University of Southampton

Faculty of Engineering, Science and Mathemetics

School of Geography

Hydraulic Modelling and Flood Inundation Mapping in a Bedrock-Confined Anabranching Network: The Mekong River in the Siphandone Wetlands, Laos

by

Tri Pham Dang Van

Thesis for the degree of Doctor of Philosophy

January 2010

UNIVERSITY OF SOUTHAMPTON

ABSTRACT

FACULTY OF ENGINEERING, SCIENCE AND MATHEMATICS
SCHOOL OF GEOGRAPHY

Doctor of Philosophy

HYDRAULIC MODELLING AND FLOOD INUNDATION MAPPING IN A BEDROCK-CONFINED ANABRANCHING NETWORK: THE MEKONG RIVER IN THE SIPHANDONE WETLANDS, LAOS

by Tri Pham Dang Van

Anabranching fluvial networks recently have become the focus of attention from environmental specialists, especially in the hydraulic field. Anabranching networks can be found in different physical environments; however, the hydraulic and geomorphological natures of such river networks are still not well known leading to on-going discussions on the definition and nature of the networks. Even though, alluvial anabranching networks generally have common features like vegetated islands, low water surface slope and stable channel planform, bedrock-confined anabranching networks also have their own characteristics inherited from the geological and structural controls imposed on the single channels that compose the network complex.

This thesis focuses on the provision of a benchmark describing the bulk hydraulic characteristics of a large bedrock-confined, anabranching river network, located within southern Laos. The network can be separated into: (i) the upper river network constituted by two bifurcations and one confluence with an interpolated bathymetry based on soundings of cross-sections along the navigation channels; and, (ii) the downstream river network characterised by a complex anabranching network with five bifurcations and five confluences for which there is no bathymetric survey.

The river network as whole is a 'composite' – partly bedrock (especially the channel-bed) and partly alluvial-filled and as such it does not accord fully with any prior description or classification of anabranching channel networks (*e.g.* Huang and Nanson, 1996). To understand the hydraulic nature of the river network, the energy approach in a one-dimensional (1D) steady-flow hydraulic model (HEC-RAS) was applied to the network. Significant challenges arose due to the lack of boundary conditions throughout the model, namely: (i) unknown splitting discharge ratios at each bifurcation; (ii) partly non-survey bathymetry; and, (iii) ungauged downstream boundary condition of one of the channel outlets. To determine the discharge entering each channel, the splitting discharge ratio at each bifurcation was defined originally by the ratio of the cross-sectional area of the first cross-section of each downstream channel and then adjusted based on the *Flow Optimization* function in HEC-RAS to minimize any rise or drop of the modelled water surface around a junction. For the channels with non-surveyed bathymetry, a SPOT satellite image was processed to construct a pseudo-bathymetry showing a range of elevations, including shallow

and deep portions of channels, rather than detailed bed elevations as would be obtained from a measured bathymetry. To define the boundary condition of the ungauged channel outlet, the water surface elevation was interpolated and validated according to predefined assumptions (*i.e.* the water surface slope along the ungauged channel was interpolated according to the available DEM and cross-sectional width extracted from a SPOT image for low discharge conditions was assumed to be similar to the gauged channels for flooding discharges).
In general, the study has helped to develop methods to model the complex river network with data constraints (*i.e.* the boundary conditions). The findings include: (i) the developed pseudo-bathymetry based on a SPOT image is useful to model a large river network using the energy approach in a 1D hydraulic model in which the cross-sectional area is important in modelling the bulk hydraulic parameters but the influence of the cross-sectional shape is subordinate; (ii) the in-channel hydraulic roughness coefficient at each cross-section may be significantly different from neighbouring values due to the variation in the local bedrock roughness and the roughness of intervening alluvial reaches; and, (iii) the hydraulic roughness of the riparian land cover along the floodplains does not contribute noticeably to the modelled stage along the river network nor to the planform extent of flooding for overbank flooding discharges. Rather, changes in land-cover, and hence the riparian roughness, are registered as small, but measureable, changes in the local velocity over the riparian floodplain and in the average in-channel velocity.

Citations:

Van, P.D.T., 2009. Hydraulic modelling and flood inundation mapping in a bedrock-confined anabranching network: The Mekong River in the Siphandone wetlands, Laos. Unpublished PhD thesis submitted to the Faculty of Engineering, Science and Mathematics, University of Southampton, England.

Contents

List of Figures

List of Tables

Declaration of Authorship

I, **Tri Pham Dang Van**, declare that the thesis entitled **Hydraulic Modelling and Flood Inundation in a Bedrock-Confined Anabranching Network: The Mekong River in the Siphandone Wetlands, Laos** and the work presented in the thesis are both my own, and have been generated by me as the results of my original research. I confirm that:

1. this work was done wholly while candidature for a research degree at this University;
2. where any part of this thesis have previously been submitted for a degree or any other qualification at this University or any other institution, this has been clearly attributed;
3. where I have quoted from the work of others, the source is always given. With the exception of such quotation, this thesis is entirely my own work;
4. where the thesis is based on work done by myself jointly with others, I have made clear exactly what was done by others and what I have contributed myself;
5. part of this work has been published as:

i) **Van, T.P.D.** and P.A. Carling, 2009. Development of a 1D hydraulic model for flood inundation mapping along the anabranched Mekong River, Siphandone, Lao PDR, as affected by recent land use changes. 7th Annual Mekong Forum. Bangkok, Thailand.

ii) **Van, P.D.T.**, P.A. Carling, T.J. Coulthard and P.A. Atkinson, 2007. Cellular Automata approach for flood forecasting in a bifurcation river system. Publs. Inst. Geophys. Pol. Acad. Sc., E-7 (401). The Eagle's Nest, Hucisko, Poland.

Signed

Date: January, 2010

Acknowledgements

My greatest thanks are to Prof. Paul Carling, the main supervisor of this PhD thesis, for his valuable encouragements and sympathies. His valuable support and guidance are highly appreciated, especially during the hardest time of the study period. Special thanks are also due Prof. Peter Atkinson, the second-supervisor, for his continued support and constructive comment on different draft versions of the thesis. In addition, specific help on supporting ideas and editing technical works from Dr. Steve Darby, Dr. Keith Richardson and Prof. Ted Milton is highly appreciated.

Thanks also go to all staff and postgraduate students, especially from whom I have great opportunities to make real friendship and to exchange knowledge, in the School of Geography, University of Southampton. Many thanks for the financial support from the Mekong River Commission, the Dorothy Hodgkin Award and the Engineering and Physical Sciences Research Council to finish this PhD study. Special appreciation is paid to the British Geomorphology Society (BSG), the International Association of Geomorphologist (IAG), the World Wildlife Fund (WWF) and the School of Geography, University of Southampton for financial support for attendance at scientific conferences. In addition, many thanks to the Optimising Access to SPOT Infrastructure for Science (O.A.S.I.S) project for the access of free SPOT images and Dr. Iwona Conlan in the Mekong River Commission for supplying relevant hydraulic data in the study area. Finally, many thanks are given to the Hunt Oil Ltd. company for a base geological map of the Siphandone wetlands.

Valuable support from the beloved family has encouraged me to overcome all the barriers; with your love, I believe I can do the best. It is never enough to just say 'Thank-you' but please accept my great and sincere appreciation for what you all have done for me.

Last but not least, a great love from my wife and 'little daughter' – Sarah is the endless source of happiness and encouragements.

'Father, Lord of heaven and earth, I thank you because you have shown to the unlearned what you have hidden from the wise and learned. Yes, Father, this was how you wanted it to happen' (Luke, 10:21).

Tri Pham Dang Van

Chapter 1: Introduction

1.1 Research context

Large rivers at the global scale are vitally important due to the great services provided with respect to the livelihood of millions of people not only directly living on the floodplains but also having contacts with the river resources like fish, potable water and agricultural products. However, such large rivers are also subject to intensive human activities increasing with the pressure of economic development; human interventions regulating temporal and spatial distributions of water resources with reservoirs and water transfer schemes have increased. In addition, global climate change is increasingly altering the physical setting of different areas in the world with different spatial and temporal distribution and at different significant levels. Kundzewicz *et al.* (2007) revealed that dramatic increasing temperature in some of Asia large river basins have intensified the water cycle and aggravated water-related natural hazards. The Mekong is the world's eighth largest river (Kummu *et al.*, 2008) but has received little scientific attention and is facing significant changes due to anthropogenic and climate pressures. However, unlike many large rivers which are alluvial, the Mekong in the southern Laos is bedrock-confined consisting of a complex network of multiple channels, with significant rocky outcrops and partial alluvial fills. The hydraulic patterns of such systems are poorly understood and addressing this scientific knowledge deficiency is a key objective of this study.

One of the present global issues is the clearance of natural forest for commercial and agricultural purposes, which might lead to more degraded land cover types (shrub or bare soil). Such a trend has happened significantly in the countries within the Lower Mekong Basin (LMB) (Figure 1.1-1) (Heinimann, 2006). The land cover changes have led to the alteration of the local hydrological regimes possibly causing the modification of the hydraulic nature of the river network by altering the sediment load and accumulated discharge from the surrounding watershed into the river network. Consequently, the changes in the hydraulic nature of a river network may lead to problems of the planform stability and channel bed evolution in the future. Such alterations may lead to changes in water supply, biodiversity of the riparian area and geomorphological nature of the river network itself, resulting in changes to the livelihood of the local people who mainly rely on the Mekong.

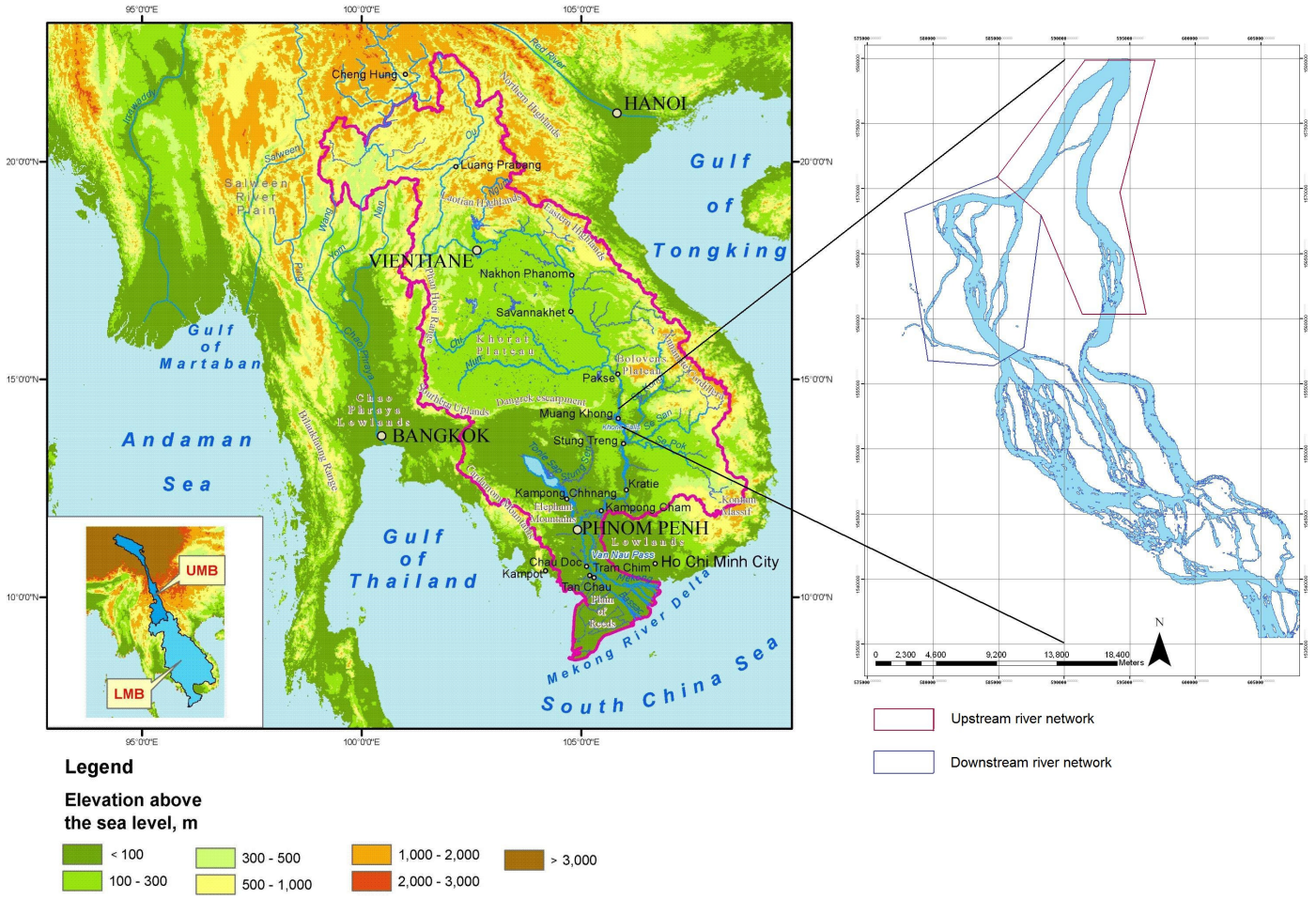

Figure 1.1-1: The Mekong River Basin and the Siphandone river network; LMB – Lower Mekong Basin and UMB – Upper Mekong Basin

Future climate change resulting in alterations of precipitation, evapo-transpiration and soil moisture may profoundly affect biodiversity, water resources (runoff and stream-flow) and therefore human livelihoods in the LMB. Different research programmes (*e.g.* Arora and Boer, 2001; Kiem *et al.*, 2004; Jacobs, 1996) have predicted different outcomes from the future climate pattern. According to Arora and Boer (2001), during the period from 2070 to 2100, there will be a decrease of the total flood discharge during the flood period of about 21 % and lower mean annual flows of about 30 %; however, according to a report from START (the global change SysTem for Analysis, Research and Training) (2006), with the increase of CO_2 concentration in the future, the LMB would receive more precipitation leading to more discharge entering different sections of the Mekong. Even though there are conflicting predictions, researchers have agreed that there would be significant changes in hydrological conditions (average temperature, seasonal distribution, precipitation, runoff and stream-flow) in different sub-areas within the LMB. Such changes might lead to great modifications of in-channel hydraulic parameters along the river network, productivity of agriculture and fisheries, and substantially altering the composition, structure and function of the regional ecosystems.

The existing dams, mainly along the Upper Mekong Basin (UMB), have significantly changed the sediment load, geomorphology and therefore hydraulic nature of the Mekong River. In addition, more hydroelectric projects have been proposed in both the UMB and LMB, which may consequently have dramatic impacts on the flow regime of the LMB. Recently, Dr. Carl Middleton from the International Rivers organization spoke on the Cable News Network (CNN) (19th June, 2009) that 'Even one dam across of the river would be devastating because what we are talking about is 70 % of the commercial fish catch migrates over long distances. So therefore if you build a project on the lower part of the river it does not matter if you build eleven or one because if you cannot get past the first dam then it cannot get past the second either'. In addition, the on-going research from the Mekong River Commission (MRC), International Rivers organization and the World Wildlife Fund (WWF) aims to understand the impacts of the proposed dams and to raise the awareness of local and international stakeholders. A typical example is the '*Open Letter on the Don Sahong Dam, Proposed for the Mainstream Mekong River, Southern Laos*' (26th Aug. 2009) (*Appendix 1*), in which signatory scientists have called for a serious

consideration for the proposed dam at the downstream end of the Siphandone wetlands, Laos.

The Siphandone wetlands (Figure 1.1-1) have been proposed to be a *RAMSAR* site according to the *Ramsar Convention on Wetlands* (Ramsar, Iran, 1971) aiming at conservation and sustainable use of natural resources. The Siphandone wetlands are rich in terms of natural resources (Daconto, 2001) and have received great attention from scientists especially in respect of aquatic biodiversity (Baird, 2001). However, little attention has been paid to the hydraulic nature of the complex river network within the area to understand how the river network behaves, which may evolve in the future, especially in the context of global and regional climate change and direct human impact.

1.2 Research problem and justification

1.2.1 Hydraulic modelling – the application for a river network with multiple outlet sections

To understand the impact of human intervention and climate change on the study area, amongst other subjects, research on the hydraulic nature of the river network to provide a benchmark of the bulk hydraulic characteristics is one of the major concerns, especially when the recorded hydraulic information of the river network (*e.g.* stage and discharge) is limited. In this study, a physical based (steady) one dimensional (1D) hydraulic model (HEC-RAS – Hydrologic Engineering Center's River Analysis System) was used to explore the hydraulic nature of the complex anabranching river network for given discharges within the Siphandone wetlands. The complex river network is divided into two sections: the upstream river network for which there is a measured bathymetry and the downstream river network with interpolated pseudo-bathymetry (representing a range of channel bed elevations, including shallow and deep channels, rather than detailed elevation) (Figure 1.1-1). Different HEC-RAS models in terms of the spatial extent and magnitude of entry discharge were developed; the upstream network models help to understand the hydraulic nature of the upstream river network with two bifurcation and one confluence at different entry discharges while the full network models (including both the upstream and downstream river network) contribute to the application of the HEC-RAS model for understanding the mean hydraulic nature of a complex network in the case of a lack of measured bathymetry.

Even though HEC-RAS models have been widely employed for a long time to estimate the flooding pattern (or wetted-section) and model the hydraulic nature (*e.g.* water surface elevation, mean velocity and Froude number) at each cross-section along natural river networks with one outlet section, the HEC-RAS model has not been applied to study a large river network with multiple outlet sections as in the Siphandone wetlands. In fact, by modelling a single river channel or simple river network with single outlet section, the requirements for the boundary conditions could be reduced to a minimum. However, to model a river network with multiple outlet sections is challenging and even more difficult if the boundary condition of one or more of the outlet sections is unrecorded, but iteratively calibrated.

2D and 3D hydraulic models have been developed to study the detailed hydraulic nature (rather than the mean conditions in a 1D hydraulic model) of the natural river network; however, due to the requirements of intensive input data and powerful computers for a large number of iterations, 2D and 3D hydraulic models have not been popular for large and remote river networks like the Siphandone river network. In fact, the model complexity is constrained by the availability of data, and therefore, to model a complex river network is challenging due to significant differences in the hydraulic nature along the river network (Costelloe *et al.*, 2006). In comparison to a 2D or 3D hydraulic model, apart from the requirement for less accurate geometry and smaller numbers of hydraulic variables to be specified (*e.g.* velocity at the entry section of the river network), a 1D hydraulic model requires extra boundary conditions (*e.g.* the entry discharge of each individual channel within a river network) in contrast to 2D or 3D hydraulic models. Actually, in a 1D hydraulic model, if a river network with several bifurcations is modelled, the splitting discharge from the upstream channel into the downstream channels needs to be specified. Such data are not always available, especially for a remote river network. Thanks to the advances of computer science, the splitting of discharge at each bifurcation in a 1D hydraulic model can be done automatically (*e.g.* the *Flow Optimization* option in HEC-RAS *v.*4.0) based on certain initial conditions on the entry discharge at each channel (presented in this study) and checked by different modelled hydraulic parameters (*i.e.* calculated water surface profile and energy gradeline along a river network through bifurcations).

1.2.2 Data collection for hydraulic modelling in a remote area of a developing country

Hydraulic data often have been collected for a long time (decades or centuries) in developed countries. However, in developing countries, such data have not been collected and archived well. In fact, often the recorded data have been stored in different computational formats and some are still only available as paper chart records or tabulated data. Furthermore, often only the main channels for navigation within a river network have been surveyed bathymetrically and gauged, and among the gauging stations not all are used to record both stage and discharge. Such issues in collecting and storing relevant data may lead to insufficient input data for building and calibrating hydraulic models.

Since the development of remote sensing techniques, remote river networks have been observed allowing the extraction of channel planform metrics (*e.g.* Schumann *et al.*, 2007). Less frequently, in clear-water shallow flows, the channel bathymetry also can be obtained using remote sensing and therefore the input bathymetric data for a hydraulic model of a river network might be available sufficiently (Katiyar and Rampal, 1991; Melsheimer and Liew, 2001; Deng *et al.*, 2008; Tripathi and Rao, 2002; Gao, 2009). However, in a large and sediment-laden river network, remote sensing imagery can provide no more than the planform of a river network (Latrubesse, 2008). The channel geometries of such river networks have not been estimated by using satellite images but rather have been measured in the field. However, this approach is not logistically realistic when a large river network like the section of the Mekong River in the Siphandone wetlands with inter-connected and myriad channels is to be studied.

1.2.3 Justification

Bedrock-confined anabranching networks which may in part be exposed bedrock and elsewhere may contain significant alluvial fill have been little studied in terms of network geometries and hydraulics. In contrast, there is a greater literature concerning alluvial anabranching and braided channel networks with consideration of their hydraulic behaviour. In addition, bedrock-confined river networks are essentially fixed in space and time whereas alluvial networks are free to adjust their channel geometries. In this study, a steady 1D hydraulic model was developed to understand the hydraulic nature of a bedrock-confined river network with multiple outlet sections,

in which the upstream boundary conditions (stage and discharge) and stage of one of the outlet sections were known. Finally, the issues encountered in successfully modelling the hydraulic behaviour of such a river network are noted and related to specific characteristics of bedrock-confined channels.

A particular challenge for the hydraulic modelling of the study river network is that there was no available information on the entry discharge for each individual channel constituting the study river network, and the bathymetry for the most downstream portion of the river network also was not available. Furthermore, most previous studies of bedrock channels applied a single value of the hydraulic roughness for a reach or group of cross-sections along the channel network. However, due to the nature of bedrock-confined channels, a cross-section along the river network within the Siphandone wetlands has different hydraulic roughness values from the neighbours according to the local channel conditions, bedrock or alluvial.

The Mekong River is increasingly receiving great attention from different international organisations (*e.g.* MRC, WWF and the International Rivers organization) due to its important and unique roles in terms of biodiversity, hydrological and hydraulic regimes and socio-economic setting. Thus, this study contributes to the understanding and provision of a benchmark concerning the generalized hydraulic nature of the Siphandone river network reflecting the conditions prevailing in the decades at the end of the 20^{th} century and the beginning of the 21^{st} century during which the flows remain essentially natural and unregulated.

The study has helped in the development of methods to model a large river network with multiple outlet sections and lack of measured input data (boundary conditions and geometry of the full river network). As such the models were calibrated according to the wetted-width section extracted from satellite imagery and the very limited available recorded data (recorded stages at the entry section and one of the outlet sections). Apart from building hydraulic models to route different entry discharges along river networks, land cover maps within the riparian zone were extracted from SPOT images (taken in 2001 and 2005) which were important to identify the influences of overbank hydraulic roughness during flooding. Furthermore, the pseudo-bathymetry was developed in the complex southern river network within the Siphandone wetlands. Such findings should encourage the application of remote

sensing imagery for interpolating bathymetry and studying the hydraulic nature of large sediment-laden river networks located in remote areas.

Even though there were not enough input data for calibration and validation of the hydraulic models separately, both the upstream and full river network model, the HEC-RAS models for the low discharge (6,450 m^3s^{-1}) were calibrated by adjusting the Manning's *n* at each cross-section and then validated by comparison with the recorded stages at the upstream and downstream boundaries and the modelled top-widths at each cross-section with those extracted from the SPOT image. In addition, the HEC-RAS models for the flood discharge were calibrated by calculating individual Manning's *n* at each cross-section and then validated by comparing the recorded stages. Furthermore, because it was considered that the in-channel Manning's *n* coefficient at each cross-section would not significantly change for all flooding discharges, the set of Manning's *n* coefficients calculated for the historical average flooding discharge (26,300 m^3s^{-1}) was applied to model the high flood discharge (45,149 m^3s^{-1}) and the modelled stages compared with those recorded at the upstream and downstream boundaries.

1.3 Research objectives

1.3.1 Main objective

To model the wetted-section and flood patterns according to different entry discharges at the upstream boundary with specific consideration given to the spatial roughness along a river network and influences of land cover change along the floodplain.

1.3.2 Specific goals

In order to meet the main objective, three specific goals were developed as follows:

(i) To quantify the discharge distribution at each junction and in-channel hydraulic parameters within each channel along a bedrock-confined river network with multiple outlet sections for low and flood discharges.

(ii) To understand the impact of the riparian hydraulic roughness on the modelled hydraulic parameters in the case of flood discharges.

(iii) To model the spatial flood extent along a large bedrock-confined river network according to different upstream discharges.

Taken together the objective and goals should not only provide insight into geomorphological processes of anabranching bedrock-confined channels within the Mekong River but also have generic applications to other bedrock-confined rivers.

1.4 Overview of the study

The thesis includes nine chapters and can be divided into three main sections, including:

The first section includes the first four chapters. Chapter 1 introduces a brief description on the current issues in the Mekong River, in general, and in the Siphandone wetlands specifically, and what issues were expected to be addressed in this PhD project. Chapter 2 reviews the available literature focusing on: (i) the hydraulic nature of both alluvial and bedrock-confined river networks; and, (ii) the hydraulic modelling applied to a single channel as well as a multi-channel network. Chapter 3 reviews the available literature on the geomorphology, geology, hydrology, hydraulics and a brief review of the sediment transport in the Mekong River generally, at Pakse gauge specifically and within the Siphandone wetlands, respectively.

The second section includes one chapter of methodology and three subsequent chapters of results. Chapter 4 illustrates a detailed description of the approach applied in the whole thesis. Chapter 5 presents results of the application of a SPOT image for pseudo-bathymetry development in a large and heavy sediment-laden river network. Chapter 6 presents: (i) a general description of the land cover pattern and land cover change in the period of 2001 – 2005; and, (ii) the HEC-RAS model for the upstream river network with the multiple outlet sections. Chapter 7 illustrates results obtained from the HEC-RAS model for the full river network with the multiple outlet sections.

Finally, the last section includes the last two chapters of discussions and conclusions. In chapter 8, a general discussion of the approaches applied in the study and what is required in the future to understand the nature of such a complex river network and their projected changes in the context of global climate change were presented. Chapter 9 summarises final conclusions on the hydraulic modelling of the bedrock-confined river network.

Chapter 2: Literature review

Introduction

The first section in this chapter summarizes the general features of alluvial and bedrock-confined river networks in terms of geomorphological and hydraulic conditions. Even though single channel reaches (straight and meandering channel) and braided networks are described briefly, special attention is paid to anabranching networks. In addition, the differences in terms of geomorphological and hydraulic nature between the multi-channel networks (braided and anabranching) are identified. Due to the general importance of the hydraulic roughness of the riparian land cover on the hydraulic models, a section on riparian hydraulic roughness is presented in the next section. Finally, literature on modelling a complex multi-channel network using physical-based hydraulic models is presented.

2.1 Geomorphology and hydraulic nature of natural river networks

Through time, different channel classifications have been introduced, for example, classification based on the stage of development (Davis, 1899), boundary conditions (or bed material) and channel patterns (or channel types) (Rosgen 1994). In this literature review, attention has been paid mainly to the channel patterns to review the differences in hydraulic and geomorphological nature of each natural channel pattern and a more intensive review is focused on the hydraulic and geomorphological descriptions of the anabranching river network.

The term ‘channel pattern’ is used to describe channel planform geometry and each pattern usually is associated with specific physical processes (flow pattern, sediment transport and planform stability) operating within a channel. Research on channel patterns requires knowledge of the physical processes leading to understanding of the physical behaviour of a channel. Such knowledge may lead to the prediction of channel dynamics (Nanson and Knighton, 1996). In fact, a general classification of channel patterns is necessary for a consistent description of channel reaches in different environments and for deeper knowledge of channel genesis and processes. However, it is important to note that such a classification should be applied to a channel reach rather than to an entire channel network (Kinghton, 1998), especially where complex multi-channel networks exist, and also depends upon stage. In

addition, there is no sharp distinction between different channel patterns in nature but rather a continuum exists from one extreme to another (Leopold *et al.*, 1992). Generally, a natural river could be considered as either a single channel reach (straight or meandering channel) or a multi-channel network (braided, anabranching or anastomosing network).

2.1.1 Classification of natural rivers

a. Single channel reach

A single channel reach with a wide range of geomorphological and hydraulic natures (Rosgen, 1994) includes two sub-classifications: straight and meandering channels (Figure 2.1-1) (Morisawa, 1985). Straight and meandering channels are both characterized by a meandering thalweg in combination with pools and riffles or alternate bars (Leopold *et al.*, 1964); however, the sinuosity index for straight channels (the ratio of channel distance to axial distance) is often less than 1.3 (van den Berg, 1995) or 1.5 (Leopold and Wolman, 1957) while it is more than 1.5 for meandering channels (Morisawa, 1985). The division between the two is normally placed at 1.5 (Leopold *et al.*, 1964). The straight channel has minor widening and incision while meandering channels are often characterised by frequent channel incision and meander widening. The point bars may be formed more intensively in the meandering channel than in the straight channel. The width/depth ratio of straight channels is smaller than 40 (Morisawa, 1985).

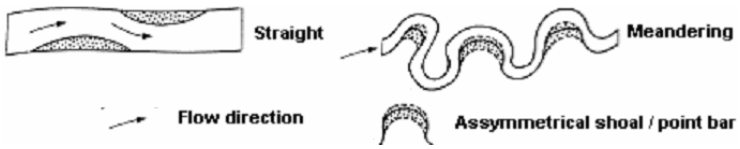

Figure 2.1-1: Channel patterns of a single channel reach (*after* Morisawa, 1985)

b. Multi-channel network

The term 'multi-channel network' generally is used to describe a braided or anabranching network (Figure 2.1-2). Even though in earlier times either the terms braiding and anabranching have been used synonymously (Leopold and Wolman, 1957; Schumm, 1971) or anabranching networks sometimes have been considered as a subset within a braided network (Richardson and Thorne, 2001), recent studies have considered anabranching networks as a separated classification with their own hydraulic and geomorphological characteristics (*e.g.* Nanson and Knighton, 1996). In

fact, the terms anabranching and braiding are mutually exclusive, and cannot be used together in a single classification (Bridge, 2003).

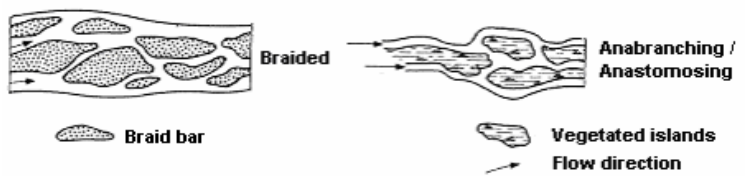

Figure 2.1-2: Channel patterns of a multi-channel network (*after* Morisawa, 1985)

Makaske (2001) suggested the channel-belt (the zone in which channel deposition or erosion may occur) as a criterion to differentiate an anabranching network from a braided network. According to Makaske (2001), an anabranching network is characterized by river patterns existing in multiple channel-belts rather than within a single channel-belt as is the case of a braided network (Figure 2.1-3). In addition, the channel-belts of an anabranching network are relatively straight and the sinuosity index of the main and major secondary channels is often less than 1.3 (Latrubesse, 2008).

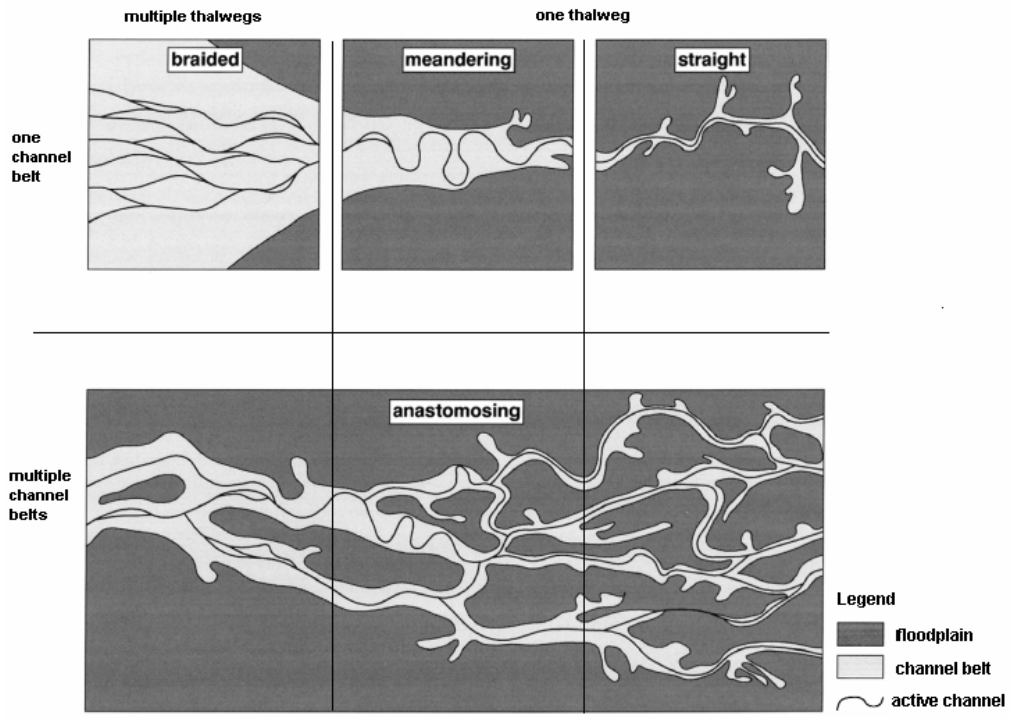

Figure 2.1-3: Classification of alluvial channels network based on the channel pattern (*after* Makaske, 2001)

Each single channel within an anabranching network could have its own geomorphological and hydraulic nature of either a single channel reach (straight and meandering channels) or a braided network (Latrubesse, 2008) which conjoin

(Knighton, 1998; Abbado *et al.*, 2005) to create the closed loops of the whole river network. Knighton (1998) described the differences between anabranching and braided networks based on entrenchment ratio, sinuosity, width/depth ratio and water surface slope criteria (Table 2.1-1). In general, an anabranching network has smaller water surface slopes and smaller width/depth ratios but higher sinuosity indices compared to a braided network. The entrenchment ratio, indicating degree of vertical containment and the access to floodplain of the flood discharges, is defined as the ratio of the floodplain width at about twice the bankfull discharge with the channel width at the bankfull discharge (Rosgen, 1994) and reflects the relationship between the channel and its floodplain. With an entrenchment ratio of greater than 2.2, the floodplain of an anabranching network is flooded more often than that of other channel types.

Table 2.1-1: Differences between braided and anabranching networks (Knighton, 1998)

	Braided network	Anabranching networks
Entrenchment ratio	N/A	> 2.2
Sinuosity	< 1.1	1.1 – 1.6
Width / Depth ratio	> 40	< 40
Water surface slope	< 0.02	< 0.005

In general, a braided network is a pattern of inter-connected smaller channels separated by braid bars consisting of mobile sediment and annual grasses, sedges and pioneer bushes (Bridge, 2003; Takagi *et al.*, 2007). The height of braided bars is usually below the bankfull height and as such the bars are inundated by high flows. Channels in a braided network individually are not hydraulically independent, but rather are linked and the entry discharge and water surface elevation in each single channel are intimately and sensitively affected by the flows in other channels (Bridge, 2003). A braided network is often characterized by erosive behaviour and continuously reforming mid-channel bars (Morisawa, 1985).

In contrast to braided networks, each channel within an anabranching network is separated by floodplains (Lane, 1957; Nanson and Knighton, 1996; Makaske, 2001). In addition, anabranching networks are characterized by relatively stable vegetated islands which are rarely flooded (Harwood and Brown, 1993; Knighton, 1998; Topa and Paszkowski, 2002; Tooth and McCarthy, 2004; Wang *et al.*, 2005) or stable alluvial or rock-cored islands (Tooth and Nanson, 2000; Brambatti and Carulli, 2001; Costelloe *et al.*, 2006), which divide flow even at the bankfull discharge. In fact,

according to Roberts (1991), over a three-year period of surveying, there was no significant change to the planform of an alluvial anabranching network. The in-channel islands are relatively large compared with the size of the individual channels (Costelloe *et al.*, 2006) but if the islands are breached, flow and sediment may be diverted from one channel to another (Tooth and Nanson, 2000). According to Bridge (2003), channels within an anabranching network are hydraulically independent, which is reflected by some channels being seasonally inactive (Broadhurst and Heritage, 1998) and different water surface elevations occur in neighbouring channels due to the lack of lateral hydraulic connectivity (Figure 2.1-4) (Broadhurst and Heritage, 1998; Heritage *et al.*, 2004; Smith *et al.*, 1997). Anabranching networks have slow rates of lateral migration and slow back accretion (Morisawa, 1985) with low water surface slope (Howard and Brown, 1993) (*i.e.* lower than the water surface slope of the braiding networks; Knighton, 1998). A high sinuosity is not an important requirement for a channel network to be considered as an anabranching network (Nanson and Knighton, 1996).

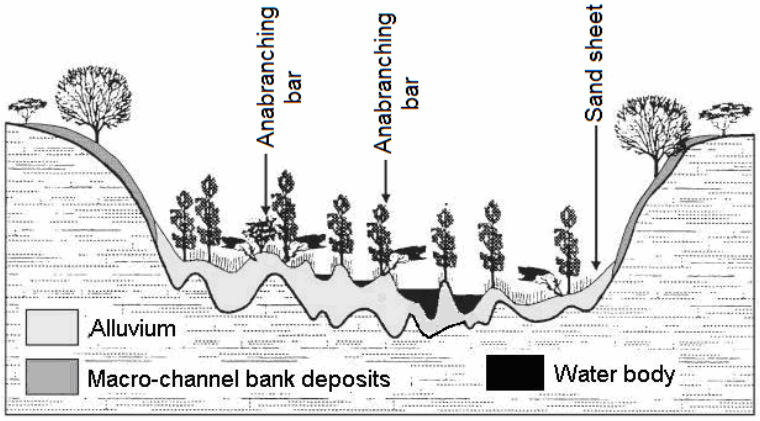

Figure 2.1-4: A cross-section of an alluvial anabranching network (*after* Heritage *et al.*, 2004)

c. Anabranching networks

Anabranching networks can be found in different physical environments including (i) bedrock-confined networks in Southern Africa (Heritage *et al.*, 2001, 2004), Australia (Costelloe *et al.*, 2006; Jansen and Nanson, 2004, Tooth and Nanson, 1999, 2000; Tooth and McCarthy, 2004; Wende and Nanson, 1998); and, (ii) alluvial networks in England (Fuller *et al.*, 2003), Ireland (Harwood and Brown, 1993), America (Smith and Smith, 1980; Smith, 1986), China (Wang *et al.*, 2005) and India (Jain and Sinha, 2004). However, the geomorphological and hydraulic nature (Nanson and Knighton, 1996) and the evolution (Judd *et al.*, 2007; Makaske, 2001) of such river networks are

not well known. Consequently, the anabranching network remains the last major category of channel patterns to be described and explained (Nanson and Huang, 1999).

In general, anabranching and anastomosing networks sometimes are used synonymously to refer to large multi-channel networks (Islam *et al.*, 2006) with an annual mean discharge of greater than 1,000 m^3s^{-1} (Latrubesse, 2008). However, Carling (2009) considers anabranching and anastomosing networks as separated channel planforms; the anastomosing networks are characterised typically by one or more channels bifurcating from the main braided or anabranching network and flowing for a considerable distance (a considerable way from the main network) before rejoining the main stem. According to Nanson and Knighton (1996), an anabranching network can be classified into six subtypes (cohesive sediment anabranching network; sand-dominated, island-forming anabranching network; mixed-load, laterally active anabranching network; sand-dominated, ridge-forming anabranching network; gravel-dominated, laterally active anabranching network; and, gravel-dominated, stable anabranching network) based on the consideration of stream energy, sediment size, and morphological characteristics (Table 2.1-2). Among the six subtypes, the first subtype (cohesive sediment anabranching network) is considered as an anastomosing network which is characterized by low gradient (which leads to high sinuosity), low stream power, cohesive sediment banks (Costelloe *et al.*, 2006) together with a low width/depth ratio and high sediment transport rate (Wang *et al.*, 2005). Note that Nanson and Knighton (1996) do not include bedrock-constrained anabranching river networks in the classification.

Table 2.1-2: Classification and features of the anabranching network (*after* Nanson and Knighton, 1996)

Type	Energy	Geomorphological features	Hydraulic features
1	Low	Cohesive and fine grained sediment Little or no lateral migration	Low width/depth ratio Low stream power (≤ 8 Wm^{-2})
2	Low	Sand-dominated channel bed Vegetated banks Low sinuosity channel pattern Island-forming within the channels network	Low stream power: 4 – 8 Wm^{-2}
3	Low	Mixed-load, laterally active meandering Channel bed sediment: mud, sand, and fine gravel	Stream power: ≈ 50 Wm^{-2}
4	High	Sand-dominated channel bed Ridge-forming characterized by long, parallel, channel-dividing ridges	Low width/depth ratio Stream power: 15 – 35 Wm^{-2}
5	High	Gravel-dominated channel bed Laterally active	Stream power: 30 – 100 Wm^{-2}
6	High	Gravel-dominated channel bed and boulders islands Stable channels network occurring in small and relatively steep basin Well-vegetated in banks and islands	Stream power: 100 – 300 Wm^{-2}

Anabranching networks often have irregular networks of multi-channel (Makaske, 2001; Topa and Paszkowski, 2002) with a sequence of confluences and bifurcations (Islam *et al.*, 2006) in a dynamic equilibrium (Jansen and Nanson, 2004). An anabranching network may develop as an individual channel evolves to become less hydraulically efficient, displacing flows onto the floodplain during periods of overbank flow and aggressive scouring of new channels (Knighton, 1998; Judd *et al.*, 2007). According to Nanson and Huang (1999), an anabranching network is the most effective channel pattern in terms of transporting both sediment and water compared to any single channel with similar water surface slope and approximately similar water surface width. The anabranching network has the advantage of concentrating stream power and maximizing bed-sediment transport. In addition, anabranching networks are considered to be resistant to bank erosion (Nanson and Knighton, 1996; Smith and Smith, 1980), therefore, the planforms of anabranching networks are more stable than braided networks.

Latrubesse (2008) briefly describes the largest anabranching networks in the world (Table 2.1-3), in which the river networks have a wide range of physical features (drainage area: 76,964 – 2,854,286 km^2, mean annual discharge: 1,200 – 123,680 m^3s^{-1}, bankful discharge: 3,200 – 161,330 m^3s^{-1}, water surface slope: 1.6×10^{-5} – 9.8×10^{-5} and width/depth (w/d) ratio: 30 – 200). Also according to Latrubesse (2008), the current approaches used to discriminate channel patterns based on analysis of variables such as water surface slope, grain size and bankfull discharge are not

appropriate for application to mega multi-channel networks, which leads to a need to define other ways to describe quantitatively a large anabranching network.

Table 2.1-3: Data on large anabranching networks at the global scale (*after* Latrubesse, 2008)

River	Gauging station	Drainage area (km^2)	Mean annual discharge (m^3s^{-1})	Bankful discharge (m^3s^{-1})	Water surface slope (10^{-5})	w/d ratio
Madeira	Abuna	1,532,002	18,630	25,000	6.0	30
Madeira Porto	Velho	954,285	19,039	30,000	4.3	33
Madeira	Manicoré	1,157,516	25,538	42,000	4.1	35
Madeira	Fazenda Vista Alegre	1,586,000	31,003	57,000	5.7	64
Japura	Acanauí	242,259	14,333	21,000	3.6	65
Japura	Vila Bittencourt	197,136	13,758	20,000	4.1	68
Solimões	Teresina	983,157	45,366	60,000	3.8	127
Solimões	Santo Antonio do Içá	1,134,540	55,538	70,000	3.4	110
Solimões (Amazon)	Itapeua	1,769,000	82,069	90,000	1.6	24
Solimões (Amazon)	Manacapuru	2,147,736	101,218	120,000	1.8	120
Amazon	Jatuarana	2,854,286	123,680	161,330	2.1	72
Upper Parana	Porto Rico	670,500	9,700	12,300	11.0	68
Parana	Corrientes	1,950,000	19,170	27,330	4.9	110
Parana	Curtiembre	2,300,000	19,500	20,500	4.8	111
Parana	Villa Urquiza	2,173,000	16,460	17,140	4.4	112
Brahmaputra	Bahadurabad	636,130	21,261	60,000	6.8	200
Araguaia	Luis Alves	117,580	1,621	3,700	10.0	76
Araguaia	Aruana	76,964	1,200	3,200	15.0	64
Araguaia	São Felix	193,923	2,700	6,000	9.8	83
Orinoco	Musinacio	1,705,383	28,723	64,600	6.0	101
Yangtze	Datong	1,705,000	25,023	87,204	9.3	130
Mekong (1)	Channoy	545,000 (*)	9,900	26,300 (+)	18.5 (-)	101 (+)

(1) Added in this study.
(*) Estimated from the SRTM; (+) Model output; (-) from Channoy to Hatxaykhoun.

According to previous studies, the anabranching river network is considered in this study as a large river network (mean annual discharge ≥ 1,200 m^3s^{-1}) and defined as (i) a multi-channel network with a sequence of bifurcations and confluences and low water surface slope; (ii) each individual channel within the river network has its own hydraulic nature and is independent to others due to the lack of hydraulic connectivity; (iii) the planform of the anabranching river network are stable; and, (iv) during the flood, the major islands are not fully inundated.

d. General comparison between natural rivers

Schumm (1985) introduced a general classification of the channel pattern in which 14 channel types are distinguished (Figure 2.1-5). The channel types are classified in three main groups, namely: bed load (type 1 – 5), mixed load (type 6 – 10) and

suspended load (type 11 – 14). The major concerns of the comparison are the distinction between the braided and anabranching river network. In fact, the anabranching network is not included in the bed load and mixed load channel types while the braided network is not present in the suspended load category. According to this classification, the anabranching networks have higher planform stability but lower *bed load / total load* ratio. In addition, both the sediment size and sediment load in anabranching networks are smaller than those in braided networks.

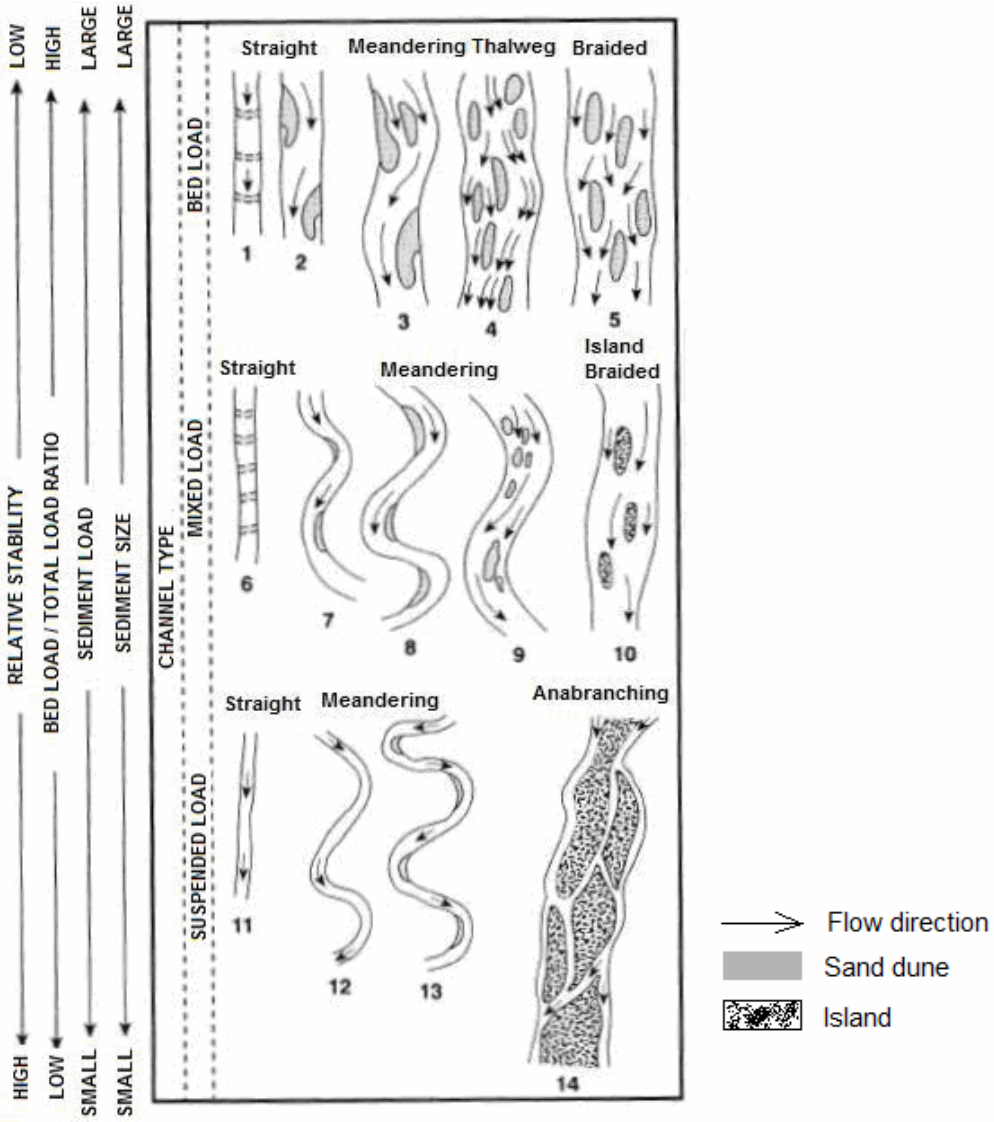

Figure 2.1-5: Classification and general descriptions of the alluvial channel pattern (*after* Kellerhals *et al.*, 1978 and Knighton, 1998)

2.1.2 Geomorphology and hydraulic nature of bedrock-confined multi-channel networks

Even though bedrock-confined anabranching networks can be found in different areas at the global scale (cited previously), such bedrock-confined anabranching networks were not considered in the classification proposed by Nanson and Knighton (1996). This section summarizes the geomorphological and hydraulic nature of the bedrock-confined anabranching network. However, there was not much information on the bedrock-confined anabranching network; therefore single bedrock-confined channels were described instead to highlight the differences between alluvial and bedrock-confined rivers. A typical planform and cross-section of a bedrock-confined anabranching network are presented in Figure 2.1-6.

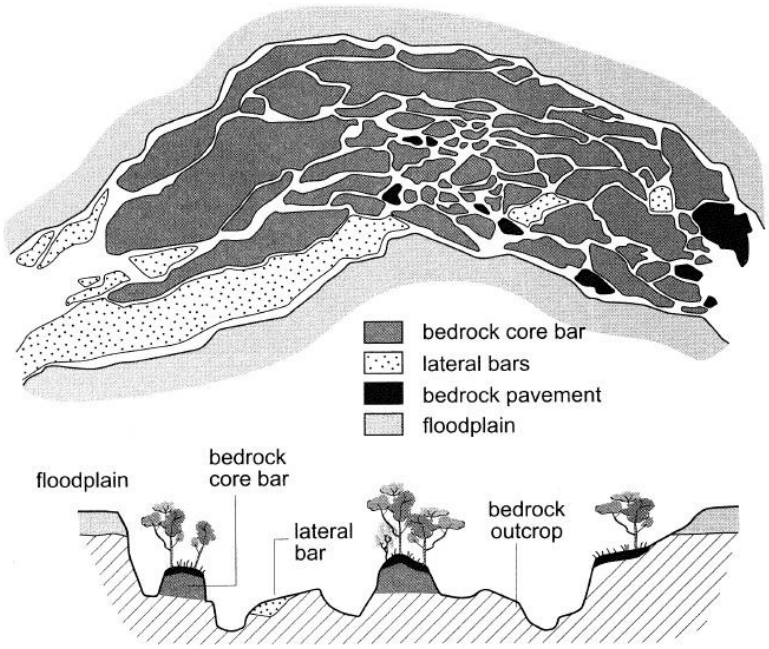

Figure 2.1-6: A typical planform and cross-section of a bedrock-confined anabranching network (Brierley and Fryirs, 2005)

a. Geomorphological characteristics of bedrock-confined anabranching networks

Different definitions of a bedrock-confined network can be found. Among those, definitions given by Schumm (1971), Wohl (1999) and Whipple (2000, 2004) are presented to show different perspectives on the bedrock-confined channels. 'Bedrock-control channels are those so confined between outcrops of rock that the material forming their bed and banks determines the morphology of the channel' (Schumm, 1971). Wohl (1999) proposed that a bedrock-confined channel is characterised as

bedrock-exposed with a direct control of bedrock on the morphology and gradient of the channel. Whipple (2004) refers to different authors (Gilbert, 1877; Howard, 1980; Howard *et al.*, 1994; Montgomery *et al.*, 1996) to define bedrock-confined channels as those that 'lack continuous alluvial cover along the channel bed even in the case of low flow discharge' and the bedrock-confined channels exist only where the transport capacity exceeds the sediment flux over the long-term. Furthermore, Tinkler and Wohl (1998) propose a more quantitative definition that a bedrock-confined channel must have a substantial proportion of the boundary (≥ 50%) as exposed bedrock or is covered by an alluvial veneer which is largely mobilised during high flows such that the underlying bedrock geometry strongly influences patterns of flow hydraulics and sediment movement. According to Turowski *et al.* (2008), the mentioned definitions contain drawbacks and cannot be used globally; another definition of bedrock-confined channel was suggested instead: 'A bedrock-confined channel cannot substantially widen, lower or shift its bed without eroding bedrock'. In short, Turowski *et al.* (2008) suggest three typical types of cross-section in the bedrock channel (Figure 2.1-7) in which type (A) represents a cross-section confined entirely in bedrock with both steep bedrock walls and exposed bedrock within channel; type (B) represents a cross-section with steep bedrock walls and alluvial fill; and, type (C) represents a cross-section with exposed bedrock bed but set in an alluvial plain.

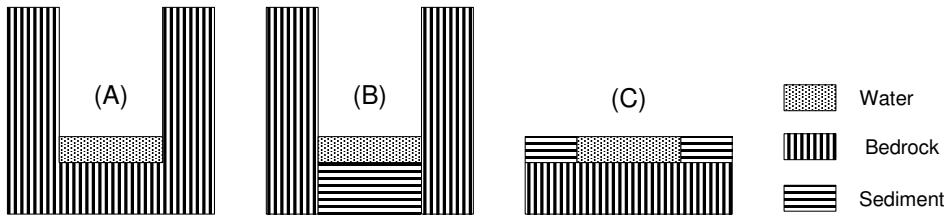

Figure 2.1-7: Types of bedrock-confined channel cross-section (*after* Turowski *et al.*, 2008)

According to Carling (2006), one of the specific features of bedrock-confined multi-channel networks is the fixed cross-section within the timeframe of individual floods and, as a consequence, flow must adjust to the channel geometry or modify the geometry by sediment deposition. In fact, morphological changes in bedrock-confined channels are generally extremely slow compared to those in alluvial channels because of the substrate resistance (Richardson and Carling, 2005). Climate, tectonic and sediment supply are the main factors which control the evolution of a bedrock-confined channel cross-section and, therefore, have important roles in adjusting the longitudinal channel bed profiles in a bedrock-confined network (Kale *et al.*, 1996;

Wobus *et al.* 2006). In the long-term, according to Stark (2006), the cross-sectional shape and the *in situ* erosion pattern are closely linked. In other words, the change of one factor has a direct impact on the other, which in turn causes a direct feedback to adjust the former. Such a feedback loop makes the channel more stable and approaches dynamic equilibrium. According to different authors (Whipple and Tucker, 1999; Stark, 2006; Wobus *et al.*, 2006), within a bedrock-confined channel, a cross-section is long-term adjusted according to eroding the channel bedrock and this process is active until a steady state of the channel is achieved in which the vertical erosion equals the tectonic advection of rock mass. The lateral erosion occurs mainly due to large floods while intermediate discharges can cause thalweg erosion, which is the main cause of evolution of a bedrock-confined channel (Knighton, 1998; Hartshorn *et al.*, 2002). In addition, above bankfull discharge, due to relatively stable channel banks, the bedrock-confined channels make new channels via the incision process (Baker and Kale, 1998; Richardson and Carling, 2006).

The bedrock-confined channel pattern principally is controlled by lithological and structural features (Ashley *et al.*, 1988) leading to more acute junction angles (Kale *et al.*, 1996) rather than alluvial channel patterns where the channel is more freely adjusted due to discharge and sediment transport. For example, even though there were no specific 'acute junction angle' values published, Tooth and Nanson (1999, 2000) described bedrock-confined anabranching rivers on the Northern Plains of arid central Australia characterized by 'abruptly' changed channel-directions at junctions or 'acute junction angles' between the channels. In addition, although Whipple *et al.* (2000) did not mention in the text-description of the bedrock-confined single channel in Alaska, by measuring the planform of the channel, the angle is up to 90^{o}. In fact, Kale *et al.* (1996) finds that major geological faults control the planform of the river networks and according to Schaller *et al.* (2005) the planform of a large river can be controlled by the structural trend. According to Tooth and McCarthy (20004), a bedrock-confined multi-channel network is strongly affected by local geology, which results in a significant but undefined impact on the in-channel processes.

b. Hydraulic features of bedrock-confined anabranching networks

Water surface slope

Generally, the water surface slopes of the bedrock-confined single channels are higher (Jamieson *et al.*, 2004; Kale, 2005) than those of the alluvial ones (Richardson and Carling, 2006) and according to Richardson and Carling (2006), the water surface slope of a single bedrock channel varies from 7.7×10^{-3} to 12×10^{-3} corresponding to very low and high discharges; in fact, the water surface slope increases with an increase of discharge. Within a bedrock anabranching network, the water surface elevations are different from one channel to another (Broadhurst and Heritage, 1998); therefore, the water surface slopes are not similar across a single cross-section within a network (Wende and Nanson, 1998; Jansen and Nanson, 2004; Tooth and McCarthy, 2004). According to Heritage *et al.* (2004) the water surface slopes within a complex network of the Sabie River range from $0.13 \times 10^{-3} – 9.9 \times 10^{-3}$ during low flow discharge to $0.27 \times 10^{-3} – 11.13 \times 10^{-3}$ during high flow discharge. In addition, the trend of water surface slope in each channel (on an alluvial base) within the anabranching network is not consistent; according to Jansen and Nanson (2004), within the three channels under study, the water surface slope in one reach significantly increases when the stage rises while in the other two reaches, the water surface slope slightly increases or decreases when the stage rises.

According to Tooth and McCarthy (2004), the bedrock-confined multi-channel network has a greater channel bed gradient compared to alluvial ones, which leads to the fact that bedrock-confined anabranching networks have steep water surface slopes (Tinkler and Wohl, 1998; Niekerk *et al.*, 1999). In addition, the water surface slope of an alluvial anabranching network is higher than that of a single channel (Knighton, 1998; Jansen and Nanson, 2004). Alluvial anabranching networks tend to have ‘smooth’ transitions in channel geometry (Schumm, 1971) including bifurcations and confluences as sediment erosion and deposition enables rapid adjustment to channel form, so water surface transitions are relatively smooth. In contrast, the water surfaces within different channels within a bedrock-confined multi-channel network may be radically different according to the lack of smooth hydraulic connectivity (Broadhurst and Heritage, 1998; Heritage *et al.*, 2004; Smith *et al.*, 1997) as bedrock control on channel form is not readily modified by erosion but only locally can be modified by

deposition of sediment (Turowski *et al.*, 2008). Rather acute channel bifurcations and other channel irregularities, often mediated by fault lines, instigate strong variation in water surface slopes.

Splitting discharge at a bifurcation within bedrock-confined anabranching networks

Flow and sediment distributions at bifurcations are important for short and long-term morphological development (Islam *et al.*, 2006). In fact, the bifurcations are sites of complex hydraulic mixing leading to unpredictable changes to channel bed and planform (Parsons *et al.*, 2007; Islam *et al.*, 2006). In addition, the ratio of splitting discharges at a bifurcation depends on the geometry, hydraulic roughness of each downstream reach (Islam *et al.*, 2006), bifurcation angles (Heer and Mosselman, 2004) and the radius of upstream bends and the slope of downstream reaches (Kleinhans, 2008). Due to issues of different water surface slopes, resistance bedrock and acute bifurcation angles within a bedrock-confined anabranching network, it is important to understand how discharge is split from the upstream channel to downstream channels at each bifurcation.

To estimate the splitting discharge at a bifurcation, the relationship between the width and discharge of channels might be useful. In fact, the relationship between discharge and cross-section width in a bedrock-confined river network is similar to that in an alluvial river network and the relationship is described as a power-law between width (W) and discharge (Q) ($W \approx Q^b$) (Wobus *et al.*, 2006). According to previous studies, for both alluvial and bedrock-confined meandering channels, (Leopold and Maddock, 1953; Parker, 1979; Whipple, 2004), the exponent (b) of the mentioned formula could range from 0.3 to 0.5. Turowski *et al.* (2008) adjust the equation ($W \approx Q^b$) based on field data of different cross-sections and find that b is determined by the bank steepness and varies according to the channel bed material ($b = 0.34 \pm 0.11$ for bedrock-confined channels and $b = 0.35 \pm 0.10$ for alluvial channels). In fact, the exponent (b) values of the bedrock and alluvial channel are quite similar. However, for the large anabranching networks, according to Latrubesse (2008), the exponent (b) is much lower and ranges from 0.01 to 0.09. Huang and Nanson (1997) use the hydraulic-geometry relation with the application of the hydraulic roughness (Manning's n) coefficient ($W/Q^{0.5} = 25.252n^{0.709}$) to express the relationship between

discharge and cross-sectional width in the study of small alluvial channels. Even though different hydraulic geometry models have been created for different channel types, according to Latrubesse (2008), the exponent (*b*) found in small channels is not applicable for large river networks.

Most hydraulic modelling studies often assume that the entry discharge into each channel of the modelled river network is known; in other words, the ratio of splitting discharge at each bifurcation is considered to be known (or measurable). In addition, most field-based observation studies often do not mention the measured hydraulic splitting discharge ratio but instead focus mainly on the sediment transport aspect (*e.g.* Kleinhans *et al.*, 2008). Therefore, in cases where there is no available splitting discharge ratio at a bifurcation, hydraulic modelling study cannot be done.

Zavadil *et al.* (2007) study a number of confluences along an alluvial network and find that the symmetry ratio (relative size of merging streams) can be used as one of the key indicators for predicting the magnitude and significance of adjustment at a Y-shaped confluence. The symmetry ratio and percentage of change in cross-sectional areas (*c*) is calculated as follows:

$$s = A_2 / A_1 \qquad \textbf{Equation 2.1-1}$$

$$c = \left(\frac{A_2 + A_1 - A_3}{A_2 + A_1}\right)100 \qquad \textbf{Equation 2.1-2}$$

where:

A_1, A_2, A_3: Mean bankfull area of the main in-coming channel, the tributary and the combined channel downstream, respectively (m^2)

s: Symmetry ratio

c: Percentage of change in cross-sectional areas (%)

Zavadil *et al.* (2007) find that the higher the symmetry ratio of a confluence (the larger the tributary), the lower percentage of change in cross-sectional area (the closer (A_1+A_2) compared to A_3); in other words, the higher the symmetry ratio (*s*), the lower the percentage of change in cross-sectional area (*c*). Such the finding of symmetry ratio might be useful to define the original splitting discharge ratio at each bifurcation along the study river network due to the lack of the available boundary condition data.

Flow velocity within a bedrock-confined anabranching network

There is a wide range of velocities within a single channel of an anabranching network with low velocities near the banks and channel bed (Richardson and Thorne, 2001). With overbank discharge conditions, flow within an alluvial anabranching network is divided laterally into zones of restricted flow velocity over the vegetated areas (often topographical ridges, scroll bars and islands) and zones of enhanced flow velocity over the vegetation-free areas (low areas and channels) (Richardson and Thorne, 2001; Wende and Nanson, 1998). According to Jansen and Nanson (2004), velocities within different channels in an anabranching network are significantly different; the velocity of each channel may peak at different values of upstream bulk total discharges.

In a detailed description of the hydraulic characteristics of an alluvial anabranching network, Tabata and Hickin (2003) noted that within different channels across a cross-section within the anabranching network, both velocity and depth have strong positive correlations with discharge leading to a conclusion that the deeper the channel, the faster the water is routed along the channels. Such an idea is supported by Jansen and Nanson (2004). Even though there is little information about the velocity distribution of flow within an anabranching network, especially a bedrock-confined one, it could be concluded that the lack of hydraulically lateral inter-connection and the influence of bedrock outcrops, faults and acute-angle bifurcations may cause differences in velocity across a single cross-section. However, in the situation with limited input data and with the application of a 1D hydraulic model, it is impossible to study the velocity distribution across a cross-section, but the mean velocity distribution within a certain channel may be explored in a downstream direction.

c. Hydraulic roughness of a bedrock-confined anabranching network

Owing to the fixed channel bed of the bedrock-confined anabranching network and assuming no (permanent) sediment deposition, there is no chance to adjust the hydraulic roughness through times as there are no significant changes of the geometry at a cross-section. The hydraulic roughness of a cross-section, which is affected mainly by the hydraulic radius, the cross-sectional shape and material of channel-bed and wall, is often expressed typically as Chezy C, Manning's n, or Darcy-Weisbach f

friction coefficients. Among these three formulae, the Manning's *n* coefficient has been widely applied.

$$C_{Chezy} = \frac{v}{\sqrt{\frac{D_H}{4}\sin S}}$$ **Equation 2.1-3**

$$n = \frac{R^{\frac{2}{3}} S^{\frac{1}{2}}}{v}$$ **Equation 2.1-4**

$$f = \frac{8gRS}{v^2}$$ **Equation 2.1-5**

where:

C_{Chezy} : Chezy coefficient ($m^{1/2}s^{-1}$)

v : Velocity (ms^{-1})

D_H : Hydraulic diameter (m)

S : Water surface slope (mm^{-1})

n: Manning's roughness coefficient ($sm^{-1/3}$)

R: Hydraulic radius (m)

f: Darcy-Weisbach friction factor

g: Acceleration due to gravity (m^2s^{-1})

In general, the hydraulic roughness at the site dominates flows at the confluences and bifurcations (Parsons *et al.*, 2007). Even though research on the hydraulic roughness coefficient of single alluvial channels has been done intensively (Chow, 1959; Barnes, 1967; Jarrett, 1984; Hicks and Mason, 1991), little attention has been paid to identifying the hydraulic roughness of an alluvial and bedrock-confined anabranching network (Heritage *et al.*, 2004). From recent research, Latrubesse (2008) concluded that the hydraulic roughness of different alluvial anabranching networks at bankfull discharge is highly consistent (Manning's *n* ranges from 0.020 to 0.035 $sm^{-1/3}$) and the anabranching network helps minimize the hydraulic roughness (Tooth and Nanson, 2000). However, the hydraulic roughness in a bedrock-confined channel is higher than

in an alluvial channel. From previous research, the flow resistance of bedrock-confined channels is widespread and sometimes high (*e.g.* Manning's *n* ranges from 0.025 – 0.04 $sm^{-1/3}$ (Carling and Grodek, 1994), 0.02 – 0.04 $sm^{-1/3}$ (Kidson *et al.*, 2006), 0.06 – 0.32 $sm^{-1/3}$ (Heritage *et al.*, 2004), 0.03 – 0.35 (Wohl and Wilcox, 2005) to 0.8 $sm^{-1/3}$ (in the peak discharge of about 100,000 m^3s^{-1} in a glacial outburst flood) (Carrivick *et al.*, 2004)). In addition, the different trends of the hydraulic roughness along the bedrock channel according to discharge could be found; for example, according to Heritage *et al.* (2004), the hydraulic roughness has a negative correlation with discharge (high hydraulic roughness at low discharge and low hydraulic roughness at high discharge), which is confirmed by Hicks and Mason (1991) and Richardson and Carling (2006); however the opposite trend was also found (*e.g.* Kidson *et al.* (2006)). Heritage *et al.* (2004) presented a comparison of the calculated Manning's *n* coefficient over a range of discharges (in-channel discharges from 1 to 100 m^3s^{-1} and overbank discharges from 1,600 to 2,100 m^3s^{-1}) in different channel types including bedrock anabranching networks, bedrock-confined anabranching networks, pool / rapid, alluvial braided network and single alluvial thread (Figure 2.1-8). In general, the lower the discharge, the higher the Manning's *n* coefficient in all channel types. However, such a trend is applicable for the in-channel discharges only. With overbank discharge, the mean Manning's *n* coefficient started increasing perhaps due to the hydraulic roughness of the land cover along the floodplain. The Manning's *n* coefficient of the bedrock-confined anabranching network type A and type B (according to the definition of Turowski *et al.*, 2008) ranged from 0.778 to 0.038 $sm^{-1/3}$ corresponding to the recorded discharge ranging from 5 to 1900 m^3s^{-1} and from 0.139 to 0.059 $sm^{-1/3}$ corresponding to the ranging of discharge from 5 to 2400 m^3s^{-1}, respectively. In addition, at the flooding discharge, the Manning's *n* coefficient of the bedrock-confined anabranching network type B remained relatively stable while it increased up to 0.8 m^3s^{-1} in the bedrock-confined anabranching network type A. Even though the Manning's *n* coefficient has been widely applied for many hydraulic studies, the Manning's *n* formula still contains well-known drawbacks: (i) it is dimensionally inhomogeneous (Chow, 1959); and, (ii) the exponent of the wetted perimeter is set to 2/3 despite the fact that from his analysis, the exponent could range from 0.6175 to 0.8395 (Laushey, 1989).

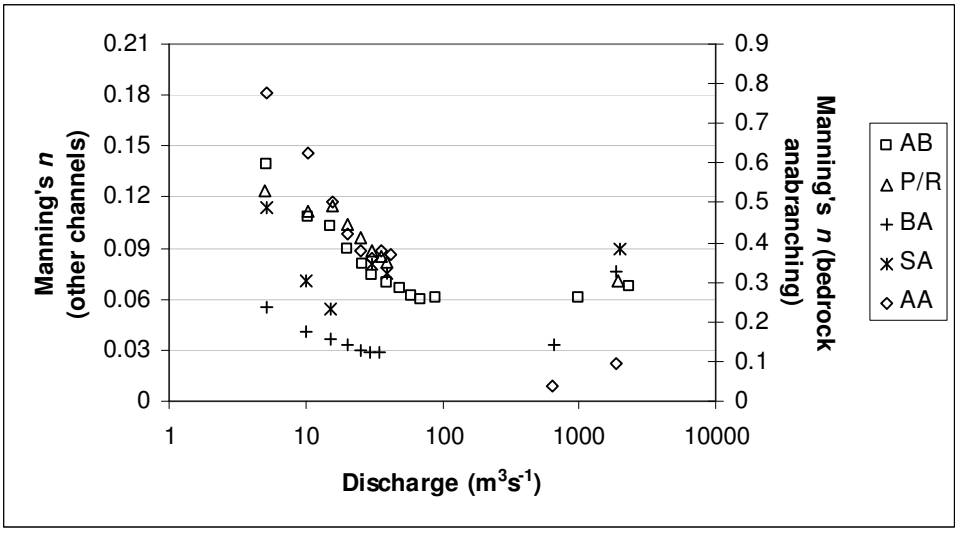

Figure 2.1-8 : Hydraulic roughness trend *vs.* discharges for different channel types (*after* Heritage *et al.*, 2004); AB – Bedrock-confined anabranching (type B) ; P/R – Pool/Riffle; BA – Braided (alluvial); SA – Single thread (alluvial); AA – Bedrock-confined anabranching (type A)

In short, the hydraulic roughness of a bedrock-confined network is widespread (from 0.02 to 0.80) and normally higher than that of the alluvial network. In addition, different hydraulic roughness trends according to the trend of discharge can be found differently in different river networks, which is mainly caused by the water surface slope trend.

d. Sediment transport along a bedrock-confined anabranching network

According to Knighton (1998), under the condition of very little or no opportunity to increase the channel gradient, the stream flow of an anabranching network can be concentrated in a number of well-defined channels, which causes the maximum transport of channel bed sediment. The anabranching network thus maximizes the sediment transporting capacity per available unit stream power (Jansen and Nanson, 2004). According to Niekerk *et al.* (1999), a bedrock anabranching network with a large channel bed slope has a greater ability for sediment transport than a mixed anabranching network with smaller channel bed slope. However, due to the high power system with maximized sediment transport capacity through a bedrock-confined anabranching network, most sediment supplied from upstream is flushed away only with localized deposition. In general, sediment transport capacity of bedrock-confined single channels exceeds the rate of sediment supplied to the channel over a long-term (Richardson and Carling, 2006; Turowski, 2008) and this sediment

transport relationship can also be found in bedrock-confined anabranching networks (Tooth and McCarthy, 2003).

2.1.3 Riparian hydraulic roughness along a bedrock-confined anabranching network

Channel vegetation, either perennially submerged or nonsubmerged, causes the hydraulic geometry exponents of single channels within a multi-channel network to differ significantly from one another (Harwood and Brown, 1993; Huang and Nanson, 1997). The flow conditions are complex where flow goes through riparian vegetation (Yagci and Kabdasli, 2008) and the hydraulic roughness of a riparian area affects the overall conveyance of a channel (Huthoff *et al.*, 2007). According to Thomas and Nisbet (2006), floodplain woodland causes a reduction in flow velocity within the floodplain, increasing the flooding level and creating a backwater effect.

The riparian vegetation causes a loss of energy and momentum of the flows and has a strong impact on the drag of flow, which appears to have a linear relationship with velocity due to deflection of the plant foliage area and reduction of the drag coefficient as the velocity increases (Fathi-Maghadam and Kouwen, 1997). According to Fathi-Maghadam and Kouwen (1997), the density of vegetation is a dominant parameter for the nonsubmerged condition. The surface area of the fronds significantly increases the momentum absorbing area of plants which, therefore, results in a decrease in the velocity of flow (Wilson and Horritt, 2002). The hydraulic roughness coefficient (Manning's n) increases as the density of riparian vegetation increases while it decreases when depth and velocity increase (Gradzinski *et al.*, 2003).

Millar (2000) concludes that bank vegetation exerts a significant and quantifiable control on alluvial channel patterns. The riparian vegetation on the in-channel alluvial islands within an anabranching network has a major role in inducing deposition and stabilizing sediments, which helps restrict extensive channel widening and lateral migration (Tooth and McCarthy, 2004). In addition, established vegetation is responsible for a range of effects (bank stabilizing by root system (Gradzinski *et al.*, 2003; Abernethy and Rutherfurd, 2001; Jansen and Nanson, 2004) and supplying coarse woody debris (Wallerstein and Thorne, 2004)) in channel-forming processes across a wide range of flows (Tabacchi *et al.*, 2000). In more detail, Tooth and Nanson (1999, 2000) explore the iterative processes between the formation and

maintenance of an alluvial anabranching network with the impact of a small indigenous shrub (the inland teatree (*Melaleuca glomerata*) with up to 3 m height) with a mix of sizes (in diameter) and age along the riparian area and within the river network; such that the land cover pattern has great influence on bankfull flow velocity, flow depth and sediment transport. Huang and Nanson (1997) find that dense trees (<6 m height) and shrubs (<3 m height) along the channel bank cause narrower channels while the in-channel vegetation (*e.g.* willows (*Salix* species) with <3 m height and other smaller trees <6 m height) causes high hydraulic roughness of the channel bed, reduces and deflects the flow velocity resulting in channel widening but has no significant influence on the channel depth. They conclude that "the possible range of variation in channel width caused by bank vegetation is less than that caused by channel bed vegetation". According to Mason *et al.* (2003), the raising of floodplain vegetation from 0.1 m to 2.0 m high and removal of hedgerows has relatively little impact on the flooding extent. In general, it seems that the hydraulic roughness of the riparian area is strongly affected by the diameter of the tree stem and the density of stems. However, shrubs and grass have little impact on the hydraulic roughness, no matter how high the shrub and grass.

According to Tooth and Nanson (2000), the impact of the land cover pattern on the development of multi-channel networks is still questioned and needs further investigation. Even though the hydraulic roughness values of different generalized land cover types can be found in different sources (*e.g.* Marsik and Waylen, 2006, Arcement and Schneider, 1989), and guidelines for choosing the proper values of the riparian hydraulic roughness are mainly available to estimate sufficiently the hydraulic roughness of the land cover of floodplains in Europe or North America, they may not be directly applied to the rest of the world and need to be adjusted according to each individual study.

To estimate the hydraulic roughness of the floodplain, apart from the base values of n_b (Table 2.1-4), an approach introduced by Arcement and Schneider (2008) includes the floodplain conditions (degree of irregularity) (Table 2.1-5), effects of obstructions (Table 2.1-6) and amount of vegetation (Table 2.1-7) in the calculation. In fact, there are many dimensions contributing to the estimation of the hydraulic roughness; therefore, it is impossible to make a single integrated table which can briefly describe

all the natures of the floodplain and the relevant Manning's n values. The final Manning's n of the floodplain at each cross-section was calculated as follows:

$$n = n_b + n_1 + n_2 + n_3 \qquad \textbf{Equation 2.1-1}$$

where,

n: Integrated Manning's n coefficient

n_b: Base value of Manning's n

n_1, n_2 and n_3: Effects of degree of irregularity, obstruction and amount of vegetation

Table 2.1-4: Base value of Manning's n_b (Arcement and Schneider, 1989)

Floodplain conditions	Median size of bed material (mm)	'n_b' value Description
Firm soil	No data	0.025 – 0.032
Coarse sand	1 – 2	0.026 – 0.035
Gravel	2 – 64	0.028 – 0.035
Cobble	64 – 256	0.030 – 0.050
Boulder	>256	0.040 – 0.070

Table 2.1-5: Degree of irregularity n_1 (Arcement and Schneider, 1989)

Floodplain conditions	'n_1' value	Description
Smooth	0.000	Compares to the smoothest, flattest floodplain attainable in a given bed material
Minor	0.001 – 0.005	Slightly irregular in shape; a few rises and dips or sloughs may be visible on the floodplain
Moderate	0.006 – 0.010	More rises and dips; sloughs and hummock may occur
Severe	0.010 – 0.020	Irregular shape; may rises and dips or slough are visible

Table 2.1-6: Effect of obstruction n_2 (Arcement and Schneider, 1989)

Floodplain conditions	'n_2' value	Description
Negligible	0.000 – 0.004	Few scattered obstructions including debris deposits, stumps, exposed roots, logs, piers, or isolated boulders which occupy less than 5 % of the cross-sectional area
Minor	0.004 – 0.005	Obstructions occupy less than 15 % of the cross-sectional area
Appreciable	0.020 – 0.030	Obstructions occupy from 15 % to 50 % of the cross-sectional area

Table 2.1-7: Amount of vegetation n_3 (Arcement and Schneider, 1989)

Floodplain conditions	'n_3' value	Description
Small	0.001 – 0.010	Dense growth of flexible turf grass or weeds growing where the average depth of flow is at least two times the height of the vegetation; supple trees growing where the average depth of flow is at least three times of the height of the vegetation
Medium	0.010 – 0.025	Turf grass growing where the average depth of flow is from one to two times the height of the vegetation; moderately dense stemy grass, weeds, or tree growing where the average depth of flow is from two to three times the height of the vegetation; brushy, moderately dense vegetation, similar to 1-to-2-year-old willow trees in the dormant season
Large	0.025 – 0.050	Turf grass growing where the average depth of flow is about equal to the height of the vegetation; trees inter-grow with some weeds and brush (none of the vegetation in foliage) where the hydraulic radius exceeds 0.607 m; or mature row crops such as small vegetables, or mature field crops where depth flow is at least twice the height of the vegetation
Very large	0.050 – 0.100	Turf grass growing where the average depth of flow is less than half the height of the vegetation; or moderate to dense brush, or heavy stand of timber with few down trees and little undergrowth where depth of flow is below branches, or mature field crops where depth of flow is less than the height of the vegetation.
Extreme	0.100 – 0.200	Dense bushy willow, mesquite and all vegetation in full foliage or heavy stand of timber, few down trees, depth of reaching branches

A more detailed description of the vegetation hydraulic roughness along the floodplain is summarised in Table 2.1-8. Such reference is just a qualitative description of the density of land cover; hydraulic modellers need to give their own adjustments on the study area to make the modelled results reflect the observed and measured data.

Table 2.1-8: Referenced hydraulic roughness (n_3) of different land cover types (Cowan, 1956)

Manning's n_3	Description
0.03	Short grass with water depth much smaller than grass height
0.04	Short grass with water depth much smaller than grass height on a slightly irregular earth surface. Trees at 10.0 m spacing, area is easy to mow
0.05	Long grass on an irregular (bumpy) surface with few trees. Irregular ground could make grass cutting Alternatively, trees at 8.0 m spacing on an even, well-grassed surface, no shrubs, no low branches
0.06	Long grass, trees at 6.0 m spacing, few shrubs. The vegetation is easy to walk through. Area not mowed, but regular maintenance is required to remove weeds and debris
0.07	Trees at 5.0 m spacing, no low branches, few shrubs, walking may be difficult in some areas
0.08	Trees at 4.0 m spacing, low branches, few shrubs, few restriction to walking
0.09	Trees at 3.0 m spacing, weeds and long grasses may exist in some locations. Walking becomes difficult due to fallen branches and woody debris
0.10	Trees at 2.0 m spacing, low branches, regular shrubs, no vines. Canopy cover possibly shades weeds and difficult to walk through
0.12	Trees at 1.5 m spacing with some low branches, a few shrubs. Slow to walk through
0.15	Trees and shrubs at 1.0 m spacing, some vines, low branches, fallen trees, difficult and slow to walk through Alternatively, a continuous coverage of woody weeds with sparse leaves and no vines
0.20	Trees and shrubs at 1.0 m spacing plus thick vine cover at flood level and fallen trees. Very difficult to walk through Alternatively, a continuous coverage of healthy shrubs and woody weeds from ground level to above flood level

2.2 Modelling complex multi-channel networks

A physical-based one-dimensional (1D), 2D or 3D hydraulic model uses complex hydraulic theories and sediment transport relationships to estimate the effects of the input parameters on a node or cross-section and then, leading to the consequent effects at the calculating object immediate upstream (sub-critical calculation) or downstream (super-critical calculation). Such models are traditionally used in engineering applications and have been applied intensively to model the wetted section along different channel networks. However, most of the modelling applications are mainly to explore the hydraulic nature (flow velocity, sediment transport and bed level changes) and inundation patterns of a single channel or a simple ⅄-shaped bifurcation (Coulthard, 2006; Parsons *et al.*, 2007).

A 1D hydraulic model considers the flow structure in the downstream direction alone. The structure of flow in the transverse direction is neglected and the mean velocity across the section is taken into account. Such a model is considered physical-based due to the established physical principles, laws and well-attested assumptions that provide the foundation for wide-spread application in hydraulic science. There are

many 1D hydraulic models (*e.g.* CCHE1D, HEC-RAS and Mike 11) and the majority assume vertically homogeneous flow conditions and apply the 1D St. Venant Shallow Water Equations for dynamic and diffusive wave and kinematic routing modelling (Pappenberger *et al.*, 2005). Such models can be applied to a multi-channel network with a single outlet section. In this study, HEC-RAS, a widely-applied hydrodynamic model allowing multiple outlet sections from a channel network, is used to study the hydraulic nature of the Siphandone river network.

HEC-RAS has been used widely to model flows in single, uniform and non-uniform channels (irrigation channels, canals, natural single-thread channels) (Table 2.2-1) and it has the ability to model complex multi-channel networks (Brunner, 2006); there are few published examples of the application of HEC-RAS for a multi-channel network so far. In general, HEC-RAS requires minimum data input (compared to 2D or 3D hydraulic models) but can be used to estimate the variation in water level along a long profile and the extent of overbank flooding (Horritt and Bates, 2002; Machado and Ahmad, 2007). However, like other hydrodynamic models, HEC-RAS also contains certain levels of uncertainty, which are examined by Pappenberger *et al.* (2005) wherein meandering channels are used as case studies to test uncertainty in the calibration of the effective hydraulic roughness coefficient. Apart from the uncertain bathymetry, the HEC-RAS mode is also uncertain due to the applied hydraulic roughness and the boundary conditions. Kasper *et al.* (2005) conclude that HEC-RAS is applicable to explore a channel with different patterns of depth-average variation in velocity across a cross-section.

Table 2.2-1: Examples of the HEC-RAS application

Author(s)	Types of channel network	Main issues of concern
Shahrokhnia and Javan (2007)	Irrigation network characterized by trapezoidal and concreted canals	Influence of the hydraulic roughness changes on the off-take discharge
Roberts *et al.* (2007)	A section of the Ottawa river with a cement weir and small sluice gates installed near the bottom	Forecasting changes in the flood regime and sediment transport before and after dam removal
Mosquera-Machado and Ahmad (2007)	A large meandering river with high velocity and alluvial river bed	Flood hazard forecasting
Thompson *et al.* (2007)	Mountainous channel including pool-riffle, plane-bed, and step-pool	Sediment mobility
Remo and Pinter (2007)	Meandering river	Developing a 1D steady flow "retro-model"
Shahrokhnia and Javan (2005)	Irrigation network characterized by trapezoidal and concreted canals	The operation of the gate The offtakes discharge changes
Pappenberger (2005)	River Morava (Czech Republic) and River Severn (the UK) –meandering rivers	Uncertainty in the calibration of effective hydraulic roughness coefficient

The advantages and disadvantages of a 1D hydraulic model

A 1D hydraulic model has been applied widely for several decades in hydraulic calculation (Merwade *et al.*, 2008) because it requires minimum input data and computer power compared to any 2D or 3D hydraulic model (Pappenberger *et al.*, 2005). This model type can be used for hydrodynamic, bedload and morphodynamic modelling (Formann *et al.,* 2007) and is appropriate to simulate long-term and long-reach channels (Cao and Carling, 2002a). Formann *et al.* (2007) present an integrated approach in which a 1D hydraulic model is applied for estimating mean channel bed aggradation or degradation and flood protection while a 2D hydraulic model is used to study hydraulic changes within the channel network (transverse flow velocity, shear stress and discharge at bifurcations).

However, 1D hydraulic modelling usually has not well reflected flow complexity due to modelled mean hydraulic parameters across a cross-section (Brion and Lane, 2008). Differences in water surface elevation across a cross-section, especially at a meandering bend, cannot be calculated in a 1D hydraulic model but must be considered using a 2D hydraulic model (Nelson *et al.*, 2003). Due to the simplicity of 1D hydraulic models, such models have inherent limitations (Merwade *et al.*, 2008). In 1D hydraulic models, the detailed river bathymetry is not required. Therefore, by default there has to be an effect (*i.e.* simplification on the modelled hydraulic results and consequences for interpretation of river processes). In addition, 1D hydraulic models cannot simulate the detailed interaction of different contiguous water bodies such as main channel and floodplain flow cells during river flooding. Finally, the 1D hydraulic model can only model the mean hydraulic parameters at each cross-section along river networks and therefore lacks the spatial distribution of hydraulic parameters across sections and between sections. However, with these limitations in mind, the key large-scale bulk flow effects of constraining flow within bedrock reaches can be explored using a 1D model.

Horritt and Bates (2002) discovered that both 1D and 2D models perform equally well for flood modelling of a meandering channel even though different models respond differently according to changes of hydraulic roughness coefficient. Even though Cao and Carling (2002a) note the drawbacks of both 1D and 2D hydraulic models (*e.g.* simplified continuity equation for water-sediment mixture, simplified continuity equation for global sediment), it can be seen that the conclusions are given according

to specific conditions of an alluvial but not bedrock channel. In addition, both 2D and 3D hydraulic models require detailed, quantitative input data, which can be difficult to obtain especially in a developing country and, therefore, such models are less popular (Downs and Thorne, 2003) compared to 1D hydraulic models. In short, according to Nelson *et al.* (2003), a 1D hydraulic model is useful especially in the case that a 1D hydraulic model can be used to answer sufficiently the considered research questions or if the input data are not fully available.

Numerical modelling for a river network with both confluences and bifurcations is still challenging according to the hydraulic complexity, including: (i) the planform geometry of the confluence and bifurcation; (ii) the ratio of discharge or momentum between the confluent and bifurcating channels; (iii) the presence and nature of any height discordance between the levels of the two channel beds; and, (iv) differences in density of discharge from the two flows (Best and Rhoads, 2008).

2.3 Modelling accuracy and acceptability

2.3.1 Calibration and validation of a hydraulic model

Calibration and validation processes need to be done to assess hydraulic model results. In general, to calibrate a model is to adjust the empirical parameters until the results obtained from the hydraulic model meet the measurements while to validate a model is to re-run the calibrated model successfully with a separate dataset (Cao and Carling, 2002b).

Calibration

Calibration is a critical step in the modelling process (Vidal *et al.*, 2007) and acccording to Aronica *et al.* (1998), to calibrate the unknown values of the model parameters is to find those as close as possible to the observed data. Calibration is defined as 'the estimation and adjustment of model parameters and constants to improve the agreement between model output and a dataset' (Rykiel, 1996). The calibration can be done based on changes of the applied parameters, which are considered to consist of two groups (Melching, 1995): (i) parameters which can be measured directly (*e.g.* cross-sectional area); and, (ii) parameters which can hardly be (if not impossible) measured directly but which can be derived or estimated (*e.g.* hydraulic roughness, expansion and contraction coefficients of energy loss). Usually,

in numerical modelling, parameters in group (ii) can be adjusted to optimize the model while parameters in group (i) can be used to validate the outcomes of model.

In hydraulic models, the hydraulic roughness is not only an important boundary condition but also bulk flow parameters are highly sensitive to the hydraulic roughness value (Vidal *et al.*, 2007, Wilson and Atkinson, 2007). According to Schumann *et al.* (2007), the majority of 1D hydraulic modelling projects assign only one value of the hydraulic roughness coefficient for the whole channel length; therefore, in some part of a channel, the wetted area is well matched with calibration data (*e.g.* satellite images) while in other parts, it is under- or over-estimated. In fact, the spatially distributed hydraulic roughness coefficient has a strong impact on the hydraulic modelling results (Wilson and Atkinson, 2007). In a bedrock-confined river network, the assumption of one hydraulic roughness value for one reach is not sufficient due to sudden changes of the channel geometry which may lead to abrupt changes of the hydraulic roughness value of one cross-section to the neighbours. Remote sensing images have been used to estimate the land cover pattern which leads to the spatially-distributed hydraulic roughness coefficient along the riparian area (Wilson and Atkinson, 2007). In fact, the assigned hydraulic roughness along the riparian area is one of the key elements of hydraulic modelling of channel flow during a period of overbank discharge (Straatsma and Baptist, 2008) and is an important factor for calibration and validation of hydraulic models (Fathi-Maghadam and Kouwen, 1997). In addition, satellite images are used to provide information on flood extend (Montanari *et al.*, 2009) and also used to estimate a hydraulic roughness value within a channel (Schumann *et al.*, 2007). However, such images have not been used to calibrate the in-channel hydraulic roughness coefficient at each individual cross-section, especially along a bedrock-confined multi-channel network. Moreover, the land-surface and riverbed elevation information also have significant contribution to the accuracy of the hydraulic model and could be achieved by field measurement (cross-section measurement (Ferguson *et al.*, 2003) and echo sounder (Lane *et al.*, 2008; Parsons *et al.*, 2005)) or extracted from satellite images (Lejot *et al.*, 2007; Mandlburger *et al.*, 2009).

Often the hydraulic roughness coefficient is section-by-section or globally adjusted such that the modelled flow parameters match well calibration data for a real channel (Verhaar *et al.*, 2008). The calibration process is done mainly using values selected

according to the experience of the user, which is time-intensive but still may not provide proper results. Alternatively, an automatic approach can be taken to calibrate the hydraulic models (Visser *et al.*, 2001) by applying the simplex algorithm to minimize the differences between the wetted area achieved from a hydraulic model and the observed data according to the change of hydraulic roughness (Manning's *n* or Darcy-Weisbach *f*).

Ramesh *et al.* (2000) develop a 1D hydraulic model based on 1D shallow water flow equations in combination with a non-linear optimization algorithm to estimate the hydraulic roughness in a multi-channel network with one confluence. It is a flume study where the channel is considered to be homogeneous and, therefore, one hydraulic roughness value can be applied for different cross-sections along the channel. The objective function of the optimization algorithm is to minimize the differences between the simulated discharge (or depth) and real data. The obtained results are the hydraulic roughness of each channel within the river network.

However, the optimisation algorithm has several drawbacks: (i) if more than one possible value meets the objective function, the results given by the OpA may not be correct (Visser *et al.*, 2001); and, (ii) the starting values of the changeable parameters also contribute to the value of the outcome of the objective function.

In HEC-RAS, apart from hydraulic roughness, other parameters (expansion and contraction coefficients, geometry) also have an impact on the result (the flooding pattern). However, Carling and Wood (1994) and Kidson *et al.* (2006) conclude that the expansion and contraction coefficients have little impact on the result and reasonable values may be selected. In addition, it is risky to adjust the geometry of the channel if there is no strong evidence from ground data. Therefore, the three variables are often kept stable during the modelling processes.

Validation

Validation has been defined as to demonstrate that a numerical model within its domain of applicability possesses a satisfactory range of accuracy consistent with the intended application of the model (Sargent, 2005) and the most common method of validation is to compare the measured results with the results obtained from modelling (after calibration) (Oreskes *et al.*, 1994). Traditionally, validation is a process whereby a calibrated model is used in similar circumstances (*e.g.* a range of

discharges different to those for which it was calibrated) for which it was not calibrated. If the model performs well against control data, it is considered validated. Apart from the traditional approach, validation can also be done according to a process of evaluating hydraulic results based on fieldwork data (Rathburn and Wohl, 2003), available database (maps; Chung and Fabbri, 2008; satellite images; Horritt, 2006) (a matching procedure whereby the outputs of the model should match well with control data). Such a validation process is important to confirm if the applied model is working properly.

In general, validation has often been accomplished on the basis of one data set which is then divided into two subsets; one for the calibration purpose and another for the validation purpose. The disadvantage with this approach is that not all available data are available for performing calibration and validation separately (Wilson and Atkinson, 2007). It is the case of doing calibration and validation of the inundation extent according to satellite images; each cross-section has its own hydraulic nature (*e.g.* the hydraulic roughness, cross-sectional shape) and the calibration process must be done for the whole set of cross-sections, not leaving half for validation.

2.3.2 Sensitivity and uncertainty analysis of a hydraulic model

In general, sensitivity analysis is undertaken to examine if the applied hydraulic model is sensitive to any applied parameters and/or variables within the studied system while uncertainty analysis is undertaken to examine the uncertainty levels of the obtained results according to the uncertainty of the input parameters. Both analyses are important to make sure that the obtained results are completely checked and understandable.

Sensitivity analysis

According to Thomas and Nicholas (2002), two type of sensitivity analysis can be distinguished: (i) sensitivity of the applied model according to the change of applied parameters; and (ii) sensitivity of the studied object according to the change of applied input. The first type of sensitivity analysis is done to examine the consistency of the changing trend of the obtained results according to variations in the applied parameters. This procedure is needed to examine if the system under study is stable according to the change of input parameters, which helps to understand the behaviour of the study object and projected behaviour of the system according to changes of

input parameters. The second type of sensitivity analysis is especially useful in hydraulic modelling of future scenarios where parameters may change in either known or unknown ways; for example, due to channel regulation or climate change.

Uncertainty analysis

Uncertainty analysis in hydraulic modelling is undertaken to quantify the modelling uncertainties and their impact, for example, on the flooding extent (Hall *et al.*, 2005). According to van Gelder (2000), uncertainty can be divided into two groups: (i) a basic lack of knowledge, or epistemic uncertainty (*e.g.* bathymetry of channel cannot be thoroughly achieved); (ii) variability of samples from the population, or inherent uncertainty (randomness) (*e.g.* location of designed cross sections), which results in an inherent non-uniqueness of optimal parameter sets in calibration; and, (iii) the complexity of the processes (*e.g.* the change of hydraulic roughness trend according to discharge at a cross section, 3D movement of water).

It is increasingly evident in hydraulics that quantifying uncertainty provides deeper knowledge on the complex system behaviour. Peppenberger *et al.* (2005) classified uncertainties in flooding inundation into five sources of uncertainty: (i) Structure – the assumptions made to simplify reality; (ii) Numerical scheme – the applied set of hydraulic equations (*e.g.* in HEC-RAS, St. Venant equations were used); (iii) Topography; (iv) Input/Output – the application of rating curves or the output of another model; and, (v) Parameters – mainly, hydraulic roughness.

Chapter 3: Study area

Introduction

The first section of Chapter 3 summarizes the available literature on the physical setting, mainly focusing on the geomorphological, hydrological and hydraulic characteristics of the Lower Mekong Basin (LMB). The second section mainly focuses on describing the hydraulic and sediment transport characteristics at the Pakse gauging station; a brief introduction of the hydrological features at the Pakse town is also presented. The third section describes in detail the geological and geomorphological features, hydrological and hydraulic characteristics and recent land cover pattern in the Siphandone wetlands. Finally, the projecting impacts of global climate change and hydropower-dams on the LMB, in general, and the Siphandone wetlands, in specific, are considered.

3.1 The Lower Mekong Basin

The Mekong River, draining a pan-shaped basin (795,000 km^2) from Tibet to the South China Sea (Gupta *et al.*, 2007) (Figure 3.1-1), is divided into two parts (Kummu, 2007): (i) the Upper Mekong Basin (UMB) including the highlands of eastern Tibet, China; and, (ii) the Lower Mekong Basin (LMB) including Myanmar, Laos, Thailand, Cambodia and Vietnam. Table 3.1-1 illustrates the territory and percentage of discharge of the six countries within the Mekong catchments; the LMB constitutes about 79 % of the total catchment area and approximately 84 % of the total annual discharge.

Table 3.1-1: Territory and discharge percentage of the six Mekong River Basin countries (*after* MRC, 2005)

Items	China	Myanmar	Laos	Thailand	Cambodia	Vietnam	Total
Area (x 10^3 km^2)	165	24	202	184	155	65	795
Catchments (%)	21	3	25	23	20	8	100
Discharge (%)	16	2	35	18	18	11	100

In the LMB, the Mekong runs through eight different geomorphological units (Figure 3.1-1) (Gupta and Liew, 2007), including: (1) the upper rock-cut section (from the China border (approximately 2,400 m +MSL) to about 5 km upstream of Vientiane, Laos (approximately 700 m +MSL)); (2) the alluvial channel section (from Vientiane to Savanakhet, Laos (approximately 470 m +MSL)); (3) the lower rock-cut channel

section (from Savanakhet to Khong Chiam, Laos (approximately 330 m +MSL)); (4) the composite section including bedrock and alluvial banks (from Khong Chiam to Siphandone, Laos (approximately 240 m +MSL)); (5) the anabranching river network over a mixed bedrock and alluvial channel bed (from Siphandone, Laos to Sambor, Cambodia (approximately 150 m +MSL)); (6) the structure-influenced alluvial channel (from Sambor to Khum Angkor Ban, Cambodia (approximately 130 m +MSL)); (7) the alluvial channel (from Khum Angkor Ban to Phnom Penh, Cambodia (approximately 110 m +MSL)); and, (8) the delta (from Phnom Penh, Cambodia to the Mekong Delta, Vietnam (approximately at similar elevation of the MSL) before draining to the South China Sea).

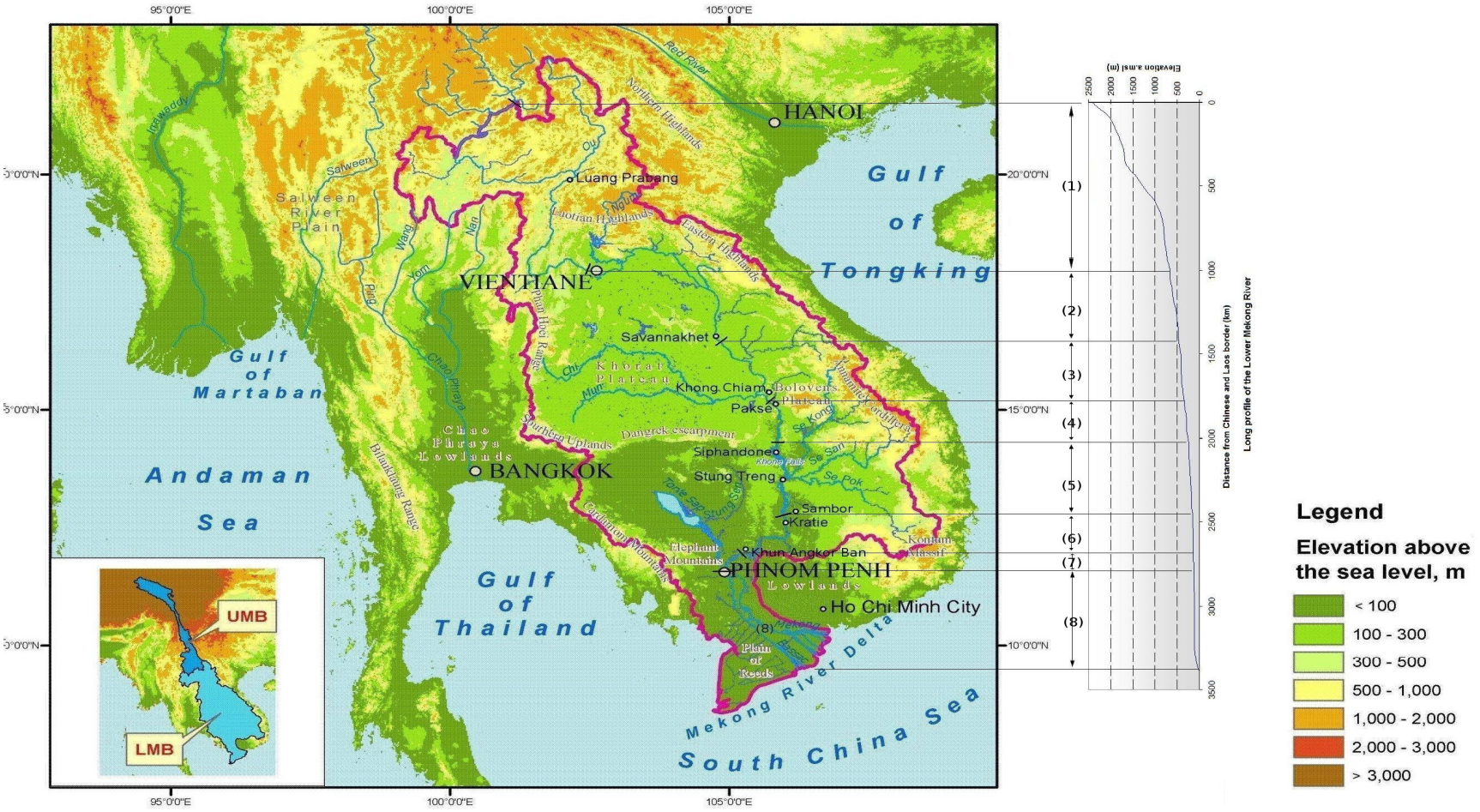

Figure 3.1-1: Geomorphological units along the LMB (*after* Gupta *et al.*, 2002; Gupta and Liew, 2007); UMB and LMB: Upper and Lower Mekong Basin, respectively

The climate of the LMB varies from cool temperate to tropical weather patterns. The average annual precipitation is about 1,680 mm across the basin (Jacobs, 1996) and about 90 % of the annual rainfall falls between June and October (Walling, 2008). However, the annual rainfall changes noticeably from the western region (Khorat Plateau) to the highlands of the northern and eastern basin (approximately from 1,000 to 2,000 and 4,000+ mm, respectively). The south-western monsoon contributes more than 85 % of the annual rainfall in the area. The annual and monthly rainfall distributions for six representative stations (Chiang Rai, Pakse, Khon Kaen, Pleiku, Phnom Penh and Chau Doc) within the subareas (Northern Region, Central Region, Khorat Plateau, Central Highlands, Cambodian Floodplain and Vietnamese Delta; Figure 3.1-1) of the LMB are shown in Figure 3.1-2 and Figure 3.1-3, respectively. Among the six subareas, the northern area of the LMB, the Central region and the Central Highlands receive high annual rainfall ranging from 1,728 to 2,192 mm while the rest is drier with low annual rainfall ranging from 1,203 to 1,321 mm.

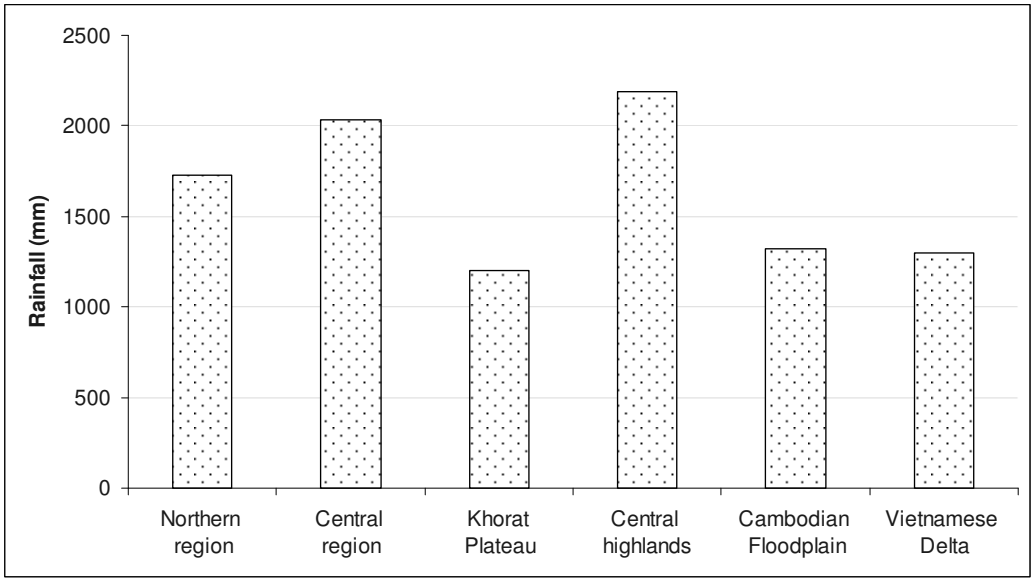

Figure 3.1-2: Annual rainfall in subareas within the LMB

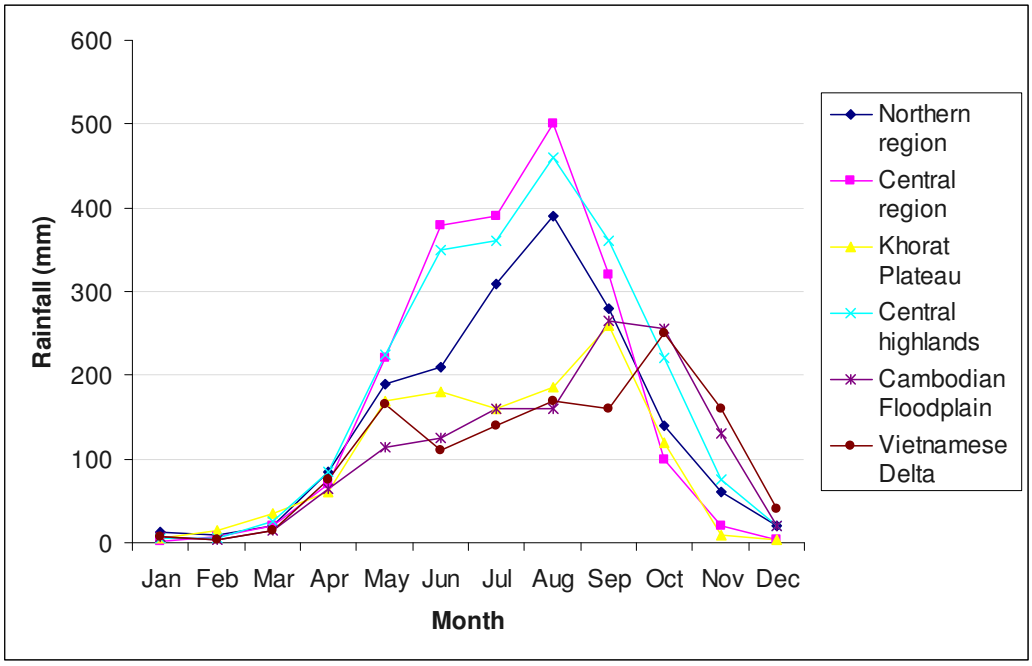

Figure 3.1-3: Monthly rainfall in subareas within the LMB

The mean annual discharge of the Mekong is about 15,000 m^3s^{-1}. Gupta and Liew (2007) give a general description of the hydraulic characteristics (channel slope, section length, channel width, low flow depth and seasonal stage change) of each geomorphological unit (described above) (Table 3.1-2). It can be seen that along the LMR, the river is significantly diverse in terms of the hydraulic characteristics.

Table 3.1-2: Characteristics of the river units within the LMB (*after* Gupta *et al.*, 2007)

Unit	Channel material	Mean slope (x 10^{-4})	Length (km)	Width (m) (x 10^3)	Low flow depth (m)	Seasonal stage change (m)
1	Rock	3	910	0.2 – 2	<5 – ~ 10	10 – 20
2	Alluvium	0.6 – 1	4100	≤ 2	≤ 5	12 – 14
3	Rock	2	200	0.4 – 2	Variable (*)	≥ 20
4	Composite	0.6	150	0.75 – 5	Variable (*)	~ 15
5	Alluvium and rock	5	200	≤ 15	8	9
6	Alluvium	0.5	225	3	~ 5	14 – 18
7	Alluvium	0.05	50	-	-	-
8	Alluvium	0.05	330	-	-	-

Note: *Variable (*)* indicates difficulty in averaging, due to many scour holes.

According to Gupta and Liew (2007), along the Mekong, there are many seasonal small tributaries with peak discharges occurring in the wet season (from May to October/November). In fact, a large portion of discharge arriving in the Mekong is from main tributaries, including: (i) Nam Ou, about 30 km upstream of Luang

Prabang; (ii) Nam Ngum below Vientiane; and, (iii) Nam Mun and Nam Chi upstream of Pakse and Se Kong, Se San and Se Pok downstream of Pakse. Figure 3.1-4 illustrates daily discharges of the Mekong at the UMB and at the confluence after the main tributaries (Num Ngum, Nam Mun and Nam Chi, Se Kong, Se San and Se Pok).

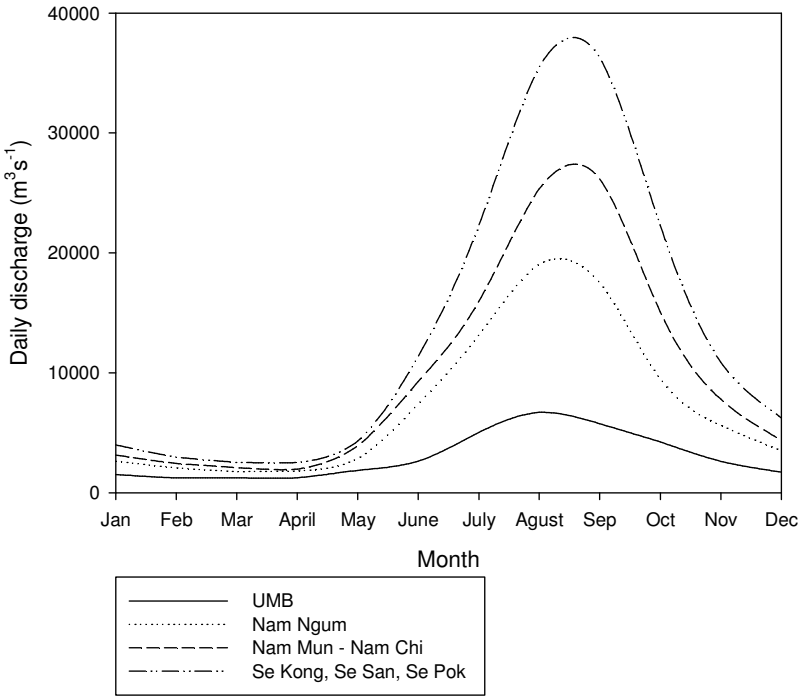

Figure 3.1-4: Discharges at selected sites in the Mekong mainstream with contribution from major tributaries (*after* MRC, 2005)

Annually, there is one flood pulse in the Mekong (Figure 3.1-4). During the wet season, the discharge is about 30 times greater than in the dry season in Pakse (Figure 3.1-1) and about 53 times in Kratie (Figure 3.1-1). In fact, more than 80 % of the annual discharge takes place from June to November and the peak flooding period, September, conveys about 20 % – 30 % of the annual discharge (Zalinge, 2003; Gupta *et al.*, 2007).

The mean annual suspended sediment load of the Mekong (discharged to the delta), which remains constant over a long history (about the last 3,000 yrs) (Ta *et al.*, 2002) due to the 'buffer' capacity (*i.e.* the ability of the buffer to resist changes in the annual sediment load), is about 160 $Mtyr^{-1}$ and the LMB contributes about 50 % of this sediment load (Walling, 2008). Metivier *et al.* (1999) also confirmed that the average discharge along the Mekong River remain constant throughout the Quaternary period. According to Gupta *et al.* (2002) a large proportion of the in-channel sediment is

delivered from its tributaries. In addition, most of the sediment in the Mekong, upstream of Cambodia, is stored inside the channel; little sediment exchange occurs between the channel and floodplain (Gupta and Liew, 2007). Owing to the sequence of land clearance, erosion and sediment transfer, more sediment will be transferred from the land surface to the river (Gupta *et al.*, 2002), but main stem dams may reduce down-system flux.

3.2 The Pakse gauging station

Along the Mekong, there are twenty-three main gauging stations where channel discharge has been collected daily. However, there are none near both the entrance and exit of the Siphandone wetlands (the study area); the nearest upstream station is at Pakse (located about 100 km north of Siphandone) (Figure 3.2-1) (MRC, 2005). However, along the Mekong from Pakse to Siphandone, there is no main tributary contributing discharge to the main channel. Therefore, the discharge recorded at Pakse was used as the entry discharge in the Siphandone wetlands for the hydraulic modelling (Chapter 6 and 7).

The Pakse gauging station is located at 15.12 N latitude and 105.80 E longitude (Kite, 2000) and the gauge zero datum above mean sea level is 86.490 m (Manusthiparom *et al.*, 2005). The cross-section of the Mekong at the Pakse gauging station is presented in Figure 3.2-2. Since 1960, the recorded stages at the Pakse gauging station are about 4.2 m, 8.3 m, 11.0 m and 12.0 m at the minimum historical level, average annual level, alarm level (critical stage) and flooding level (overbank stage), respectively.

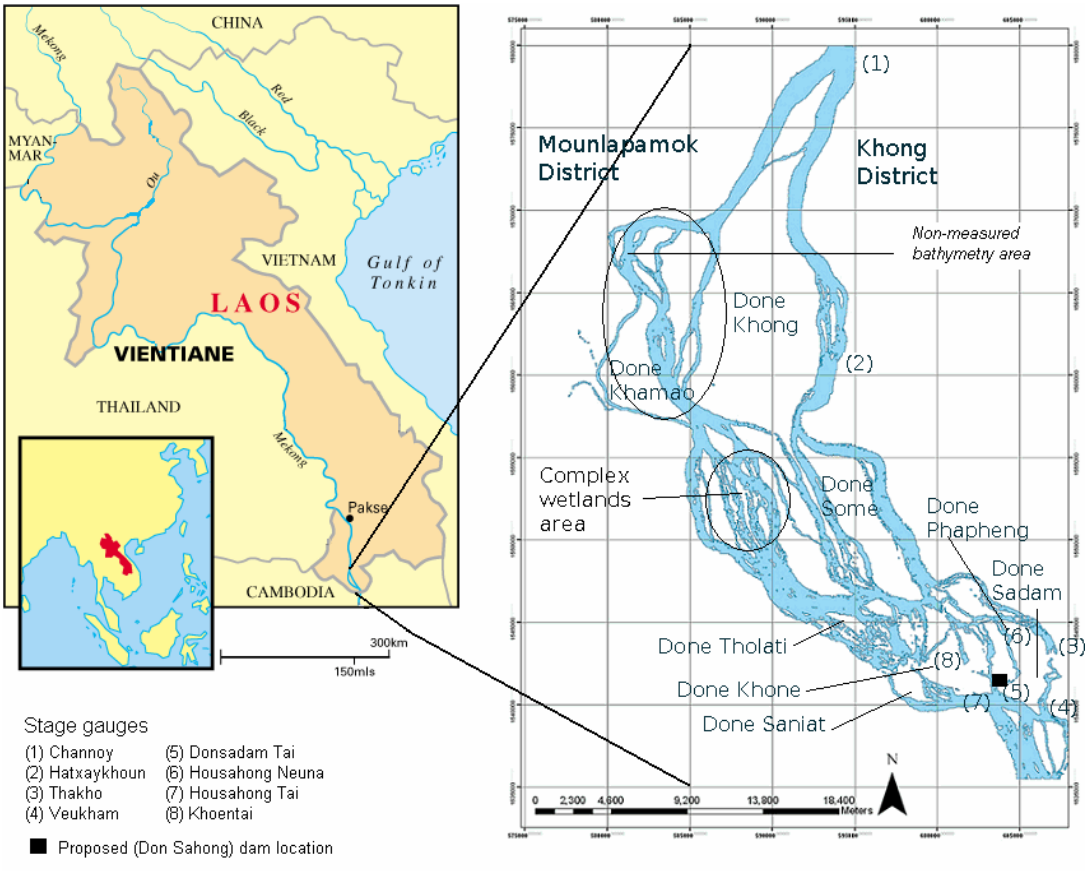

Figure 3.2-1: The Pakse gauging station and the Siphandone wetlands and locations of the stage gauges

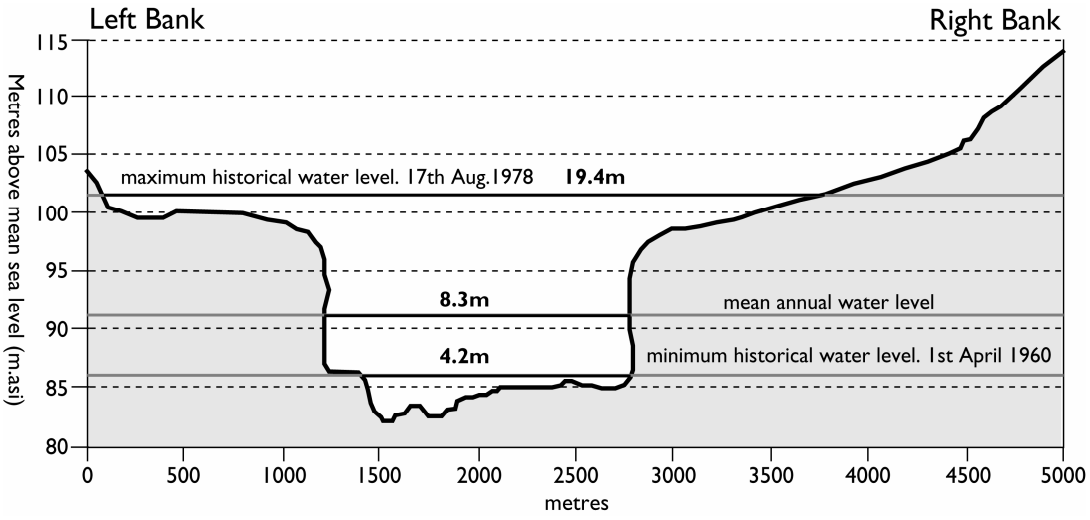

Figure 3.2-2: Cross-section at the Pakse gauging station

The Pakse gauging station is located in a section of bedrock channel bed with high steep alluvial banks (Gupta and Liew, 2007). The average water surface slope at bankfull discharge is about 6 x 10^{-5} mm^{-1} (Gupta and Liew, 2007) and at the lowest discharge is about 9.32 x 10^{-5} mm^{-1} (Conlan, 2008). The width/depth ratio at the

bankfull discharge at the Pakse gauging station is about 54.5. The historically reasonably stable rating curves demonstrating the stability of the rated cross-section are presented as Equation 3.2-1 and Equation 3.2-2 (MRC, 2006):

$$H = (Q / 454.7)^{-1.012} \qquad \textbf{Equation 3.2-1}$$

or

$$Q = 454.7(H + 1.6)^{1.7} \qquad \textbf{Equation 3.2-2}$$

where:

H: Channel stage (m)

Q: Discharge (m^3s^{-1})

The average discharge of the maximum flood flow, average flow and minimum at Pakse were about 37,700, 9,900 and 1,600 m^3s^{-1}. Figure 3.2-3 presents the maximum, average and minimum annual discharge from 1960 to 2005 (MRC, 2005) at the Pakse gauging station. The annual maximum flooding discharge ranges from 24,600 m^3s^{-1} to 56,000 m^3s^{-1}, the annual average discharge ranges from 6,800 m^3s^{-1} to 12,700 m^3s^{-1} and the annual average minimum discharge ranges from 1,060 m^3s^{-1} to 2,220 m^3s^{-1}. The annual hydrograph in the year 2000 is presented (Figure 3.2-4 and Figure 3.2-5) as an example showing daily discharge at the Pakse gauging station and the trend of discharge over a single year and presents the flow duration curve in the year 2000.

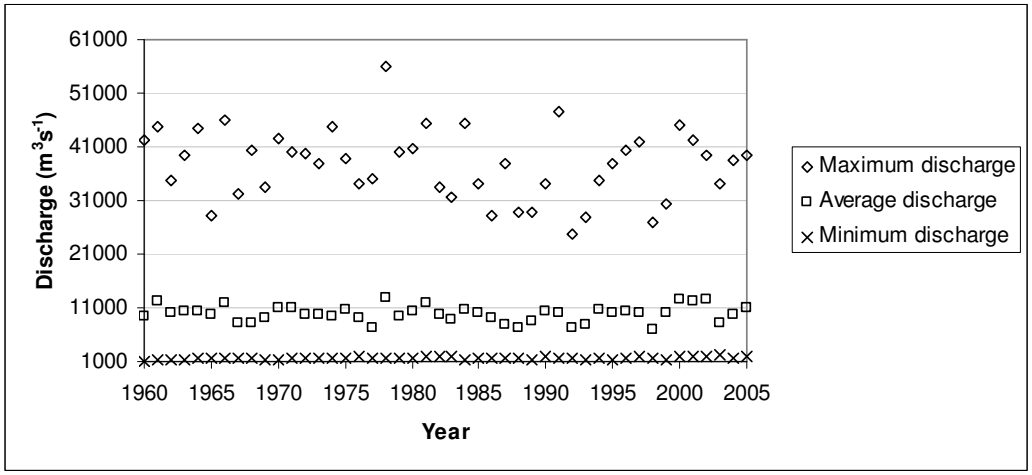

Figure 3.2-3: Annual maximum and average discharge at Pakse from 1960 to 2005

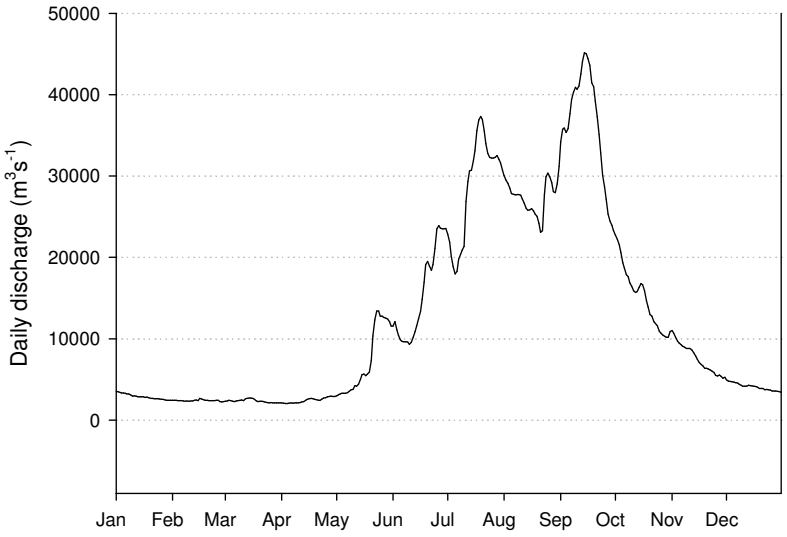

Figure 3.2-4: Hydrograph at the Pakse gauging station in 2000

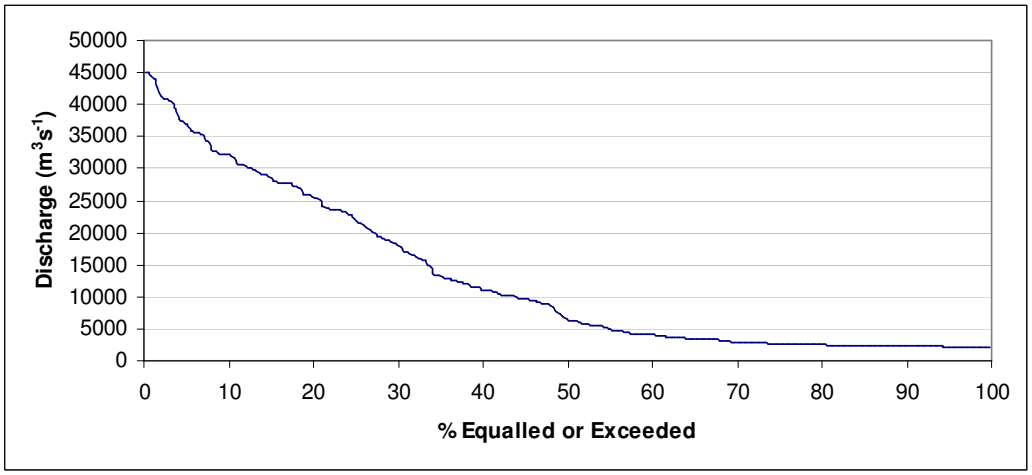

Figure 3.2-5: Flow duration curve at Pakse in 2000

The mean monthly discharge (from 1960 to 2005) is presented in Figure 3.2-6. In general, the lowest discharge takes place in March and April when the average discharge is about 1,840 and 1,800 m^3s^{-1}, respectively. After that, discharge rises sharply until reaching the peaks of 26,200 and 26,300 m^3s^{-1} in August and September, respectively. In addition, the trend of the discharge follows that of the rainfall pattern; the maximum rainfall is about 500 mm in August, with a peak flooding discharge lagging by approximately one month.

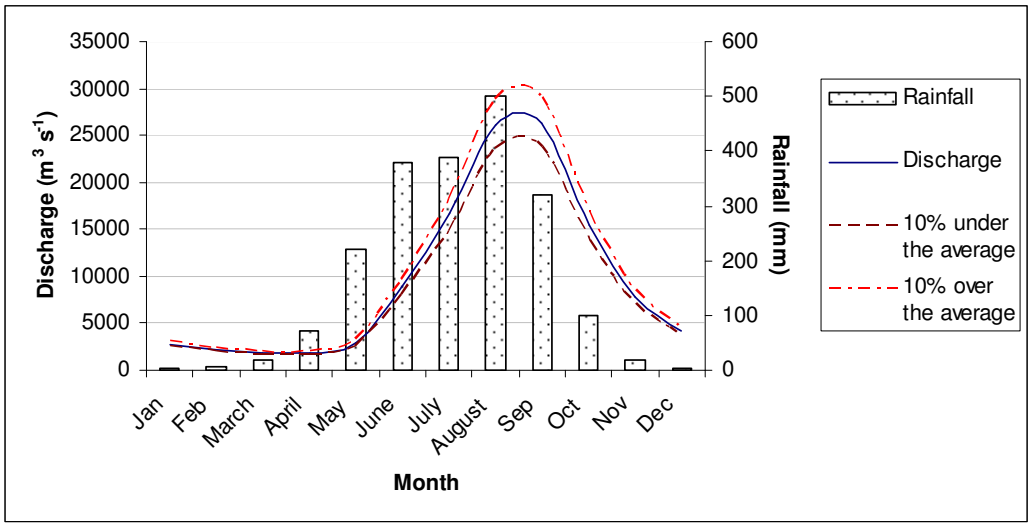

Figure 3.2-6: Monthly average discharge and rainfall from 1960 to 2004 at Pakse (*after* MRC, 2005)

Figure 3.2-7 illustrates the measured annual suspended sediment loads and total annual discharge in different years at the Pakse gauging station. There is a wide range of sediment loads in Pakse (from 63 to 330 Mt in 1967 and 1978, respectively) with no overall trend showing temporal changes. Even though the construction of major dams on the headwaters in China in 2002 seemed to have little impact on the sediment load along the LMB, with the proposed dams in the whole Mekong Basin (including both UMB and LMB), the sediment load is expected to decrease (Walling, 2008). In addition, according to the unpublished data of Yamanashi University, the grain-size distribution of bed material at Pakse was collected and analysed (Figure 3.2-8). The coarsest grain-size (D_{90}) was 4.75 mm with the lowest proportion of about 0.34 % while the highest proportion of about 25.47 % stands for the sediment size of > 0.425 mm.

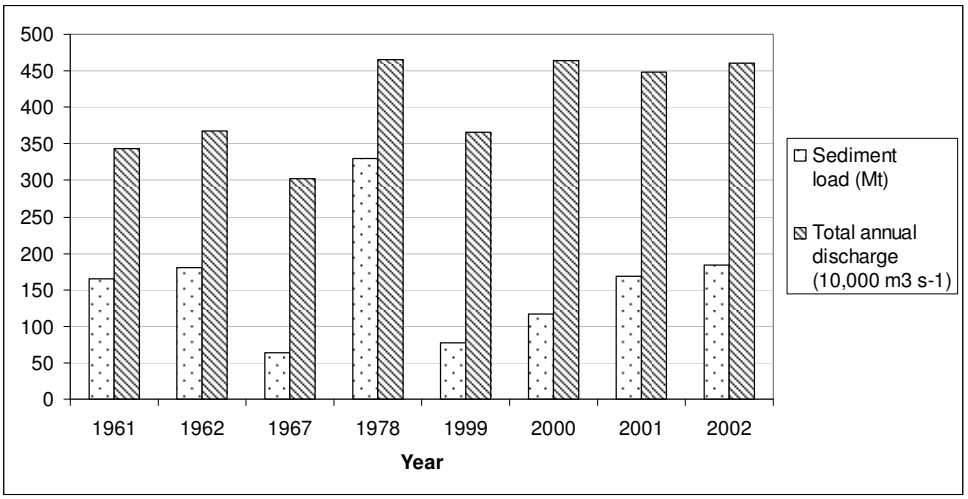

Figure 3.2-7: Sediment load at the Pakse gauging station (*after* Harden and Sundborg, 1992 and Walling, 2008); Sediment load – Mt, Total discharge – 10,000 m^3s^{-1}

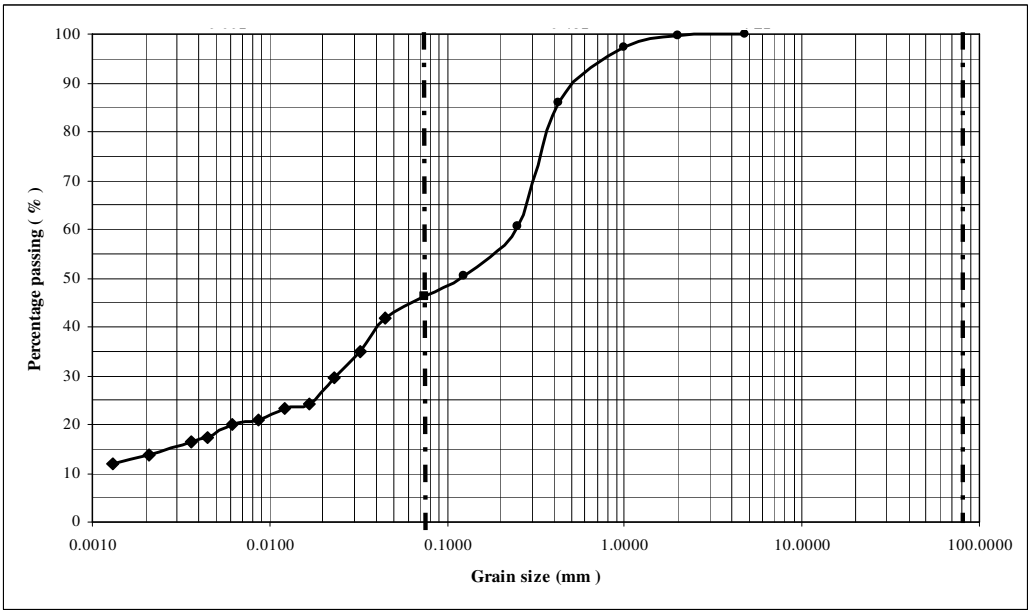

Figure 3.2-8: Bed material – Grain-size distribution curve at Pakse (Unpublished data of Yamanashi University)

3.3 The Siphandone wetlands

The Siphandone wetlands stretch from latitude 13°54' N to 14°18' N and from longitude 105°44' E to 106°00' E and are located within the fifth geomorphological unit (anabranching river network over a mixed bedrock and alluvial channel bed; Gupta and Liew, 2007) (Figure 3.2-1). Figure 3.3-1 and Figure 3.3-2 presents the watershed surrounding the Siphandone wetlands and the river network and pictures showing the actual present of some specific locations, respectively.

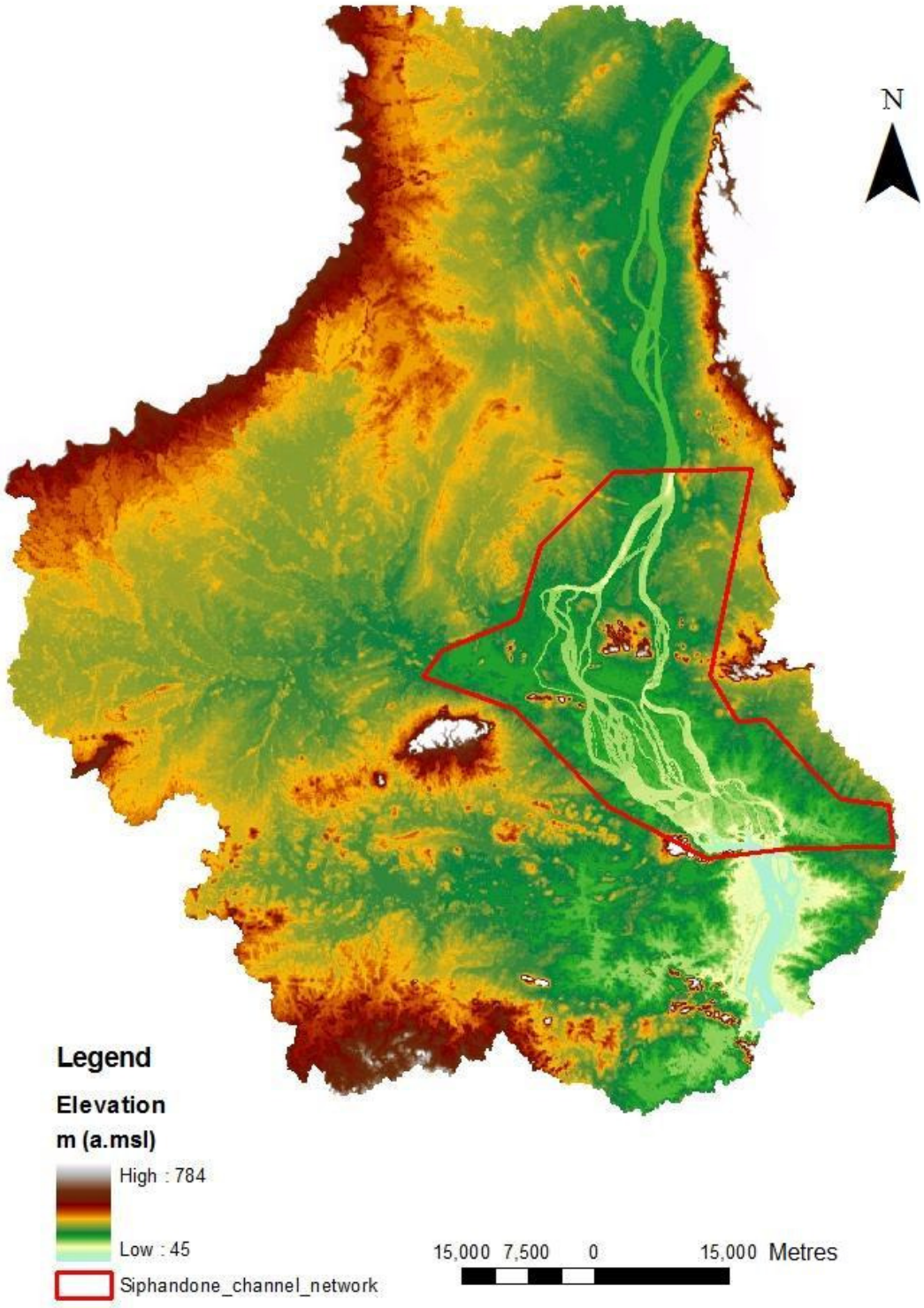

Figure 3.3-1: Watershed surrounding the Siphandone wetlands and the river network

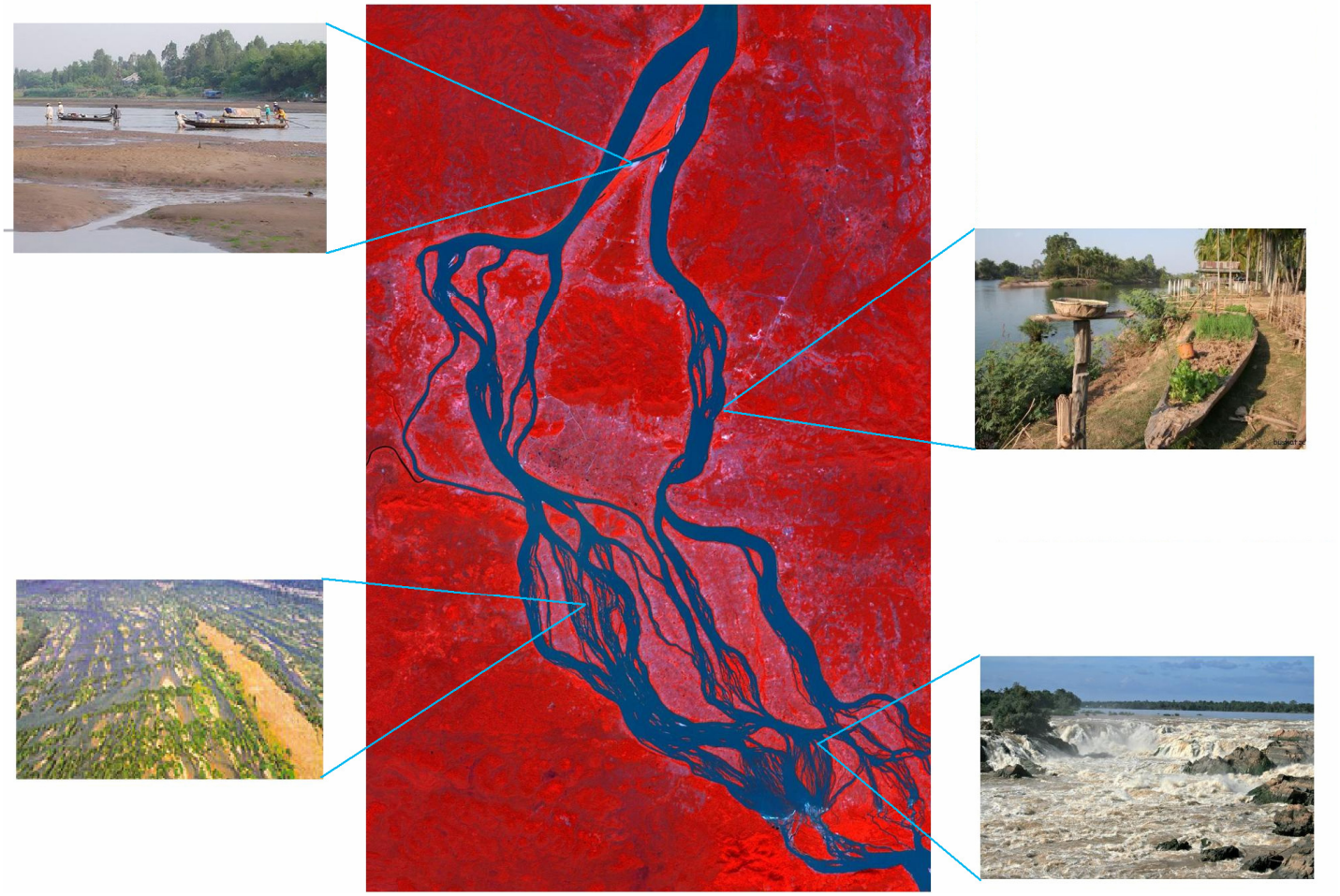

Figure 3.3-2: The Siphandone river network, Laos

3.3.1 Geomorphological and geological features

According to Brambati and Carulli (2001), the Siphandone wetlands can be divided into six geomorphological units. presents the spatial distribution of each geomorphological unit, including: Unit 1 – Khong island hills, Unit 2 – Khong island plain, Unit 3 – Great islands, Unit 4 – Small islands, Unit 5 – Done Som, Done Hangkhon, Done Phapeng and Hangkhon areas and Unit 6 – Area between Done Tholati. In general, the first geomorphological unit is located in the Done Khong hills and in the hills located along the right bank of the channel network with the land surface elevation up to over 200 m +MSL and the valley contours follow the fault system (North West-South East). The second geomorphological unit is the Done Khong plain and area in the right bank of the channel network stretching down to Unit 5. It is characterized by the reddish silt found in the Northern hills and the hill foots are covered by a thick layer of reddish-brown silt. The third unit is distributed mainly in the south and west of the study area. It is characterised by a flat land surface with elevation of about 89 m +MSL in the northern end and about 91– 93 m +MSL at the southern end of the unit. The fourth unit can be found in the centre and south of the channel network. It is characterised by the 'camel hump' shaped islands with the elevation of the island surfaces of about 82 – 85 m +MSL. In addition, according to the field survey from Brambati and Carulli (2001), they found that there are newly developed sand banks around the islands of this geomorphological unit; however, such alluvial deposition may be ephemeral and could be washed away by the annual flood. The fifth geomorphological unit can be found in the south of the study area with a series of hills with the average land surface elevation of about 70 m +MSL and separated by faults (North West-South East) (and Figure 3.3-4). The last geomorphological unit is characterised by the thin layer of alluvial deposits blanketing the channel bed and sandstone banks outcrops.

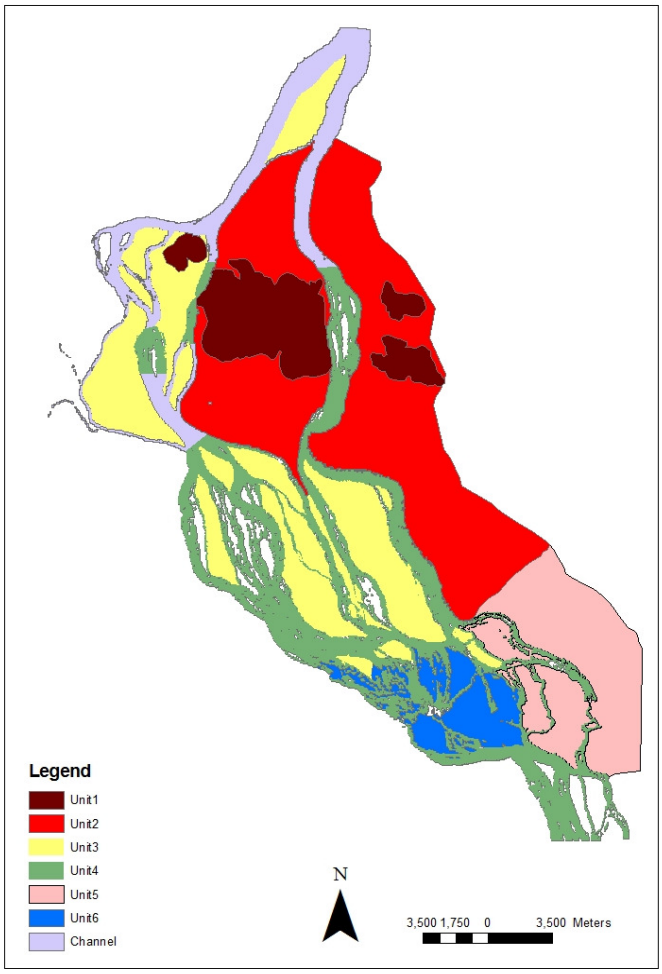

Figure 3.3-3: Geomorphological features of the Siphandone wetlands (*after* Brambati and Carulli, 2001); Notes: Unit 1: Khong island hills; Unit 2: Khong island plain; Unit 3: Great islands; Unit 4: Small islands; Unit 5: Done Som, Done Hangkhon, Done Phapeng and Hangkhon; Unit 6: Area between Done Tholati.

Two main morphological elements can be distinguished in the study area (Brambati and Carulli, 2001), including: (i) hills formed by the cleavage acid volcanic rocks featuring fault in a North North West-South South East and East-West direction. Such faults have resulted in the development of the planform of the river network; and, (ii) alluvial deposit consisting of medium to fine-grained quartz-feldspathic white sands. In addition, according to Brambati and Carulli (2001), the islands in Siphandone (except Done Khong) can be divided into three main classes with reference to the dry seasonal water surface elevation (about 82 m +MSL) (the islands in the first, the second and the third classes with altitudes of 8-10 m, 6-7 m and 3-5 m, respectively). As such the classification is given in accordance to the elevation of the island in relation to the water surface during the dry season and is determined based on field

observations of morphological units of the great and small islands (Figure 3.3-3). The islands are rock-cored and surrounded by accumulation of channel sediment. In the case of the low level islands, the sides are steep, eroded and with the occurrence of sand and silt bars at the lower levels. The local removal of the thin alluvial cover is evidence of an erosive phenomenon. Such features can be observed in the south of Tholati, which is characterized by a continuous outcrop of south-dipping torbiditic (also considered as aquitards; an impermeable layer along an aquifer) sandstones. The large islands (*e.g.* Done Khong, Done Khamao and Done Som; Figure 3.2-1) are rock-cored and usually have stable alluvial banks, which could be explained either by the large islands coinciding with areas having less fluvial energy (for instance, Done Khamao bordered to the west by a minor channel), or the size of the islands makes them intrinsically more stable.

The fault system has led to the formation of raised blocks, which are transverse to the channel gradient and which obstruct the primary course of the channel network. The channel network is compelled either to go round or dissect the obstructions. A further East-West fault trend often also affects the course of the channels, which turn at acute angles toward both east and west at various points. In the south, the course of the river network is also affected by outcrops of stable sandstone dipping to the south. These obstructions mainly consist of the hills rising in the middle of Done Khong. The second unit is alluvial deposits consisting of medium to fine grained quartz-feldspathic white sands, which cover the underlying formations (acid volcanic rocks in the north and torbiditic sandstones in the south) and consist of a thin layer of sand which grows gradually thicker from the south (4 – 6 m) to the north (10 – 12 m). The thinning of these alluvial deposits, from north to south, is reflected in the degree of instability of the rocky-cored alluvial islands, especially during flooding events (Brambati and Carulli, 2001).

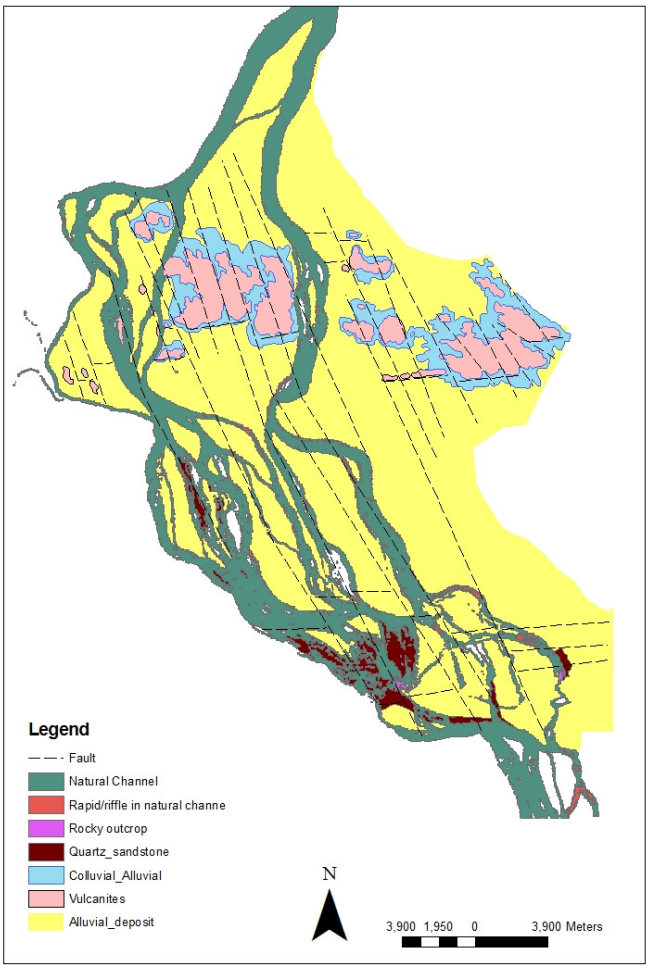

Figure 3.3-4: Simplified geological features of the Siphandone wetlands (Brambati and Carulli, 2001)

The basic structure and geology of the Siphandone wetlands was compiled and simplified from unpublished maps (Figure 3.3-5), including: (i) the photogeological map (1:100,000) of the Pakse area of Laos, sheet 4 created in 1991; and, (ii) the photogeological synthesis map (1:250,000) of the Pakse area, Laos – surface structures obtained courtesy of the Hunt Oil Ltd. Company, Singapore.

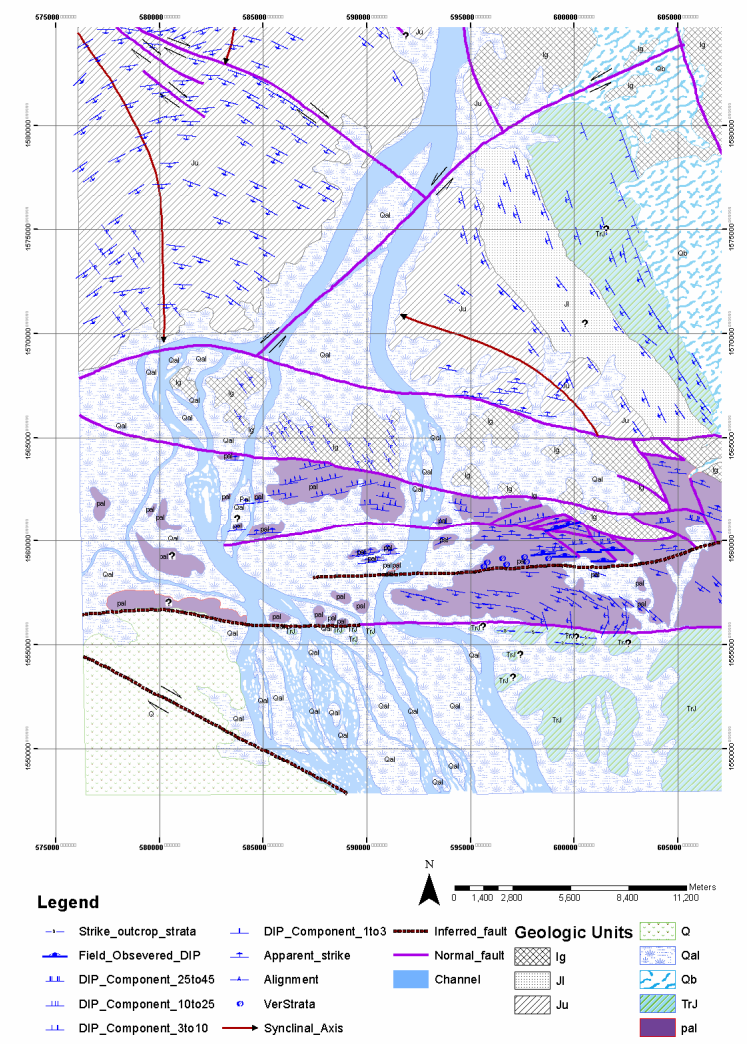

Figure 3.3-5: Basic structure and geology of the Siphandone wetlands (*Source:* Hunt Oil Ltd.) (Ig: Igneous rocks; Jl: Lower Jurassic sand stone; Ju: Upper Jurassic sand stone; Q: Quarternary rocks; Qal: Alluvial, gravel, sand, silt and clay; Qb: Basalt flow; TrJ: Upper Triassic and/or Lower Jurassic marine rocks; pal: Paleozoic volcanic rocks)

3.3.2 Channel banks stability

A general assessment by Brambati and Carulli (2001) has argued for widespread conditions of degradation of the channel banks, due partly to the rapid evolution of the riverine islands system. It seems that some small islands may be the product of a degradation process of former larger islands. The stability of channel banks has been reported in terms of four qualitative classes: stable, mainly stable, mainly eroded and eroded (Table 3.3-1) (Brambati and Carulli, 2001).

Table 3.3-1: Conditions of river bank stability within Siphandone (*after* Brambati and Carulli, 2001)

	Mainly stable	Stable	Eroded	Mainly eroded
Km	23.0	21.0	46.0	36.0
%	18.2	16.7	36.5	28.6

The prevailing condition of 'instability' throughout the study area is emphasized by the fact that only 16.7 % of the surveyed channel banks could be classified as stable; a slightly larger proportion (18.2 %) is classified as mainly stable. In fact, according to Brambati and Carulli (2001), this latter proportion show signs of local, incipient and acute erosion. The islands might therefore be considered more realistically as unstable areas which could be subject to further erosion in the near future. In addition, the most unstable areas are located in the south-central part of the study area (Unit 4;), where the islands are somewhat smaller than those in other areas and of lower elevation. These island systems are therefore liable to being eroded along their outer edges and also risk being submerged by high floods. However, this does not mean that other islands are not subject to inundation: local inhabitants report that most of the larger islands have been flooded occasionally along the edges and that bank erosion is increasing due to clearing riparian vegetation. The only islands that are partly free from flooding are those with an altitude of 10 – 12 m in comparison with the minimum water surface elevation. The groups of small islands and sand banks with an elevation between 2 and 7 m above the dry season water level have, thus, been identified as areas subject to inundation (Brambati and Carulli, 2001).

The high frequency of channel banks undergoing erosion (36.5 %) stands out; if those dominated by erosion (28.6 %) are added, the total figure of 65.1 % indicates that erosion of the riverine system in the study area is considerable. The critical nature of the situation is further exacerbated if consideration is given to the additional 18.2 % of bank length classified as potentially subject to erosive phenomena in the near future (Brambati and Carulli, 2001).

However, earlier research on the alluvial anabranching network (Nanson and Knighton, 1996; Smith and Smith, 1980) and bedrock-confined anabranching networks (Baker and Kale, 1998; Richardson and Carling, 2006; Stark, 2006) show that the anabranching network is mainly stable. Without quantitative data related to bankline erosion rate, the lateral instability of a bedrock-confined anabranching network within the Siphandone wetlands reported by Brambati and Carulli (2001) is questionable and requires further assessment.

3.3.3 Hydrological and hydraulic characteristics

The climate in Siphandone is monsoonal and similar to the general pattern recorded at Pakse. The rainy season extends from May to October/November with high monthly maximum rainfall ranging from 150 to 500 mm, while during the dry season (November/December – April), the monthly mean rainfall is about 0 to 21 mm. The average annual rainfall in Done Khong during 1979 – 1997 was about 1,753 mm. Figure 3.3-6 shows the monthly rainfall in Done Khong and the recorded water surface elevation at different temporary stage gauges (Channoy, Hatxaykhoun, Thakho, Veukham, Khoentai, Housahong Neua, Housahong Tai and Donsadam Tai (Figure 3.2-1)) in Siphandone. During the dry season, the river network has low stage in which some channels were dry during the lowest-discharge period while the water level rises rapidly in June and afterwards, during the rainy season. The flooding period reaches its peak in August – September, which causes inundation of the seasonal islands, especially in the complex wetlands area (Figure 3.2-1). The gauging stations were used for a specific project from 1998 to 2005 and therefore no further information was collected at those gauging stations after 2005. Except the Channoy stage gauge located in the North and Hatxaykhoun stage gauge located in the central Siphandone, the rest are located in the South and outside of the study area where the river network is replaced by a complex network of small channels and waterfalls. Details of the stage gauge stations are presented in Table 3.3-2 and the cross-sections at Channoy and Hatxaykhoun extracted from the available DEM are presented in Figure 3.3-7 and Figure 3.3-8.

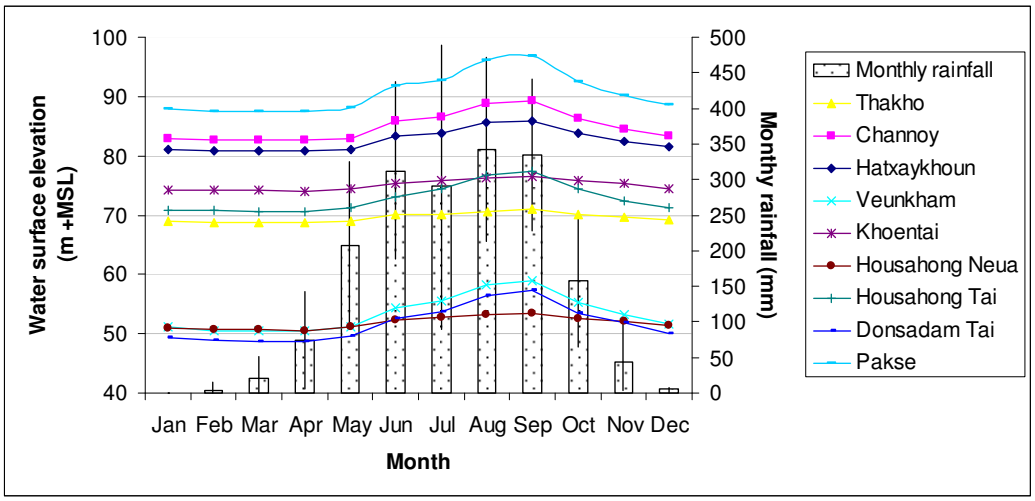

Figure 3.3-6: Monthly average water levels at different stage gauges (tabulated in MRC, 2005) and monthly rainfall in Done Khong (tabulated in Daconto, 2001)

Table 3.3-2: Location and zero gauge of the stage gauges within Siphandone

No.	Name	Location	Zero gauge (m)
1	Channoy	1583724N / 595762E	81.633
2	Hatxaykhoun	1560925N / 594031E	79.669
3	Thakho	1544726N / 606275E	65.331
4	Veukham	1539651N / 606761E	46.280
5	Khoentai	1544088N / 599860E	70.856
6	Housahong Neua	1544835N / 602960E	47.280
7	Housahong Tai	1541559N / 603602E	66.840
8	Donsadam Tai	1540800N / 603937E	44.484

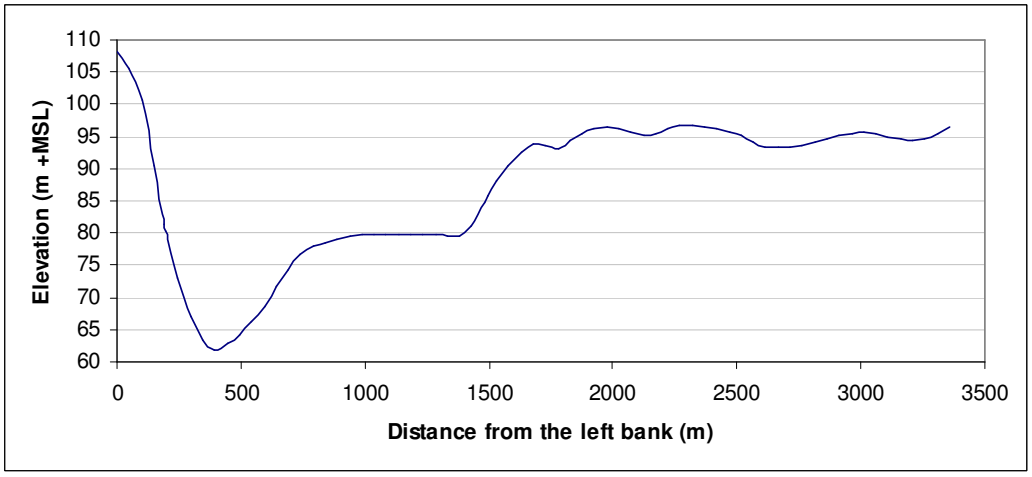

Figure 3.3-7: Cross-section at Channoy

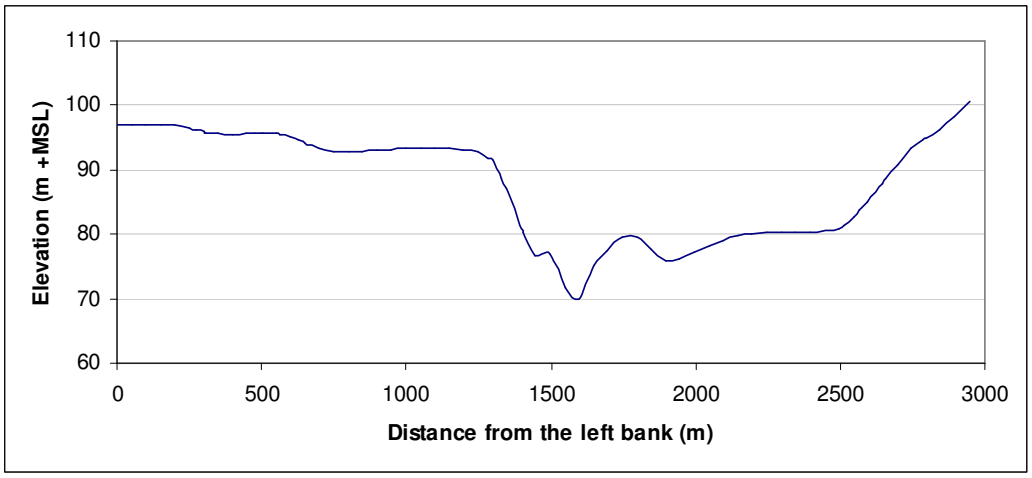

Figure 3.3-8: Cross-section at Hatxaykhoun

According to Gupta and Liew (2007), the general regional channel slope through this area is about 5.0 x 10^{-4}. However, because it is a bedrock-confined anabranching network, the water surface elevation of a channel might be different from another channel at the same latitude and similar moment of observation leading to different water surface slopes along each channel as well. For example, on the 10th January, 1998, the water surface elevation at different stage gauge stations at the southern area of Siphandone (Khoentai, Thakho, Veukham, Donsadam Tai; Figure 3.2-1) was 74.30, 68.89, 51.22 and 49.35 m +MSL, respectively. In addition, according to data obtained in the field in January, 2008, at an average discharge (from 08th to 14th January, 2008) of about 2,461 m^3s^{-1} (recorded at the Pakse gauging station), the water surface slope in the main channel from Channoy to Hatxaykhoun was 0.000074, two orders of magnitude less than the regional slope reported by Gupta and Liew (2007).

Figure 3.3-9 presents the local water surface slope trend from Channoy to Hatxaykhoun over the daily surveyed period (1998 – 2005) according to the upstream discharge recorded at the Pakse gauging station. Figure 3.3-9 shows that, between Channoy and Hatxaykhoun, the higher the discharge, the higher the slope, which can also be found at Pakse. Such a relationship is contrary to expectation as usually water surface slope reduces in an alluvial system at high discharge (Leopold and Wolman, 1957); however, it agrees with the results from Richardson and Carling (2006) that in a bedrock channel, the water surface slope increases when the upstream discharge rises.

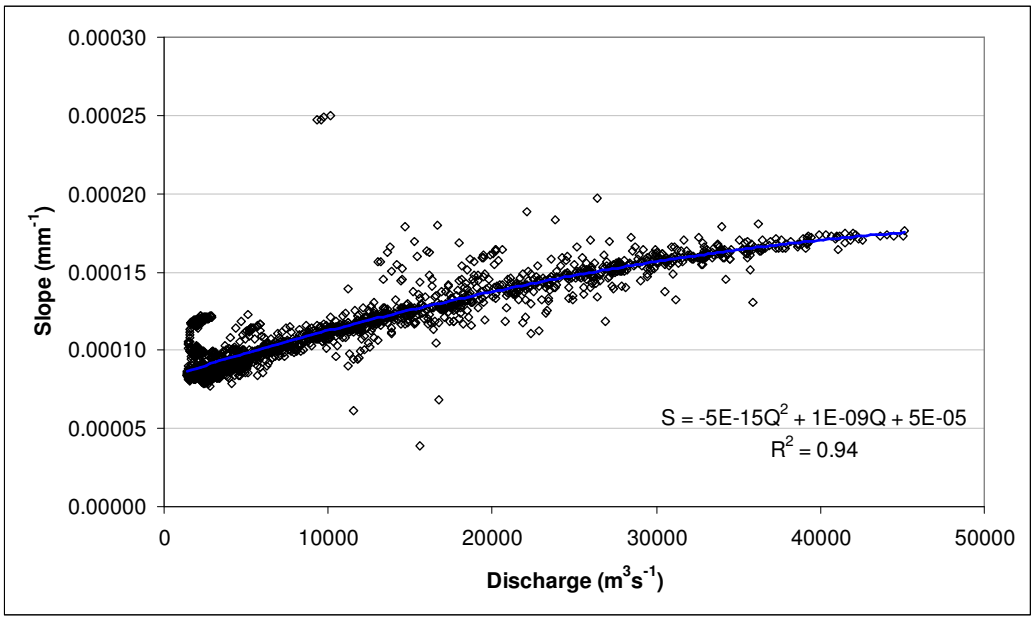

Figure 3.3-9: Upstream discharge (at the Pakse gauging station) *vs.* water surface slope from Channoy to Hatxaykhoun

Data from the historical discharge (1998 – 2005) collected at the Pakse gauging station and stage collected at the gauge stage at Channoy are plotted in Figure 3.3-10. There is a close relationship between the two variables; in fact, for the whole period of observation, the R^2 was equal to 0.94.

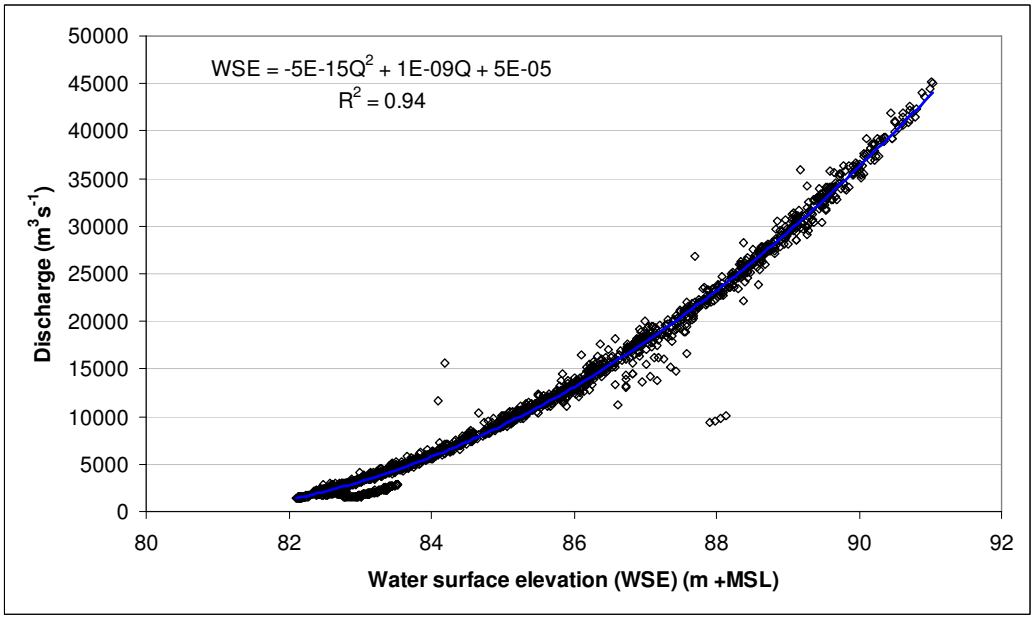

Figure 3.3-10:Discharge (at the Pakse gauging station) *vs.* stage (at the Channoy stage gauge)

The full river network and junctions are presented in Figure 3.3-11. Along the network, there were 18 bifurcations, 1 trifurcation and 14 confluences with the

maximum and minimum angles (θ_1 and θ_2) measured along the planform extracted from the SPOT image between channels of 0^o and 81^o, respectively (Table 3.3-3). The angle at each junction was measured as illustrated in Figure 3.3-12.

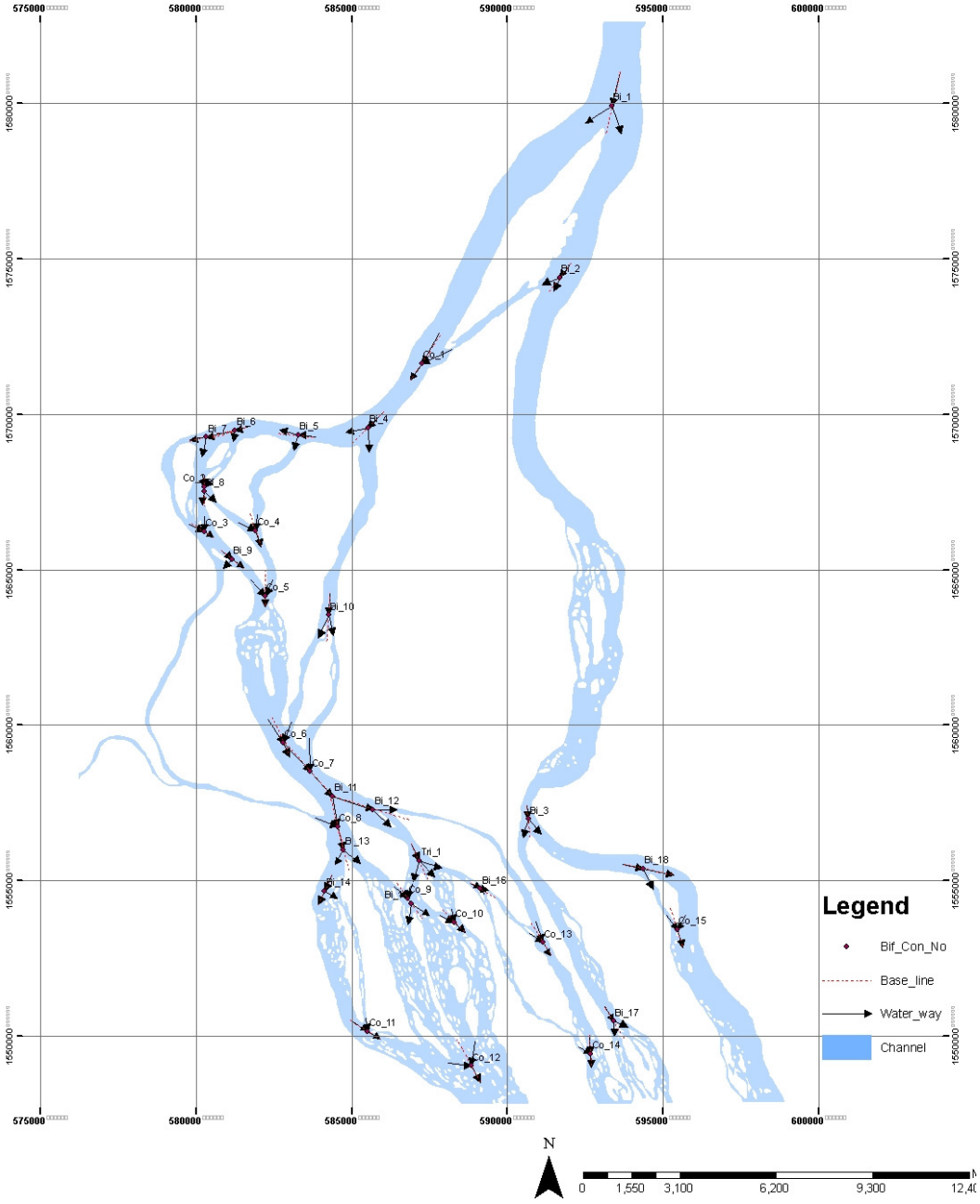

Figure 3.3-11: Main bifurcations and confluences along the Siphandone river network

Table 3.3-3: Angle between the upstream and downstream channels at each junction

Junction	Bifurcation	
	θ_1	θ_2
Bi_1	32	44
Bi_2	14	28
Bi_3	39	22
Bi_4	46	32
Bi_5	76	12
Bi_6	72	0
Bi_7	65	6
Bi_8	49	5
Bi_9	8	89
Bi_10	19	21
Bi_11	24	36
Bi_12	15	28
Bi_13	37	44
Bi_14	81	0
Bi_15	18	43
Bi_16	16	17
Bi_17	38	28
Bi_18	0	54
	Trifurcation	
	Left-	**Middle-**	**Right-**
Tri_1	39	20	48
	Confluence	
	θ_1	θ_2
Co_1	32	5
Co_2	42	5
Co_3	59	6
Co_4	24	47
Co_5	24	42
Co_6	45	10
Co_7	39	2
Co_8	3	55
Co_9	54	10
Co_10	32	25
Co_11	45	0
Co_12	35	58
Co_13	12	14
Co_14	0	60

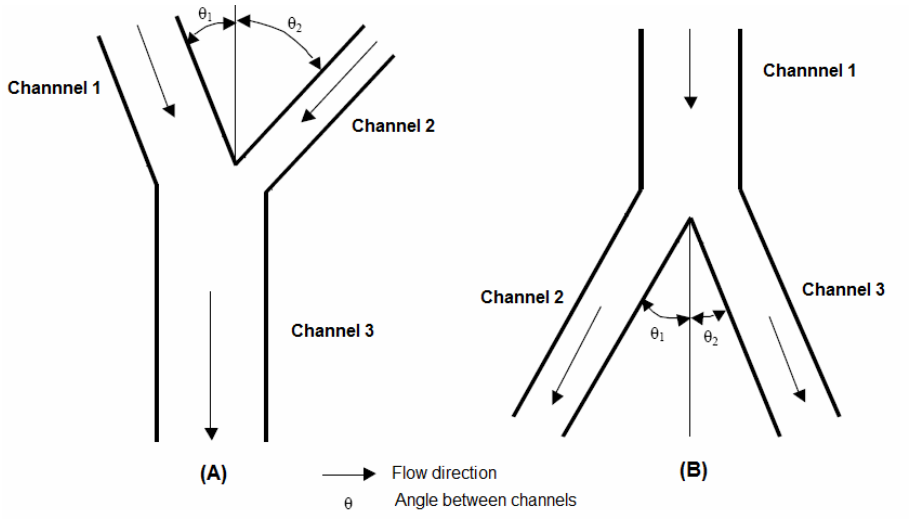

Figure 3.3-12: Measured angles at each junction; (A) at a confluence and (B) at a bifurcation

3.3.4 Recent land cover and land cover change

Siphandone consists of a complex landscape. In some islands, developed soil can be found with well-developed vegetation including up to 30 m-hight trees and paddy fields (Gupta *et al.*, 2007). According to Altobelli and Daconto (2001), the land cover in Siphandone is classified into eight classes (Table 3.3-4). The spatial distribution of land cover can be seen on the land cover map for 2001 (MRC, 2005) (Figure 3.3-13).

According to Alfredo (2001), agriculture (mainly rice paddies) dominates most of the large islands and the corridor along the left channel bank (from Channoy to Thakho). Rice paddy also extends further east into a mosaic of the deciduous dipterocarp-oak forest and secondary growth areas. The latter class represents the largest proportion in total area of land cover, which indicates a significant impact of human pressure on the natural vegetation, due to encroachment of farming areas into the woodlands. The main forest area can be seen in Done Khong and the mixed evergreen-deciduous forest area in the northern part of the island. The southern islands with their thinner alluvial deposit and irregular topography are less suitable for any agricultural activities and therefore preserve some forest cover.

Similar to the currently rapid livelihood development in the LMB (MacAlister and Mahaxay, 2009), land cover pattern in Siphandone has changed quite significantly (mainly from dry forest into mixed forest, dry scrub or agriculture, especially rice paddy). Such changes might have strong impacts on changes in the hydraulic roughness within the riparian area, which would lead to variation of the hydraulic

nature of floods. MRC (2005) produced a static land cover map for 2001 (Figure 3.3-13) but there are no maps of the land cover change over time.

Table 3.3-4: Land cover types within Siphandone (*after* Alfredo and Daconto, 2001)

Land cover type	Area (km^2)	%
1. Deciduous Dipterocarp-Oak Forest (DOF)	113.9	16.2
2. Mixed Evergreen-Deciduous Forest (MXF)	45.8	6.5
3. Secondary growth	206.4	29.3
4. Sand bank/Bar vegetation	30.1	4.3
5. Boong area (*)	12.1	1.7
6. Rice paddies	141.4	20.1
7. Bare soil	40.7	5.8
8. Water	113.4	16.1
Total	**703.8**	**100**

(*) *Boong area* – shallow, rocky places with permanent flow are characterized by having dense tufts or small islands of vegetation (mainly *Telectadium edule* (Asclepiadaceae) mixed with *Homonia riparia* (Euphorbiaceae), *Rotula aquatica* (Boraginaceae) and other shrubs and grass) on sandstone bedrock where there is a general absence of sand (Maxwell, 2001).

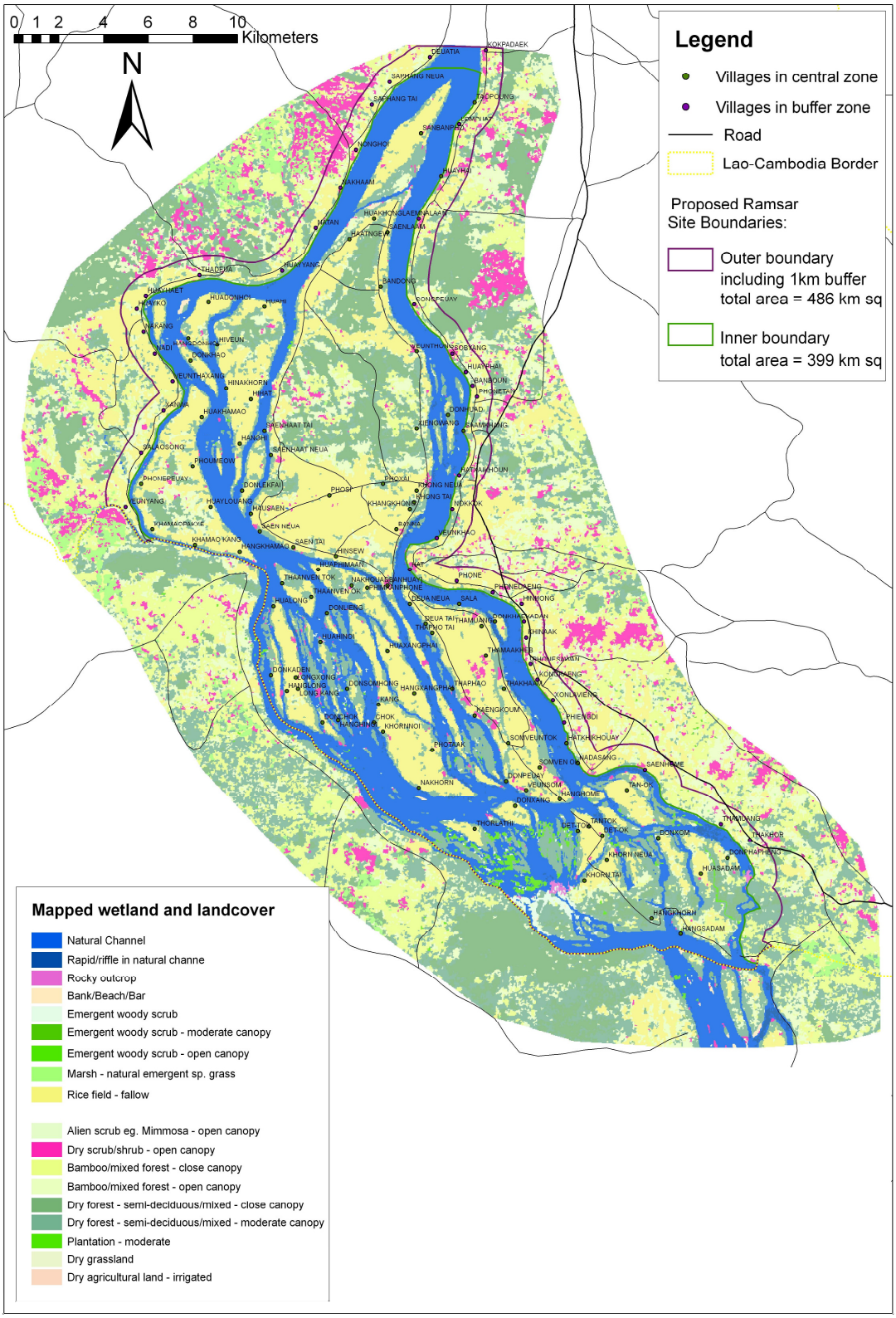

Figure 3.3-13: Land cover map for 2001 (MacAlister and Mahaxay, 2009)

3.4 Impacts of climate change on the physical setting along the Lower Mekong River

Global climate change is having different impacts on different regions at the global scale. In addition, according to Jacobs (1996), even though the impact of climate change in LMB is complex and it is difficult to make long term climate change projections, the area will continue to experience annual climate variability as in the situation today.

In LMB, different research on the impact of climate change has resulted in different outcomes in terms of predicted hydrological patterns. According to Arora and Boer (2001) there will be a decrease of the total flooding discharge during the flooding period of about 21 % and lower mean annual flows of about 30 %; however, according to a report from START (the global change *S*ys*T*em for *A*nalysis, *R*esearch and *T*raining) (2006), with the increase of CO_2 concentration in the future, the LMB would receive more precipitation leading to more discharge entering different sections of the Mekong. Even though there are conflicting predictions, researchers have agreed that there would be significant changes in hydrological conditions (average temperature, seasonal distribution, precipitation, runoff and stream-flow) in different sub-areas within the LMB, leading to the changes in the in-channel hydraulic parameters along the river network, productivity of agriculture and fisheries, and substantially altering the composition, structure, and function of the region's ecosystems. In addition, according to Kiem *et al.* (2004), the El Nino event, an abnormal warming of the surface ocean waters in the eastern tropical Pacific leading to less precipitation in the land surface (and more precipitation in the Pacific), has been studied to understand the impact on the regional and local hydrological and hydraulic regime. Kiem *et al.* (2004) conclude that (i) the magnitude of the annual average maximum daily flow is lower during the El Nino event; (ii) the number of high discharge events (> 30,000 m^3s^{-1}) during the El Nino event is lower than that of the normal year; and, (iii) the daily increases in discharge prior to peak events during El Nino event is significantly higher.

According to a workshop organized by the WWF in 2009, the future climate change in the Siphandone wetlands could result in changes of the hydrological and hydraulic setting. First, the hydrological regime would change in terms of rainfall and temperature/radiation. Such changes of the hydrological regime lead to changes of

hydraulic parameters such as total annual discharge, seasonal discharge and peak discharge of flood and drought. In addition, the changes in hydrological regime would also impact on the sediment load from the land surface into the river network as well as the stability of channel banks. The hydraulic parameters of the river network and channel morphology are closely linked where the changes of one factor may affect the nature of another factor which in turn sends a feedback to the previous one. Furthermore, the changes of the channel morphology may have strong impacts on the living environment of the local flora and fauna population in terms of changing in size of pool and riffle / sand bar along the river network.

3.5 Impacts of hydropower-dams construction and operation on the physical setting along the LMR

The annual sediment load at Khone Falls is estimated to be about 132 Mty^{-1} (Pantulu, 1986). The on-going changes of the physical settings resulting from dam construction, deforestation, agriculture, gravel mining (within the channel network) and road construction within the study area as well as the upstream and downstream activities might lead to increases in the annual sediment load. In contrast, the dam operation in the upstream section of the Mekong may result in less sediment transported into the study area. In fact, the change of sediment loads along the Mekong in general and along the Siphandone wetlands is currently a crucial issue, but there has been no research in this field in the area so far.

Dam construction on the UMB retained sediment and caused a series of downstream effects (Fu *et al.*, 2008). Lu and Siew (2006) generally described the impacts of dam construction and operation along the UMR on the water and sediment discharge along the LMR. They found that the infilling of the Manwan reservoir in 1992 caused water levels and sediment concentration to fall to record lows in different segments along the LMR. According to Fu *et al.* (2008), during the period from 1993 to 2003, the Manwan dam trapped about 26.9 – 28.5 ton annually. After the dam construction, during the dry season, flows generally declined and the differences in water levels fluctuated considerably. In addition, according to Wang and Lu (2008), during the entire period from 1962 to 2003, at the five main gauging stations (*i.e.* Chiang Saen, Luang Prabang, Nong Khai, Mukdahan and Khong Chiam) along the LMR, the sediment load (before and after the operation of the Manwan dam) had different responses to human activities and climate variations. In fact, at Chiang Saen – the

nearest gauging station to the Manwan dam, the construction of the dam likely brought extra sediment into the stream while during the operation of the dam, the sediment was trapped causing a decrease of the sediment load. Apart from the impact from the Manwan dam, the sediment load change can be caused by the climate factors as well. In fact, Wang and Lu (2008) found that the sediment load decreased due to climate change. However, such changes due to dam construction and operation were less significant further downstream (Fu *et al.*, 2008). According to Lu and Siew (2006) and Kummu and Varis (2007), the decrease of sediment load due to the Manwan dam might have been balanced before reaching Luang Prabang. In addition, the Manwan dam construction and operation did not have a significant impact on the sediment load at the four gauging station downstream.

In the Siphandone wetlands, the Don Sahong dam is proposed to be built. Even though no research has been conducted to study the impacts of such construction in terms of hydraulic and sediment transport, the international biologists argued that such a new dam would significantly change the wetlands conditions and therefore lead to changes of the local flora and fauna populations (Baird, 2009).

Chapter 4: Methodology

Introduction

A general framework is presented to briefly describe the overall procedure employed to model the wetted-section and flooding patterns according to different entry discharges along the river network. The approach to preparing the spatial data, including the measured and pseudo-bathymetry of the river network and land cover (change) maps, are then presented in detail. To model the river network, first, a raster-based model is described as a simple approach to estimate the possible inundated area when the (average and high) flood discharge is routed along the river network; this approach is useful to estimate the flooding extent before building a physical-based hydraulic model (HEC-RAS – Hydrologic Engineering Center's River Analysis System). Detailed description of the 1D hydraulic model (HEC-RAS) in terms of basic calculations and development of hydraulic models for a river network is presented as the main approach to understand the hydraulic nature of the river network. Finally, the CAESAR (Cellular Automaton Evolutionary Slope And River) model and the Optimization Algorithm (OpA) are presented as alternatives to model the river network with limited input data.

4.1 General framework

The study was done following the general procedure presented in Figure 4.1-1, in which two main processes were identified, namely: (A) Preparation of the spatial data; and, (B) Application of HEC-RAS for the river network. First, SPOT (Satellite Pour l'Observation de la Terre) images a with ground resolution of 20 m were used to create the land cover maps of the study area which then were used to calculate the land cover change in the period of 2001 and 2005 and estimate the hydraulic roughness coefficient (Manning's *n*) of the floodplain. Apart from that, the SPOT images were also used to estimate the wetted-width along the river network in the low entry discharge (which was recorded at the Pakse gauging station on the date the SPOT image was taken) and interpolate a pseudo-bathymetry (representing a range of channel bed elevations, including shallow and deep channel, rather than detailed elevation as the measured bathymetry) of the downstream river network. The SRTM (Shuttle Radar Topography Mission) with a ground resolution of 90 m showing the elevation of the land surface was integrated with the Hydrographic Atlas (showing the

measured bathymetry in the presentation of cross-section interpolated from the random hydrographic depth sounding with the accuracy of 0.01 m) representing the measured bathymetry along the upstream river network and the interpolated pseudo-bathymetry along the downstream river network to create an integrated DEM (Digital Elevation Model) of the study area. The second process of this study was to apply the steady 1D hydraulic model (HEC-RAS) to model the wetted-section along the upstream (Chapter 6) and full (Chapter 7) river network according to the low (6,450 m^3s^{-1}) corresponding to the recorded lowest discharge of the available SPOT images and the mean historical and highest flood discharges (26,300 m^3s^{-1} and 45,169 m^3s^{-1}, respectively). The available boundary conditions of the HEC-RAS model included the recorded discharges at the entry section of the river network (assumed to be equal to that recorded at the Pakse gauging station; Chapter 3, Figure 3.2-1) and the recorded stages at the entry section (Channoy; Chapter 3, Figure 3.2-1) and at the downstream end of the left branch (Hatxaykhoun; Chapter 3, Figure 3.2-1) of the river network. In addition, the hydraulic roughness coefficient (Manning's *n*) at each cross-section along the river network was calculated individually. The outcomes of the HEC-RAS model were the wetted-section and the hydraulic parameters at each cross-section along the river network.

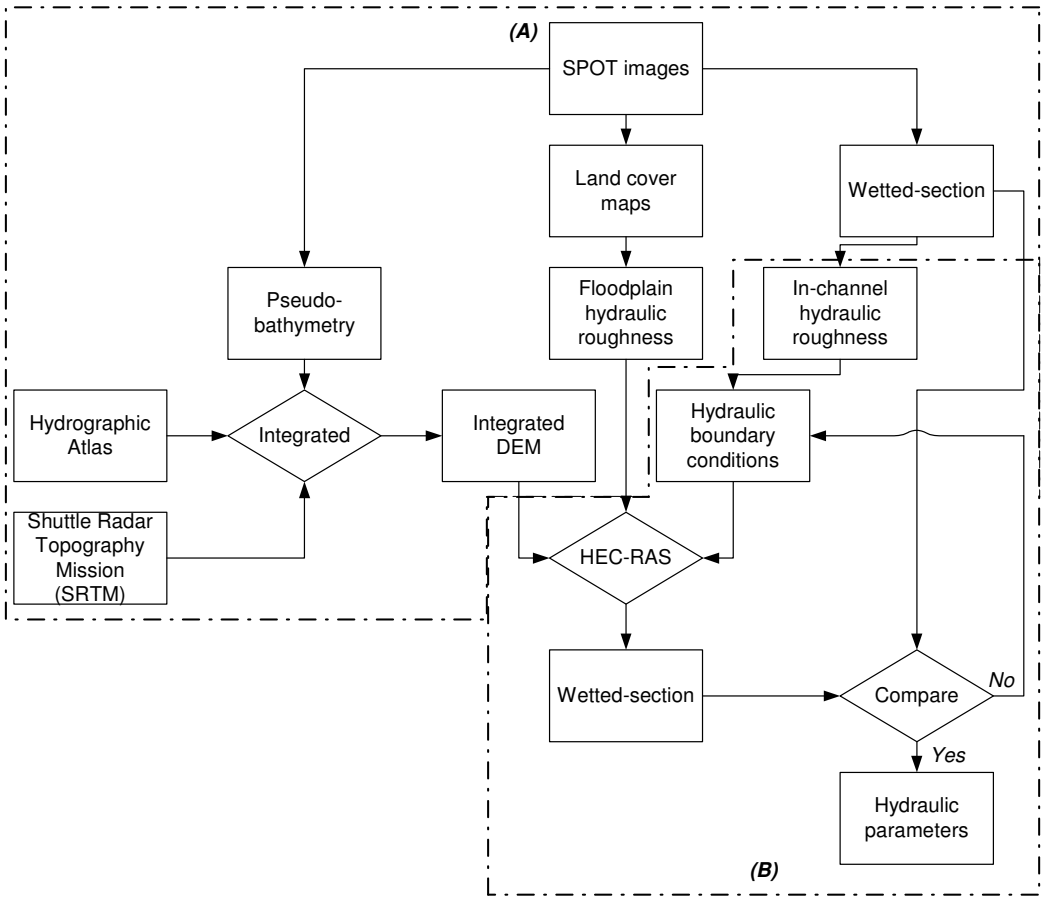

Figure 4.1-1: General approach to study the hydraulic parameters of a river network

4.2 Spatial data preparation for the one-dimensional (1D) hydraulic modelling

4.2.1 Land cover and land cover change mapping from SPOT images

To create the land cover map in the study area, two multi-spectral three-band atmospherically-corrected SPOT images taken in 2001 and 2005 (Figure 4.2-1) were analysed in ENVI 4.5. Seven land cover types extracted from the land cover map created according to the MRC 2003 (Chapter 3, section 3.3) were grouped into five classes (paddy rice field, shrub, natural forest, degraded forest, bare soil). Such simplified land cover map was then used to select the Manning's *n* coefficient along the floodplain for the HEC-RAS models, in which the maximum number of the assigned Manning's *n* at each cross-section could not be greater than twenty. To understand the impacts of the land cover change on the flood scenarios, the sensitivity analysis of the hydraulic models according to different hypothetical scenarios was done. Before applying the supervised classification analysis, cloud-cover and cloud-

shadow were masked and excluded in the images. On the SPOT images, the cloud-cover was identified according to the high reflectance of the feature (often the reflectance value in the middle of the cloud-cover feature was 255 – the maximum reflectance in remote sensing imagery) compared to the surrounding features, and the cloud shadow was detected in the surrounding areas of the identified cloud with low reflectance compared to the neighbours. The *Regions of Interest* (ROIs) (the training areas or the image subsets created to extract statistics for image operation; ENVI, 2008) were collected according to the land cover map created by the MRC (2003). The ROIs was created according to the following rules: (i) the ROIs was scattered over the whole image where the features found in the SPOT images were similar to those found in the available land cover map; (ii) the ROIs should be homogeneous (similar reflectance of all bands); and, (iii) the ROIs should only cover the area with the known (or strongly expected to be) land cover type. The supervised classification technique (*Maximum Likelihood;* Campbell, 2002) was applied to create the land cover map in which a single cell might be classified into different land cover types compared to the neighbours (also called *noise*). To eliminate the 'noise', the filtering technique (*Majority Analysis*) was applied to change spurious pixels within a large area of a single class to that class (ENVI, 2008) using a 'filter window' (Kernel size) of 3 x3 pixels. Finally, the accuracy assessment (*Confusion Matrix*) was done to show the accuracy of the classification results by comparing the classification results with ground data (collected during the fieldtrip in 2008) (ENVI, 2008); in other words, the accuracy assessment was done to evaluate the acceptability of the classified land cover type. The supervised classification procedure for land cover analysis is presented in Figure 4.2-2. The land cover change map was created based on the calculation of the two land cover patterns in 2001 and 2005 due to the following formula: *Land_cover_change_map = Land_cover_map (2001) x 10 + Land_cover_map (2005)*. In the *land cover change map*, the pixels with the code of similar digit in tens and units (*e.g.* 22) reflects no change while the pixels with the code of different digits in tens and units (*e.g.* 12) reflects the change of land cover type (*e.g.* from land cover type 1 in 2001 to land cover type 2 in 2005).

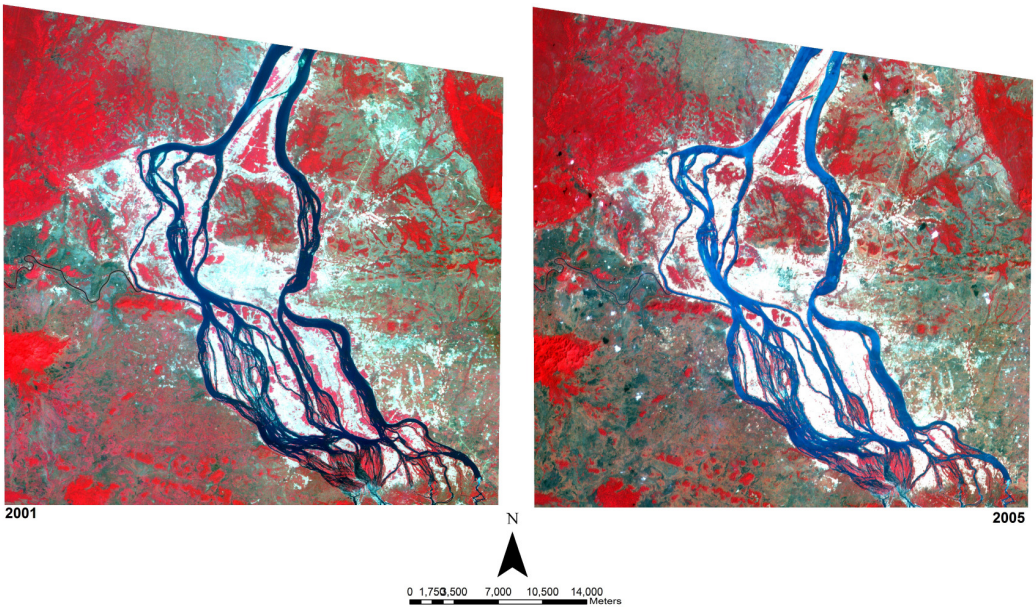

Figure 4.2-1: Satellite images covered the Siphandone wetlands (SPOT 1 taken in 03rd March 2001 and SPOT 2 taken in 18th February 2005)

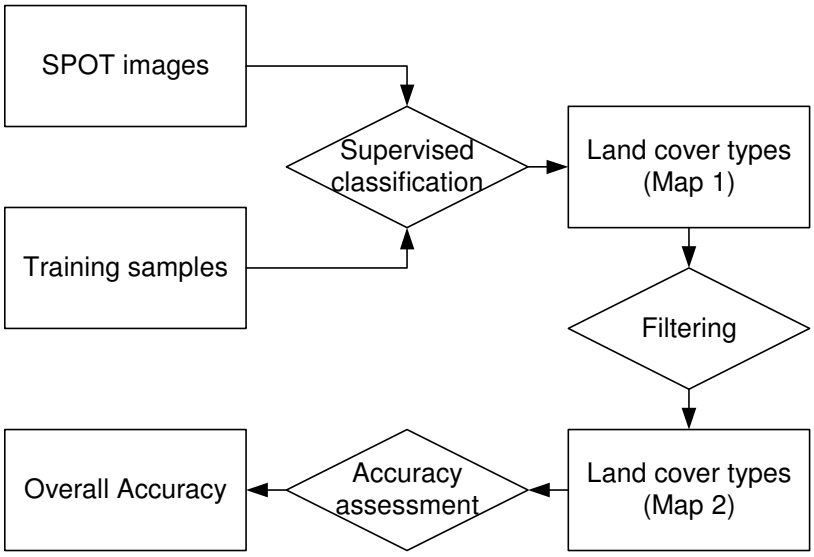

Figure 4.2-2: Procedure of supervised classification analysis for the land cover pattern in 2001 and 2005

4.2.2 SPOT image processing for pseudo-bathymetry interpolation

In order to develop the full river network HEC-RAS models, geometry of the river network was required. However, along the downstream river network, there was no measured bathymetry. In addition, even though SRTM data were used to estimate the bathymetry of a large river during the low discharge when the channel bed was mainly exposed (Patro *et al.*, 2009), the SRTM data did not contain the channel bed elevation in the study area (Figure 4.2-3); therefore, a novel approach was developed

to estimate the pseudo-bathymetry due to the combination of reflectance of the red and green bands in a SPOT image. The interpolated pseudo-bathymetry will be validated via the application of the HEC-RAS models.

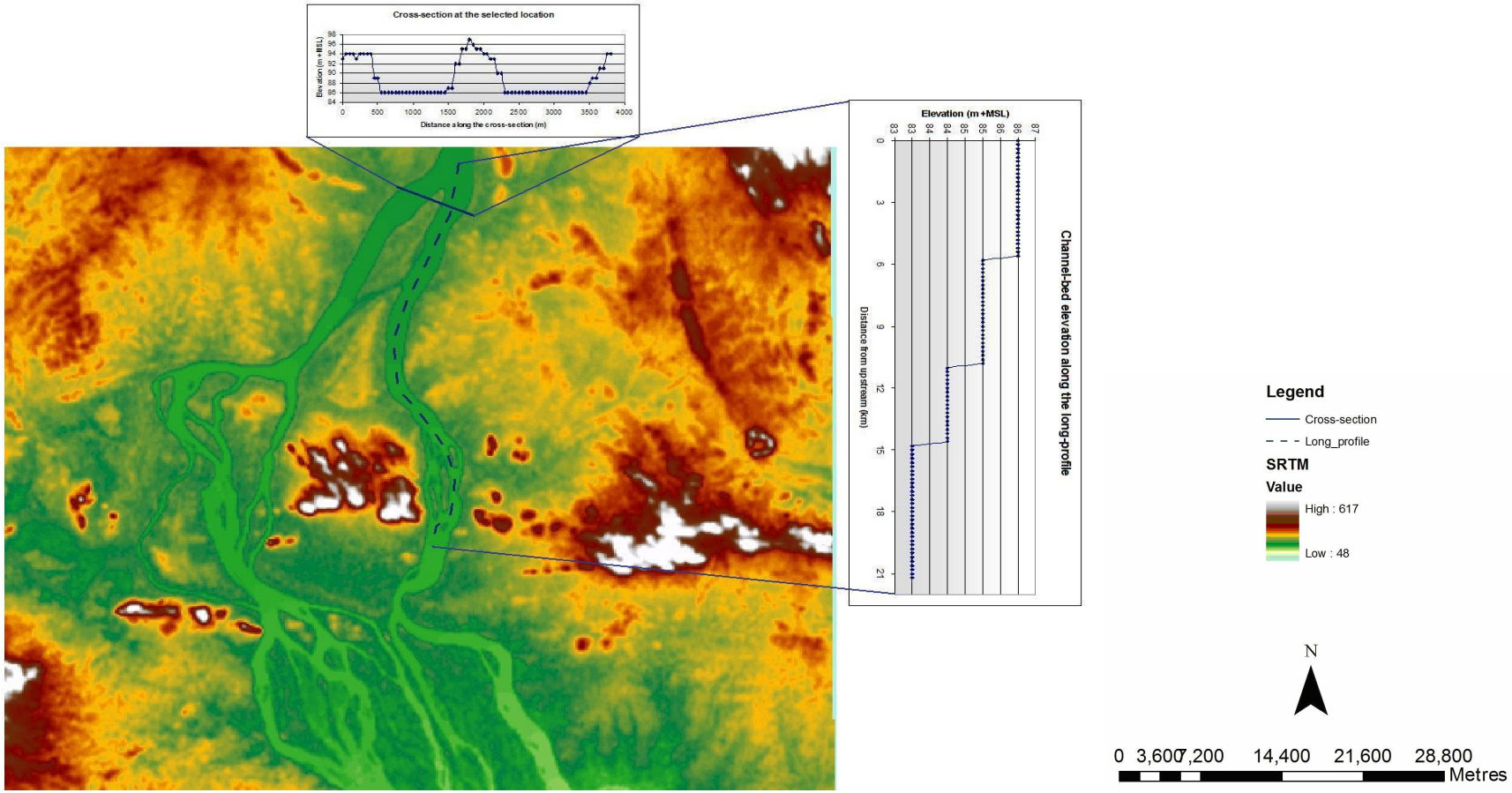

Figure 4.2-3: SRTM raster layer in the study area

According to Melsheimer and Liew (2001), the reflectance from a SPOT image contains information on the water depth and therefore can be used to interpolate the bathymetry; in fact, along the water body in a SPOT image, the darker hues represent deep water while the brighter hues represent shallow water. With clear water, Band 1 (green) (0.50 μm – 0.59 μm) has penetration depth of light of the order of 10 m (Melsheimer and Liew, 2001) and even down to 20 m (Campbell, 1999) and therefore contains information on the bathymetry. In fact, the green band has a strong penetration capacity (Tripathi and Rao, 2002; Gao, 2009) and could be useful to estimate the water depth. However, no previous research had been done to investigate the penetration depth of Band 2 (red). Melsheimer and Liew (2001) suggested to include Band 2 in the interpolation of the bathymetry and to separate different zones of water depth for better interpolation of the bathymetry of each segment with significant differences in the gemomorphological features. However, Melsheimer and Liew (2001) and other researchers have not considered the application of SPOT imagery for heavy sediment-laden large river networks, which is a great challenge of the study. Figure 4.2-4 briefly illustrates the procedure to generate the pseudo-bathymetry from a SPOT image.

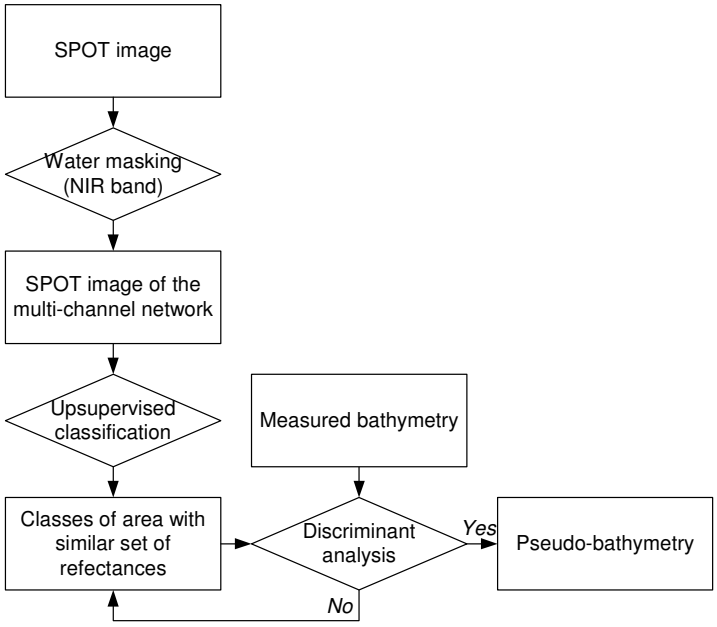

Figure 4.2-4: Procedure for interpolating the pseudo-bathymetry from a SPOT image

The pseudo-bathymetry was first interpolated for the upstream river network where the measured bathymetry was available to validate the approach of interpolating a SPOT image for the pseudo-bathymetry. Then, the approach was applied to

interpolate the pseudo-bathymetry along the downstream river network. The pseudo-bathymetry was developed with the hypothesis that 'the optical bathymetry is underpinned by the principle that the total amount of radiative energy reflected from a water column is a function of water depth' (Gao, 2009), and therefore, the combination of reflectance of band 1 (green) and band 2 (red) of a SPOT image reflects ranges of water depth in a large and sediment-laden river network and therefore can be used to interpolate a pseudo-bathymetry. To interpolate the bathymetry of a seabed, Melsheimer and Liew (2001) assumed that the attenuation of the SPOT signal is spatially homogeneous. However, this assumption is weak in this study due to the nature of a heavy sediment-laden river network. Therefore, the first assumption in this study is that a constant suspended sediment concentration exists throughout the water column across the river and therefore the higher the water column, the greater the sediment load and the darker hue in the image due to signal attenuation by the sediment mass (verified by the examination of the applied SPOT image and field data). In nature, sediment concentrations tend to be higher where the flow energy is greatest. Velocity and depth tend to be greatest in mid-channel and thus shear stress, $\tau = \rho gRS$, and turbulence, $\mathrm{Re} = {}^{UD}\!/_{v}$, (*see* Section 4.7) will tend to peak in the central portion or the deeper faster channel flow; this is considered as the second assumption. Thus if suspended sediment concentrations are not uniform, they will have a tendency to increase in deeper waters and thus reinforce the attenuation of the signal. The third assumption was that flow velocity and turbidity are not significantly different within segments along the river network with similar geomorphological natures.

In order to interpolate the pseudo-bathymetry of the river network, an available SPOT image related to the lowest-recorded entry discharge (compared to other available SPOT images) was used in order to minimize the impact of sediment load and water column height on the pseudo-bathymetry interpolation. In order to minimize the miss-interpolation caused by the parts near the channel banks where water depth co-varying with the mixing of land cover might lead to reflectance transects, a water mask was created by using the near infrared band (NIR) (Melsheimer and Liew, 2001) and then shrunk to eliminate the mixed pixels at the edges. The unsupervised classification interpolation was done in ENVI *v.*4.5 to interpolate the regions of different reflectance based on the combination of the green and red band reflectance. Tripathi and Rao

(2002) differentiated eleven depth zones when the bathymetry of a seabed was analysed. However, due to the different nature of the transparency of the water (according to the density of suspended material) in the study area, initially ten classes were classified from the water body, which would then be combined into two classes (shallow and deep class) according to the *discriminant analysis* result. In fact, with the preliminary trials, the correlation between the measured bathymetry and classification of reflection using more than two classes was low (the correlation at a certain class was often less than 0.50). In general, the *general proportion correct* and the *proportion correct* of each class according to the *discriminant analysis* (Ehrenfeld and Littauer, 1964) analysed in Minitab *v.*15 were expected to be larger than 0.6; in other words, more than 60 % of the sample population from each class matches the observed data was expected. Preliminary trials showed that the best correlation between the defined classes and the measured bathymetry was about 0.68 but usually not better than 0.6; therefore, the correlation value at 0.60 is a requirement and the correlation between the two variables less than 0.60 was rejected.

At different segments along the river network, the reflectance of a SPOT image might reflect different ranges of measured bathymetry (Melsheimer and Liew, 2001). Such differences could be caused by (i) significant changes of the bathymetry along the long profile of the river network; and, (ii) the sediment load concentration between the segments. In order to interpolate the pseudo-bathymetry of the upstream river network, the river network was divided into different segments based on the measured bathymetry according to the Hydrographic Atlas. The interpolated pseudo-bathymetry was compared with classified measured bathymetry to indentify which segments were not interpolated within an expected similarity (equal or larger than 60%). The segments along the upstream river network were then adjusted iteratively to maximize the value of the proportion correct so as to improve the pseudo-bathymetry interpolation.

Even though the discriminant analysis result showed similar *proportion correct*, the cross-sectional area at each delineated cross-section might be different. Consequently, it is important to interpolate different pseudo-bathymetries at each cross-section and then the cross-sectional areas extracted from the measured bathymetry and the pseudo-bathymetries were compared at the mean stage along the upstream river network on the date when the SPOT image was taken. In this study, according to the

preliminary analysis, two pseudo-bathymetries were developed to sufficiently reflect the measured bathymetry, namely: (i) the first pseudo-bathymetry – developed based on three segments along Channel 2 and 3 and two segments along Channel 4 and 5; and, (ii) the second pseudo-bathymetry – developed based on three segments along Channel 2 and 3 and three segments along Channel 4 and 5. The pseudo-bathymetry which created least difference in terms of cross-sectional area compared to the measured bathymetry was chosen as a base to interpolate the pseudo-bathymetry of the downstream river network.

The geomorphological features along the downstream river network were also referred in order to help create the pseudo-bathymetry. According to Bambati and Carulli (2001), the 'side channels' were occasionally dry during the dry season while other parts were shallow or deep at distinguished geomorphological units. Therefore, the 'shallow' and 'deep' channels along the downstream river network were interpolated according to the relationships between the SPOT interpolation and the 'shallow' and 'deep' segments along Channel 4 and 5, respectively. Such geomorphological features will be further discussed in Chapter 5.

4.2.3 The integrated DEM

In the Hydrographical Atlas, the bathymetry was measured along the main navigation channels. The sections of channel with the measured bathymetry data are presented in Figure 4.2-5.

Figure 4.2-5: Channel sections with available measured bathymetry in the study area (*Source*: the Hydrographic Atlas)

Figure 4.2-6 illustrates the procedure to integrate different sources of information into one integrated DEM. In order to create an integrated DEM, in which both the elevation of the land surface and the bathymetry of the full river network were presented, the measured bathymetry data (the measured cross-sections extracted from the Hydrographic Atlas with the average distance between the cross-sections was from about 200 m to 450 m), the pseudo-bathymetry data (developed from the SPOT image) and a point layer which was interpolated from the SRTM to represent the land surface elevation were merged and then interpolated (according to the *Natural Neighbor* approach (Sibson, 1981; Watson, 1992) in ArcGIS *v.*9.3) into an integrated DEM.

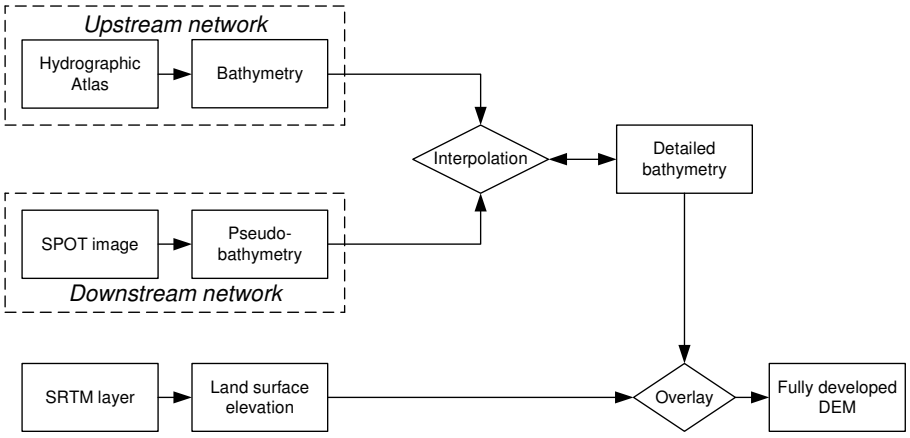

Figure 4.2-6: Procedure for developing an integrated DEM

4.3 Raster-based model for wetted-section mapping

A tilted DEM was applied to estimate the wetted-section along the river network with a common water surface slope throughout the whole network. This approach was applied in order to estimate the 'possible' flooding extent for the complex river network (based on the recorded stages at Channoy and Haxaykhoun) so that the cross-section delineated in the HEC-RAS model may cover the likely-estimated inundated area. Figure 4.3-1 illustrates how to tilt the DEM according to a common slope. The elevation of the first row of the DEM was constrained to its original value but the rest were tilted according to a pre-defined angle (α) corresponding to the water surface slope calculated according to the differences in water surface elevation at Channoy and Hatxaykhoun and the distance between the two stations (approximately 20,000 m). From the second row of the DEM onwards, the elevation was re-calculated based on its own original elevation plus the tangent of the predefined angle and then multiplied by the raster cell size (50 m). Because the slope was small, the tangent of the slope could be considered as the value of the slope itself (Equation 4.3-1). The wetted-section and the flooding patterns along the river network were estimated based on the stages recorded at Channoy horizontally flowing through the tilted-DEM.

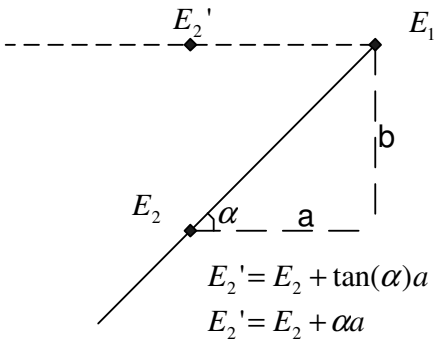

Figure 4.3-1: Tilted-DEM approach

$$E_2' = E_2 + \alpha a$$ **Equation 4.3-1**

where,

E_1: Water surface elevation at the upstream cell (m)

E_2 and E_2': Water surface elevation at the downstream cell before and after tilted (m)

a: Cell size (m)

b: Elevation differences (m)

α: Water surface slope (mm^{-1})

4.4 A one dimensional (1D) physical-based hydraulic model

4.4.1 The steady-flow calculation in HEC-RAS

A subcritical-1D steady state calculation in HEC-RAS was applied according to the following assumptions: (i) Flow is comparatively steady (the hydraulic nature of a point within a cross-section remains constant over time) along the full river network; (ii) Flow varies gradually between cross-sections (spatially changes along a long profile); (iii) The water surface slope is less than 10%; and, (iv) Flow is considered 1D (only velocity variation along a long profile is considered). The computational procedure is undertaken based on the solution of the 1D energy and momentum equations. In this study, it was assumed that the hydraulic nature does not change rapidly along the river network. Therefore, the energy equation was applied instead of the momentum approach. In addition, due to the lack of the measured bathymetry along the downstream river network, the momentum approach which requires very well-defined bathymetry for the centroid of each cross-section could not be applied.

The energy equation used in HEC-RAS is the 1D St Venant equation to simulate the open-channel flow. Horizontal exchange of discharge between channels and floodplains are assumed to be insignificant and the discharge is distributed according to the conveyance. The assumption is fulfilled in this study because the river network is large and therefore the discharge going beyond the banks during the flooding period is not significant compared to the total conveyed discharge. The in-channel discharge can be calculated (Equation 4.4-1), in which the ratio between the in-channel and total discharge was calculated as presented in Equation 4.4-2 and the floodplain conveyance was calculated as presented in Equation 4.4-3.

$$Q_c = \phi Q \qquad \textbf{Equation 4.4-1}$$

where:

Q_c: Discharge in channel (m^3s^{-1})

Q: Total discharge (m^3s^{-1})

ϕ: Ratio between the discharge in channel and the total flow

$$\phi = \frac{K_c}{K_c + K_f} \qquad \textbf{Equation 4.4-2}$$

where:

K_c: Conveyance in channel (m^3s^{-1})

K_f: Conveyance in the floodplains (m^3s^{-1})

$$K_f = K_{lob} + K_{rob} \qquad \textbf{Equation 4.4-3}$$

where:

K_{lob} and K_{rob}: Conveyance in the left (lob) and right over bank (rob), respectively (m^3s^{-1})

In addition, the conveyance and the 1D energy equations are defined as illustrated in Equation 4.4-4 and Equation 4.4-5, respectively.

$$K = \frac{A^{5/3}}{nP^{2/3}}$$ **Equation 4.4-4**

where:

P: Wetted perimeter (m)

A: Cross-sectional area (m^2)

n: Manning's roughness coefficient ($sm^{-1/3}$)

$$S_c = \frac{\phi^2 Q^2 n_c^{\,2}}{R_c^{\frac{4}{3}} A_c^{\,2}}$$ **Equation 4.4-5**

$$S_f = \frac{(1-\phi)^2 Q^2 n_f^{\,2}}{R_f^{\frac{4}{3}} A_f^{\,2}}$$ **Equation 4.4-6**

where:

A_c, A_f: Cross-sectional area of channel and floodplain, respectively (m^2)

x_c, x_f: Distance along channel and floodplain, respectively (m)

R_c, R_f: In-channel and floodplain hydraulic radius, respectively (m)

S_c, S_f: In-channel and floodplain friction slope, respectively (mm^{-1})

ϕ: Ratio between the discharge in channel and the total flow

The cross-section is subdivided into different units with uniformly distributed velocity to calculate the conveyance over a single cross-section over the floodplain (Figure 4.4-1). In this approach, the cross-section is subdivided due to different Manning's n coefficients assigned to each subdivision. The conveyance is then summed to get the in-channel, left and right overbank conveyance.

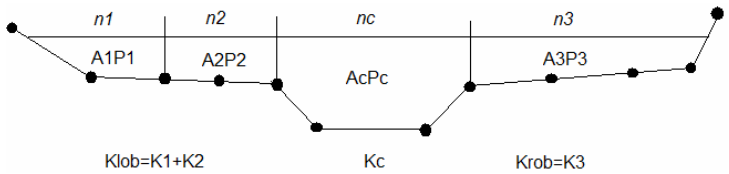

Figure 4.4-1: HEC-RAS conveyance subdivision method

The following is the general computational procedure for the subcritical hydraulic calculation, starting from the most downstream cross-section:

(i) Assume a water surface elevation at the immediate upstream cross-section;

(ii) Based on the assumed water surface elevation, determine the corresponding total conveyance and velocity head;

(iii) With the values identified from step (ii), compute S_f and solve the following equation for h_e.

$$h_e = LS_f + C\left|\frac{\alpha_2 V_2^2}{2g} - \frac{\alpha_1 V_1^2}{2g}\right| \qquad \textbf{Equation 4.4-7}$$

where:

h_e: Energy head loss between two cross-sections (m)

L: Discharge weighted reach length (dimensionless parameter)

$\overline{S}_f$: Representative friction slope between two cross-sections (mm^{-1})

C: Expansion or contraction loss coefficient (dimensionless parameter)

α: Velocity weighted coefficient (dimensionless parameter)

V: Mean velocity (ms^{-1})

g: Gravitational acceleration (m^2s^{-1})

(iv) With the value from steps (2) and (3), solve the following equation for the water surface

$$Y_2 + Z_2 + \frac{\alpha_2 V_2^2}{2g} = Y_1 + Z_1 + \frac{\alpha_1 V_1^2}{2g} + h_e \qquad \textbf{Equation 4.4-8}$$

where:

Y: Depth of water at cross-sections (m)

Z: Elevation of the main channel inverts (m)

Compare the computed value of water surface with the value assumed in step (i); repeat steps (i) through (iv) until the values agree to within 0.003 m (a default value in HEC-RAS), or a user-defined tolerance.

4.4.2 Development of HEC-RAS models for a river network with multiple outlet sections

a. The HEC-RAS model development

The cross-sections along the river network were developed in HEC-GeoRAS, an extension of HEC-RAS developed for ArcGIS, to extract the cross-sectional shape (geometry) for the HEC-RAS model. The planform of the river network was complex (*i.e.* different sinuosity values along the river network) and the channel bed was highly changeable. In fact, the cross-sections were not developed with similar distances but developed iteratively to reflect significant changes of cross-section and obtain an acceptable modelled energy gradeline (*i.e.* the energy head slope between the two neighbour cross-sections was smaller than 1.0×10^{-3} mm^{-1}). The cross-section was developed with a straight line for the channel-section to reflect the mean hydraulic nature of the flow (*e.g.* velocity). Along the floodplain, the cross-section was aligned according to the geometry of the land surface at each cross-section. The initial set of the cross-sections was developed to represent the downstream changes of the channel geometry (Figure 4.4-2). The differences in modelled water surface elevations or the energy head lost between the next two cross-sections along a channel were checked; if the water surface slope were smaller than 0.1 mm^{-1}, there was no need to interpolate cross-sections between the cross-sections, otherwise, additional cross-sections (in the middle of the two cross-sections) were interpolated in HEC-RAS until the slope became smaller than 1.0×10^{-3} mm^{-1} (Totz, 2003).

The individual cross-sections developed for the HEC-RAS model do not cross each other but some intersect, especially for the cross-sections around junctions. In fact, at junctions, where the channel banks had often low elevation, the modelled water surface elevation would be higher than the elevation of the banks, especially in the flooding models, but the extent of the resultant flood was not known a *priori*. The cross-sections were developed with the join of cross-sections at one end where the cross-sections of two neighbouring channels (*e.g.* Channel 2 and 4; Figure 4.4-2) join on an intervening island, the joining point was defined as the local maximum in the conjoined sections profile.

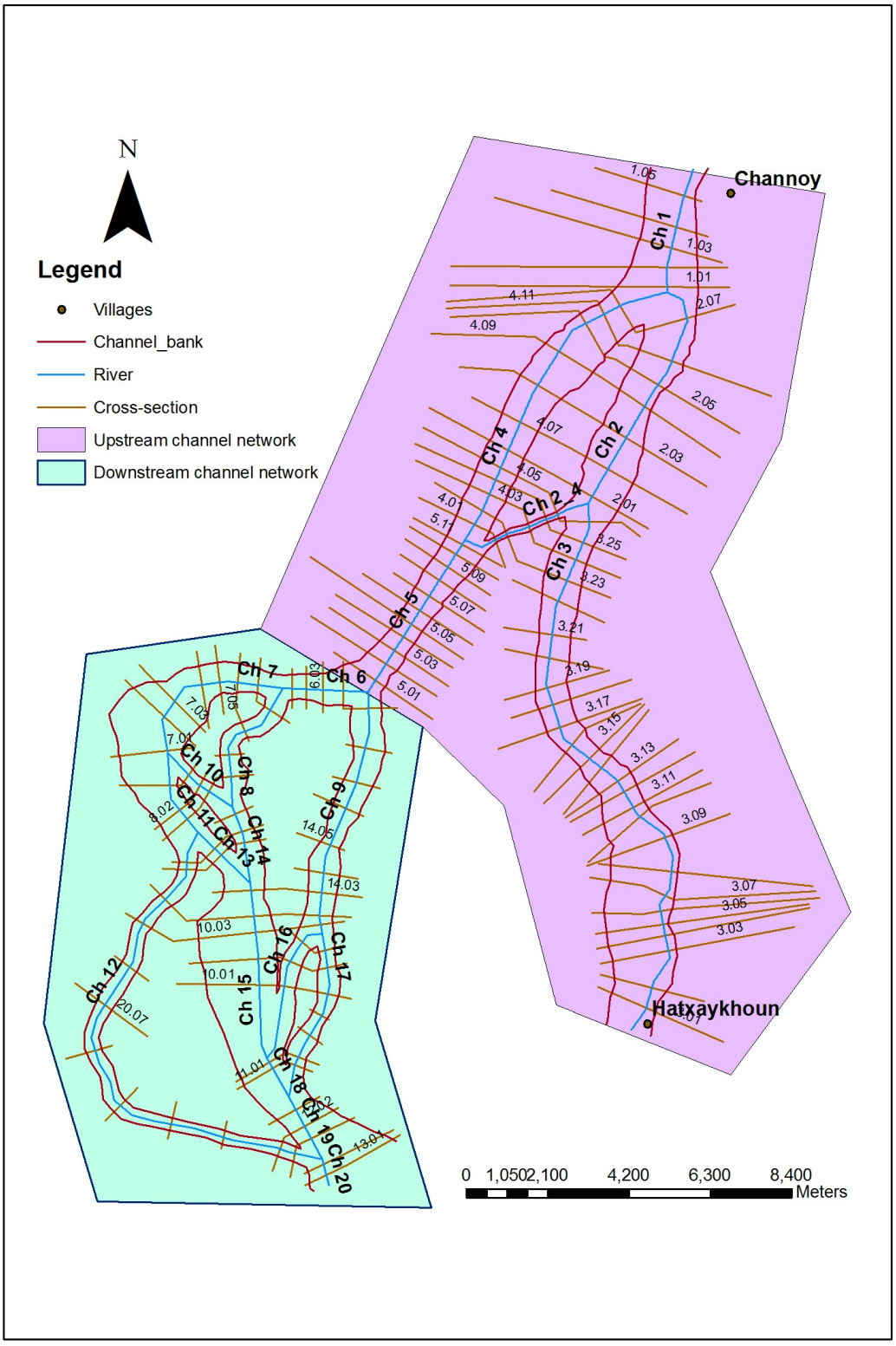

Figure 4.4-2: HEC-RAS models developed for both low and flood discharges

At the Channoy stage gauge, the recorded water surface elevations were used as the upstream boundary conditions of the HEC-RAS model. There was no information on

discharge at the Channoy stage gauge; therefore, the recorded discharges at the Pakse gauging station were used instead. Along Channel 2 and Channel 3, the downstream boundary conditions were the recorded stages at the Hatxaykhoun stage gauge.

Along Channel 4 and Channel 5, in the low entry discharge scenario, there was no available recorded stage other than the channel geometry extracted from the available DEM and the top-width at each cross-section extracted from the SPOT image. By using WinXSPRO, a software package designed to analyze stream channel cross-section data for geometric and hydraulic parameters, the water surface elevation at each cross-section corresponding to the top-width were identified. Based on the interpolated slope, the water surface elevation at the end of Channel 5 could be calculated. In addition, the literature review showed different water surface slopes between channels along anabranching networks during low discharges but there was no information for the high discharge conditions. Consequently, for the flood discharge scenarios (average and high flood discharges), the water surface slope was assumed to be similar over the full river network (the water surface slopes along Channel 4 and 5 were assumed to be equal to that along Channel 2 and 3); the calculated slopes from Channoy to Hatxaykhoun were applied to Channel 4 and 5 as well, as the initial constraint and subsequently, the water surface slope was adjusted if required. The approach applied to calculate the boundary conditions along Channel 4 and 5 would be further developed to identify the boundary conditions (water surface slope and stages) at the downstream river network. The full river network models would use the calculated Manning's *n* coefficient at each cross-section along the upstream river network and the calculated water surface elevations at each cross-section along Channel 4 and Channel 5 based on the full river network were compared to those calculated based on the upstream river network to check the results.

Another important input data set is the entry discharge into each single channel of the river network. However, there was no available information on the splitting discharge at each bifurcation along the study river network. Most research concerning junctions mainly focused on understanding the fluvial processes (Kleinhans *et al.*, 2008; Makeske *et al.*, 2009; Richardson and Thorne, 2001) along a river network but no information was provided on the splitting discharge at a bifurcation. The symmetry ratio was used by Zavadil *et al.* (2007) just to examine the magnitude of channel adjustment at confluences. In the Mekong, the lack of field data and basic knowledge

on the splitting discharge at each bifurcation led to the requirement for an assumption on the splitting discharge. In this study, the assumption was that the ratio of cross-sectional areas of the first cross-section of the channels downstream of a bifurcation node was similar to that of the splitting discharge at each bifurcation. The *Flow Optimization* option was applied at all bifurcations along the river network in order to minimize any rise or drop of water surface profile by changing the initial assumed entry discharge into each channel downstream. In addition, in the HEC-RAS model, at each confluence, the discharge entering the downstream channel was automatically calculated as the summation of the discharges of the on-coming channels.

b. Boundary conditions

The downstream water surface elevation at the Hatxaykhoun gauge, the end of Channel 3, would be used as the model boundary condition while the upstream water surface elevation at the Channoy gauge would be used to validate the hydraulic models by comparing the modelled water surface elevation with the recorded water surface elevation at the gauge. In addition, the boundary conditions at the end of Channel 5 were the interpolated water surface elevation as described previously and then corrected until the modelled water surface elevations at Channoy met the pre-defined ones and there was no significant jump or drop along the water surface profile, especially at each bifurcation.

The in-channel hydraulic roughness (Manning's n) was calculated as presented in Section 4.5 while the hydraulic roughness on the floodplain for the flood discharge models was set according to the published literature with reference to the land cover pattern on the floodplain. Five land cover types (paddy rice field, shrub, natural forest, degraded forest, bare soil) were distinguished in the area and the hydraulic roughness of each land cover type will be presented in Chapter 6.

c. Default settings of the HEC-RAS model

The default values for expansion and contraction coefficients (0.3 and 0.1, respectively) are retained in this study. In fact, such default values are applicable to subcritical flow calculation (Totz, 2003) and widely accepted (Carling and Grodek, 1994; Peppenberger *et al*, 2005; Mosquera-Machado and Ahmad, 2007; Thompson *et al.*, 2007; Remo and Pinter, 2007) and will only be changed if there is strong evidence

of abrupt changes of flow direction leading to differences of the expansion and/or contraction coefficients along a channel (Totz, 2003).

4.5 Calibration and validation of the HEC-RAS model

4.5.1 The upstream river network

a. The HEC-RAS modelling using the measured DEM

- **Low discharge scenario**

The approach described in this section was not applied to the cross-channel (Channel 2_4) for the low discharge model as there was no relevant data to calculate or to estimate the water surface slope in the channel. By field observation, the cross-channel was sand-bed and according to Latrubesse (2005) and many others the Manning's *n* coefficient of this channel type was about 0.02. This value of the Manning's *n* was applied to Channel 2_4 and then adjusted so that the modelled water surface elevation at Channoy met the recorded one at the upstream boundary.

To calibrate the HEC-RAS model in the low discharge scenario (Figure 4.5-1), the top-width at each cross-section was identified according to the SPOT image (taken in 2003) (Figure 4.5-2). By using WinXSPRO, the water surface elevation at each cross-section corresponding to the predefined top-width was identified. The Manning's *n* roughness coefficient was calculated at each cross-section in MS Excel according to the adjusted version of the Manning's equation (Equation 4.5-1) and then applied in HEC-RAS. At a bifurcation, in theory, the difference in water surface elevations at the last cross-section of the upstream channel and the first cross-section of the downstream channel should be less than 0.03 m while the distance between the two cross-sections should not be larger than 30 m (Totz, 2003). It means that in the large river network where the distance between cross-sections was much larger than 30 m, the water surface slope between the two cross-sections could be used instead and the slope should not be larger than 1.0×10^{-3}. If the modelled water surface slope between the two cross-sections was larger than 1.0×10^{-3}, the interpolated water surface slope at the end of Channel 5 (*normal depth* - the depth corresponding to uniform flow (Chow, 1959) and calculated according to the cross-sectional shape, water surface slope and discharge) of the HEC-RAS model would be adjusted.

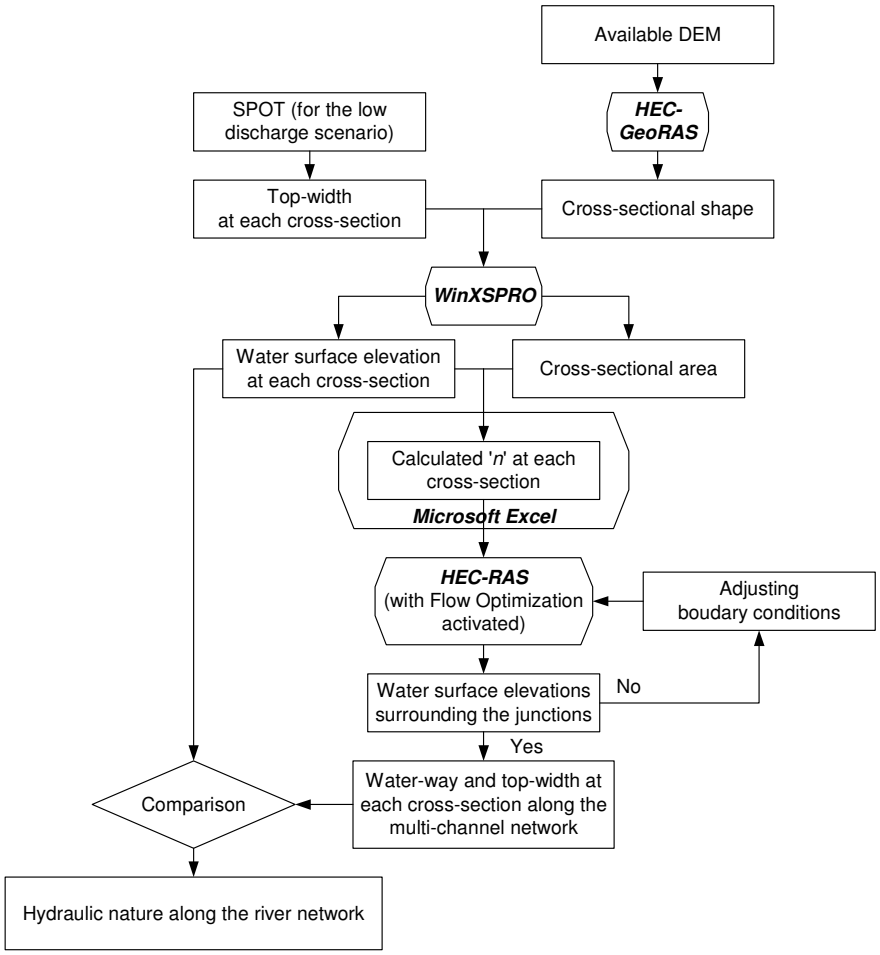

Figure 4.5-1: Routine to calibrate the hydraulic roughness along the upstream river network in the low discharge

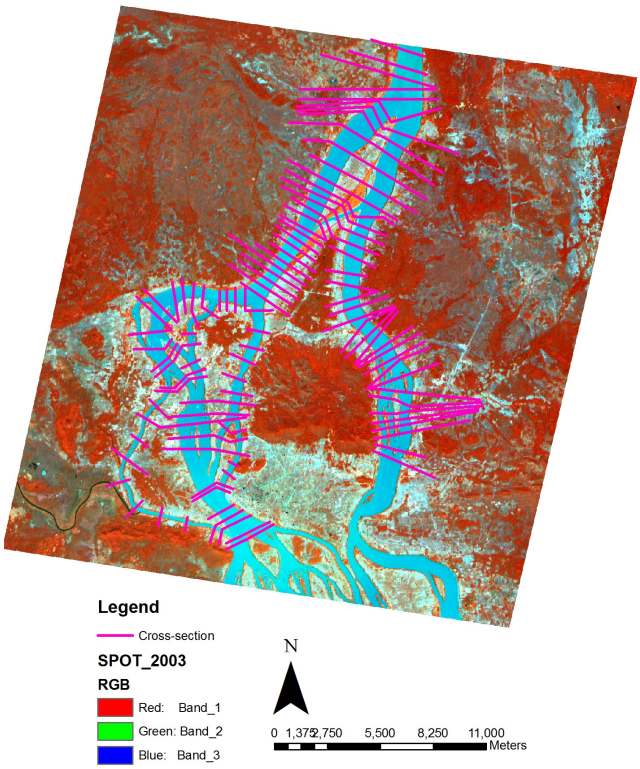

Figure 4.5-2: SPOT 2 (taken in 30th October, 2003) and cross-sections developed for the HEC-RAS models

The (base) in-channel hydraulic roughness (Manning's *n*) was calculated as follows (Equation 4.5-1):

$$n_b = \frac{1}{QW^{2/3}} A^{5/3} S^{1/2} \qquad \textbf{Equation 4.5-1}$$

where:

n_b: The (base) in-channel Manning's *n* hydraulic roughness ($sm^{-1/3}$)

Q: Entry discharge (m^3s^{-1})

A: Cross-sectional area (m^2)

S: Water surface slope (mm^{-1})

W: Top-width at a cross-section (m)

The applied Manning's *n* (according to Equation 4.5-1) was the base Manning's n_b adjusted according to the effect of the obstruction (islands) and degree of meandering (Equation 4.5-2) (Aldridge and Garett, 1973). Table 4.5-1 illustrates the value of the adjusted factors corresponding to the brief description geometry.

$$n = (n_b + n_*)m$$ **Equation 4.5-2**

where,

n_b: Base n value for channel

n_*: Effect of obstruction

m: Degree of meandering

The 'm' factor was selected according to the sinuosity of the different segments along the river network (Table 4.5-1). The sinuosity was calculated as the ratio between the total length of channels per unit length of river. The former was measured along the starting and ending point of the channel segment while the latter was measured along the thalweg of the channels.

Table 4.5-1: Effect of geometry on the hydraulic roughness of the channel (Arcement and Schneider, 2008)

Description	Adjusted value	Description
Effect of obstructions	0.000	No island found in the cross-section
(n_*) including vegetation	0.045	Islands found in the cross-section
Degree of meandering	1.000	Range of channel sinuosity: [1.0 to 1.2]
	1.150	Range of channel sinuosity: [1.2 to 1.5]

- **Flood discharge scenario**

Pilgrim (1976) showed that average in-channel velocity is a non-linear function of discharge but reaches an asymptotic value at high flows. Even though, Pilgrim (1976) did not mention the water surface slope, especially along a multi-channel network, it can be used as a base for the assumption that the water surface slopes along channels within the upstream river network were similar in the flooding scenario. In fact, according to Carling and Wood (1994) and Wohl (2007), the local water surface slope was fluctuated highly in the low discharge but such variation became insignificant when the discharge reached the bankfull one. To identify the hydraulic roughness value at each cross-section in MS Excel, a common water surface slope (S = 1.28 x 10^{-4} and 1.68 x 10^{-4} for the average flood and high flood, respectively which were calculated according to the recorded stages along Channoy and Hatxaykhoun) was applied to all channels except Channel 2_4. The water surface slope in Channel 2_4 was calculated according to the difference between water surface elevation at the first cross-section of Channel 3 and 5 and the distance along the cross-channel. The water surface elevation at each cross-section was calculated according to the initial slope

and the distance between the cross-section and its neighbour. With the defined water surface elevation, the cross-sectional area and top-width at each cross-section were identified by using WinXSPRO. The base Manning's n_b at each cross-section was calculated (in MS Excel) and further adjusted according to Equation 4.5-2 and applied in HEC-RAS. The model would be checked by the acceptable water surface slope (less than or equal to 1.0 x 10^{-3} mm^{-1}) between the last cross-section of the upstream channel and the first two cross-sections of the two downstream channels. If the model was not validated, the boundary condition of the HEC-RAS model would be adjusted. Figure 4.5-3 illustrates steps for calculating the hydraulic roughness at each cross-section and modelling the flooding pattern along the upstream river network in HEC-RAS.

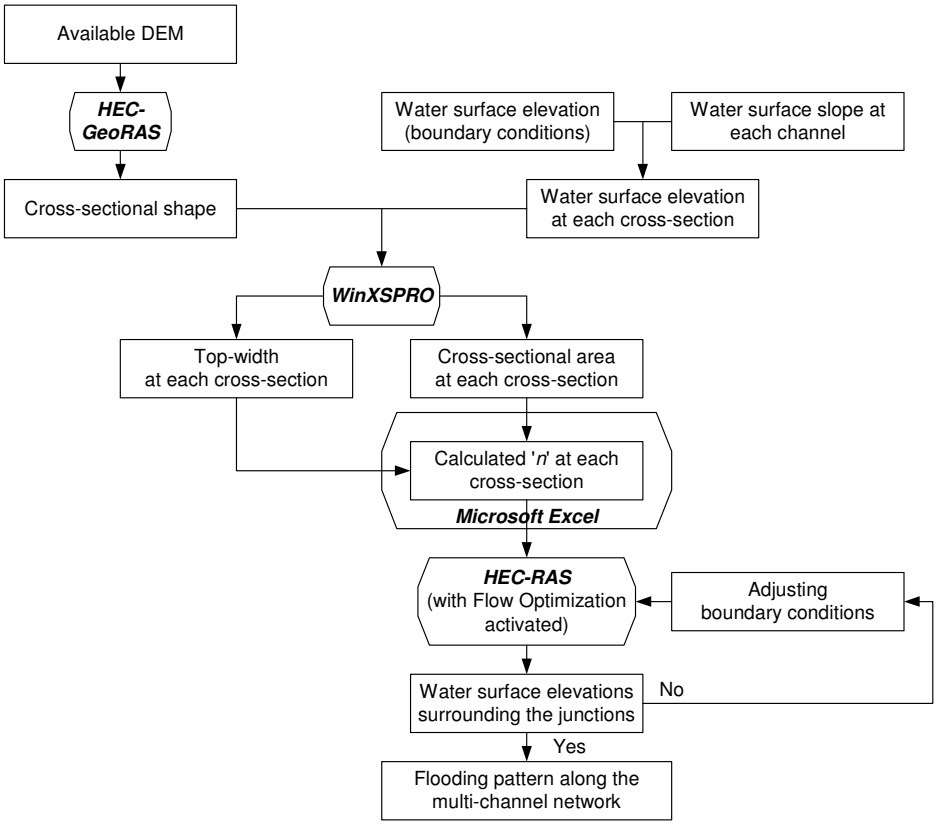

Figure 4.5-3: Routine to calibrate the hydraulic roughness along the upstream river network in the flood discharge

b. The HEC-RAS model using pseudo-bathymetry

To examine the impact of using pseudo-bathymetry on the results of the 1D hydraulic modelling, two types of analysis were done: (i) Applying the identical boundary conditions and hydraulic roughness coefficient at each cross-section for the pseudo-bathymetry; and (ii) Changing the boundary conditions (from the known water surface

elevation to the water surface slope) and hydraulic roughness coefficient along Channel 4 and 5 (from those calculated according to the measured bathymetry to those calculated according to the pseudo-bathymetry), from which the pseudo-bathymetry of the downstream river network would be developed. The modelled water surface profiles calculated according to the pseudo-bathymetry would then be compared to those obtained from the measured bathymetry HEC-RAS model to validate if the pseudo-bathymetry was acceptable to develop the HEC-RAS model for the full river network.

4.5.2 The downstream river network

The water surface elevation is often different from one bedrock-confined channel to its neighbours (Broadhurst and Heritage, 1998); therefore, the water surface slope might be different between channels along the downstream river network. Even though the top-width at each cross-section was extracted from the SPOT image, according to the poor quality of the available DEM (channels appeared in the DEM to be either wider or narrower than the natural channels), the water surface elevation at each cross-section along the downstream river network might not be estimated accurately. In addition, the number of delineated cross-sections along each channel in the downstream river network was not sufficient to correctly interpolate the water surface slope leading to inaccurate estimation of the Manning's *n* coefficient at each cross-section.

According to Hicks and Mason (1991), the lowest Manning's *n* coefficient along the alluvial-filled bedrock channel was 0.009. However, to make the full river network model work (*i.e.* to eliminate the drop or rise of water surface profile, especially at each bifurcation and to minimize the differences between the modelled and recorded stages at the stage gauges), the minimal value of the hydraulic roughness along the downstream network was iteratively defined as greater than 0.007 in the low discharge and 0.009 in flood discharge models. The lower boundary (at the end of the downstream river network) was calibrated iteratively based on the *normal depth* (water surface slope) to make the modelled water surface elevations along the upstream river network meet those in the upstream river network model (Chapter 6).

4.6 Other possible approaches for river network modelling

Different approaches had been tried to model the river network in the Siphandone wetlands. Principally, the approaches met the requirements of the study. However, due to the complexity of the river network, the obtained results were not acceptable therefore will not be presented in the successive chapters of results. However, discussions are briefly given to explain why the approaches were not successful and how they might be improved (Chapter 8).

4.6.1 A reduced complexity (raster-based) model (CAESAR - Cellular Automaton Evolutionary Slope And River)

There are available models using reduced complexity theory for landscape modelling (Coulthard and Macklin, 2001), channel evolution (Murray and Paola, 1994, 1997) and flood estimation (Rinaldi *et al.*, 2005). Amongst others, CAESAR is a popular reduced complexity model which can be used to estimate flood pattern (according to flood discharge) and water way using low discharge) along a complex river network (Coulthard, 1996).

To route water along a channel network, CAESAR uses a four-dimensional scanning algorithm as illustrated in Figure 4.6-1. The first scan (Box 1) is taken from right to left (looking downstream) and discharge is routed from the current cell to a set of neighbouring cells with lower elevation. In the case where there is no cell with lower elevation relative to the current cell, but the combination of the bed elevation and water column is higher than the combined elevation of the neighbouring cells, discharge is retained in the current cell up to the height of the obstruction whilst the rest is routed onwards. When a 'valley' is reached, the scan continues 'uphill' without moving any discharge (Box 2). Next, a similar calculation is performed in Box 3 but in the opposite direction of that performing in Box 1. The last scan directs discharge downstream (Box 4). The surface flow is routed as in the described scanning routing and the proportion routed to the neighbouring cells is calculated as presented in Equation 4.6-1.

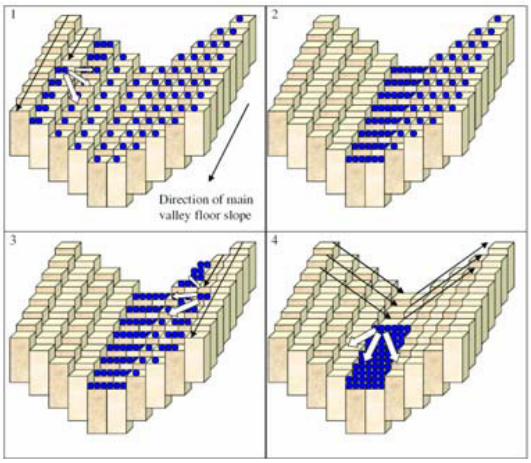

Figure 4.6-1: Schematic of the scanning algorithm (Coulthard *et al.*, 2002)

$$Q_i = Q^{S_i}/\sum S_i \qquad \textbf{Equation 4.6-1}$$

where:

Q: Discharge at the current cell (m^3s^{-1})

Q_i: Discharge delivered to the neighbouring cell i from the current cell (m^3s^{-1})

S_i: Local water surface slope of the current cell and its neighbours (cell i) (mm^{-1})

The differences in slope between diagonal neighbours are accounted for dividing by $\sqrt{2D_x^2}$ (where, D_x – the grid cell size, m). The depth is calculated using a rearrangement of the Manning's equation (Equation 4.6-2) and the discharge water is then routed (Equation 4.6-3).

$$d = (Qn/S^{0.5})^{(3/5)} \qquad \textbf{Equation 4.6-2}$$

$$Q_i = Q^{(e+d)-e_i}/\sum (e+d)-e_i \qquad \textbf{Equation 4.6-3}$$

where:

d: Remaining water depth at the current cell (m)

n: The Manning's hydraulic roughness coefficient ($sm^{-1/3}$)

S: Mean water surface slope (mm^{-1})

e: Combined elevation (the bed elevation and the water column) (m)

4.6.2 The Optimization Algorithm (OpA)

The OpA (based on Solver module in Microsoft Excel) could be applied to automatically calibrate the roughness at each cross-section along the river network to make the model match the measured top-width at each cross-section (extracted from the SPOT image). Because the hydraulic roughness of a channel is affected by the channel bed nature and other parameters like sinuosity, the hydraulic roughness set alone cannot resolve if the channel bed is bedrock or not. However, in the case of the study area, most parts of the river network have low sinuosity (especially in the northern bifurcation); therefore, the hydraulic roughness alone is suggested to be able to reflect the channel bed nature.

In the OpA, the changing variables are the Manning's *n* coefficient at each cross-section with the following constraint: $0.009 \leq n \leq 0.9$ where 0.009 is the smallest hydraulic roughness for a large alluvial channel (Latrubesse, 2008) and 0.9 is the greatest hydraulic roughness for a bedrock-influenced channel (Heritage *et al.*, 2004, Kidson *et al.*, 2006; Carrivick, 2009). The objective function (Equation 4.6-4) is the summation of differences in the width of the wet area of each cross-section achieved from a SPOT image and from the HEC-RAS model:

$$f(x) = \sum Difference\,in\,width\,of\ wetted\,area\,achieved\ from\,SPOT\,and\,HEC-RAS$$

$$f(x) \rightarrow \min \qquad \textbf{Equation 4.6-4}$$

Figure 4.6-2 illustrates the framework of coupling of HEC-RAS (Task A) and the OpA (Task C). Task (A) is to model the flow within the channel network with reference to a single Manning's *n* coefficient and the ratio of splitting discharge at each junction was identified according to the ratio of the first cross-section of each downstream reach. Task (B) is to identify the wetted-width (at each cross-section) from the SPOT image. After that, task (C) is utilized to minimize differences between the SPOT image and the HEC-RAS model at each cross-section based on the OpA. In task (C), the objective function (to minimise differences between the top width at each cross-section achieved in HEC-RAS and from the SPOT image), the changing parameters (Manning's *n* coefficient (at each cross-section)) and the constraints of the optimized model, including: (i) the summation of discharges within the two downstream branches was the discharge at the entry reach; (ii) the acceptable ratio of

discharges entering each downstream branch; and, (iii) Manning's *n* coefficient at each cross-section must be greater than or equal to 0.009 and less than or equal to 0.9, must be clarified.

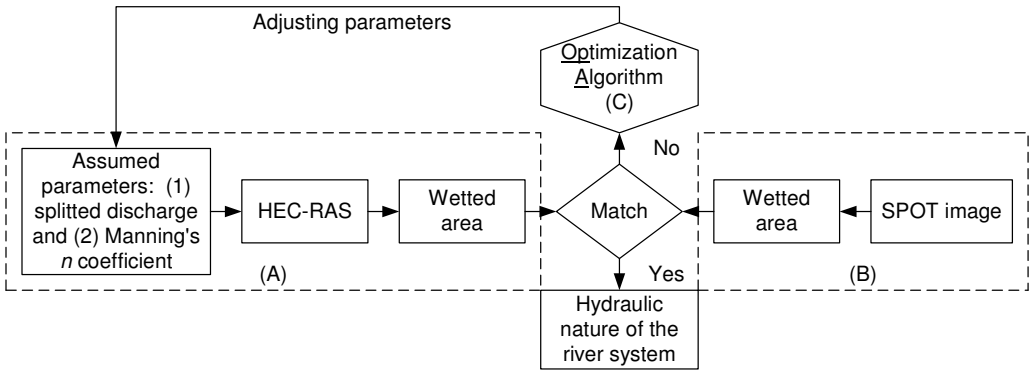

Figure 4.6-2: The coupling of the Optimization Algorithm and HEC-RAS

4.7 Considered hydraulic parameters

In the 1D hydraulic modelling, the mean hydraulic parameters at each cross-section were considered. The important hydraulic parameters presented in this research were:

- *Mean velocity:*

$$U = \frac{Q}{A} \qquad \textbf{Equation 4.7-1}$$

- *Froude number*:

$$Fr = \frac{U}{\sqrt{gD}} \qquad \textbf{Equation 4.7-2}$$

- *Shields parameter*:

$$\tau_* = \frac{RS}{(\frac{\rho_s}{\rho} - 1)d_s} \qquad \textbf{Equation 4.7-3}$$

- *Particle Reynolds number*

$$\mathrm{Re}_* = \frac{U_* d_s}{\upsilon} \qquad \textbf{Equation 4.7-4}$$

where,

U: Mean velocity at each cross-section (ms^{-1})

Q: Entry discharge (m^3s^{-1})

A: Cross-sectional area (m^2)

Fr: Froude number (dimensionless)

g: Gravity constant (ms^{-2})

D: Hydraulic depth (m)

R: Hydraulic depth (m)

Re_*: Particle Reynolds number

S: Water surface slope (mm^{-1})

d_s: Sediment size (m)

U_*: Shear velocity

ρ and ρ_s: Fluid and sediment density (kgm^{-3})

τ : Shear stress (Pa)

v: Kinematic viscosity (m^2s^{-1})

In addition, at-a-station hydraulic geometry analysis (Leopold and Maddock, 1953) was done at Pakse and Channoy (for the general discussion (Chapter 8) on understanding the hydraulic geometry at different river networks)_according to the following equations (Equation 4.7-5, Equation 4.7-6 and Equation 4.7-7, in which the exponents indicate rate of increase in hydraulic variables (W, D, U) with increasing discharge (Q)):

$$W = aQ^b \qquad \textbf{Equation 4.7-5}$$

$$D = cQ^f \qquad \textbf{Equation 4.7-6}$$

$$U = kQ^m \qquad \textbf{Equation 4.7-7}$$

Given the power-law forms, the continuity relation can be shown in Equation 4.7-8, Equation 4.7-9 and Equation 4.7-10.

$$Q = WDU \quad \textbf{Equation 4.7-8}$$

$$ack = 1 \quad \textbf{Equation 4.7-9}$$

$$b + f + m = 1 \quad \textbf{Equation 4.7-10}$$

where,

W: Top-width at the cross-section

a, c, k, b, f and m: Constant

Summary

This chapter presents the approaches to model the complex bedrock-confined anabranching network with the lack of input data. The 1D steady flow calculations were applied with three levels of the upstream discharges corresponding to the low flow and average and high flood discharges. The boundary conditions were based on the recorded stage at the stage gauge and interpolated based on the SPOT image. The bathymetry was created according to the measured cross-section along the navigating channels (upstream river network) and the pseudo-bathymetry along the complex anabranching network (downstream river network) was interpolated in accordance with the SPOT image. The hydraulic roughness was calculated at each individual cross-section based on: (i) the channel geometry extracted from the interpolated bathymetry; and, (ii) predefined entry discharge into each individual channel, which is automatically adjusted based on the *Flow Optimization* option in HEC-RAS.

Chapter 5: Pseudo-bathymetry interpolation and the application of a raster based model for wetted-section mapping

Introduction

Development of a full DEM including detailed geometry of a remote river network and floodplains, which could then be used for hydraulic modelling, was challenging. This chapter presents a novel approach to derive a pseudo-bathymetry (the geometry of the river network interpolated according to a range of elevation (*e.g.* shallow and deep section corresponding to high and deep channel bed), but no detailed elevations showing the continuous surface of the channel bed). The pseudo-bathymetry was developed in accordance with a combination of the red and green band reflectance from a SPOT image for the study river network. The approach was validated by comparing the developed pseudo-bathymetry to the measured bathymetry along the upstream river network and then the method was applied to estimate the pseudo-bathymetry for the downstream river network (Chapter 4, Figure 4.4-2) with reference to the documented geomorphological features of the channels. In addition, a raster based approach (tilted-DEM approach) was applied to estimate the 'likely' wetted-section along the river network with a common water surface slope employed over the full river network. This raster based approach was used to estimate the areas possibly prone to flooding which would be used as a reference for determining the possible extent of cross-sections in a 1D hydraulic model, especially in the case of flood discharges.

5.1 Bathymetry interpolation

Among the available SPOT images, the image taken on 18th February 2005 was used to interpolate the pseudo-bathymetry. In fact, the entry discharge of the Siphandone river network was smallest (2,024 m^3s^{-1}) on the 18th February 2005 compared to other dates when the SPOT images were available so that the water column was lowest and the sediment load was assumed to be small compared with the load in other images at other times.

5.1.1 Masking the river network

A mask of the river network created to focus the unsupervised classification analysis on the channel network is presented in Figure 5.1-1. Because the unsupervised classification technique was applied to differentiate zones of the water body based on different combinations of reflectance of the red and green bands, the raster cells (on the SPOT image) near the channel banks were cropped out so that the classification results would not be distorted by other features nearby the banks (*e.g.* in-channel and in-bank vegetation). By iteratively constraining the pixel at the edge of the river network, the wetted-section was shrunk with the pixel values ranging from 1 to 75 in the near infrared (NIR) band. Due to the constraints, some wetted-area was not mapped in the mask of the channel network, marked by the ellipses (Figure 5.1-1). However, the wetted 'cropped-out' areas were mainly along the channel banks or along the channel 2_4 (Figure 5.1-1), relatively narrower and shallower than the main channels, where there was no measured bathymetry; therefore, the mask did not have any strong impact on the pseudo-bathymetry interpolation or the later analysis.

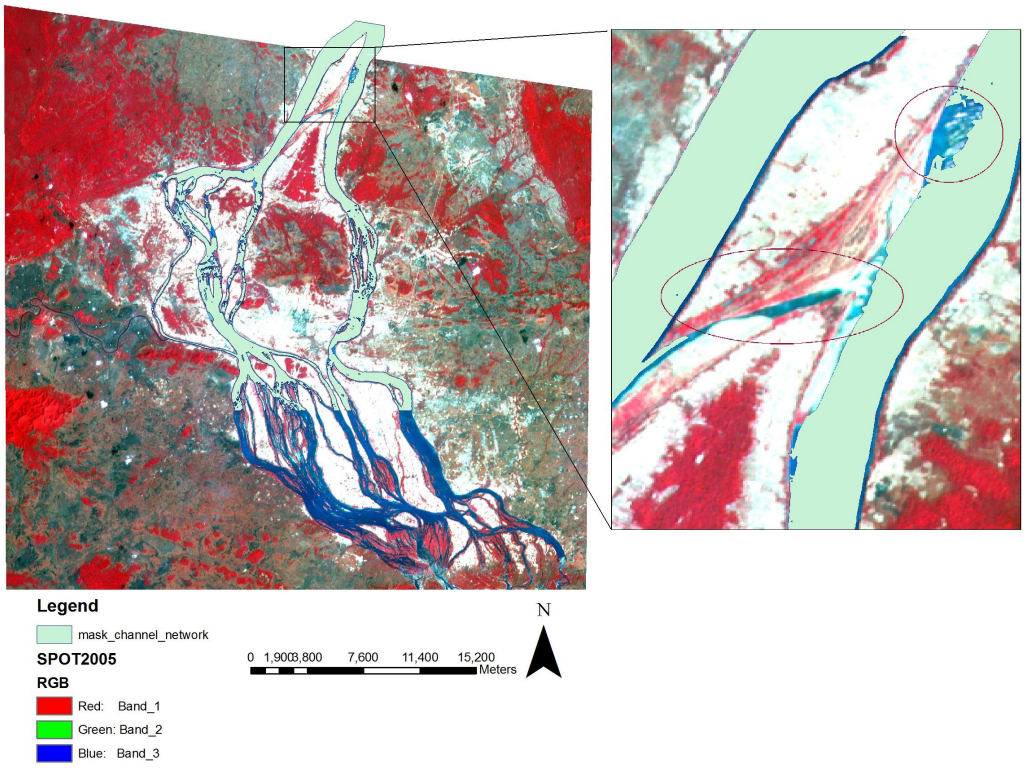

Figure 5.1-1: Water masking by the near inferred band

5.1.2 Interpolation of SPOT image for the upstream river network

The result of water body classification is presented in Figure 5.1-2, from which different zones of combination of reflectance could be realized. Along the eastern channels (Channel 2 and Channel 3), the most upstream section was mostly classified as classes 5, 6 and 7 while the upper middle was mainly classified as classes 8 and 9, the lower middle was mainly classified as classes 7 and 8, and the most downstream section was mostly classified as classes 2, 3 and 4. Along the right channels (Channel 4 and Channel 5), the upstream section was mainly classified with class 4 while the middle was a mix of classes 4, 5, 6 and 7 and the downstream channel was mostly classified as classes 4 and 5.

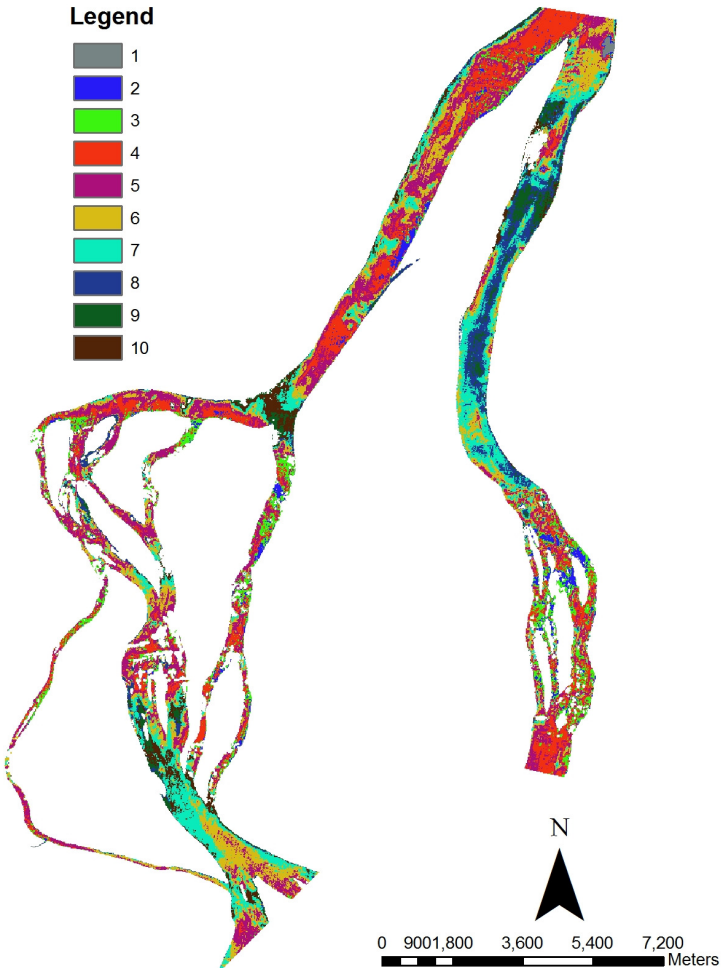

Figure 5.1-2: Classes after the unsupervised classification; Legend shows class units

To understand the relationship between the combinations of reflectance from the SPOT image at different segments of the river network and the measured bathymetry, a *discriminant analysis* (Chapter 4, section 4.2.2) between the measured bathymetry

and the river network classification was done. Two analyses of defining segments within the river network were accomplished, including: (i) Analysis 1 – Three segments along Channel 2 and Channel 3 and two segments along Channel 4 and Channel 5 were set; and, (ii) Analysis 2 – Three segments along Channel 2 and Channel 3 and three segments along Channel 4 and Channel 5 were determined. Different segments along the upstream river network in the two analyses are shown in Figure 5.1-3 and Figure 5.1-4. Note, because the relationship between the spectral values of the red and blue bands and the measured bathymetry along Channel 4 and Channel 5 would be used to interpolate the pseudo-bathymetry of the downstream river network, the main differences between the two analyses were the subdivisions along Channel 4 and Channel 5. Table 5.1-1 and Table 5.1-2 present results of the *discriminant analysis* for the two analyses.

The comparisons between the interpolated pseudo-bathymetries and a two-class bathymetry extracted from the measured bathymetry were presented in Figure 5.1-3 and Figure 5.1-4, which show the *similarity* and *difference* between the interpolated pseudo-bathymetry and the two-class measured bathymetry, respectively. The relationship between the classes defined in Figure 5.1-2 and the average channel bed elevation (which was calculated according to the measured bathymetry) along each segment in Analysis 1 and 2 are presented in Table 5.1-1 and Table 5.1-2, accordingly. Along the left channels, the pseudo-bathymetry at all segments in Analysis 1 was different from Analysis 2 from -0.02 m to +0.30 m and in general, the pseudo-bathymetry created from Analysis 1 was higher than Analysis 2 in terms of the interpolated altitude. However, because the subdivided segments along the right channels were different both in numbers and spatial distribution, the average pseudo-bathymetry was significantly different between the two analyses. In general, except the fact that the altitude interpolated according to pseudo-bathymetry in segment 4 in Analysis 2 was higher than that in Analysis 1, the rest of the channels along the right channel was assigned a lower altitude in Analysis 2 than that in Analysis 1.

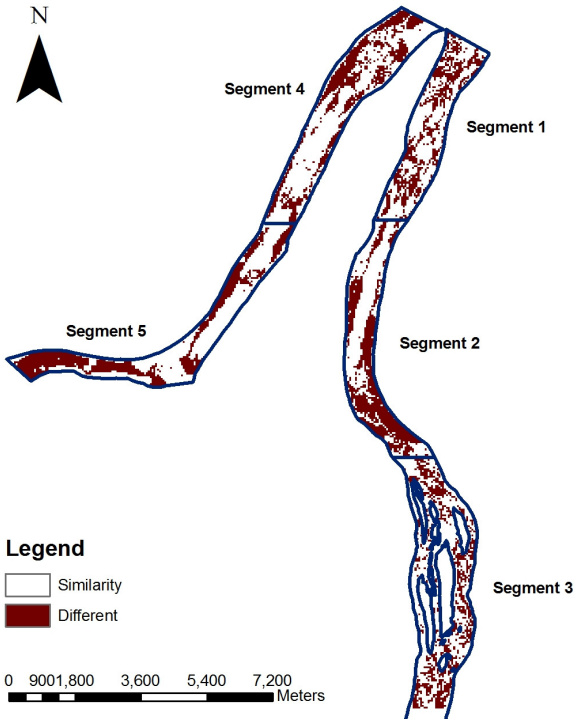

Figure 5.1-3: Comparison between the interpolated pseudo-bathymetry and the two-class bathymetry extracted from measured bathymetry (Analysis 1)

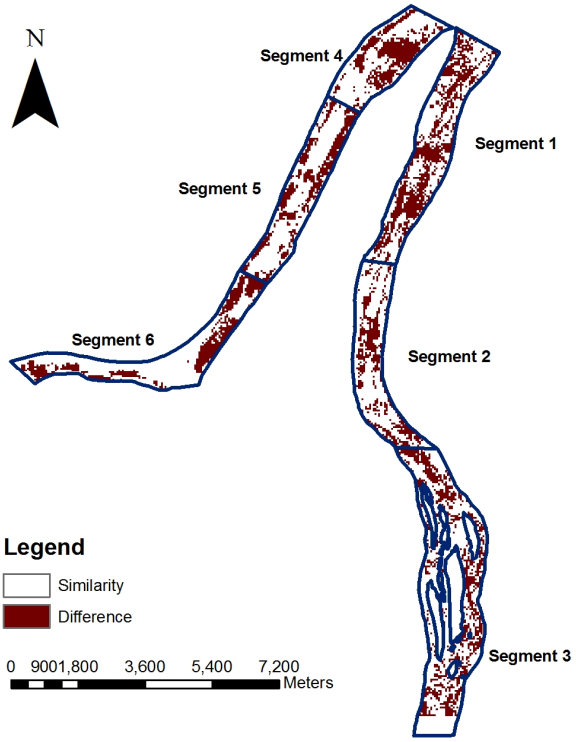

Figure 5.1-4: Comparison between the interpolated pseudo-bathymetry and the two-class bathymetry extracted from measured bathymetry (Analysis 2)

Table 5.1-1: Channel bed elevation of each class of different segments along the upstream river network (Analysis 1)

Segment	Classes	Mean channel bed elevation (m +MSL)
Segment 1	6, 9 and 10	79.315
	2, 3, 4, 5, 7 and 8	78.513
Segment 2	3, 4, 5, 6, 7 and 10	78.360
	7, 8 and 9	77.725
Segment 3	2, 3, 5, 6, 7, 8, 9 and 10	79.119
	1 and 4	78.271
Segment 4	2, 3, 4 and 8	78.763
	5, 6, 7 and 10	77.407
Segment 5	2, 3, 4, 5 and 6	76.201
	7, 8, 9 and 10	74.690

Table 5.1-2: Channel bed elevation of each class of different segments along the upstream river network (Analysis 2)

Segment	Classes	Mean channel bed elevation (m +MSL)
Segment 1	6, 9 and 10	79.072
	2, 3, 4, 5, 7 and 8	78.351
Segment 2	6, 7 and 10	78.136
	5, 8 and 9	77.338
Segment 3	2, 3, 5, 6, 7, 8, 9 and 10	79.090
	1 and 4	78.298
Segment 4	2, 3, 7, 8 and 9	79.431
	4, 5, 6 and 10	78.721
Segment 5	1, 2, 3, 4, 5, 8 and 9	76.827
	6, 7 and 10	75.282
Segment 6	3, 6, 7, 8, 9 and 10	76.256
	2, 4 and 5	73.438

The percentage of planview differences between the classified measured bathymetry and the pseudo-bathymetry is presented in Table 5.1-3. Details of the *discriminant analysis* and descriptive statistics for the pseudo-bathymetry along the upstream river can be found in *Appendix 2*.

Table 5.1-3: Proportion correct of the planview between the classified measured bathymetry and pseudo-bathymetry

Segment	*Proportion correct*	
	Analysis 1	Analysis 2
Segment 1	0.623	0.562
Segment 2	0.523	0.677
Segment 3	0.687	0.678
Segment 4	0.631	0.610
Segment 5	0.587	0.652
Segment 6	N/A	0.689
Whole network	0.615	0.646

Figure 5.1-5 and Figure 5.1-6 present the long profile along Channel 2 to Channel 3 and Channel 4 to Channel 5 based on the measured bathymetry and the interpolated pseudo-bathymetries. Even though there are differences between the interpolated pseudo-bathymetry and the measured bathymetry, the differences between the measured bathymetry and the pseudo-bathymetry in Analysis 2 is smaller than those in Analysis 1, especially along Channel 4 and Channel 5.

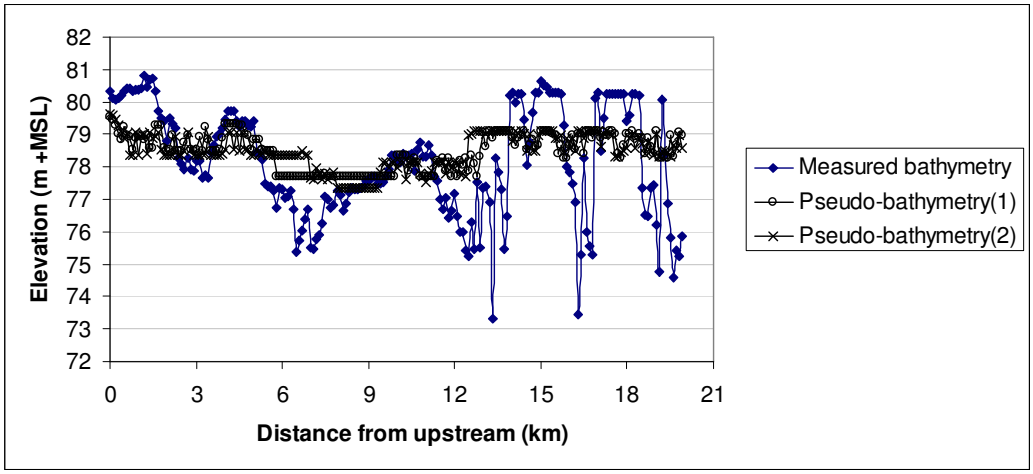

Figure 5.1-5: The long profile along Channel 2 and Channel 3 according to the interpolated pseudo-bathymetry; (1) – Analysis 1 and (2) – Analysis 2

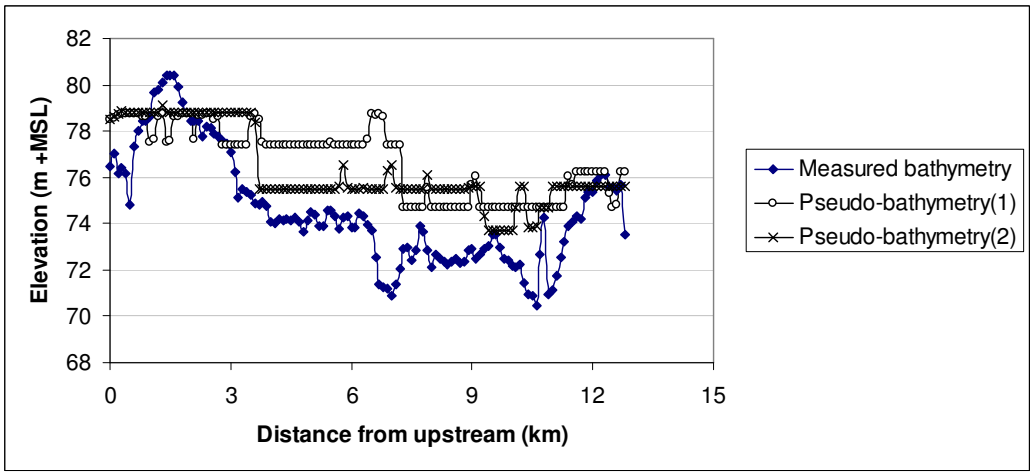

Figure 5.1-6: The long profile along Channel 4 and Channel 5 according to the interpolated pseudo-bathymetry; (1) – Analysis 1 and (2) – Analysis 2

The cross-sectional area comparison was done at low stage (83 m +MSL) equally distributed along the river network. Figure 5.1-7 and Figure 5.1-8 present a comparison between the measured and cross-sectional areas interpolated according to the pseudo-bathymetry at each cross-section along the upstream river network in two analyses. In general, the differences between the cross-sectional areas in Analysis 1 and 2 were from -54.97 % to +44.51 % and from -29.19 % to +34.56 %, respectively. However, the significant differences between cross-sectional areas in Analysis 1 mainly came from Channel 4 while the differences in Analysis 2 came from Channel 2. In addition, the average differences between the cross-sectional areas along different channels are presented in Table 5.1-4. Except for the higher differences in Channel 2 in Analysis 2, the other channels along the river network have lower

differences in Analysis 2 compared to Analysis 1. Therefore, Analysis 2 should be referred to interpolate the pseudo-bathymetry along Channel 4 and Channel 5.

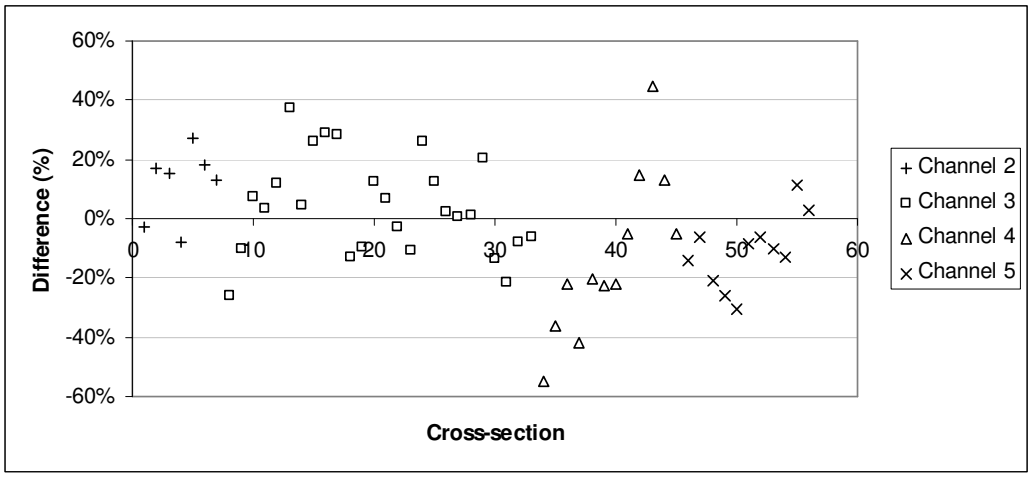

Figure 5.1-7: Comparison between the measured and 'pseudo' cross-sectional area (Analysis 1)

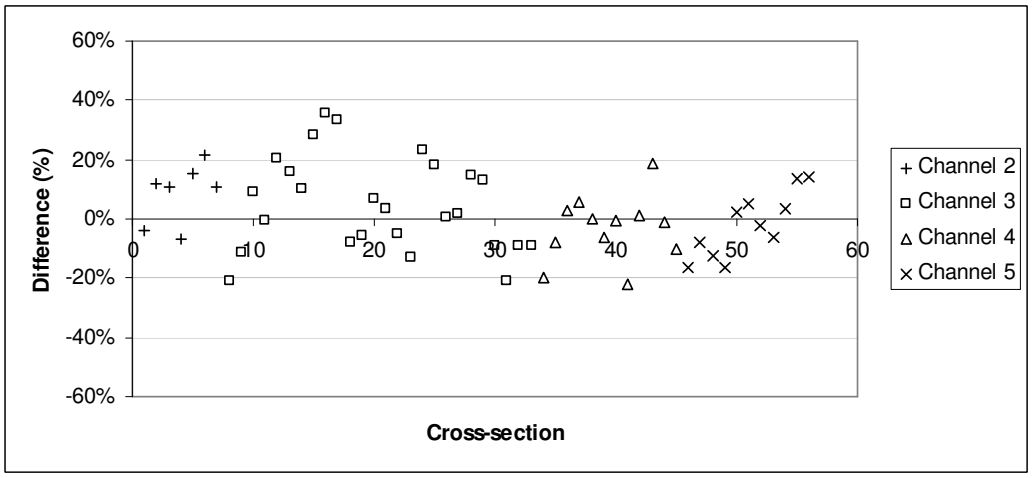

Figure 5.1-8: Comparison between the measured and 'pseudo' cross-sectional area (Analysis 2)

Table 5.1-4: Average differences (in percentage) of the cross-sectional areas in two analyses

Channel	Analysis 1	Analysis 2
Channel 2	11.37	16.14
Channel 3	4.16	3.01
Channel 4	13.16	0.81
Channel 5	10.93	8.15

5.1.3 Interpolation of SPOT image for the downstream river network

According to the smaller differences between the measured and interpolated cross-sectional areas in Analysis 2, this analysis was selected to interpolate the pseudo-bathymetry of the downstream river network. According to the measured bathymetry, Segment 6 in Analyses 2 was deep and actually deeper than any segment along the

downstream river network; therefore, the relationship between the band spectral values and the measured bathymetry was not applied to interpolate the pseudo-bathymetry of the downstream river network. Channel 12 was considered as a shallow channel which was seasonally dry during the dry season and the channels alongside the small islands geomorphologic unit was described as 'shallow' with a measured depth of about 2 – 3 m (Figure 5.1-9) (Brambati and Carulli, 2001). Therefore, such channels were interpolated according to the relationship found between the SPOT reflectance and measured bathymetry in Segment 4 which was considered shallow according to the measured bathymetry. In addition, according to the MRC (2003), along the downstream river network, the depth of the channels was smaller than 7.0 m (except the local deep-pools in the southern most of the downstream river network; Figure 5.1-9). Therefore, the relationship found between the SPOT reflectance and measured bathymetry in Segment 5 was used. The interpolated channel bed elevation according to the pseudo-bathymetry along Profile 1 and Profile 2 (Figure 5.1-9) is presented in Figure 5.1-10; the ellipses represent the small-islands geomorphologic unit. Finally, Figure 5.1-11 presents the full DEM of the study area interpolated from: (i) SRTM for the land surface elevation; (ii) the measured bathymetry (*i.e.* Hydrographic Atlas) along the upstream river network; and, (iii) the interpolated pseudo-bathymetry for the downstream river network.

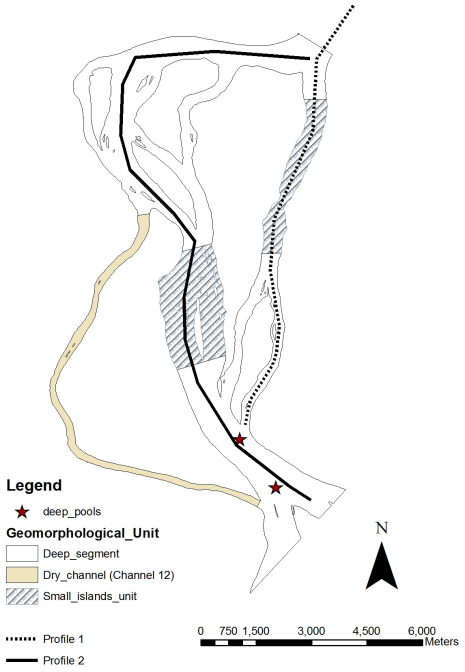

Figure 5.1-9: Different morphological units in the downstream river network (*after* Brambati and Carulli, 2001)

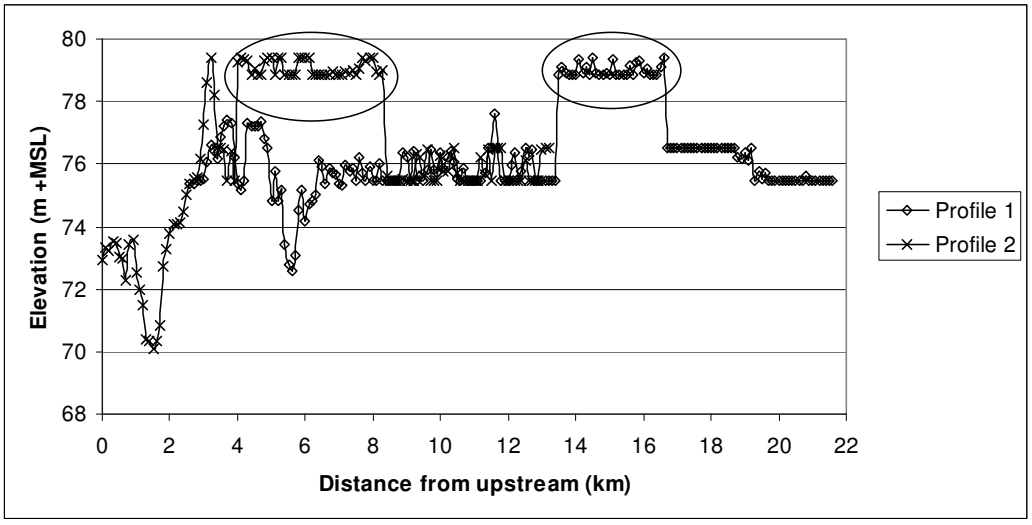

Figure 5.1-10: The pseudo-bathymetry along the downstream river network (*see* Figure 5.1-9 for Profile 1 and Profile 2)

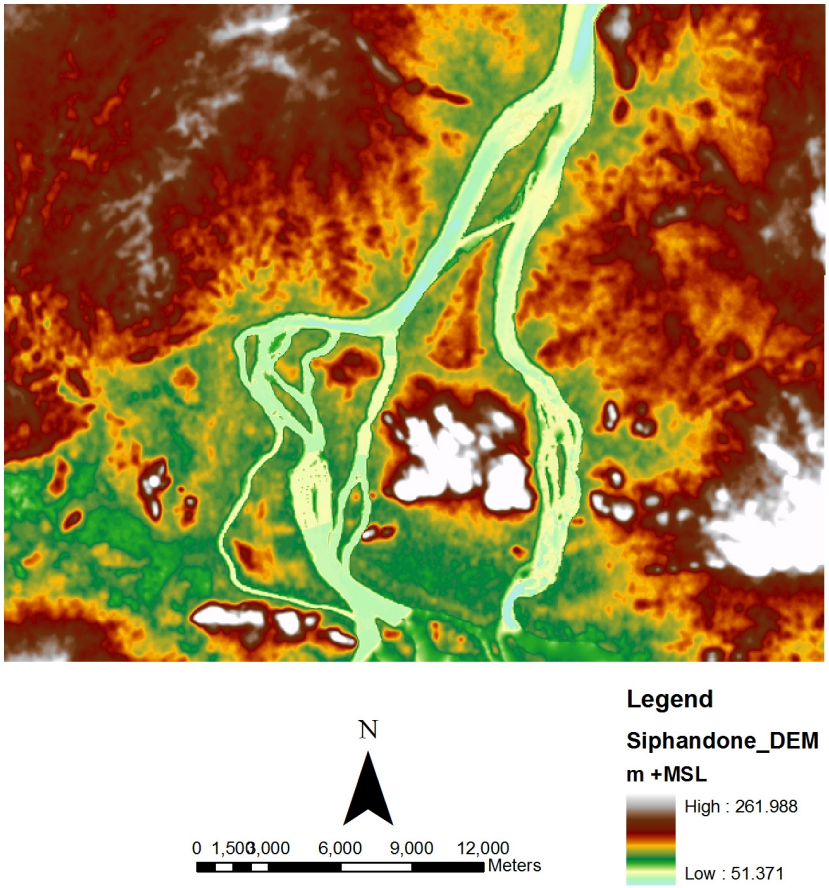

Figure 5.1-11: The integrated DEM of the study area

5.2 Raster based model (tilted-DEM) for wetted-section mapping along the river network

The tilted-DEM model with a common water surface slope throughout the full river network was used to project the areas prone to flooding and the 'possible' extent of the flood, if any. The findings from this model were useful for developing a 1D hydraulic model (HEC-RAS) in the next chapters in terms of delineating cross-sections which might cover all the riparian areas which were suspected to be inundated during the floods along the studied river network.

The tilted-DEM approach was applied for the two versions of the DEM, namely: (i) DEM with the measured bathymetry of the upstream river network and the interpolated pseudo-bathymetry of the downstream river network; and, (ii) DEM with the pseudo-bathymetry applied along the full river network. Three analyses with three entry discharges (low discharge (6,450 m^3s^{-1}), historically recorded average flood discharge (23,600 m^3s^{-1}) and large flood discharge (45,149 m^3s^{-1})) were applied to see if with a common water surface slope along the full river network, the flooding extent might be locally or globally significant throughout the river network. The common water surface slopes (Table 5.2-1) were calculated according to the recorded stages at Channoy and Hatxaykhoun and the distance between the two stage gauges (about 20 km). Figure 5.2-1 and Figure 5.2-2 present the wetted-section along the river network according to the low entry discharge, average flood discharge and high flood discharge. Even though the entry discharge increased significantly from different analyses, the simulated wetted-sections just slightly increased of about 12 % and 19 % in the average and high flood discharge (compared with the low discharge scenario), accordingly and the main regions causing the changes were the sand bars which were often dry in the dry season and inundated during the flooding period (the 'zoom-in' image in Figure 5.2-1 and Figure 5.2-2).

Table 5.2-1: Upstream discharge and the water surface slope from Channoy to Hatxaykhoun

Upstream discharge (m^3s^{-1})	Water surface elevation at Channoy (m+MSL)	Water surface elevation at Hatxaykhoun (m+MSL)	Slope (mm^{-1})
6,450	84.09	81.93	0.0001017
26,300	88.53	85.53	0.0001502
45,149	91.26	87.32	0.0001749

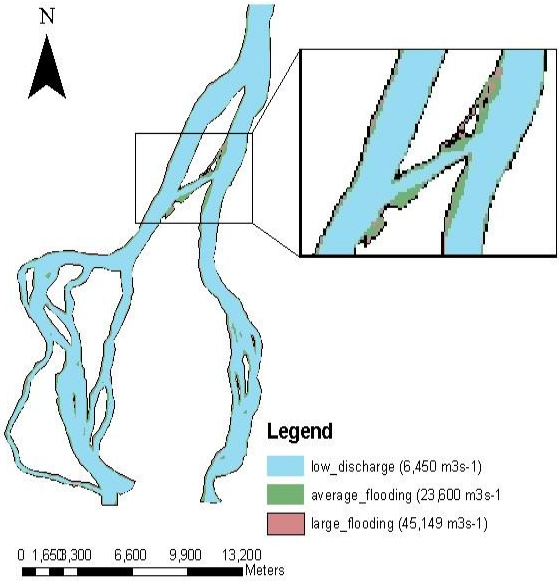

Figure 5.2-1: Wetted-section estimated from the measured bathymetry for the upstream river network and the pseudo-bathymetry for the downstream river network

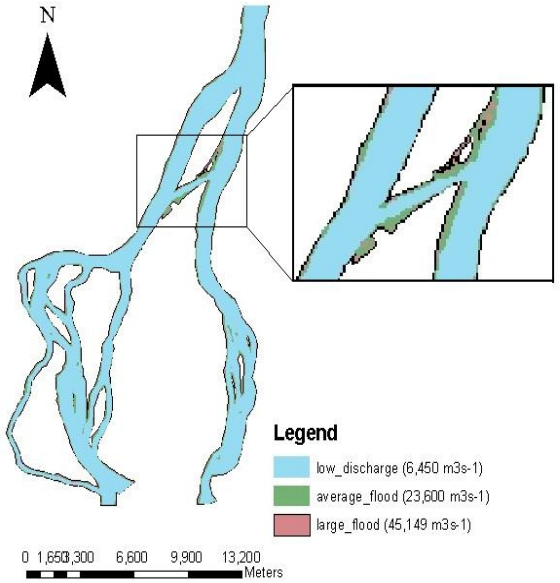

Figure 5.2-2: Wetted-section estimated from the pseudo-bathymetry for both the upstream and downstream river network

5.3 Discussion

Several previous studies were developed to extract the bathymetry of the ocean by using different optical signatures (Katiyar and Rampal, 1991; Melsheimer and Liew, 2001; Deng *et al.*, 2008; Tripathi and Trao, 2002; Gao, 2009). Among others, Melsheimer and Liew (2001) used SPOT images to extract the bathymetry of the Malaysia sea while Deng *et al.* (2008) applied the Lansat-7 ETM+ and QuickBird images to interpolate the bathymetry of the Beilum Estuary, China. In this study,

Landsat-7 with a spatial resolution of 30 m was not used because the resolution is poorer than the 20 m resolution of the available SPOT image. In addition, QuickBird with a fine spatial resolution of 2.44 m was not available in the study area. According to the results obtained from Melsheimer and Liew (2001), the SPOT image with resolution of 20 m was applied to interpolate the pseudo-bathymetry. In addition, due to the objective of the present study (*i.e.* to interpolate a pseudo-bathymetry along the river network), the SPOT image with 20 m resolution was sufficient.

Boruah *et al.* (2008) used the Indian Remote Sensing satellite images (with four spectral bands ranging from 0.45 to 1.70 μm) to successfully (85 % accuracy) qualitatively classify the channel bed into three classes (deep, medium and shallow water) under the application of the unsupervised classification technique in ENVI *v.*4.1. The application was done along a large and heavy sediment-laden river network. However, Boruah *et al.* (2008) did not consider the actual depth of the channel, which is a crucial requirement in this study. In addition, by using four available bands, Boruah *et al.* (2008) defined three classified depths while there were only two classified depths in this study with the application of the two bands.

With the poor results of the interpolated bathymetry when ten classes of depth were classified along the upstream river network, the study shows that the SPOT image, as expected, cannot be used to interpolate the detailed bathymetry of a large sediment-laden river network. Moreover, to estimate the pseudo-bathymetry of a channel, it is necessary to distinguish the channel into different segments with similar geometries (*e.g.* shallow, average or deep segment). In fact, local environmental conditions (*i.e.* sediment load in different segments of a channel) have strong influences on the interpolation of bathymetry information from a satellite image (Melsheimer and Liew, 2001); therefore, a single combination of the two bands reflectance in the SPOT image reflects different values of the measured bathymetry at different segments along a channel.

The approach applied in this study did not consider the 'smoothing' analysis (Tripathi and Rao, 2002) for the applied SPOT image. By applying the 'smoothing' approach (*majority filter*), the 'noise' of the interpolated bathymetry could be minimised and therefore a 'smoother' bathymetry could be created. However, such analysis was not applied in this study because the results of the unsupervised classification techniques did not show any significant chaos (Figure 5.1-2). To strengthen the application of the

SPOT image for pseudo-bathymetry interpolation, it is necessary to get the ground data to calibrate and validate the model and to better define segments along the river network (*i.e.* to determine the SPOT reflectance of that segment with measured bathymetry data which can be used to interpolate the pseudo-bathymetry of other segments). In addition, the general geometry of the upstream and downstream river network might be considerably different due to the differences in the (channel-) pattern of the river networks (*i.e.* meandering and anabranching network for the upstream and downstream river network, respectively). It is suggested that further adjustment of this method should be done, especially the ground data (spatial distribution of the suspended sediment) for calibrating the models is significantly important. The assumptions made for the analysis of the pseudo-bathymetry (Chapter 4, section 4.2.2) could not be validated in this Chapter but would only be validated when the calculated hydraulic parameters along the downstream river network were within the acceptable range in comparison to those along the upstream river network (*see* Chapter 6).

The reflectance of a SPOT image over the water-body along the river network can be affected by the following possibilities: (i) Lower reflectance in the high water column; and, (ii) The smoothness of the water surface has significant impact on the reflectance (*i.e.* the turbulent water surface reflects high reflectance). In addition, because there was no information on the sediment load across a cross-section, it was assumed that the sediment load concentration was equally distributed across a channel. Due to the unsupervised classification technique with the combination of the red and green bands, different zones of combined classes were classified with the combination of the two possibilities. Even though the *proportion correct* between the measured and pseudo-bathymetry was small (< 70%), the differences between cross-sectional areas extracted from the measured and pseudo-bathymetry were ranging from about -20 % to less than +40 %, in which majority of the differences was within -20 % and +20 %. The interpolation of the pseudo-bathymetry and its application for a steady 1D hydraulic model with the energy approach would confirm if the pseudo-bathymetry extracted from the SPOT image is applicable.

In the interpolation of the SPOT image for the pseudo-bathymetry of the upstream river network, the *proportion correct* achieved from the *discriminant analysis* of more than 0.6 might be caused by a large proportion of the deep section of the river

network. However, the main aim of such interpolation was to determine different depth classifications (*i.e.* shallow and deep; Table 5.1-2) and estimate the average depth of each classification of a channel. The integrated DEM with the interpolated pseudo-bathymetry would then be used to develop a 1D hydraulic model with the energy calculation and, therefore, the cross-sectional area was more important than the shape of the cross-section (Chapter 8, section 8.4). In addition, according to Kolding (2002), there were relatively small deep-pools (100 x 100 m in planview) located in Channel 19 and 20 (Figure 5.1-9). Such geomorphological features were reflected by the deep class in the pseudo-bathymetry.

With the iterative procedure for interpolating the pseudo-bathymetry from the SPOT image, it is not necessary to have more than two analyses of dividing the river network into different segments. In addition, the main focus is the interpolation of the pseudo-bathymetry for the right channels because the relationship between the right channels bathymetry and the SPOT reflectance would be used to interpolate the pseudo-bathymetry of the downstream river network. In addition, according to the literature (*e.g.* Brambati and Carulli, 2001), the downstream river network can be simplified into two main geomorphological units. Therefore, in this study, the maximum number of segments along Channel 4 and 5 was three of which two shallow segments were chosen for interpolating the pseudo-bathymetry along the downstream river network.

Small differences between the wetted-sections (in the tilted-DEM approach) resulted from different upstream discharges might be caused by the steep river banks of the cross-sections along the river network (*e.g.* Chapter 3, Figure 3.3-6 and Figure 3.3-7). It leads to the idea that to calibrate the hydraulic model, it is necessary to not only consider the differences between the modelled top-width and the measured one (extracted from the SPOT image) at each cross-section but also to compare the modelled stages with the recorded water surface elevation as well. Even though the tilted-DEM approach is simple, the approach can give an original impression of the flood extent along the study river network. It is useful in the case that a remote river network is modelled (like in this study) and there was no prior information on how extensive the floods might be.

Chapter 6: One dimensional (1D) hydraulic modelling for the upstream bedrock-confined river network

Introduction

The main aim of Chapter 6 is to model the mean hydraulic parameters (*i.e.* discharge, velocity and Froude number) at each cross-section along the bedrock-confined upstream river network (Chapter 4, Figure 4.4-2); therefore, the wetted-section and flooding patterns in accordance with the low entry discharge (6,450 m^3s^{-1}) and flood entry discharges (historical average and high flood discharge of 26,300 m^3s^{-1} and 45,149 m^3s^{-1}, respectively) are modelled accordingly. The subcritical calculation together with the energy approach of the 1D steady gradually varied flow simulation in the HEC-RAS model was used to model the river network with two outlet sections where the geometry was available according to the measured bathymetry. To calibrate the HEC-RAS model, the in-channel hydraulic roughness coefficients (Manning's *n*) were calculated at each cross-section (Chapter 4, section 4.5). In addition, to model the flooding patterns resulting from the entry flood discharges, the floodplain hydraulic roughness was also required; therefore, the land cover maps of 2001 and 2005 created from the SPOT images were presented as a base to estimate the hydraulic roughness of the floodplain. A comparison between the two land cover patterns was made also to examine the magnitude and the spatial pattern of changes.

With the application of the HEC-RAS model for the measured bathymetry, the modelled stages at all applied entry discharges met the recorded data at Channoy and Hatxaykhoun (the upstream and downstream boundary conditions, respectively). In addition, there was no significant drop or rise along the water surface profile, especially at the junctions. The ratio of the cross-sectional areas of the first pair of cross-sections along the downstream channels could be used as an initial condition for splitting discharge at each junction (*i.e.* the ratio of the entry discharge at each channel after a junction was assumed equal to the ratio of the cross-sectional areas). The pseudo-bathymetry was developed along the upstream river network to examine if the pseudo-bathymetry extracted from SPOT image could be applied to model a larger river network, extended downstream (Chapter 7). In fact, the HEC-RAS models developed based on the pseudo-bathymetry also demonstrated that the modelled stages at all applied entry discharges matched the recorded data quite well. In

addition, the modelled stages in line with the flood discharges along the upstream river network were similar between all scenarios of land cover pattern. Even though the modelled water surface profiles resulting from all scenarios were not significantly different from each other, the mean riparian velocity significantly changed, especially between the current and the future hypothetical land cover pattern in which the area was mainly rice paddy field.

6.1 Chapter structure

This chapter is an essential part of the study, in which the modelled hydraulic characteristics of the river network are presented. The general structure of the chapter is presented in Figure 6.1-1. The hydraulic models were developed based on the interpolated in-channel hydraulic roughness and the reviewed floodplain hydraulic roughness. The modelled hydraulic nature of the river network were presented for each upstream entry discharge (low discharge and mean and high flood discharge) in terms of the entry discharge entering each channel, cross-sectional area, mean velocity and Froude number.

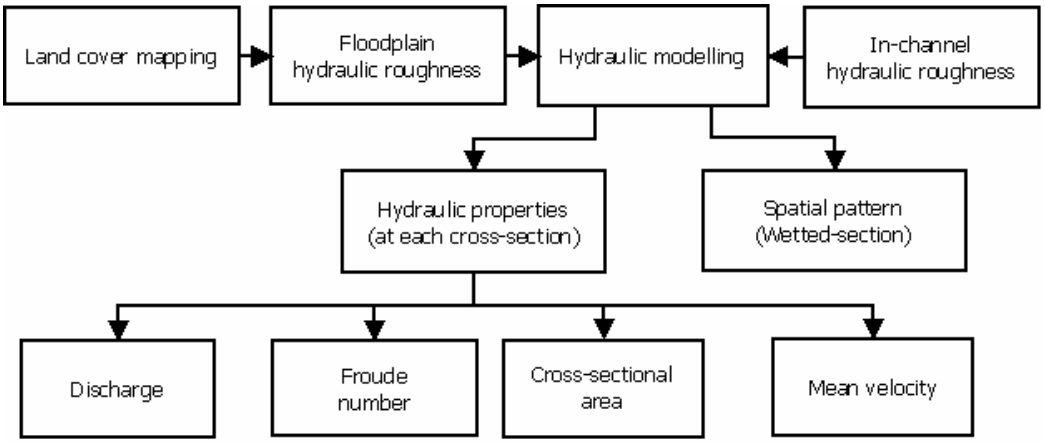

Figure 6.1-1: Structure of Chapter 6

6.2 Land cover mapping and the hydraulic roughness of each land cover type

6.2.1 Land cover and land cover change maps

Within the study area, the main land cover types (*i.e.* natural forest, degraded forest (or cut forest), shrub, rice paddy and bare-soil (including sand bars)) could be recognized in both SPOT images (2001 and 2005). The land cover maps created from the SPOT images are presented in Figure 6.2-1. The areas of each land cover type in 2001 and 2005 are presented in Table 6.2-1 and results of the accuracy assessment for

SPOT 2001 and 2005 are 87.08 % and 83.64 %, respectively. Among the classified classes, bare-soil was misclassified with the dry paddy field. In fact, during the periods when the SPOT images were taken, the paddy fields were mostly harvested and dry; therefore the reflectance of the paddy rice field and the bare-soil was not very well differentiated (*i.e.* the accuracy for the bare-soil in 2001 and 2005 was 76.87 % and 68.51 %, respectively). Table 6.2-2 illustrates the changes of the land cover pattern in the period of 2001 – 2005. In general, there were noticeable decreases in the area of the natural and degraded forest while the area of shrub and rice field significantly increased. The percentage of natural forest area decreased from 13.23 % to 8.61 % in 2001 and 2005, accordingly. The degraded forest represents a large proportion of the whole land surface; however, the proportion went down from 44.10 % in 2001 to 37.67 % in 2005. In contrast, shrub increased significantly from 16.72 % to 26.81 % in 2001 and 2005, respectively.

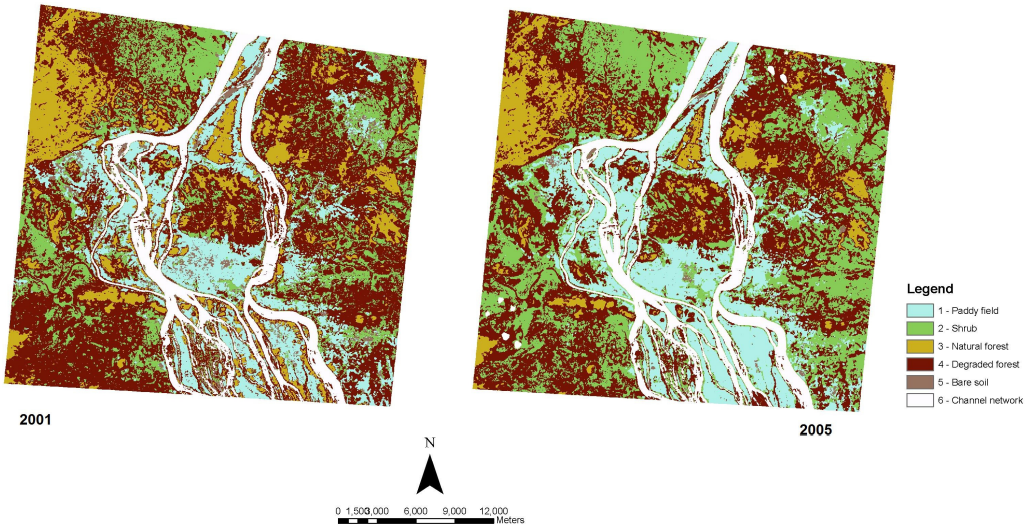

Figure 6.2-1: Land cover map extracted from the SPOT image 2001 and 2005

Table 6.2-1: Area and percentage of each land cover type over the study area

Land cover type	2001		2005		Differences in %
	Area (km^2)	%	Area (km^2)	%	
Rice field	117.81	13.88	138.23	16.32	2.44
Shrub	141.88	16.72	227.06	26.81	10.09
Natural forest	112.26	13.23	72.92	8.61	-4.62
Degraded forest	374.22	44.10	319.09	37.67	-6.43
Bare soil	22.00	2.59	5.24	0.62	-1.97
Channel	80.38	9.47	84.47	9.97	0.50

Table 6.2-2 presents the area of each land cover type in 2001 and 2005. The most significant change occurred where 90.37 km^2 of the degraded forest (code 4) was

changed into shrub (code 2) from 2001 to 2005. In 2005, the degraded forest had been converted from shrub where the area was not continuously cut and vegetation kept growing or the natural forest had been replaced by degraded forest where the forest had been exploited. The latter occurred dispersedly over the whole area while the former had happened more heavily in the east of the study area. The spatial pattern of land cover change in the period 2001 – 2005 is presented in Figure 6.2-2, in which the code in the map shows areas which were covered by a certain land cover type in 2005 had changed from another land cover type in 2001. Among the changes, rice paddy, shrub and degraded forest were the significant changes. In fact, more rice fields were established along the upstream river network while shrub and degraded forest were scattered over the whole study area.

Table 6.2-2: Land cover pattern in area (km^2) in 2001 and 2005

		Year 2005						
	Code	1	2	3	4	5	6	**Total**
Year 2001	1	**94.15**	17.42	0.00	4.24	*1.97*	0.02	117.80
	2	8.19	**107.81**	0.00	*24.82*	0.29	0.71	141.82
	3	*12.11*	1.89	**66.97**	*30.63*	0.35	0.14	112.08
	4	*12.45*	*90.37*	*5.94*	**257.47**	0.46	*6.23*	372.92
	5	11.25	7.26	0.00	1.05	**1.77**	0.66	22.00
	6	0.08	2.31	0.00	0.87	0.40	**76.72**	80.38
	Total	138.23	227.06	72.92	319.09	5.24	84.47	

Notes: 1 – Rice field, 2 – Shrub, 3 – Natural forest, 4 – Degraded forest, 5 – Bare soil and 6 – Channels.

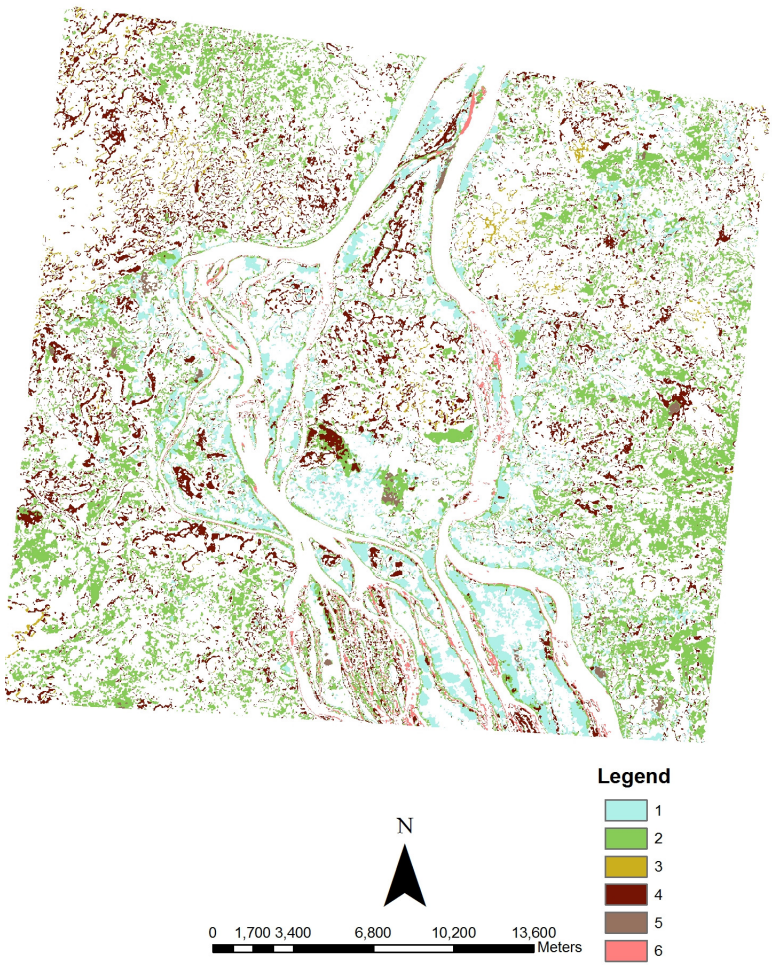

Figure 6.2-2: Land cover change map in the period of 2001 and 2005; 1 – Rice field, 2 – Shrub, 3 – Natural forest, 4 – Degraded forest, 5 – Bare soil and 6 – Channels

6.2.2 Hydraulic roughness for each land cover type

For the flood discharge scenarios, each cross-section of the HEC-RAS model was divided into three main parts, including two sections of the (left and right) riparian zone and a section of the channel. To identify the hydraulic roughness coefficient (Manning's *n*) of the floodplain sections, the land cover map created in 2005 was used to reflect the latest land cover pattern in the study area and the referenced hydraulic roughness values (Cowan, 1956) of each land cover type was identified (Table 6.2-3)

Table 6.2-3: Hydraulic roughness value of each land cover type in the floodplain in the study area (*after* Cowan, 1956)

No.	Land cover type	Referenced roughness
1	Bare soil	0.03
2	Shrub	0.10
3	Degraded forest	0.15
4	Natural forest	0.20
5	Rice paddy	0.04

6.3 Boundary conditions of the hydraulic models

6.3.1 Water surface slope and the downstream boundary condition along Channel 4 and 5 in the low discharge

The water surface slope required to set the downstream boundary condition of the hydraulic model was interpolated according to the water surface elevation at each cross-section extracted from the SPOT image and the DEM. Figure 6.3-1 presents the water surface elevation (WSE) (based on the wetted-width extracted from the SPOT image and the measured DEM) at each cross-section and the linear interpolation of the water surface elevation along Channel 1, Channel 4 and Channel 5. Due to the relatively poor quality of the DEM, the interpolated water surface elevation fluctuated highly along Channel 4 and Channel 5. However, even though the R^2 was small (R^2 = 0.334), the interpolation was acceptable because the water surface elevation at the first cross-section of Channel 1 (at Channoy) was 84.03 m, which was relatively close to the recorded stage (84.09 m). Based on the linear interpolation, the water surface slope along Channel 4 and 5 was 1.59 x 10^{-4} mm^{-1} which was not significantly different from the slope measured along Channel 2 and 3 (1.02 x 10^{-4} mm^{-1}).

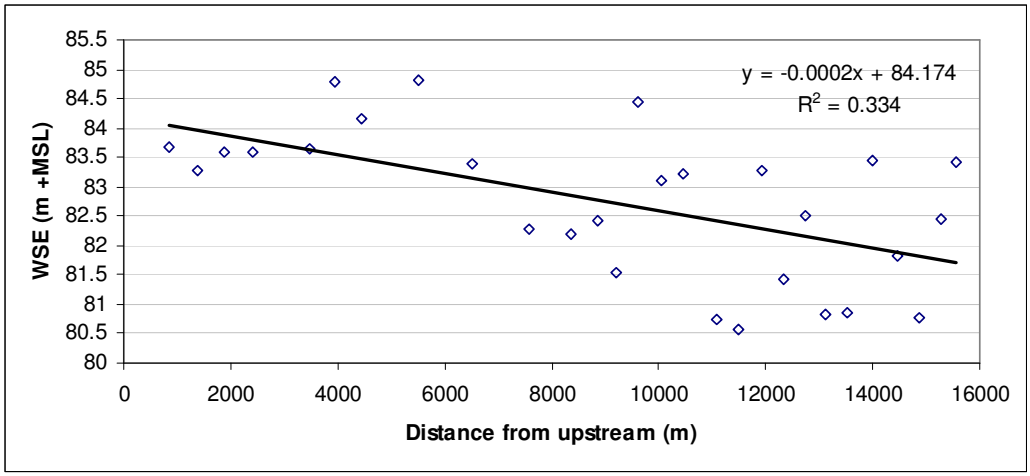

Figure 6.3-1: Water surface elevation at each cross-section along Channel 1, 4 and 5

6.3.2 Factors affecting the hydraulic roughness

In this study, due to the nature of the bedrock-constraint river network, the form hydraulic roughness was the main concern due to significant changes of the cross-sectional areas of the neighbouring cross-sections. In addition, the skin roughness was considered as minor contribution to the total hydraulic roughness at each cross-section and therefore was neglected in the hydraulic models.

a. Obstruction

Obstruction, in this study considered as islands, is acknowledged as an important source leading to increase of the in-channel hydraulic roughness. Along the upstream river network, islands appear along the terminal segment of Channel 3 only and n_* from cross-section 2 to 10 was assigned to be 0.045 (*see* Chapter 4, Table 4.5-1).

b. Degree of meandering (*m*)

Five segments along the upstream river network were divided as presented in Figure 6.3-2. The calculated sinuosity index and the estimated '*m*' are presented in Table 6.3-1 (*see* Chapter 4, Table 4.5.1). Most segments within the upstream river network were given a sinuosity index (SI) of around 1.2 or less and therefore the '*m*' coefficient was assigned equal to 1. However, for Segment 3 with a SI of about 1.18 (close to the range of 1.2 – 1.5), the '*m*' coefficient was assigned equal to 1.15 (Table 6.3-1).

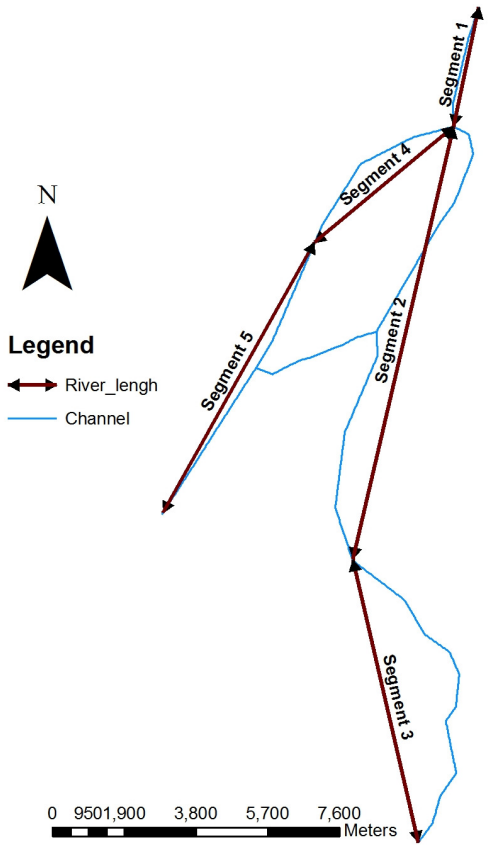

Figure 6.3-2: Divided segment along the upstream river network

Table 6.3-1: Calculated sinuosity index and the adjusted sinuosity factor (*m*)

Segment	Sinuosity index	*m*
Segment 1	1.00	1.00
Segment 2	1.07	1.00
Segment 3	1.18	1.15
Segment 4	1.06	1.00
Segment 5	1.00	1.00

6.3.3 The calculated hydraulic roughness coefficient at each cross-section in the low discharge

With the water surface slope along Channel 1, 2 and 3 of 1.02 x 10^{-4} mm^{-1} and along Channel 4 and 5 of 1.59 x 10^{-4} mm^{-1}, the base Manning's *n* (n_b) coefficient at each cross-section is presented in Figure 6.3-3. Even though most of the calculated Manning's *n* values were higher than 0.009 (Chapter 4, section 4.6.2), the calculated Manning's *n* at cross-section 2, 6 and 9 along Channel 3 and some of the cross-sections along Channel 2_4 were smaller than 0.009 (Chapter 4, section 4.5).

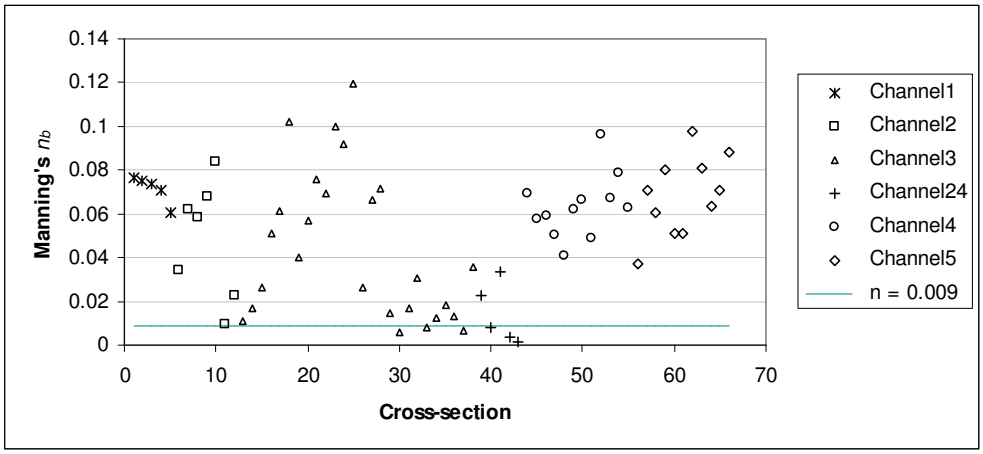

Figure 6.3-3: Base Manning's n_b at each cross-section along the upstream river network with the low discharge (6,450 m^3s^{-1})

Figure 6.3-4 presents the calculated Manning's *n* at each cross-section along the upstream river network. On average, the Manning's *n* coefficients along Channel 4 and 5 were similar to those along Channel 1 and higher than those along Channel 2 and Channel 3. However, the local Manning's *n* coefficient along Channel 3 was high, up to 0.14, where the cross-sectional area was largest amongst other cross-sections. In addition, the Manning's *n* coefficient along Channel 2_4 was iteratively assigned to 0.035 to make the model meet the recorded stage at Channoy and Hatxaykhoun. In general, the Manning's *n* coefficient at each cross-section along Channel 4 and Channel 5 was higher than that along Channel 2 and Channel 3.

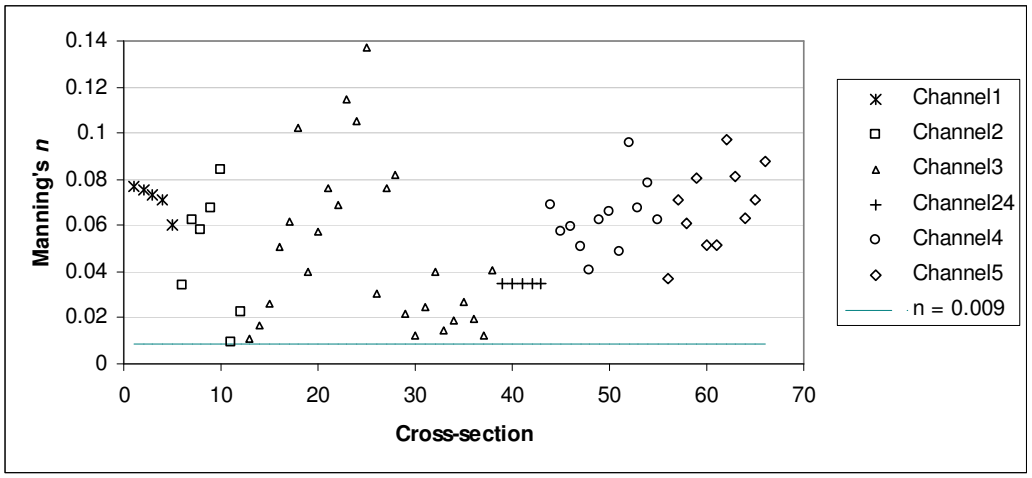

Figure 6.3-4: Calculated Manning's *n* coefficient at each cross-section along the upstream river network with the low discharge (6,450 m^3s^{-1})

6.3.4 The calculated hydraulic roughness coefficient at each cross-section in the flood discharge

The base and integrated Manning's *n* in the flood discharge at each cross-section along the upstream river network are presented in Figure 6.3-5 and Figure 6.3-6, respectively. It could be seen that after integration with other geometry factors, the Manning's *n* at each cross-section along Channel 3 was higher mainly due to the sinuosity index and the irregularity of the channel caused by the islands. In general, the Manning's *n* coefficients at each cross-section along Channel 4 and 5 were higher than those along Channel 2, Channel 3 and Channel 2_4.

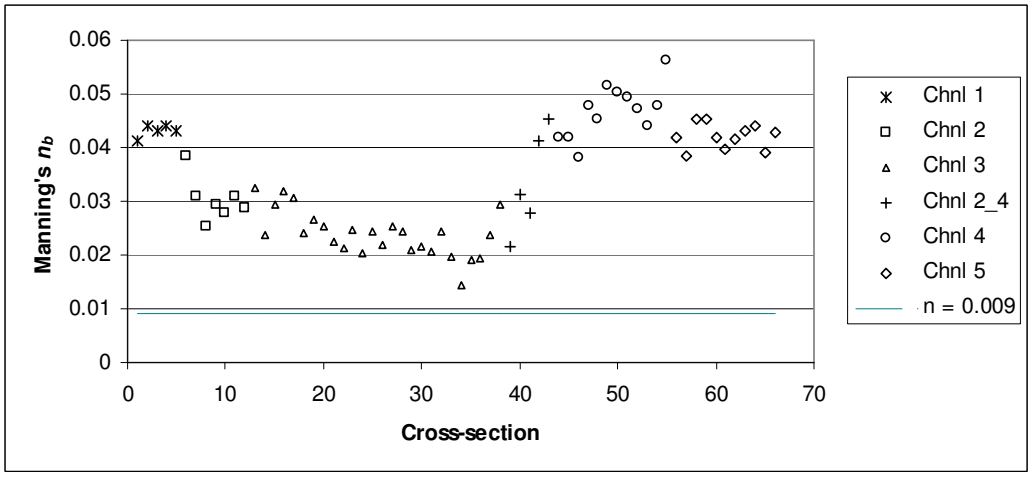

Figure 6.3-5: Base Manning's n_b at each cross-section along the upstream river network with the average flood discharge (26,300 m^3s^{-1})

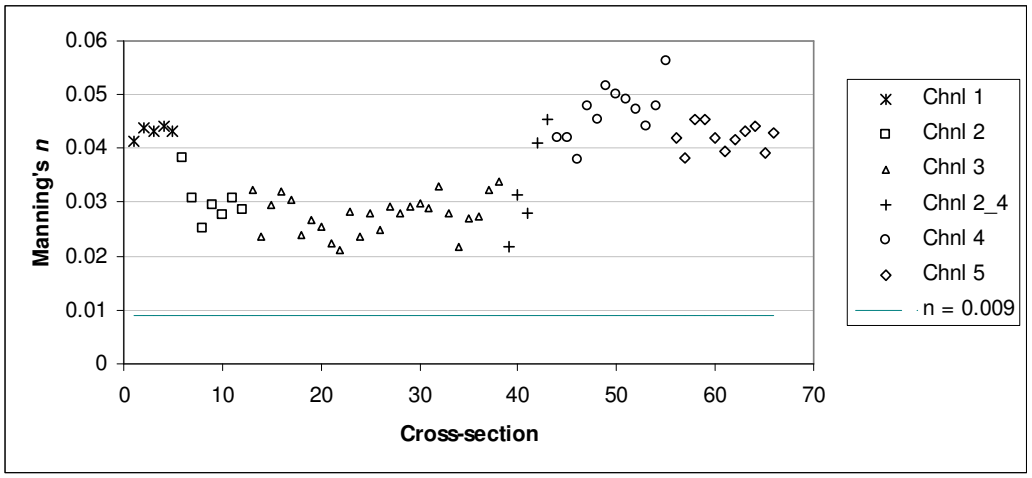

Figure 6.3-6: Calculated Manning's *n* coefficient at each cross-section along the upstream river network with the average flood discharge (26,300 m^3s^{-1})

6.4 Hydraulic modelling for the low discharge (6,450 m^3s^{-1}) with measured DEM

6.4.1 Individual hydraulic roughness coefficient at each cross-section

The modelled water surface (WS) profiles and energy gradeline along the upstream river network according to individual hydraulic roughness coefficient at each cross-section are presented in Figure 6.4-1, Figure 6.4-2 and Figure 6.4-3. In the figures, the minimum channel elevation (Min Ch El), water surface elevation (WSE) and energy gradeline elevation (E. G. Elev) are also presented. The modelled water surface elevations at Channoy, Hatxaykhoun and the end of Channel 5 were 84.17 m +MSL, 0.08 m higher than the recorded stage (84.09 m +MSL), 81.93 m +MSL and 81.46 m +MSL, respectively.

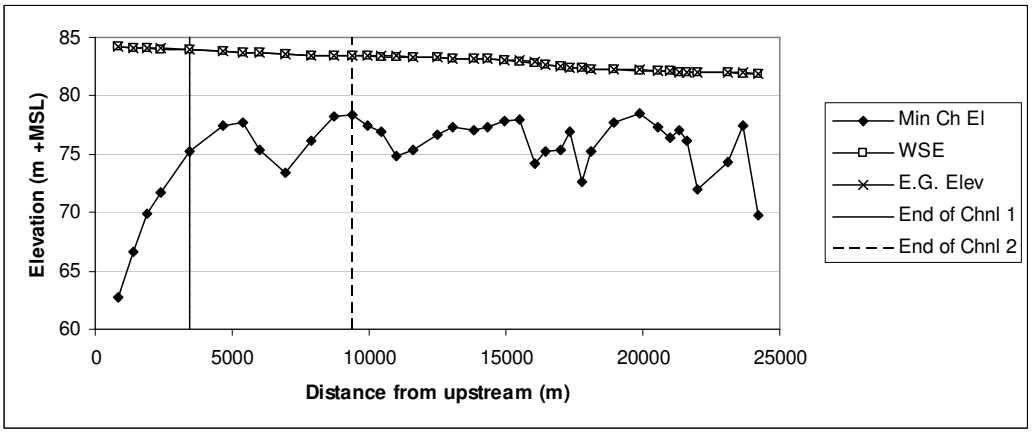

Figure 6.4-1: Water surface profile and energy gradeline along Channel 1, 2 and 3 in the low discharge scenario

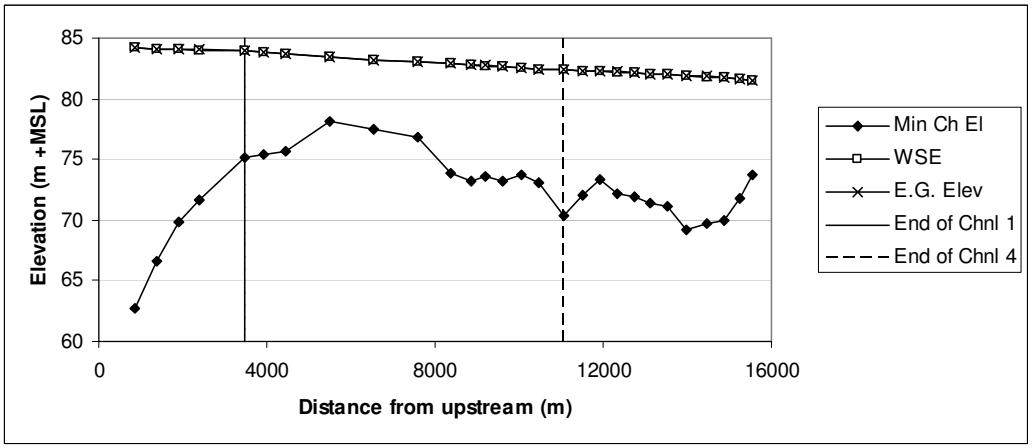

Figure 6.4-2: Water surface profile and energy gradeline along Channel 1, 4 and 5 in the low discharge scenario

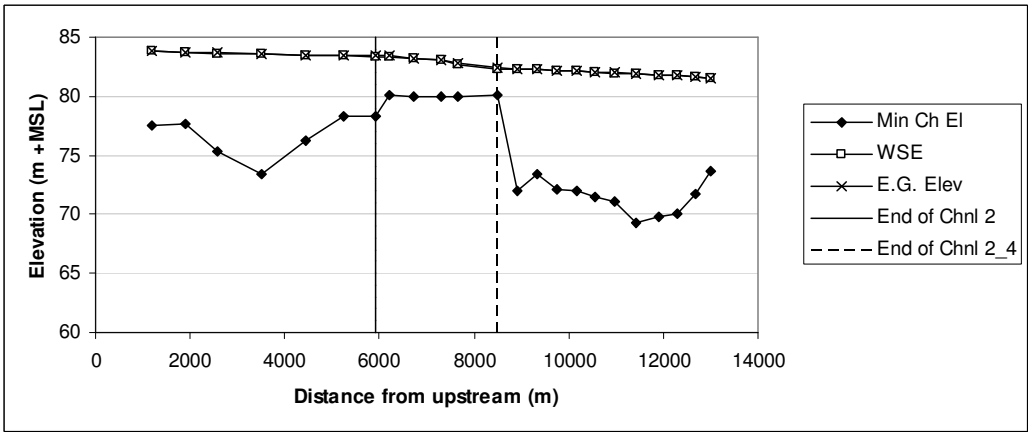

Figure 6.4-3: Water surface profile and energy gradeline along Channel 2, 2_4 and 5 in the low discharge scenario

To validate the modelled top-width at each cross-section, the modelled top-width was compared to the top-width extracted from the SPOT image. Figure 6.4-4 shows the linear comparison between the modelled top-width and the top-width extracted from the SPOT image for each cross-section. With the R^2 of 0.945, the modelled top-width met the SPOT image quite well. Figure 6.4-5 illustrates the percentage of differences at each cross-section, in which the positive difference indicates wider top-width calculated in the HEC-RAS model than that extracted from the SPOT image. The maximum difference was 180.32 % which came from the cross-channel (Channel 2_4). In fact, the widths of all the cross-sections along Channel 2_4 were not large (maximum 180 m wide) and that channel was created with the general estimated channel bed elevation based on the field observation (according to the digital global position system) and the planform of Channel 2_4 was imitated from the planform

extracted from the SPOT image. Apart from the cross-channel, the differences in the modelled and the SPOT top-width were less than 20%; except cross-section 2.02 of Channel 2 and 3.09 of Channel 3. In addition, the differences were higher along Channel 2 and 3 and less along Channel 4 and 5. The main cause of the high differences between the top-width extracted from the SPOT image and that extracted from the HEC-RAS model is the poor quality of the applied DEM. In fact, along Channel 3, there are islands which were not well reflected in the DEM.

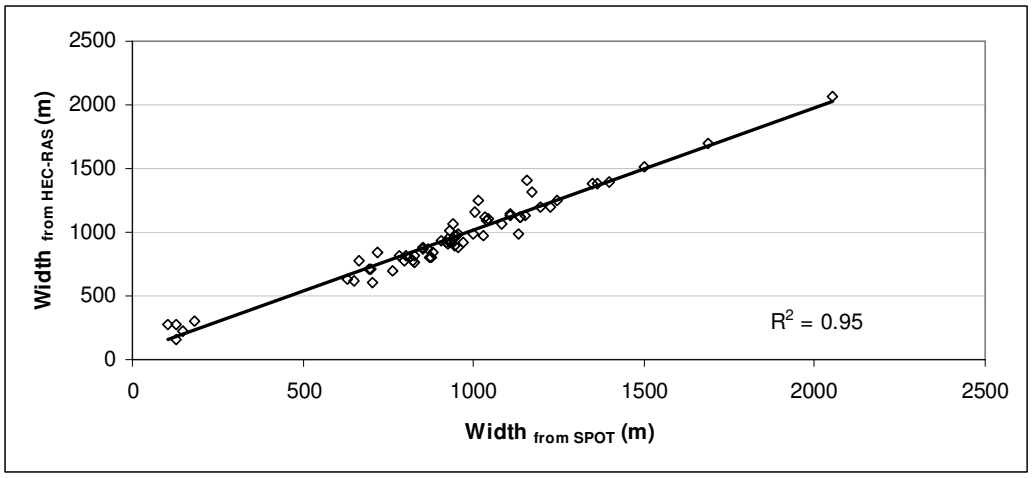

Figure 6.4-4: Linear comparison between the modelled top-width and that extracted from SPOT

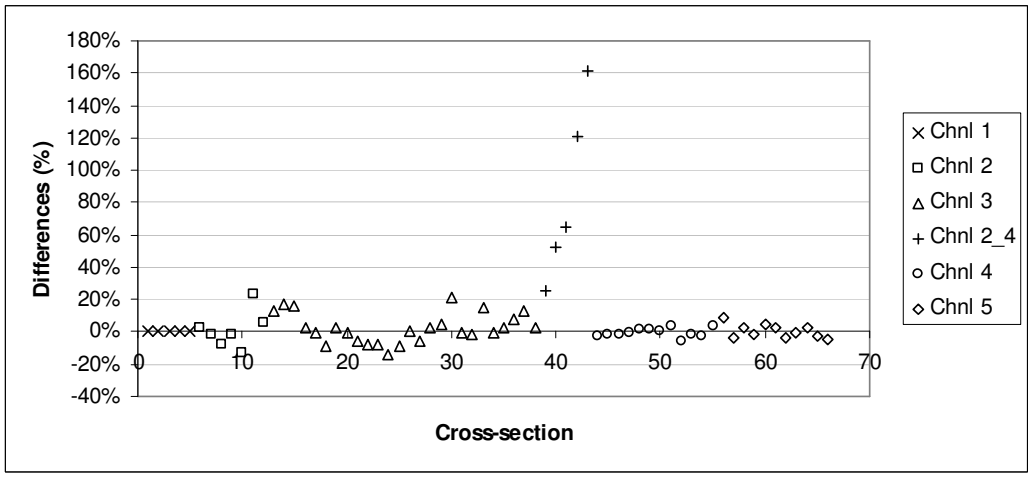

Figure 6.4-5: Differences in percentage between the modelled top-width and that extracted from SPOT

Figure 6.4-6 presents the calculated Froude number at each cross-section along the upstream river network, which shows that with the low calculated Froude number (from 0.05 to 0.35), the flow in the low discharge was highly sub-critical. The highest Froude number was found along Channel 2_4 due to the high in-channel velocity. The

high Froude number was also found in the last cross-section along Channel 3 where the islands could be found; in fact, due to the presence of the islands, the cross-sectional areas along the downstream segment of Channel 3 was smaller than those along the upstream segment of the channel. In addition, the Froude number along Channel 1, Channel 4 and Channel 5 was smaller than that along Channel 2 and Channel 3 due to the higher hydraulic radius along Channel 1, Channel 4 and Channel 5.

In general, the mean in-channel velocity along Channel 1 was the highest while the mean in-channel velocity along Channel 2_4 was the smallest among other channels. In each channel, because the entry discharge of each cross-section along a channel remained constraint, the mean in-channel velocity increased when the cross-sectional area decreased. Figure 6.4-7 presents the water-way obtained from the HEC-RAS model according to the low entry discharge (6,450 m^3s^{-1}).

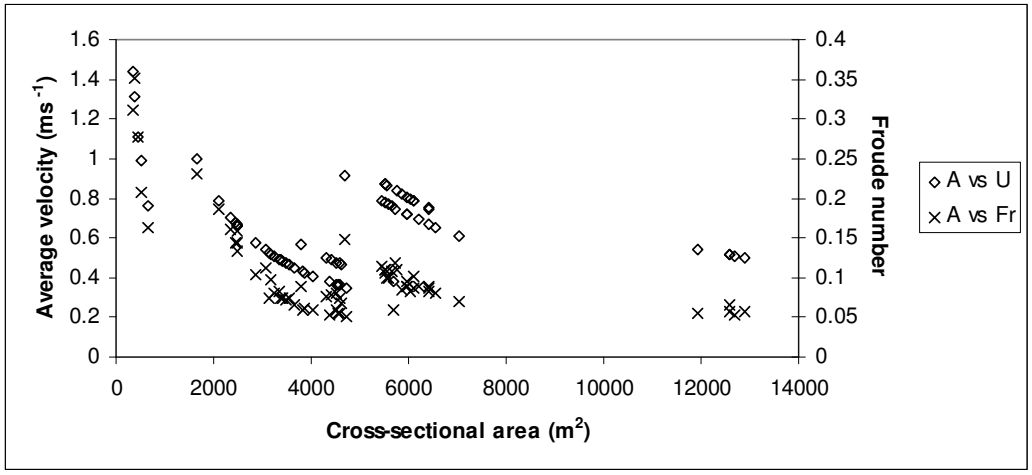

Figure 6.4-6: Froude number, mean in-channel velocity and cross-sectional area at each cross-section along the upstream river network (in low discharge simulation)

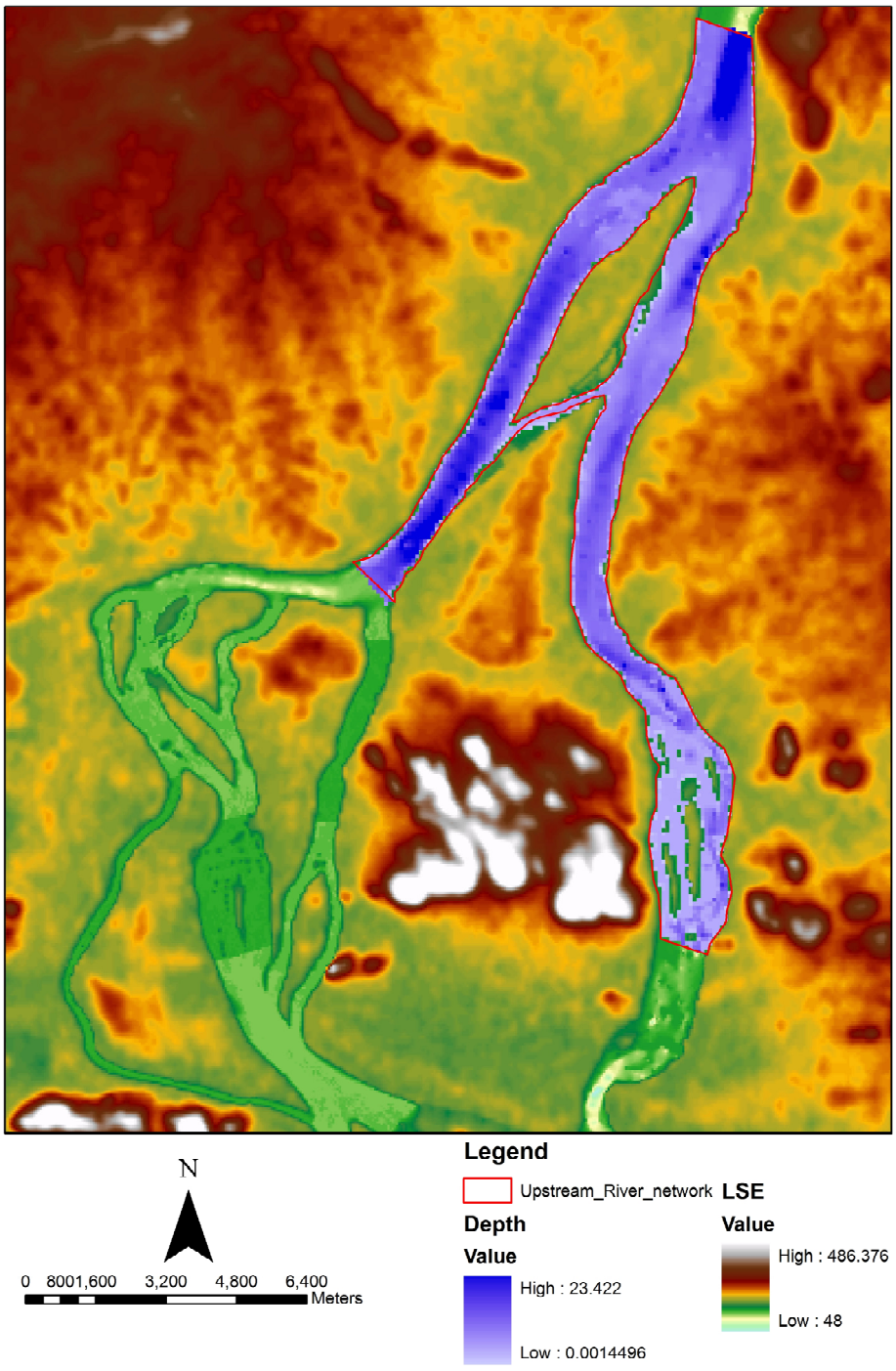

Figure 6.4-7: Modelled water-way according to low discharge (6,450 m^3s^{-1}) based on the measured bathymetry

6.4.2 Mean hydraulic roughness coefficient for each channel

To examine the impact of the assigned hydraulic roughness coefficient on the HEC-RAS results, the model was run with (i) the entry discharge of each channel was remained similar to what it were in the previous models; and (ii) the mean Manning's

n value of each channel rather than individual Manning's *n* value at each cross-section. The mean Manning's *n* value was calculated as the average '*n*' of each cross-section along a channel. The modelled water surface elevations at the beginning and the end of each channel along the upstream river network and the applied mean Manning's *n* coefficient at each channel are presented in Table 6.4-1. With the applied mean Manning's *n* coefficient at each reach, the water surface elevation (WSE) at the first bifurcation was not well modelled. In fact, there was a drop at the end of Channel 1 (84.10 m +MSL) and the beginning of Channel 2 (83.90 m +MSL). In addition, the recorded stage at the upstream boundary was 84.09 m +MSL while the modelled stage was 84.28 m +MSL.

Table 6.4-1: Mean Manning's *n* coefficient at each channel

Channel	Manning's *n*	WSE (m +MSL)	
		Upstream	Downstream
Channel 1	0.071	84.28	84.10
Channel 2	0.048	83.90	83.56
Channel 3	0.048	83.56	81.93
Channel 2_4	0.065	83.59	82.69
Channel 4	0.063	84.09	82.75
Channel 5	0.068	82.48	81.70

6.5 Hydraulic modelling for the low discharge (6,450 m^3s^{-1}) with interpolated the pseudo-bathymetry

Two analyses were developed to examine the water surface profiles along the upstream river network in the case of the pseudo-bathymetry: (i) Analysis 1: The application of the calculated Manning's *n* set calculated according to the measured bathymetry for the full upstream river network; and, (ii) Analysis 2: The Manning's *n* set along Channel 4 was calculated according to the pseudo-bathymetry and then applied in the HEC-RAS model together with the previous Manning's *n* set calculated based on the measured bathymetry. The latter analysis was done in order to examine if the Manning's *n* coefficient calculated according to the pseudo-bathymetry could be used together with the pseudo-bathymetry to model the river network. It is, in fact, an evidence to confirm if the pseudo-bathymetry could be used to determine the hydraulic roughness at each cross-section along the downstream river network and if the calculated Manning's *n* together with the pseudo-bathymetry could be used as the boundary conditions for the hydraulic model for the full river network.

6.5.1 Analysis 1

Analysis 1 was done with (i) similar water surface elevation at Hatxaykhoun (81.93 m+MSL) and similar Manning's *n* set as they were in the measured bathymetry HEC-RAS model; and, (ii) the water surface elevation at the end of Channel 5 was 81.27 m+MSL, 0.19 m below boundary condition set in the measured bathymetry HEC-RAS model. The comparison in the modelled stages between the HEC-RAS models with the application of the measured bathymetry and pseudo-bathymetry is presented in Figure 6.5-1 ,in which the positive values represent higher stage modelled from the pseudo-bathymetry compared to the measured bathymetry. In general, with lower downstream boundary conditions, the modelled water surface elevation at each cross-section along the upstream river network based on the pseudo-bathymetry was higher than those based on the measured bathymetry. The difference in the modelled stage at each cross-section was from -0.18 m to +0.24 m.

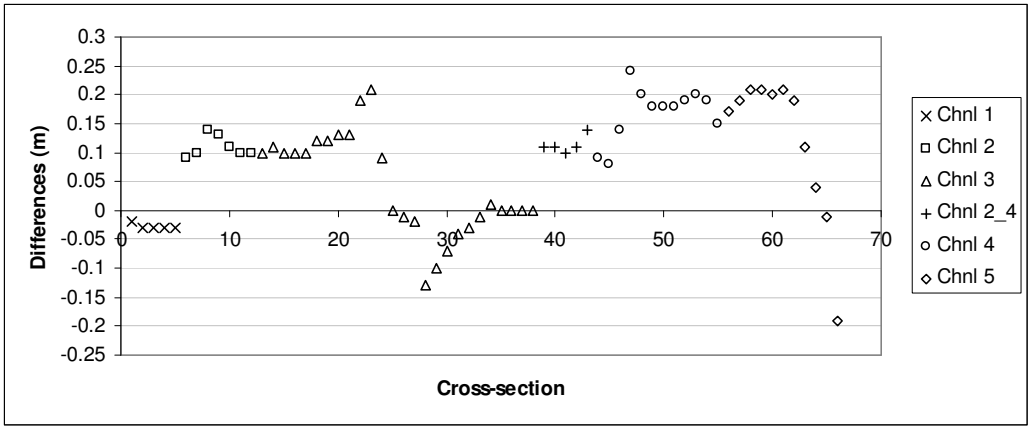

Figure 6.5-1: Differences in stages at each cross-section in the low discharge scenario

Figure 6.5-2 illustrates the relationship between the Froude number and the mean in-channel velocity at each cross-section along the upstream river network. The Froude number ranged from 0.05 to 0.34 and the mean in-channel velocity ranged from 0.34 ms^{-1} to 1.47 ms^{-1}.

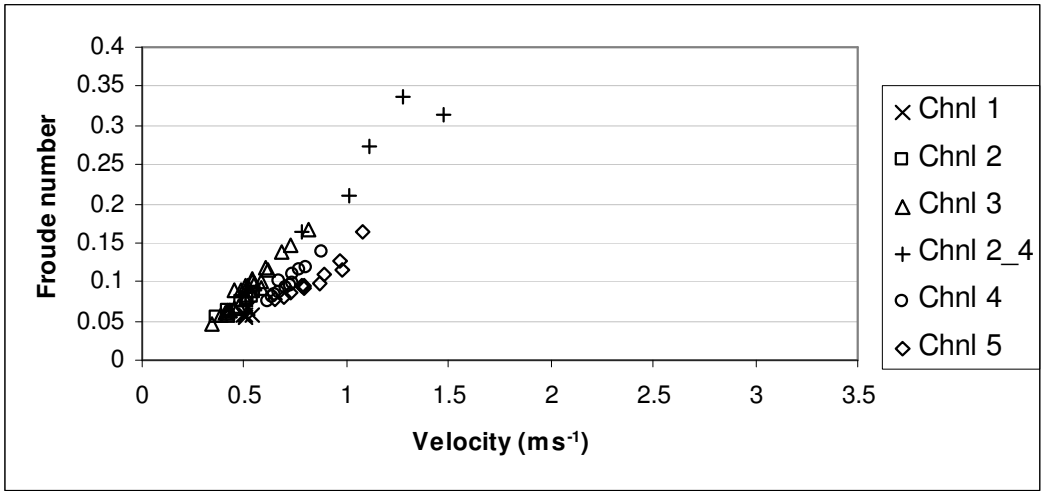

Figure 6.5-2: Froude number *vs.* mean in-channel velocity at each cross-section along the upstream river network (Analysis 1)

6.5.2 Analysis 2

Figure 6.5-3 presents the calculated Manning's *n* along Channel 4 based on the measured and pseudo-bathymetry, in which the cross-section number was presented following the downstream direction. In general, the Manning's *n* coefficients calculated according to the measured bathymetry were higher than those calculated according to the pseudo-bathymetry. Given a similar discharge entering Channel 4 in two cases, the cross-sectional area at each cross-section calculated according to the pseudo-bathymetry was smaller than that calculated according to the measured bathymetry.

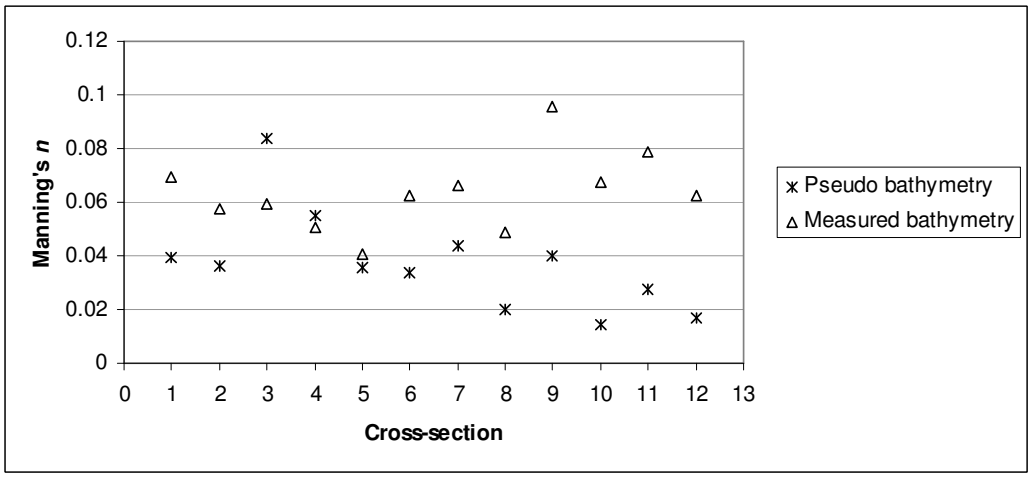

Figure 6.5-3: Calculated Manning's *n* according to the measured and pseudo-bathymetry along Channel 4 in the low discharge scenario

Analysis 2 was done with (i) similar water surface elevation at Hatxaykhoun (81.93 m +MSL) and similar Manning's *n* set along all channels as they were in the measured bathymetry HEC-RAS model except Channel 4; (ii) the water surface elevation at the end of Channel 5 was 81.37 m +MSL, 0.09 m below the boundary condition set in the measured bathymetry HEC-RAS model; and, (iii) The Manning's *n* coefficient at each cross-section along Channel 4 was calculated according to the cross-sectional area extracted from the pseudo-bathymetry. The comparison in the modelled stages between the HEC-RAS models with the application of the measured bathymetry and pseudo-bathymetry is presented in Figure 6.5-4, in which the positive values represent higher stage modelled from the pseudo-bathymetry compared to the measured bathymetry. In general, with lower downstream boundary conditions, the modelled water surface elevation at each cross-section along upstream river network based on the pseudo-bathymetry was higher than those based on the measured bathymetry. The difference in the modelled stage at each cross-section was from -0.23 m to +0.32 m.

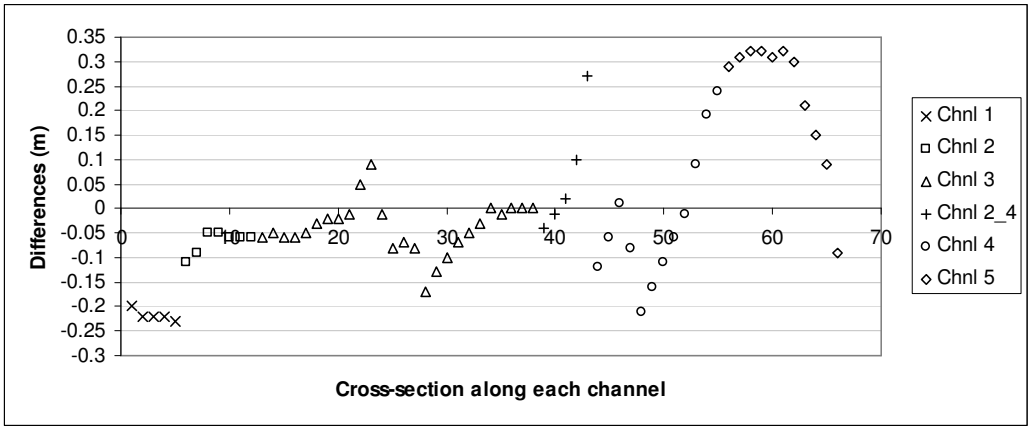

Figure 6.5-4: Differences in stages at each cross-section in the low discharge scenario

Figure 6.5-5 presents the relationship between the Froude number and the mean in-channel velocity at each cross-section along the upstream river network. The Froude number ranged from 0.05 to 0.28 and the mean in-channel velocity ranged from 0.32 ms^{-1} to 1.29 ms^{-1}.

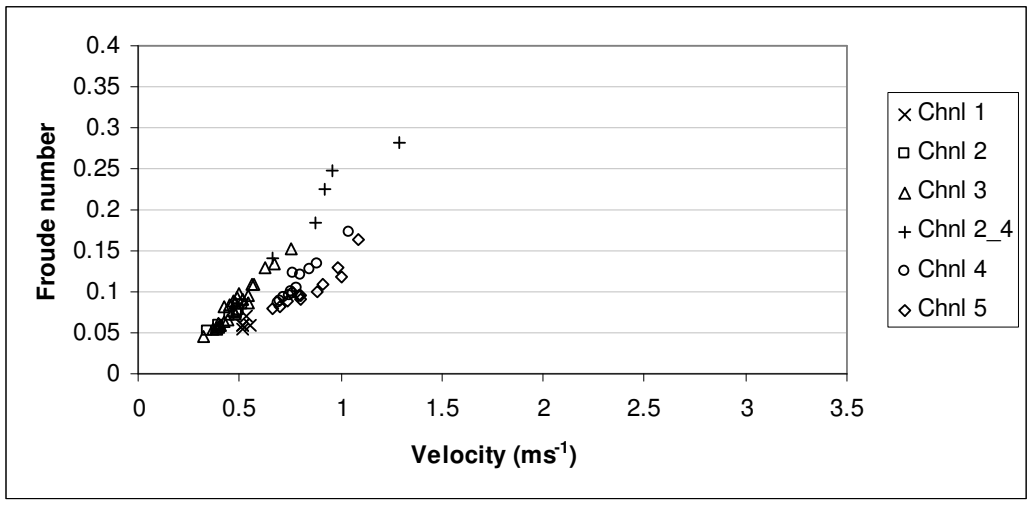

Figure 6.5-5: Froude number *vs.* mean in-channel velocity at each cross-section along the upstream river network (Analysis 2)

6.6 Hydraulic modelling for the flood discharge

6.6.1 Spatial pattern of the historical average flood discharge (26,300 m^3s^{-1})

a. Measured DEM

The water surface profiles and energy gradeline are presented in Figure 6.6-1, Figure 6.6-2 and Figure 6.6-3, accordingly. The modelled stage at Channoy, Hatxaykhoun and the end of Channel 5 were 88.56 m +MSL (higher than the recorded stage of 88.53 m +MSL), 85.53 m +MSL and 86.45 m +MSL (lower than the interpolated stage of 86.64 m +MSL), respectively.

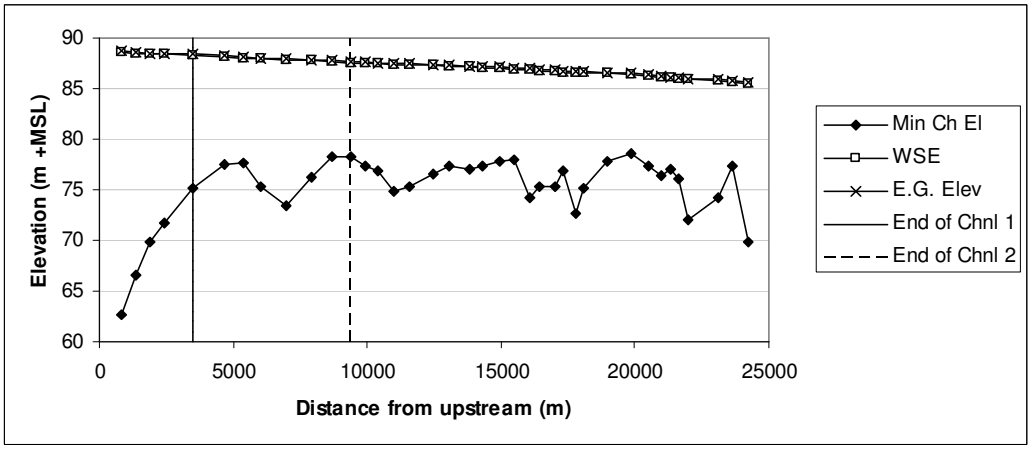

Figure 6.6-1: Water surface profile and energy gradeline along Channel 1, 2 and 3 in the average flood discharge scenario

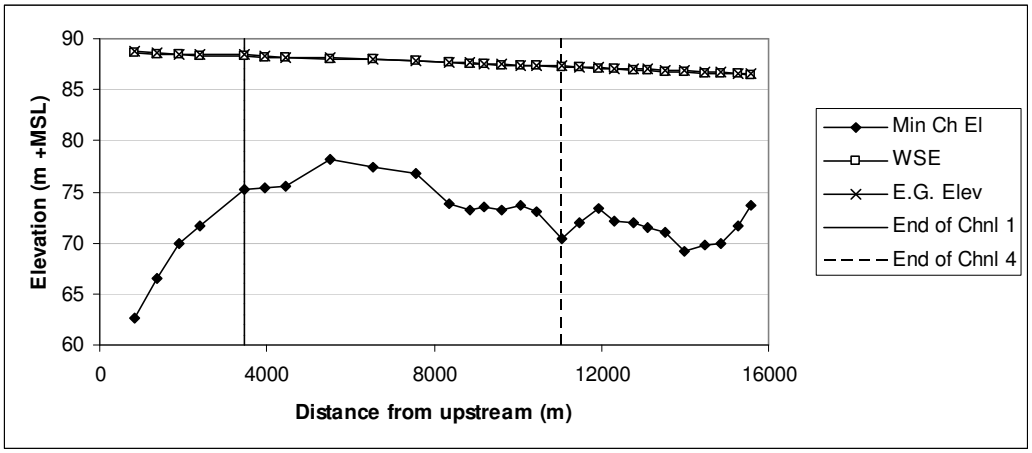

Figure 6.6-2: Water surface profile and energy gradeline along Channel 1, 4 and 5 in the average flood discharge scenario

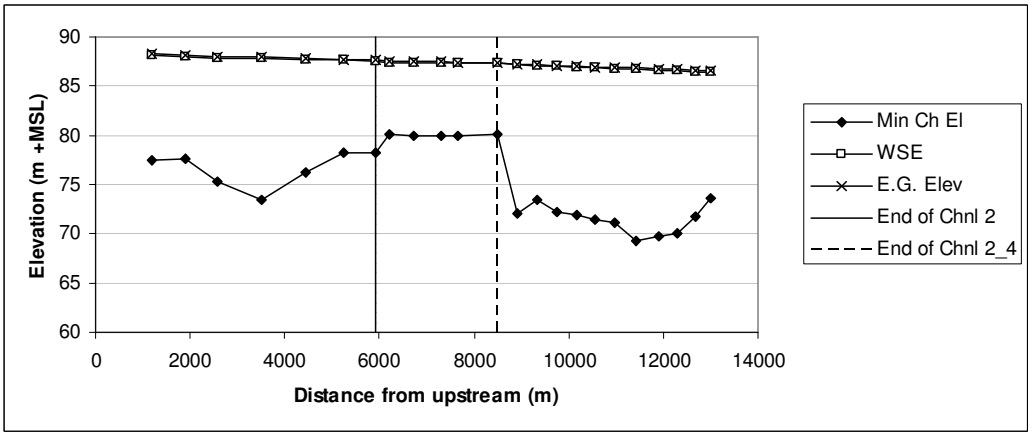

Figure 6.6-3: Water surface profile and energy gradeline along Channel 2, 2_4 and 5 in the average flood discharge scenario

Figure 6.6-4 illustrates the Froude number (ranging from 0.10 to 0.29) along the upstream river network, which shows that the flow was highly sub-critical. The range of mean in-channel velocity along the upstream river network was from 0.81 ms^{-1} to 2.02 ms^{-1} in which the lowest mean in-channel velocity could be found along Channel 2_4 and the highest mean in-channel velocity could be found along the terminal segment of Channel 3 according to the low cross-sectional areas. In general, as in the low discharge model, the mean in-channel velocity along Channel 1 was the highest while the mean in-channel velocity along Channel 2_4 was the smallest among other channels within the upstream river networks. In addition, in the low discharge scenario, along each individual channel, the mean in-channel velocity increased when the cross-sectional area decreased.

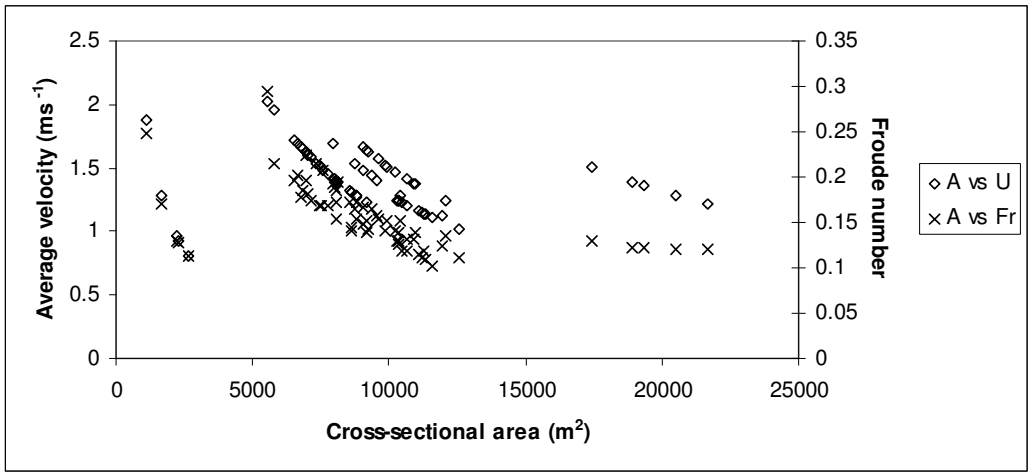

Figure 6.6-4: Froude number, mean in-channel velocity and cross-sectional area at each cross-section along the upstream river network in average flood discharge scenario

Figure 6.6-5 presents the mean velocity in the left and right riparian zone in comparison with the mean in-channel velocity in the average flood discharge. The maximum mean velocity in the riparian zone was 0.46 ms^{-1}; much smaller than the maximum mean in-channel velocity of 2.33 ms^{-1}. In addition, the discharge entering the left and right riparian zones is presented in Figure 6.6-6. In fact, the percentage of the discharge entering the left and right riparian zones was so small (maximum of 1.74% of the total discharge at a cross-section) due to very small mean riparian velocity and the flooded area compared to the mean in-channel velocity and the in-channel discharge. Figure 6.6-7 presents the flooding pattern according to the average flood discharge (26,300 m^3s^{-1}) and the wetted-area along the riparian zone was 5.16 km^2.

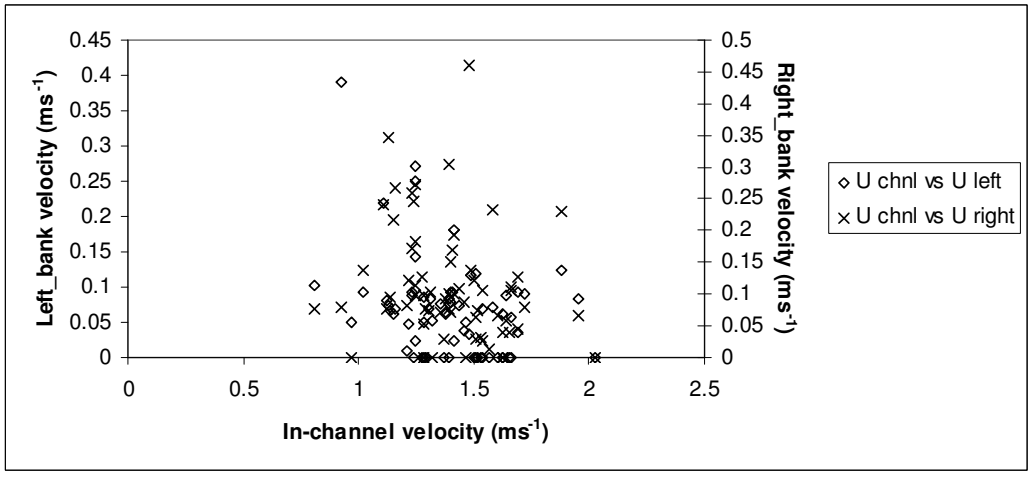

Figure 6.6-5: Mean floodplain and in-channel velocity in the average flood discharge scenario

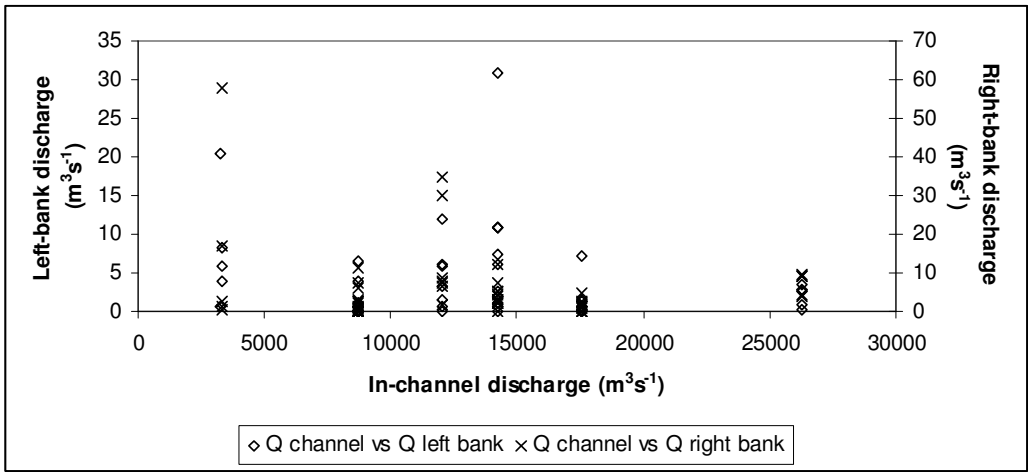

Figure 6.6-6: Discharge entering the left and right banks and the main channel in the average flood discharge scenario

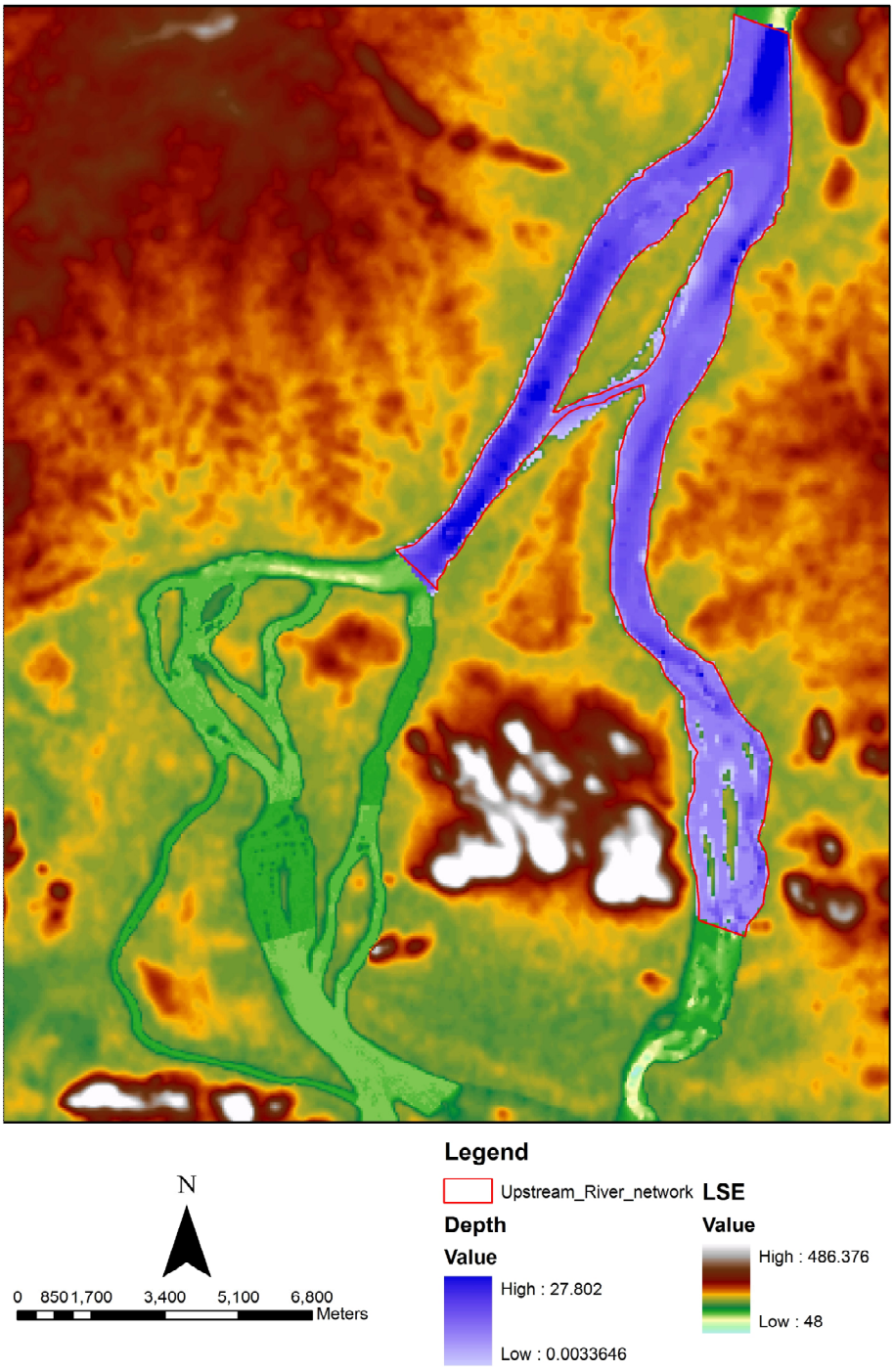

Figure 6.6-7: Modelled flooding pattern according to average flood discharge (26,300 m^3s^{-1}) based on the measured bathymetry

b. Pseudo-bathymetry

Figure 6.6-8 presents the calculated Manning's *n* at each cross-section along Channel 4 according to the average flood discharge (26,300 m^3s^{-1}). The values calculated

according to the pseudo-bathymetry were similar to those calculated based on the measured bathymetry.

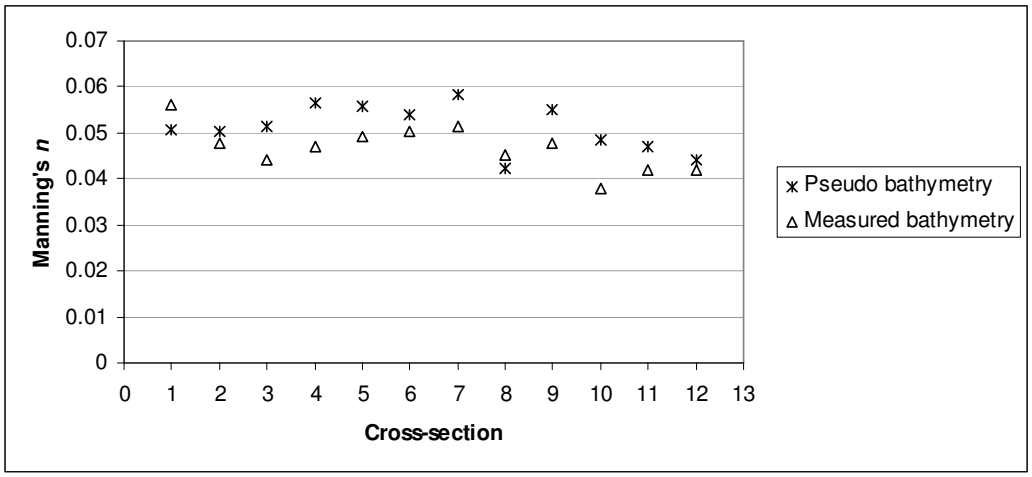

Figure 6.6-8: Calculated Manning's *n* according to the measured and pseudo-bathymetry along Channel 4 in the average flood discharge scenario

The calculated water surface slope along Channel 4 and 5 was 1.28 x 10^{-4} mm^{-1}; however, to minimize the hydraulic drop and/or rise at each bifurcation and to make the model meet the recorded stage at Channoy and Haxaykhoun, the slope was adjusted to 1.98 x 10^{-4} mm^{-1}. According to the calculated Manning's *n* based on the pseudo-bathymetry, the modelled water surface elevations at Channoy, Hatxaykhoun and the end of Channel 5 were 88.60 m +MSL, 85.53 m +MSL and 86.49 m +MSL, respectively. The water surface profiles along the upstream river network based on the pseudo-bathymetry were presented in Figure 6.6-9, Figure 6.6-10 and Figure 6.6-11.

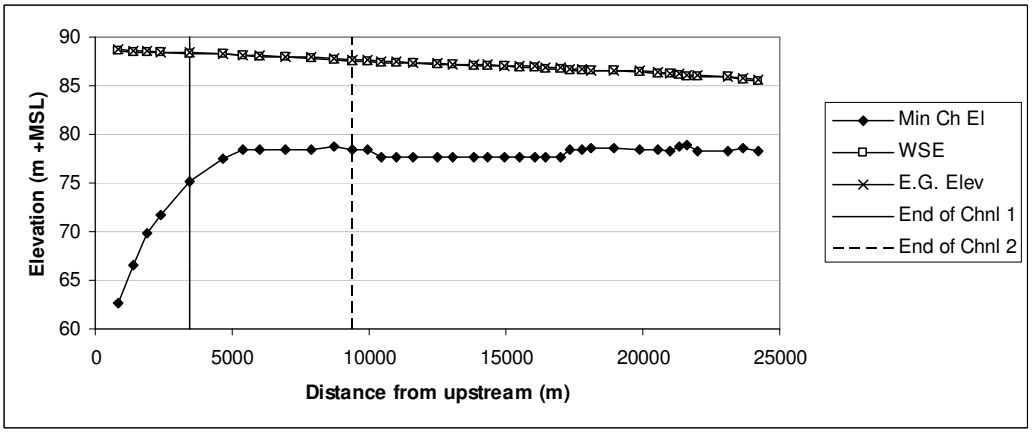

Figure 6.6-9: Water surface profile and energy gradeline along Channel 1, 2 and 3 in the average flood discharge scenario

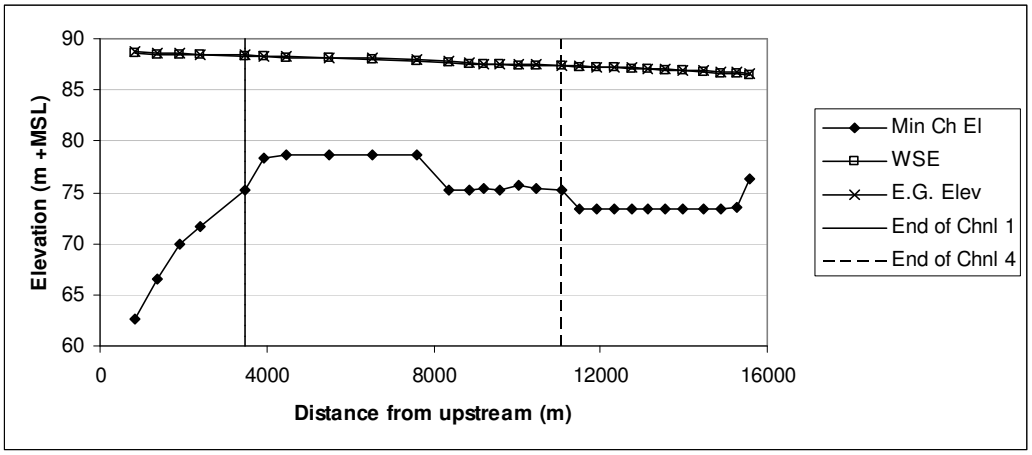

Figure 6.6-10: Water surface profile and energy gradeline along Channel 1, 4 and 5 in the average flood discharge scenario

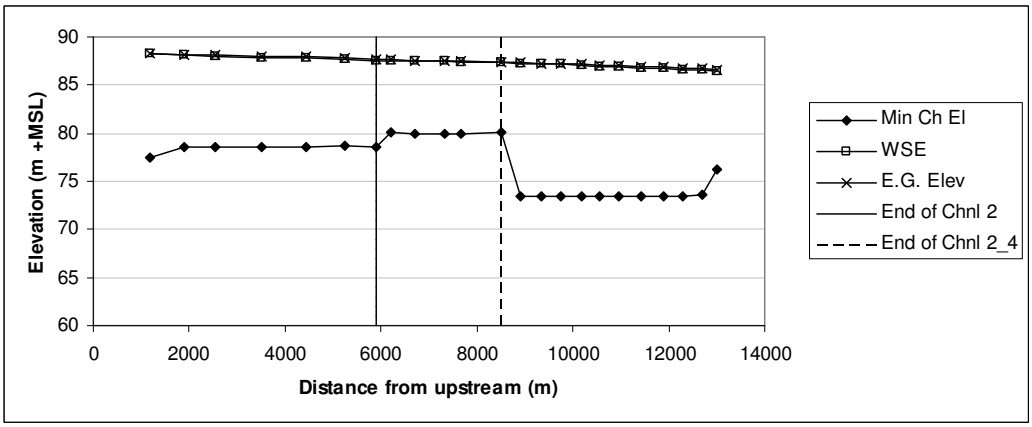

Figure 6.6-11: Water surface profile and energy gradeline along Channel 2, 2_4 and 5 in the average flood discharge scenario

Figure 6.6-12 presents the relationship between the Froude number and mean in-channel velocity at each cross-section along the river network. The Froude number ranged from 0.10 to 0.26 and the mean in-channel velocity ranged from 0.76 ms^{-1} to 1.92 ms^{-1}. In addition, there was a wide range of the modelled cross-sectional area (from 1,200 m^2 to 21,782 m^2) with the highest cross-sectional areas along Channel 1 and the lowest along Channel 2_4.

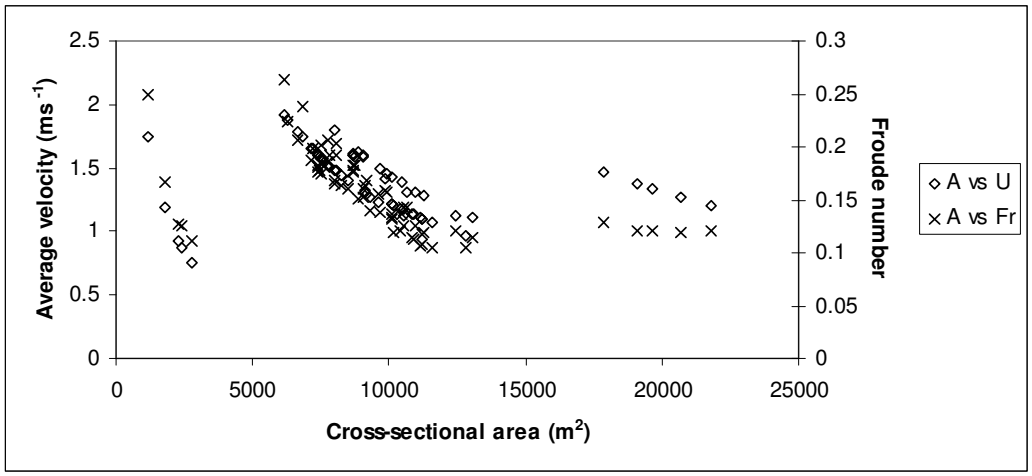

Figure 6.6-12: Froude number, mean in-channel velocity and cross-sectional area at each cross-section along the upstream river network in average flood discharge scenario

presents the modelled water surface elevation at each cross-section calculated according to the measured and pseudo-bathymetry. The water surface profiles in the two analyses were similar from each other and the absolute differences in stage are presented in Figure 6.6-13. The maximum differences appeared in Channel 3 (cross-section number 3.06) with the difference between the modelled water surface elevations being 0.15 m. In general, models based on the two bathymetries created quite well-matched results in terms of water surface elevation.

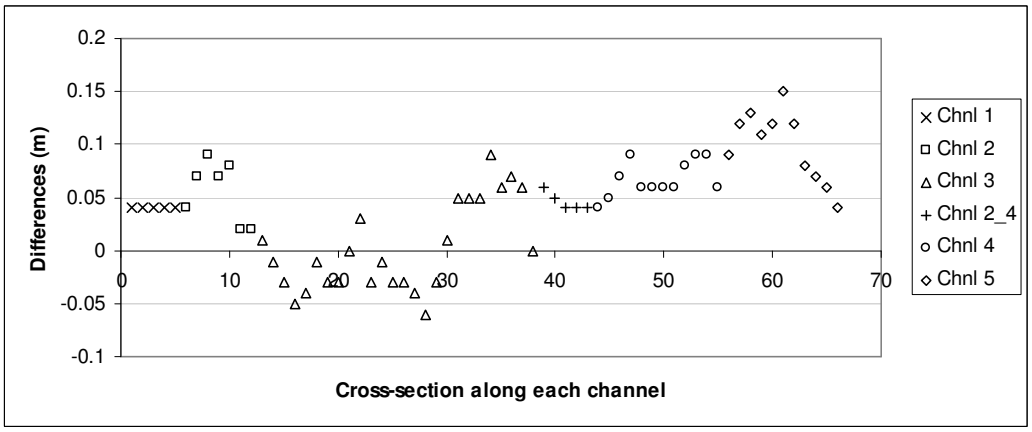

Figure 6.6-13: Differences in stages at each cross-section in the average flood discharge scenario

c. Hypothetical scenarios of land cover pattern based on the measured bathymetry

Figure 6.6-14 presents the differences in the modelled water surface elevation at each cross-section in different scenarios of land cover pattern. The modelled water surface elevations calculated according to the past land cover pattern were slightly higher than

those calculated according to the current one while the modelled water surface elevations calculated in the future land cover pattern were slightly lower than those calculated according to the current one. However, such differences were not significant and the mean value of differences was about 0 m and 0.03 m in comparison between the past to current land cover pattern and between the future to current land cover pattern, respectively. In addition, the mean in-channel velocities at each cross-section in all scenarios of the land cover pattern were quite similar, except some local differences. In fact, the mean in-channel velocity was quite similar between the models calculated according to the past and current land cover patterns. However, when the natural land cover was cleared for agriculture (*i.e.* the future land cover pattern), the local in-channel velocity slightly decreased where the relatively rough floodplain was found in the current land cover pattern and replaced by a 'smooth' floodplain in the future (*e.g.* changing from the natural forest into the rice paddy) (Figure 6.6-15).

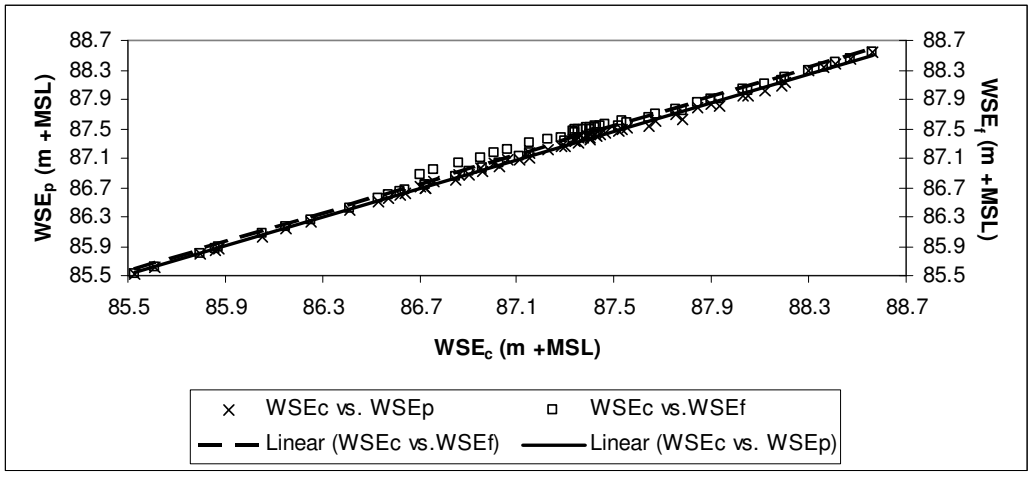

Figure 6.6-14: Modelled WSE at each cross-section according to the land cover change in the average flood discharge scenario; WSEc, p, f – Water surface elevation for the current, past and future land cover pattern, respectively

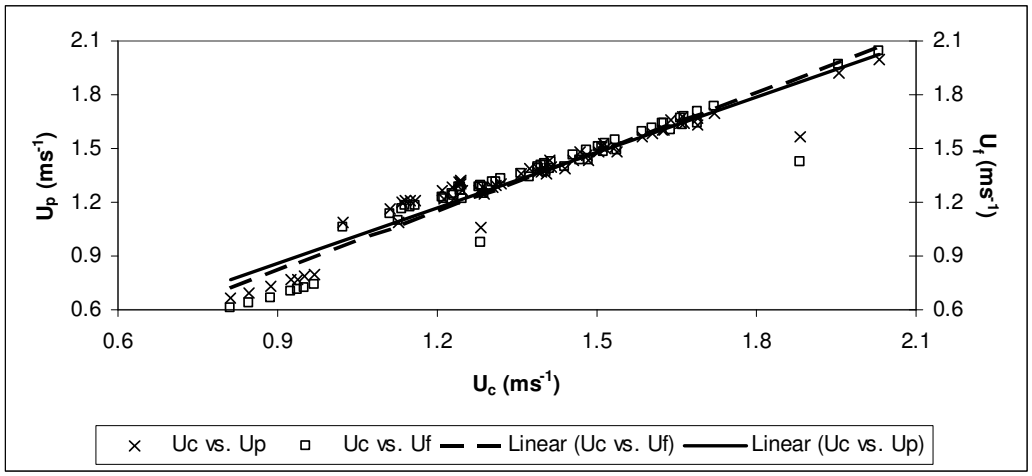

Figure 6.6-15: Modelled mean in-channel velocity at each cross-section according to the land cover change in the average flood discharge scenario; Uc, p, f – Water surface elevation for the current, past and future land cover pattern, respectively

Figure 6.6-16 and Figure 6.6-17 present the differences in the mean riparian velocity according to different land cover patterns along the left and right banks, respectively. Along both the left and right banks, the mean riparian velocity increased from the past to current and future land cover patterns, which indicates that the rougher the floodplain, the slower the flow.

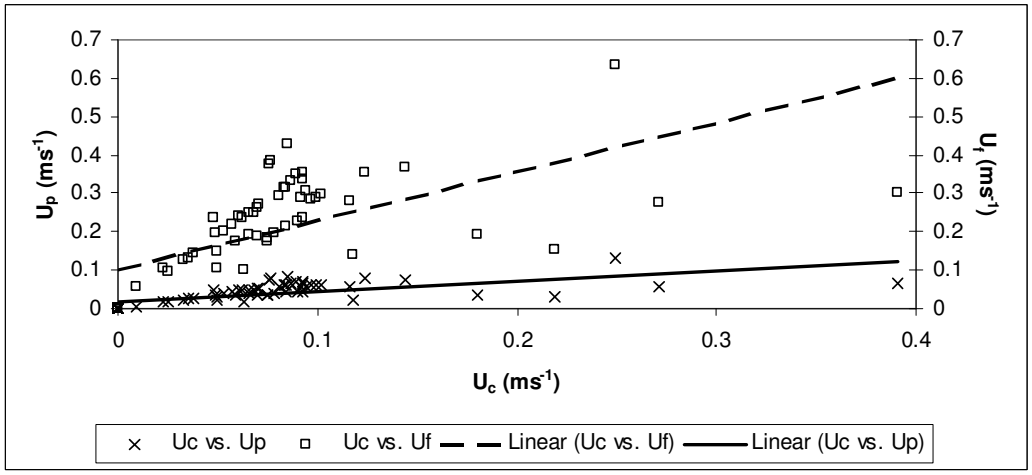

Figure 6.6-16: Modelled mean velocity in the floodplain along the left bank in the average flood discharge scenario; Uc, p, f – Water surface elevation for the current, past and future land cover pattern, respectively

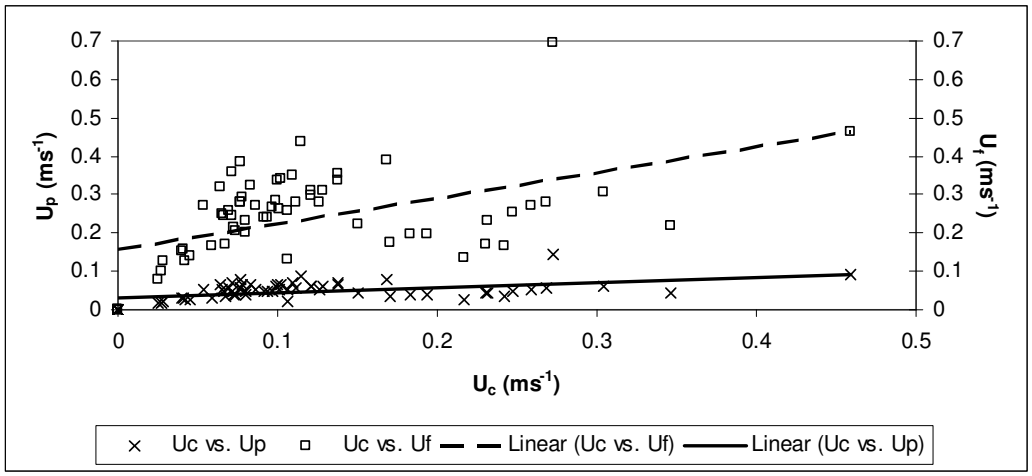

Figure 6.6-17: Modelled mean velocity in the floodplain along the right bank in the average flood discharge scenario; Uc, p, f – Water surface elevation for the current, past and future land cover pattern, respectively

6.6.2 Spatial pattern of the historical high flood discharge (45,149 m^3s^{-1})

According to the assumption that the Manning's *n* coefficient at each cross-section along the upstream river network was stable in the flood discharge, the set of calculated Manning's *n* according to the historical average flood discharge was applied for the hydraulic model in the high flood discharge. The boundary conditions in the large flood discharge were: (i) the recorded stages at Channoy (91.21 m +MSL) and Hatxaykhoun (87.32 m +MSL); and, (ii) the interpolated stage at the downstream end cross-section along Channel 5 (87.81 m +MSL).

a. Based on the measured DEM

The modelled water surface profiles and energy gradeline are presented in Figure 6.6-18, Figure 6.6-19 and Figure 6.6-20. The modelled stage at Channoy was 91.21 m +MSL, lower than the recorded stage of about 0.05 m.

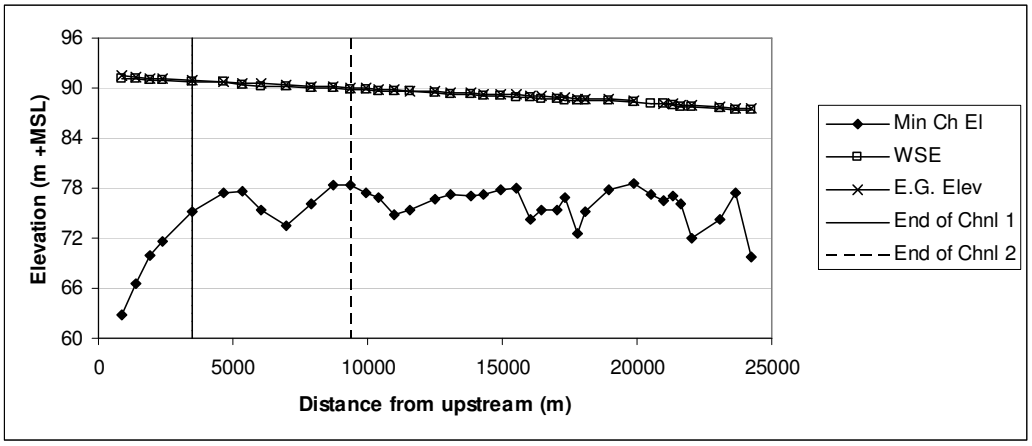

Figure 6.6-18: Water surface profile and energy gradeline along Channel 1, 2 and 3 in the high flood discharge scenario

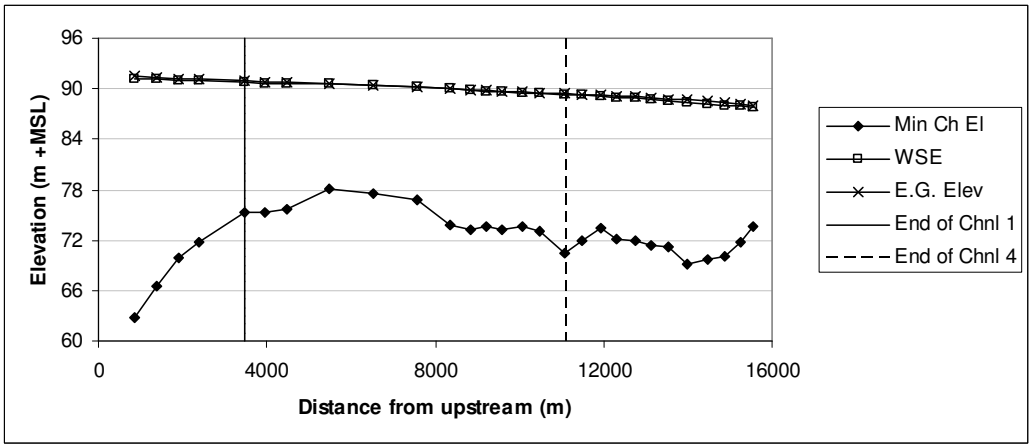

Figure 6.6-19: Water surface profile and energy gradeline along Channel 1, 4, and 5 in the high flood discharge scenario

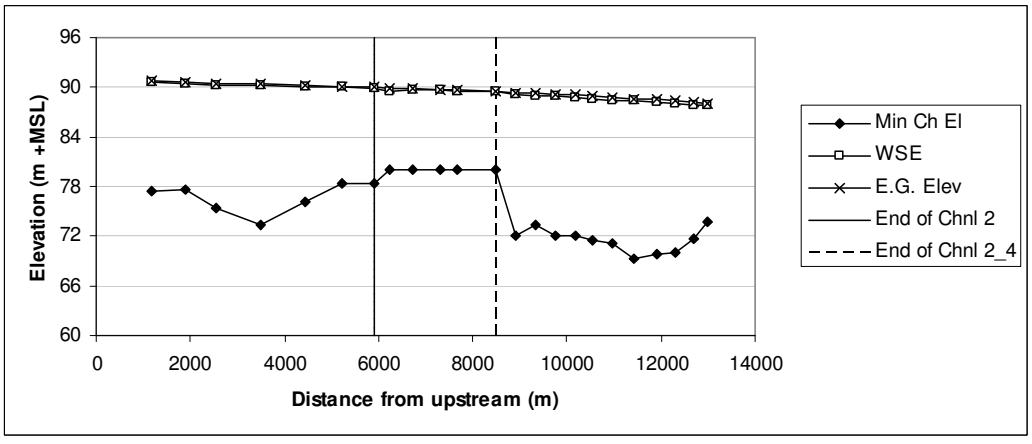

Figure 6.6-20: Water surface profile and energy gradeline along Channel 2, 2_4 and 5 in the high flood discharge scenario

Along the upstream river network, the calculated Froude number ranged from 0.13 to 0.31 (Figure 6.6-21) (much smaller than 1). Therefore, the flow could be considered as sub-critical flow. The mean in-channel velocity ranged from 1.19 ms^{-1} to 2.72 ms^{-1} in which the minimum mean in-channel velocity appeared along the cross-channel while the maximum mean in-channel velocity appeared along Channel 3. As it was in the low discharge and average flood discharge models, the cross-sectional area has a strong negative relationship with mean in-channel velocity (*i.e.* along each channel, the lower cross-sectional area, the higher mean in-channel velocity).

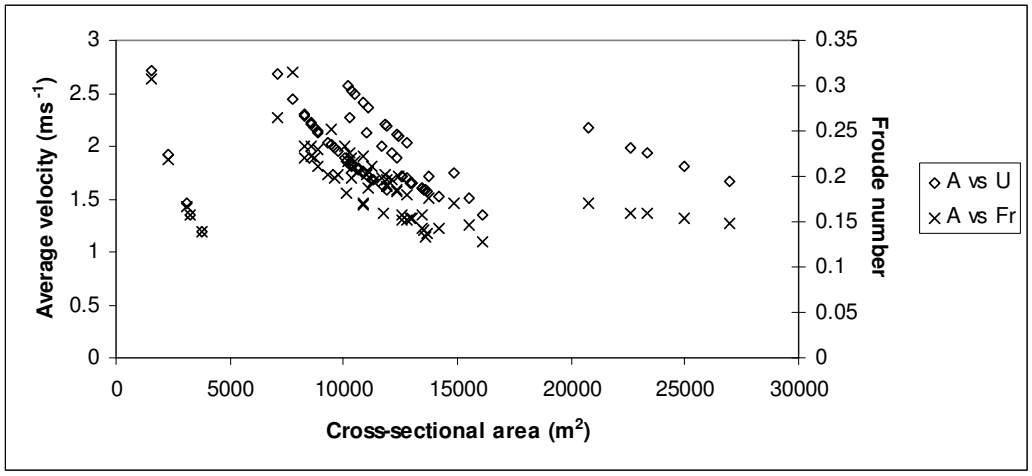

Figure 6.6-21: Froude number, mean in-channel velocity and cross-sectional area at each cross-section along the upstream river network in high flood discharge simulation

Figure 6.6-22 presents the mean velocity in the left and right riparian zones in comparison with the mean in-channel velocity in the high flood discharge. The maximum mean velocity in the riparian zone was 0.31 ms^{-1}, much smaller than the maximum mean in-channel velocity of 2.94 ms^{-1}. In addition, the discharge enters the left and right riparian zones is presented in Figure 6.6-23. The percentage of the discharge entering the left and right riparian zones was very small (maximum of 5.85% of the total discharge at a cross-section) due to very relatively small mean riparian velocity and wetted-area along the riparian zones compared to those in the main channel. The flooding pattern according to the high flood discharge (45,149 m^3s^{-1}) was presented in Figure 6.6-24 and the wetted-area along the floodplain was 7.51 km^2.

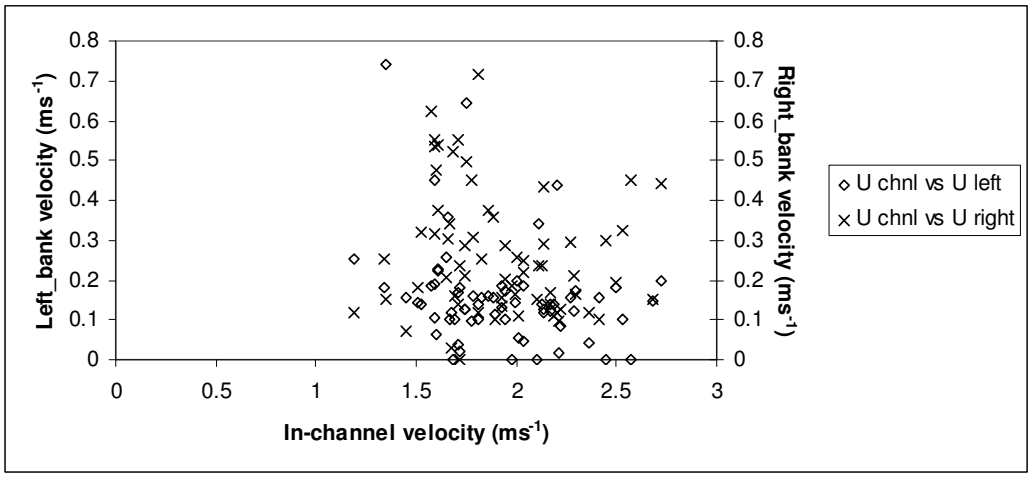

Figure 6.6-22: Mean riparian velocity and mean in-channel velocity in the high flood discharge

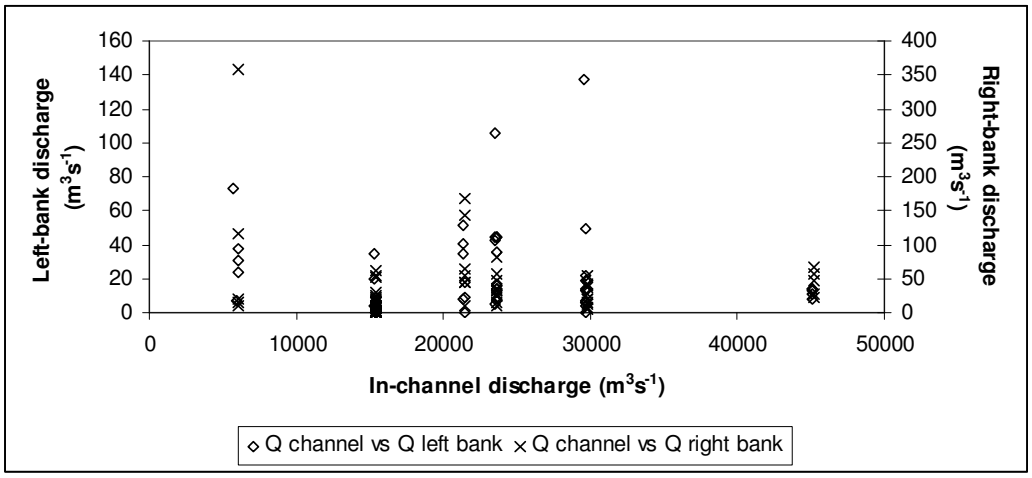

Figure 6.6-23: Discharge entering the left and right banks and the main channel in the high flood discharge

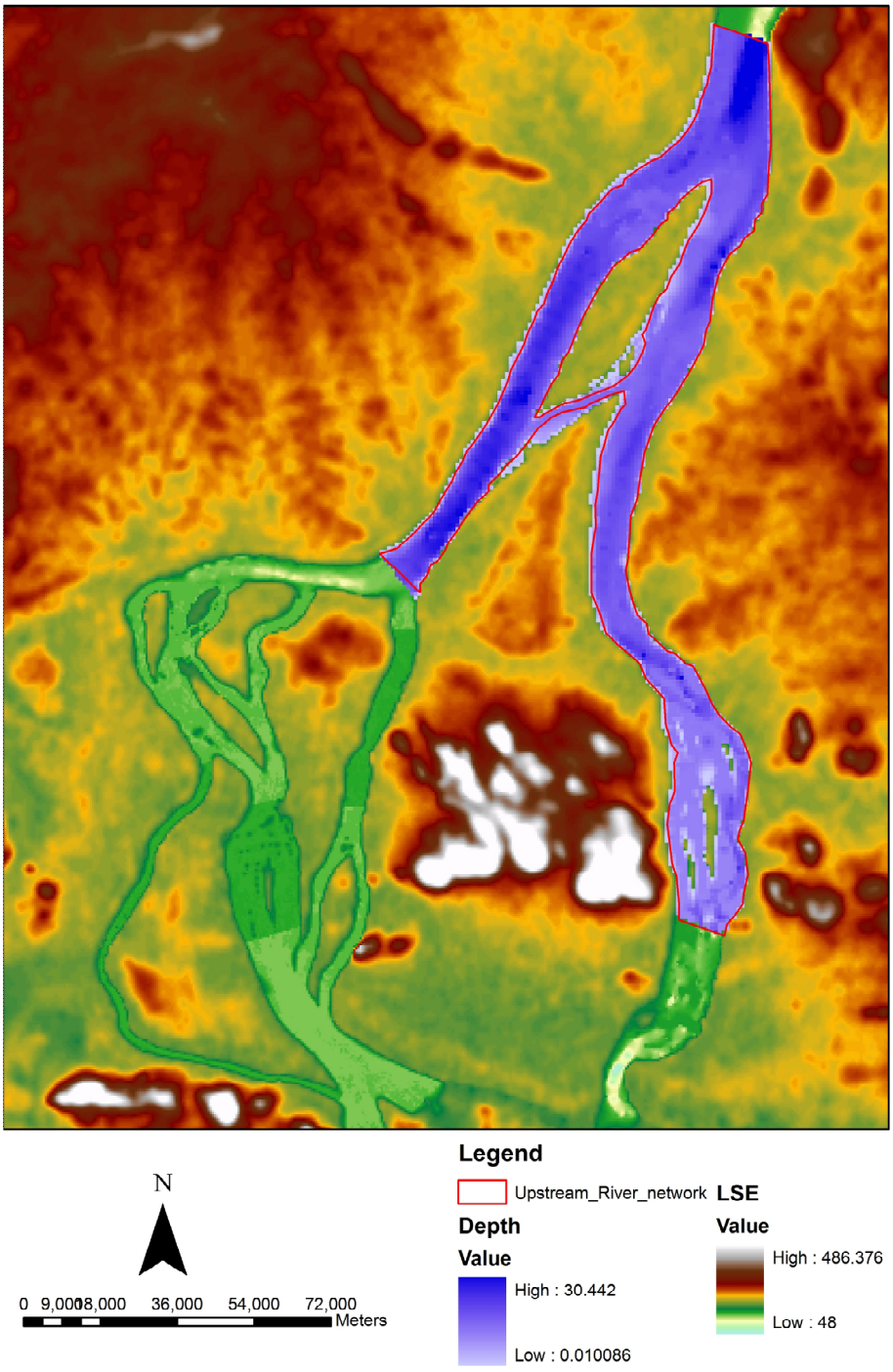

Figure 6.6-24: Modelled flooding pattern according to high flood discharge (45,149 m^3s^{-1}) based on the measured bathymetry

b. Based on the pseudo-bathymetry

By applying the water surface slope at Channel 5 at 3.0 x 10^{-4} mm^{-1} (even though the calculated slope was 1.68 x 10^{-4} mm^{-1}), the modelled water surface elevation at upstream was 91.33 m which was higher than the recorded stage of about 0.17 m.

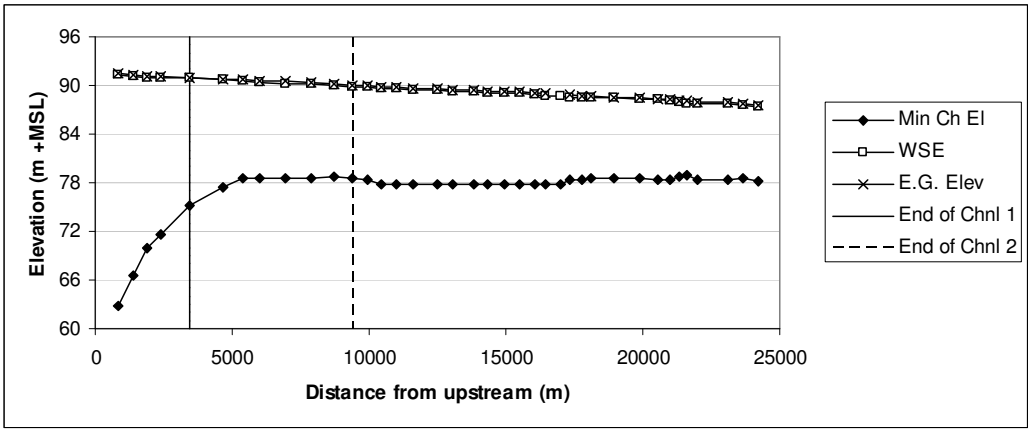

Figure 6.6-25: Water surface profile and energy gradeline along Channel 1, 2 and 3 in the high flood discharge scenario

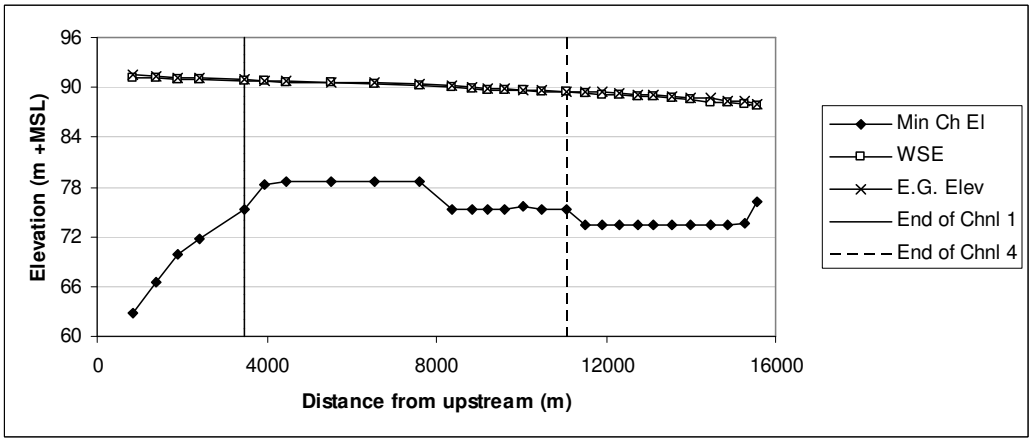

Figure 6.6-26: Water surface profile and energy gradeline along Channel 1, 4 and 5 in the high flood discharge scenario

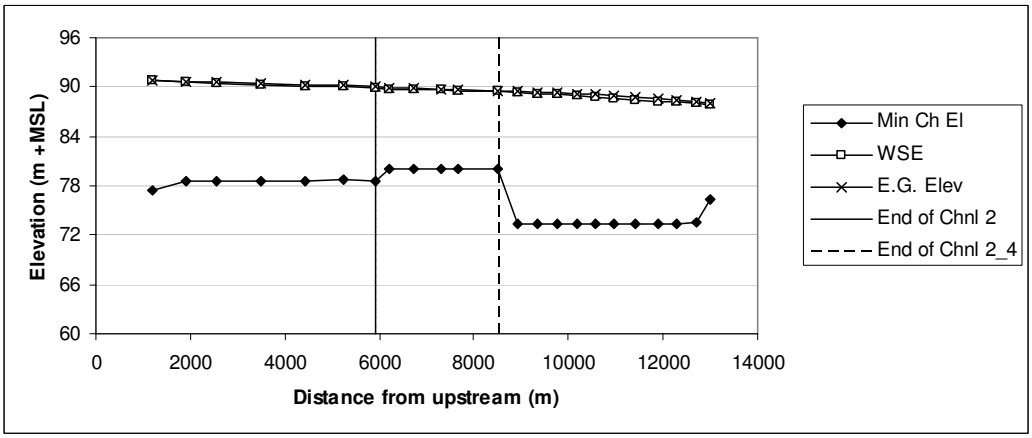

Figure 6.6-27: Water surface profile and energy gradeline along Channel 2, 2_4 and 5 in the high flood discharge scenario

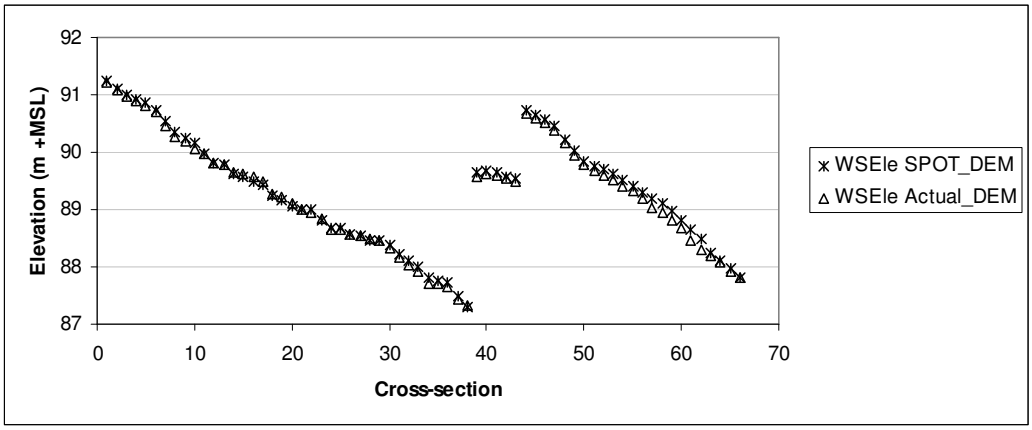

Figure 6.6-28: Modelled water surface profiles according to the measured and pseudo-bathymetry in the high flood discharge scenario

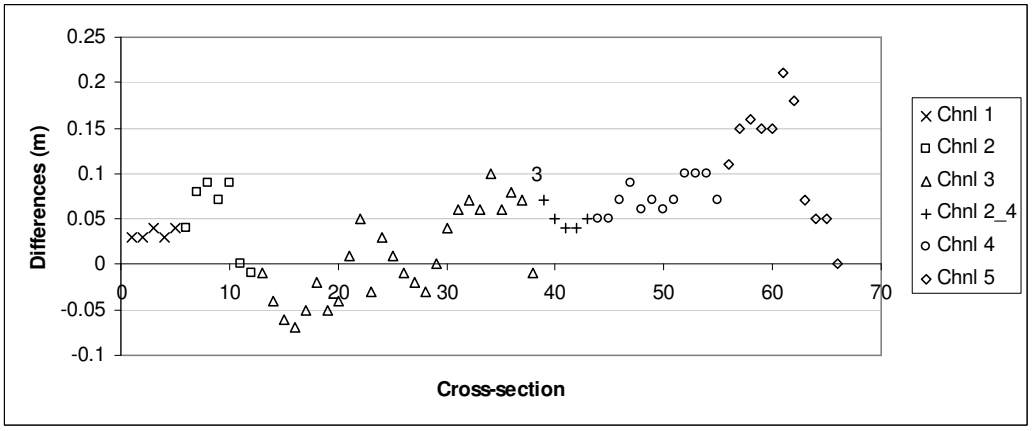

Figure 6.6-29: Differences in stages at each cross-section in the high flood discharge scenario

Figure 6.6-30 presents the relationship between the Froude number and mean in-channel velocity at each cross-section along the upstream river network. The Froude number ranged from 0.12 to 0.30 and the mean in-channel velocity ranged from 1.11 ms^{-1} to 2.78 ms^{-1}. Figure 6.6-30 also presents the relationship between the cross-sectional area and mean in-channel velocity at each cross-section in which the cross-sectional area ranged from 1,721 m^2 to 27,181 m^2. In fact, the relationship between the Froude number and the cross-sectional area *vs.* mean in-channel velocity was similar to those when the measured bathymetry was applied.

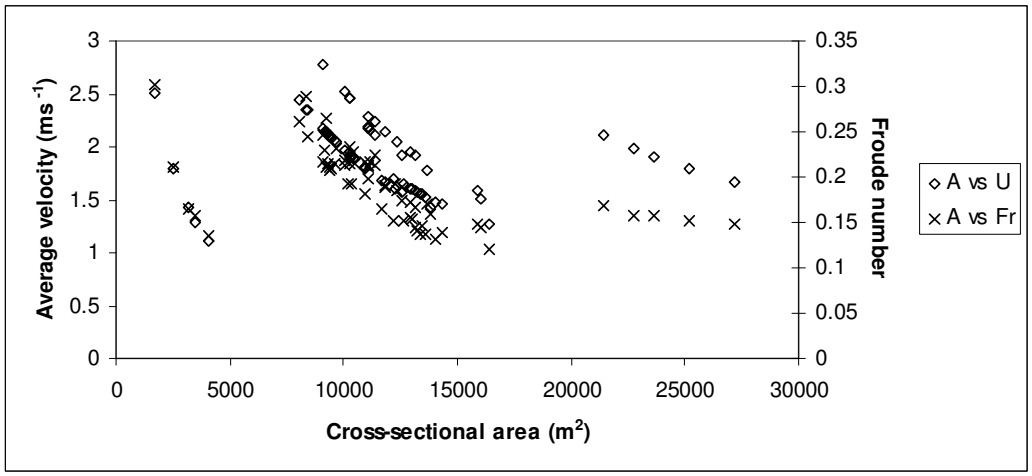

Figure 6.6-30: Froude number, mean in-channel velocity and cross-sectional area at each cross-section along the upstream river network in high flood discharge simulation

c. Hypothetical scenarios of land cover pattern based on the measured bathymetry

Figure 6.6-31 presents the differences in the modelled water surface elevation at each cross-section in different scenarios of land cover pattern. Similar to the modelled results according to the average flood discharge, the modelled water surface elevations calculated according to the past land cover pattern were slightly higher than those calculated according to the current one which in turn were slightly higher than those calculated according to the future one. However, such differences were not significant and the mean value of differences was about 0 m and 0.05 m in comparison between the past to current land cover pattern and between the future to current land cover pattern, respectively. In addition, also similar to the average flood discharge scenario, the mean in-channel velocity at each cross-section in all scenarios of the land cover pattern was quite similar, except some local differences (Figure 6.6-32).

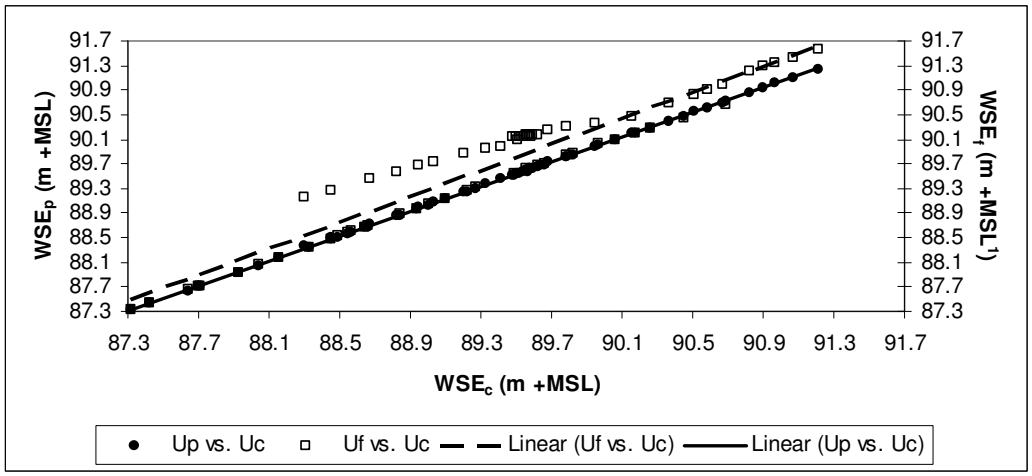

Figure 6.6-31: Modelled WSE at each cross-section according to the land cover change in the high flood discharge scenario; $WSE_{c, p, f}$ – Water surface elevation for the current, past, and future land cover pattern, respectively

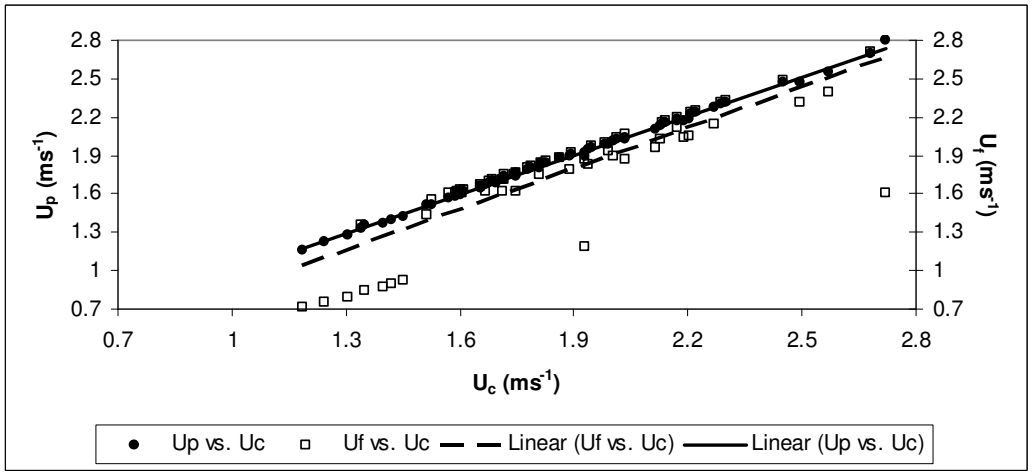

Figure 6.6-32: Modelled mean in-channel velocity at each cross-section according to the land cover change in the high flood discharge scenario; $U_{c, p, f}$ – Water surface elevation for the current, past, and future land cover pattern, respectively

Figure 6.6-33 and Figure 6.6-34 present the differences in the mean riparian velocity between the current *vs.* past land cover pattern and current *vs.* future land cover pattern, respectively. In general, the rougher land surface, the slower the flow.

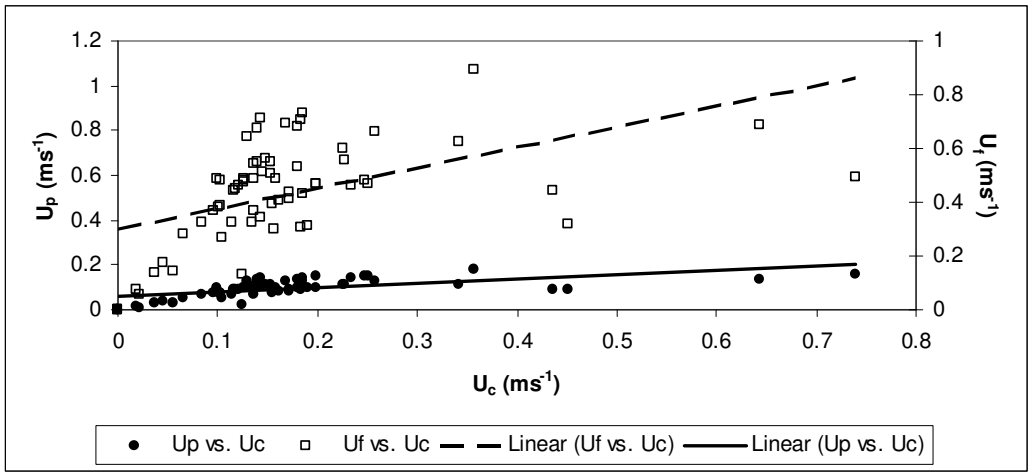

Figure 6.6-33: Modelled mean velocity in the floodplain along the left bank in the high flood discharge scenario; $U_{c,\,p,\,f}$ – Water surface elevation for the current, past, and future land cover pattern, respectively

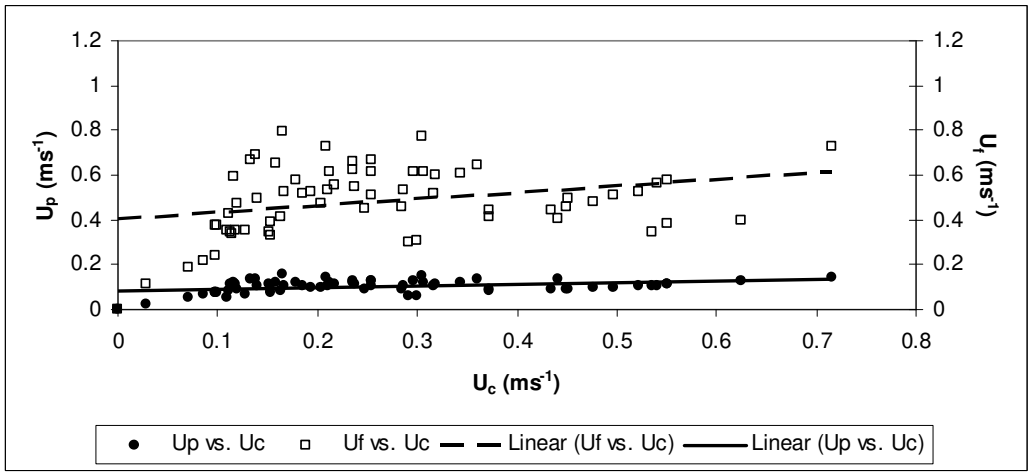

Figure 6.6-34: Modelled mean velocity in the floodplain along the right bank in the high flood discharge scenario; $U_{c,\,p,\,f}$ – Water surface elevation for the current, past, and future land cover pattern, respectively

6.7 The hydraulic properties along Siphandone and at the Pakse gauging station in all three scenarios of entry discharge

Figure 6.7-1 illustrates a comparison between the calculated mean velocities in three scenarios of entry discharge. Even though there were significant differences in the mean in-channel velocity at each cross-section, the mean in-channel velocity in all cross-sections in the low discharge was the smallest (0.62 ± 0.16 ms^{-1}) while the figure was the highest in the high flood discharge (1.90 ± 0.46 ms^{-1}); the mean in-

channel velocity in all cross-sections in the average flood discharge was 1.41 ± 0.31 ms^{-1}. Figure 6.7-2 illustrates a comparison between the calculated water surface slopes in three scenarios of entry discharge. The water surface slope in the low discharge scenario changed significantly from one cross-section to another. The mean water surface slope over the upstream river network was 2.0 x 10^{-4} mm^{-1} and the standard deviation in the water surface slope was 2.28 x 10^{-4} mm^{-1}. However, in the flood discharge scenarios, the water surface slopes were more stable in all cross-sections. In fact, the mean water surface slopes in the average and high flood discharge were 1.2 x 10^{-4} mm^{-1} and 1.6 x 10^{-4} mm^{-1}, respectively while the standard deviations in the water surface slope in the average and high flood discharge were 3.3 x 10^{-4} mm^{-1} and 5.0 x 10^{-5} mm^{-1}, respectively. In general, the higher mean in-channel velocity together with the lower water surface slope from Pakse to Channoy led to smaller Manning's *n* in Pakse than in Siphandone (Figure 6.7-3).

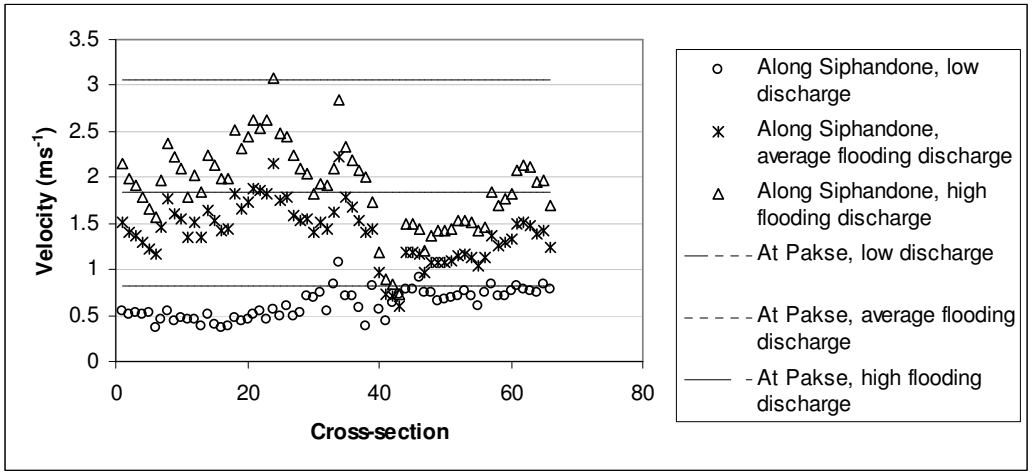

Figure 6.7-1: Comparison of the calculated mean in-channel velocity at Pakse and along the Siphandone river network

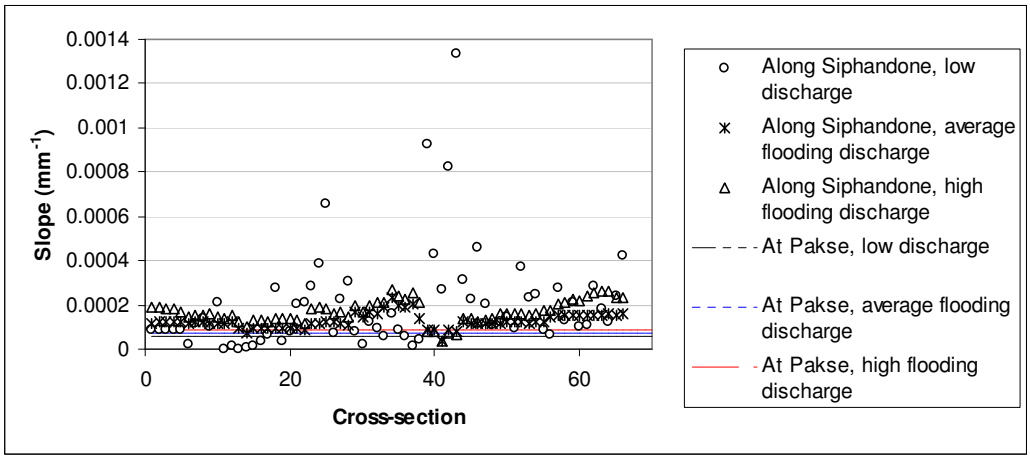

Figure 6.7-2: Comparison of the calculated water surface slope from Pakse to Channoy and along the Siphandone river network

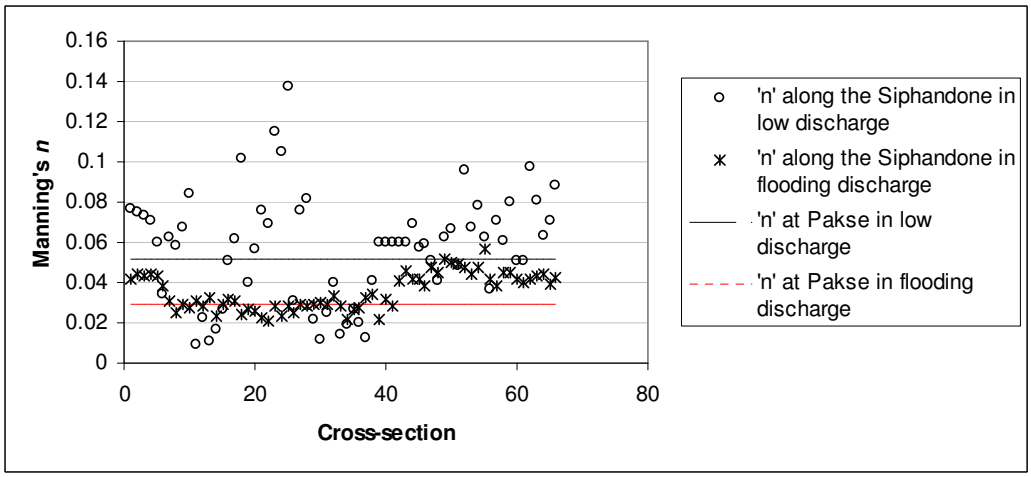

Figure 6.7-3: Comparison of the calculated Manning's *n* at Pakse and along the Siphandone river network

6.8 Discussion

The land cover pattern in the Siphandone wetlands changed significantly even in a short period (2001 – 2005). More agriculture (rice paddy) was practised along the upstream river network corridor. In hilly areas, the natural forest and degraded forest existed in 2001 were converted into shrub, a more degraded land cover type by 2005. Due to a large proportion of the discharge routed in the channel section of a cross-section in the large river network, the land cover changes leading to changes in the riparian hydraulic roughness did not have a significant impact on the flood extent. However, the mean velocity along the riparian zone changed according to the assigned hydraulic roughness (*i.e.* the rougher the surface, the slower the flow); therefore, it may lead to geomorphological changes of the floodplain. In addition, the

SPOT image taken on 18th February, 2005 was not applied to calculate the hydraulic roughness at each cross-section in this chapter because with the low discharge (2,024 m^3s^{-1}) on the due date, the cross-channel (Channel 2_4) was partly dry and therefore the cross-channel could not be modelled.

In the energy approach of a 1D hydraulic modelling, the cross-sectional area was more important than the cross-sectional shape. Therefore, the pseudo-bathymetry could be used to estimate the water-way and flooding pattern along the upstream river network. Table 6.8-1 presents the *p*-values from the *2-Sample t-test* (Fleming and Nellis, 2000) to compare between the mean values of the modelled Froude number, mean in-channel velocity, cross-sectional area and water surface elevation (WSE) resulting from the measured and pseudo-bathymetry HEC-RAS models. It is concluded that because all the *p*-values were greater than 0.1, there were no significant differences between the modelled hydraulic parameters resulting from the measured and pseudo-bathymetry HEC-RAS models. In other words, the pseudo-bathymetry is further developed for the downstream river network which could be used to extract the geometry of the HEC-RAS model.

Table 6.8-1: The *p*-value from the *2-Sample t-test* analysis for modelled hydraulic parameters according to the measured and pseudo-bathymetry HEC-RAS model

	Low Discharge	Average Flood Discharge	Large Flood Discharge
Froude number	0.620	0.844	0.878
Mean in-channel velocity	0.677	1.000	0.895
Cross-sectional area	0.924	0.872	0.889
WSE	0.740	0.966	0.729

The splitting discharge at each bifurcation according to the ratio of the cross-sectional areas of the first cross-section of each channel downstream allowed an initial calculation of the hydraulic roughness (Manning's *n*) at each cross-section along the river network. In addition, such predefined entry discharge at each channel would then be used as the initial set of entry discharges for the HEC-RAS model. This approach was particularly helpful where there was no input data for hydraulic modelling on the splitting discharge at each bifurcation.

The cross-sections along the upstream river network had steep banks. Therefore, the top-widths extracted from the SPOT image were not significantly different from those resulting from the HEC-RAS model. To evaluate the simulated results based on the pseudo-bathymetry, the stages at each cross-section were compared to those

calculated according to the measured DEM. Figure 6.8-1, Figure 6.8-2 and Figure 6.8-3 present a comparison between the modelled cross-sectional areas resulting from the measured and pseudo-bathymetry HEC-RAS model in the case of the low discharge, average and high flood discharge with the R^2 = 0.950, 0.965 and 0.967, respectively. In fact, the differences in the low discharge scenario were higher than those in the flood discharge. Therefore, the interpolated pseudo-bathymetry was particularly useful to model the flooding pattern in a complex river network without any measured bathymetry at some river segments. In addition, there were no significant differences between the modelled Froude number and in-channel velocity based on the measured and pseudo-bathymetry in all cases of the applied upstream discharges. Table 6.8-2 shows the minimum, average, maximum and standard deviation of each geometrical aspect, including cross-sectional area, top-width and hydraulic depth (which were calculated according to the low entry discharge) along the river network. It can be seen that the geometry of the upstream river network was complex; therefore, it was not realistic to apply only one Manning's *n* coefficient for the full river network. In fact, by using the mean value of the Manning's *n* of each channel and of the whole reach, the modelled results did not match the measured data well (section 6.3.2).

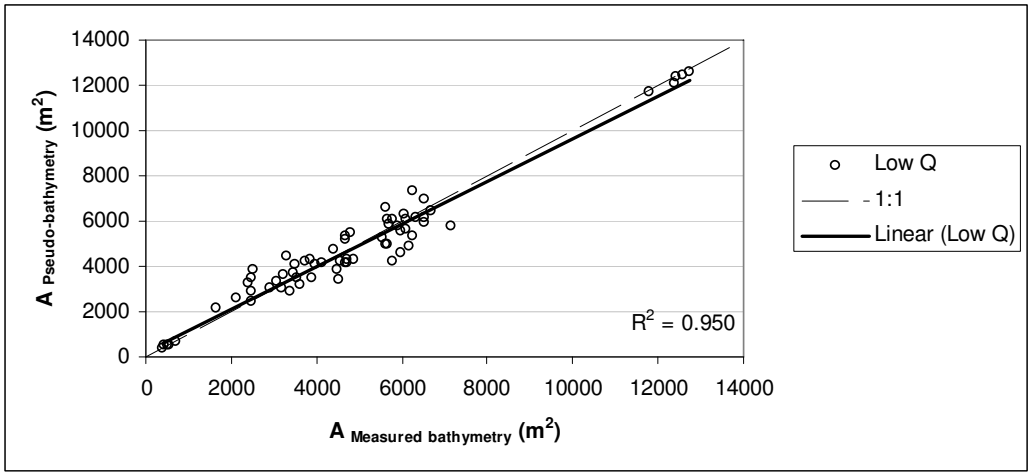

Figure 6.8-1: Comparison between the cross-sectional area (A) calculated from the measured and pseudo-bathymetry in the low discharge

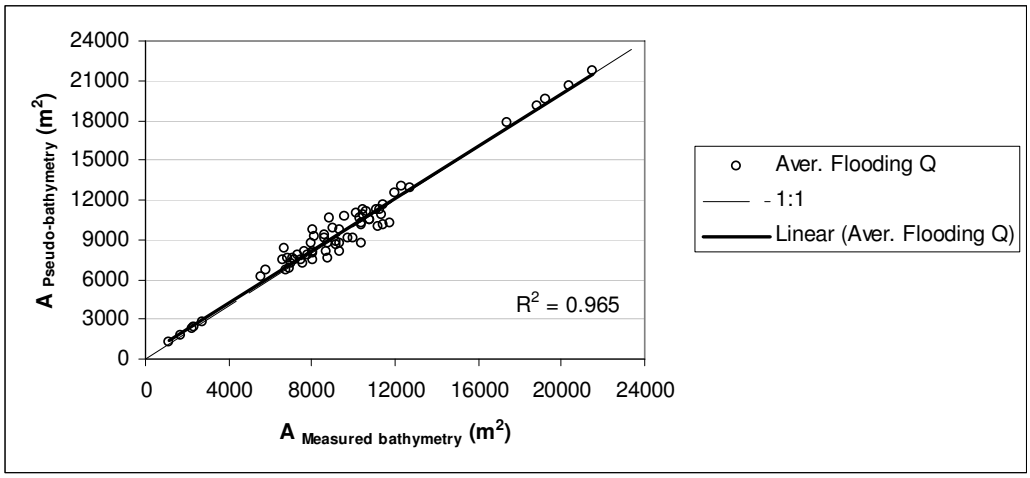

Figure 6.8-2: Comparison between the cross-sectional area (A) calculated from the measured and pseudo-bathymetry in the average flood discharge

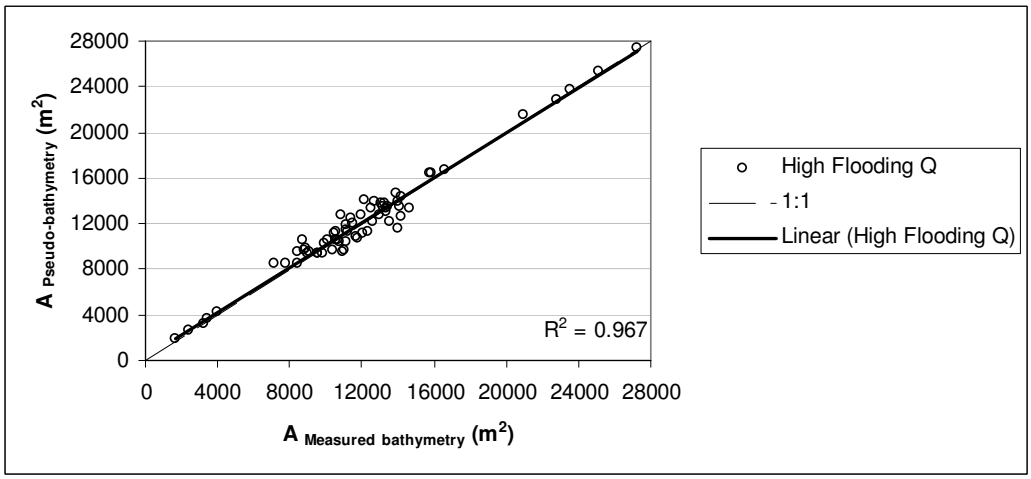

Figure 6.8-3: Comparison between the cross-sectional area (A) calculated from the measured and pseudo-bathymetry in the high flood discharge

Table 6.8-2: Summary of geometry along the upstream river network

	Cross-sectional area (m^2)	Top_width (m)	Hydraulic depth (m)
Min	1663.11	605.58	1.79
Average	5278.27	1011.51	5.31
Max	12761.23	2058.11	9.74
Standard deviation	2543.44	263.42	2.08

The mean velocity corresponding to the low discharge, average and high flood discharge at each cross-section along the upstream river network is presented in Figure 6.8-4. The mean in-channel velocity along the cross-channel (Channel 2_4) was much higher than that along other channels in the upstream river network because of the low Manning's *n* coefficients along the cross-channel (Figure 6.8-5) compared to those in other channels. In addition, the calculated in-channel hydraulic roughness

coefficients at each cross-section along Channel 4 and 5 were higher than those along Channel 2 and 3 at all applied entry discharges, which might reflect the existence of the bedrock outcrops along Channel 4 and 5. During the flood discharge, the hydraulic roughness coefficients along the cross-channel were quite similar to those along other channels; the mean in-channel velocity was quite similar over the whole upstream river network. Moreover, the findings also confirm that the hydraulic roughness coefficient calculated for the average flood discharge could be similar to a full range of flood discharges.

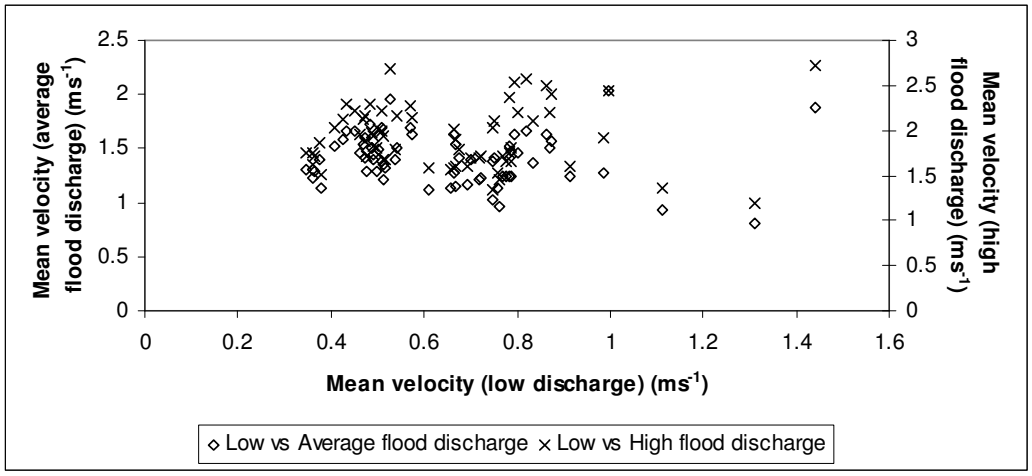

Figure 6.8-4: Mean velocity at each cross-section in low discharge, average and high flood discharge simulation

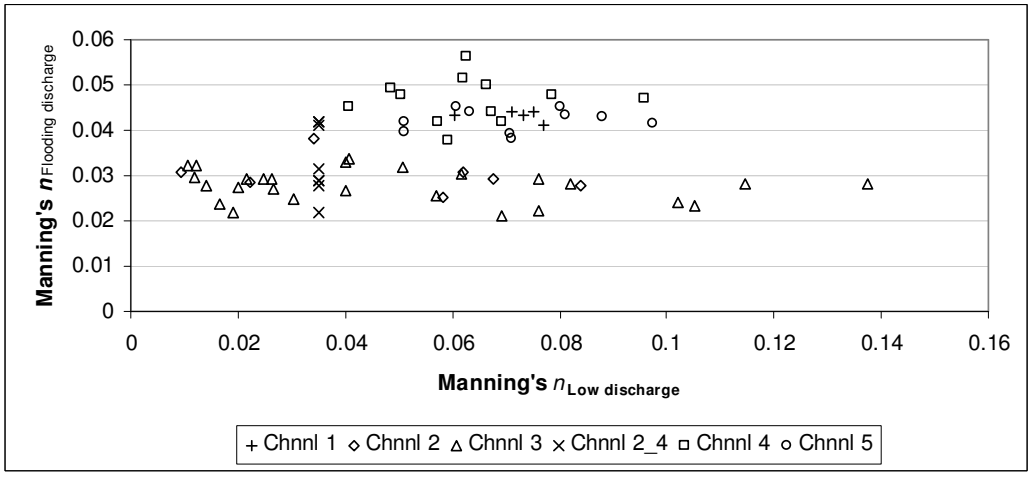

Figure 6.8-5: The calculated Manning's *n* at each cross-section in the low (6,450 m^3s^{-1}) and flood discharge scenario

By analysing the geometry of individual cross-sections along the upstream river network, the hydraulic roughness at each cross-section could be estimated and with the application of the energy approach of the 1D hydraulic model, the estimated hydraulic roughness was validated (according to the measured water surface elevation at the upstream and downstream boundary condition and the top-width according to the SPOT image). In the low discharge scenario, the water surface slope may change rapidly. Therefore, the application of one water surface slope for every cross-section along a channel (as it was in the flooding scenario) was not realistic. The SPOT image was used to extract the top-width at each cross-section; based on the extracted top-width and the applied DEM, the water surface elevation at each cross-section could be estimated and therefore the local water surface slope from one cross-section to the neighbour could be calculated (Chapter 4, section 4.5). Even though there existed cross-sections with low Manning's *n* coefficient, they often had small cross-sectional area as well, leading to higher flow velocity. The relationship between the calculated Manning's *n* and the cross-sectional area of each cross-section is found in Figure 6.8-6 in which the mean Manning's *n* was 0.057 and the standard deviation of the mean Manning's *n* was 0.027. In the flood discharge scenario, the water surface slope was mostly stable along the network. Therefore, a general slope could be used to calculate the hydraulic roughness coefficient at each cross-section. The relationship between the Manning's *n* and the cross-sectional area could be found in Figure 6.8-7 in which the mean Manning's *n* value was 0.035 and the standard deviation of the mean Manning's *n* was 0.009.

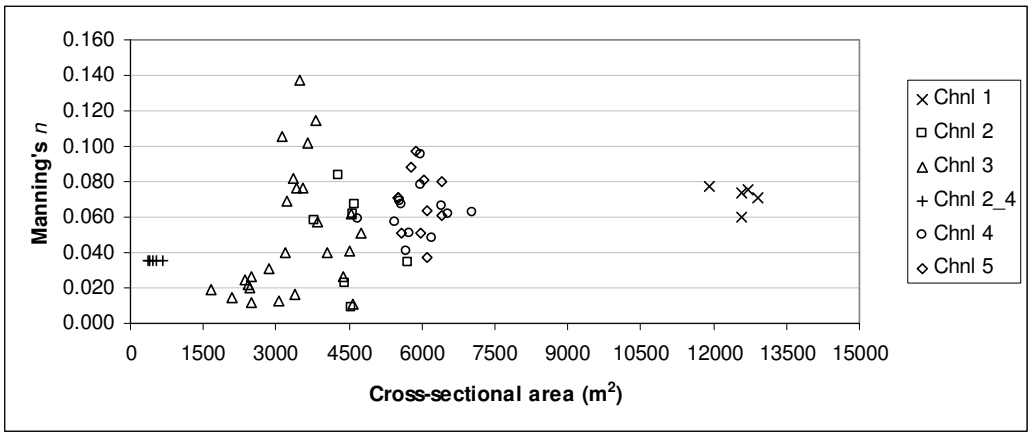

Figure 6.8-6: Manning's *n vs.* cross-sectional area in the low discharge scenario

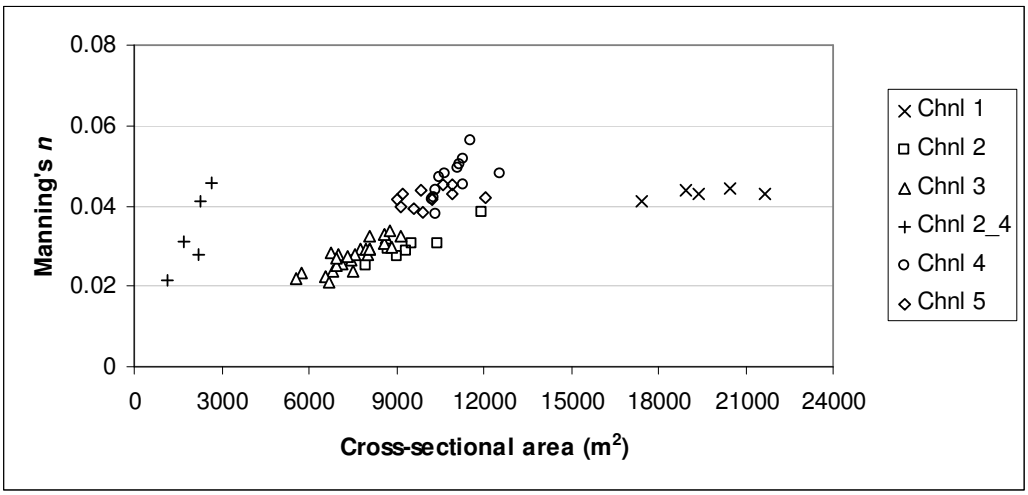

Figure 6.8-7: Manning's *n vs.* cross-sectional area in the flood discharge scenario

The calculated Manning's *n* coefficient at each cross-section along the upstream river network was different along a channel and such differences along different channels within the river network were even higher. In fact, the findings agree with the conclusions from other scientists (Carling, 2009; Gupta and Liew, 2007) that this section of the Mekong River is a bedrock-confined river network. Due to the differences in the river bed material and the cross-sectional areas at given discharges, the assumption of one value of the assigned Manning's *n* coefficient along the whole channel was not realistic. However, the hydraulic roughness trend along the river network in the low discharge scenario fluctuated significantly while it is more stable in the flood discharge scenario. In the low discharge simulation, together with the nature of the river network, due to the quality of the extracted cross-section from the developed DEM, the calculated Manning's *n* at each cross-section along a channel was highly fluctuated. The standard deviation of the calculated Manning's *n* along the river network in the low discharge and flood discharge was 0.028 and 0.009, respectively. Such differences can be explained by higher standard deviation of the cross-sectional area and hydraulic radius along the upstream river network in the low discharge compared to those in the flood discharge (Table 6.8-3). In fact, the Manning's *n* coefficient calculated at each cross-section along the upstream river network (from 0.009 to 0.14 in the low discharge and from 0.02 to 0.06 in the flood discharge) was within the range of published values (Barnes, 1967; Hicks and Mason, 1991; Kidson *et al.*, 2006; Richardson and Carling, 2006; Carrivick, 2009; Chapter 2, section 2.1.2.c).

Table 6.8-3: Standard deviation of the cross-sectional area and hydraulic radius in the low and average flood discharge

Low discharge		Flood discharge	
Cross-sectional area (m^2)	Hydraulic radius (m)	Cross-sectional area (m^2)	Hydraulic radius (m)
0.221	0.266	0.188	0.264

For the low discharge, according to the large differences in water surface elevation (interpolated based on the applied DEM and the top-width extracted from the SPOT image) of the first cross-sections of each channel downstream after each bifurcation, the cross-sectional area calculated according to the water surface elevations of the first cross-section of each downstream channel did not well match the cross-sectional areas calculated in the HEC-RAS model. Table 6.8-4 illustrates the distributed discharge into channels after each bifurcation calculated according to the extracted water surface elevations and according to the HEC-RAS model in the low discharge scenario. In general, the differences of the entry discharge of downstream channels of a bifurcation were ±5 %. However, for flood discharge (Table 6.8-5 and Table 6.8-6) where the water surface slope was assumed to be similar over the whole network, the ratio of cross-sectional areas used to calculate the Manning's *n* at each cross-section was reflected approximately from the HEC-RAS model.

Table 6.8-4: Cross-sectional areas after each bifurcation in the low discharge scenario

	HEC discharge (m^3s^{-1})	Percentage of discharge	SPOT discharge (m^3s^{-1})	Percentage of discharge
Bifurcation 1				
Channel 2	2090.32	32.41%	2427.32	37.63%
Channel 4	4359.68	67.59%	4022.68	62.37%
Bifurcation 2				
Channel 3	1774.50	84.89%	2186.65	90.09%
Cross-channel	315.82	15.11%	240.67	9.91%

Table 6.8-5: Cross-sectional areas after each bifurcation in the average flood discharge scenario

	HEC discharge (m^3s^{-1})	Percentage of discharge	SPOT discharge (m^3s^{-1})	Percentage of discharge
Bifurcation 1				
Channel 2	14054.65	53.47%	14023.25	53.32%
Channel 4	12229.59	46.53%	12276.75	46.68%
Bifurcation 2				
Channel 3	12392.38	88.21%	12471.79	88.94%
Cross-channel	1656.13	11.79%	1551.46	11.06%

Table 6.8-6: Cross-sectional areas after each bifurcation in the high flood discharge scenario

	HEC discharge (m^3s^{-1})	Percentage of discharge	SPOT discharge (m^3s^{-1})	Percentage of discharge
Bifurcation 1				
Channel 2	24992.04	55.50%	24073.60	53.32%
Channel 4	20036.80	44.50%	21075.40	46.68%
Bifurcation 2				
Channel 3	22067.99	88.57%	21410.22	88.94%
Cross-channel	2847.54	11.43%	2663.38	11.06%

Except for some high local water surface slopes from one cross-section to the neighbour, the general water surface slope along the river network in the low discharge was lower than that in the flood discharge (Figure 6.8-8). In fact, the recorded water surface slope between Channoy and Hatxaykhoun was from 4.07 x 10^{-5} mm^{-1} to 2.63 x 10^{-4} mm^{-1} corresponding to the full range of recorded entry discharge (at Channoy) from 1,300 m^3s^{-1} to 45,100 m^3s^{-1}, respectively.

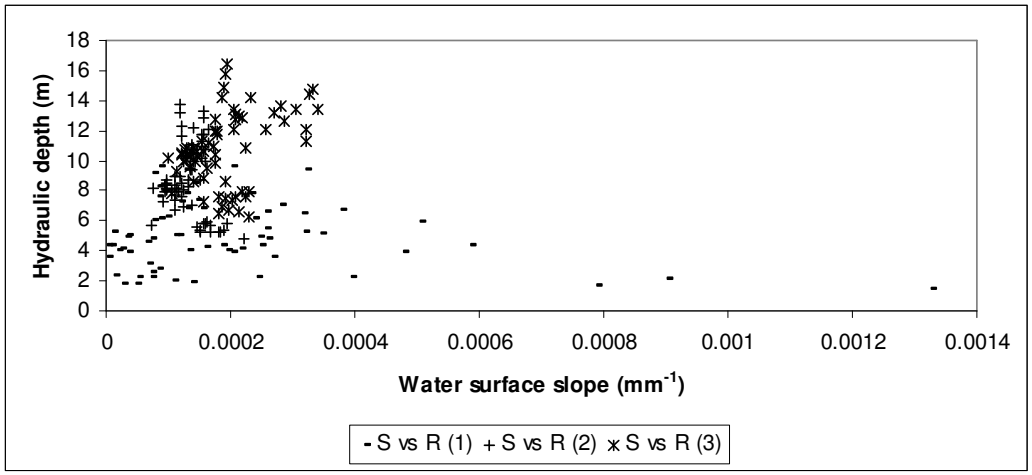

Figure 6.8-8: Hydraulic radius *vs.* water surface slope along the upstream river network; Notes: (1) – Low discharge; (2) – Mean flood discharge; (3) – High flood discharge

Figure 6.8-9 and Figure 6.8-10 present the modelled hydraulic depth and mean in-channel velocity in relation to the modelled Froude number based on the measured and pseudo-bathymetry, respectively. It can be seen that the higher the hydraulic depth (caused by the higher entry discharge), the higher the mean in-channel velocity. Due to the higher magnitude of increase of velocity compared to that of the hydraulic depth in accordance with a unit increase of the entry discharge, the calculated Froude number was highest with the high flood discharge while it was lowest in the low discharge. In addition, the trend of increasing in-channel velocity at all cross-sections along the river network with increasing discharge similar to the results obtained by

Wohl (2007). The calculated sets of the Froude number based on the measured and pseudo-bathymetry were not significantly different (Table 6.8-7). In all applied entry discharges, the Froude number calculated according to the measured bathymetry was higher than that calculated according to the pseudo-bathymetry. Due to the higher magnitude of increase of the mean in-channel velocity compared to the magnitude of increase of the square root of the hydraulic depth, the Froude number calculated according to the measured bathymetry was higher than that calculated according to the pseudo-bathymetry.

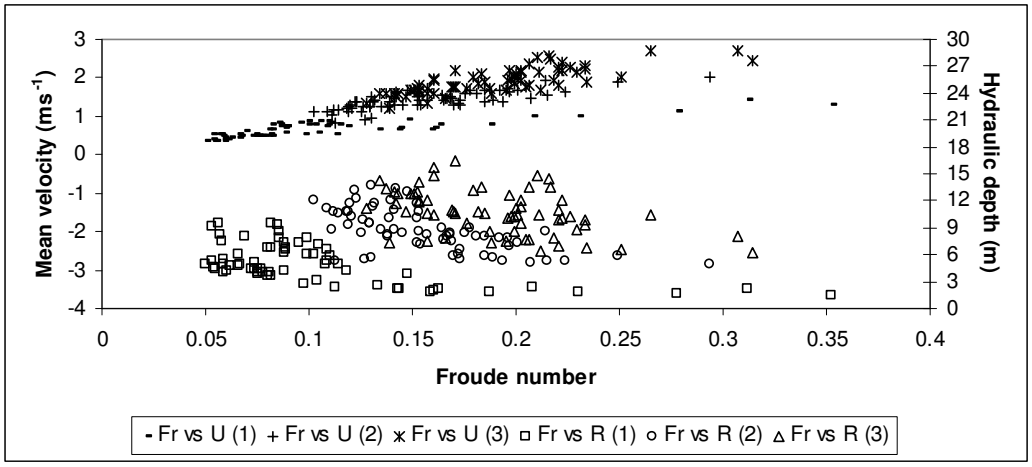

Figure 6.8-9: Hydraulic depth, mean in-channel velocity *vs.* Froude number in all applied entry discharges along the upstream river network based on the measured bathymetry

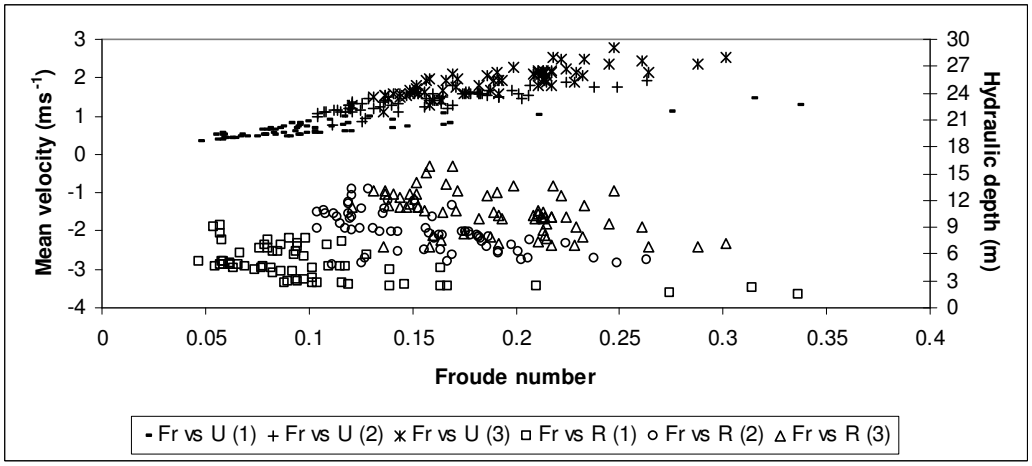

Figure 6.8-10: Hydraulic depth, mean in-channel velocity *vs.* Froude number in all applied entry discharges along the upstream river network based on the pseudo-bathymetry

Table 6.8-7: Range of the modelled hydraulic parameters along the upstream river network according to the low discharge (*L*), average (*A*) and high (*H*) flood discharge

Parameters	(*L*) scenario		(*A*) scenario		(*H*) scenario	
	(*M*)	(*P*)	(*M*)	(*P*)	(*M*)	(*P*)
Fr_{Min}	0.050	0.045	0.102	0.104	0.128	0.121
Fr_{Max}	0.352	0.281	0.294	0.263	0.314	0.301
U_{Min}	0.348	0.319	0.811	0.756	1.186	1.109
U_{Max}	1.441	1.292	2.029	1.918	2.721	2.784
RMin	1.41	1.52	4.86	4.76	6.22	6.73
R_{Max}	9.59	9.08	13.80	13.31	16.44	15.90

Notes: *Fr* – Froude number; *U* – Mean in-channel velocity; *R* – Hydraulic depth; (*M*) Measured bathymetry; (*P*) Pseudo-bathymetry.

Chapter 7: Extension of the 1D hydraulic modelling for the full bedrock-confined river network

Introduction

Even though short reaches of river networks have been modelled successfully by using 2D or 3D hydraulic models, due to the highly computational cost and intensively required input data (detailed bathymetry and measured hydraulic parameters at the entry section of the river network), the 2D or 3D hydraulic models cannot be applied to a large river network with insufficient input data. This chapter presents extensions of the previous models presented in Chapter 6 to a complex anabranching river network (Chapter 4, Figure 4.4-2). Due to lack of input data, the following were not known: (i) the entry discharge of each individual channel constituting the river network; (ii) the detailed bathymetry of most of the downstream river network; and, (iii) the downstream boundary of one outlet section. The modelled hydraulic parameters of the river network in the Siphandone wetlands under low discharge (6,450 m^3s^{-1}) and the historical average and high flood discharge corresponding to 26,300 m^3s^{-1} and 45,149 m^3s^{-1}, respectively are presented. To set initially the entry discharge of each channel, the cross-sectional ratio was applied as the ratio of the splitting discharge at each bifurcation and then iteratively adjusted according to the acute angle between the upstream and downstream channels (routing less water into the acute downstream channel). In addition, there was no available recorded stage at the end of the downstream river network; the 'normal depth' (water surface slope) was applied for the downstream boundary condition of the downstream river network. The results show that the modelled stages at the end of Channel 3 and 5 were similar to those of the upstream river network modelled in all three levels of the entry discharge (low flow, and average and high flood discharges).

The results presented in this chapter include: (i) the Manning's *n* coefficient and the hydraulic characteristics at each cross-section and entry discharge of each channel of the downstream river network in the low and flood discharges; and, (ii) the modelled water surface profiles and the spatial extents of the water-way in the low discharge model and the flooding pattern in the flood discharge models along the full complex river network.

7.1 Splitting discharge at the acute bifurcating angle

To minimise the rise and/or drop of the water surface at each bifurcation along the downstream river network, the splitting discharge ratio from the upstream channel to the downstream channels was adjusted where the acute angle was found (Bi_4, Bi_5, Bi_6 and Bi_9; Chapter 3; Figure 3.3-12). In fact, the ratio was first applied to route discharge downstream according to the assumption of the splitting ratio and then adjusted by reducing the routed discharge (from 5% to 15%) entering the acute channel. The adjusted splitting discharge was applied iteratively in both the low discharge and average flood discharge scenarios to calculate the Manning's *n* coefficient at each cross-section and to set the initial boundary condition of the HEC-RAS model. The iterations were terminated when there was no significant rise or drop of the modelled stage (differences in water surface elevation between the last cross-section of the upstream channel and the first cross-section of the first downstream channel were not greater than 3 mm) at each bifurcation along the river network.

7.2 Hydraulic modelling in the case of the low discharge (6,450 m^3s^{-1})

The Manning's *n* coefficients at each cross-section along the upstream river network were similar to what they were in the upstream river network model (Chapter 6, section 6.2.4). The calculated Manning's *n* at each cross-section along the downstream river network is presented in Figure 7.2-1. In Figure 7.2-1, the minimum Manning's *n* coefficient along the downstream river network was constrained to equal 0.007 or greater while the maximum Manning's *n* coefficient (0.033) was found to be much lower than that in the upstream river network (0.137).

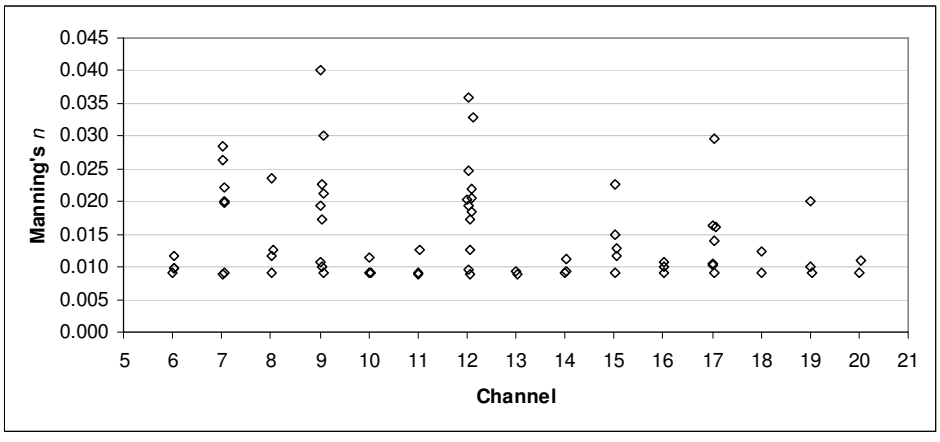

Figure 7.2-1: Manning's *n* coefficient at each cross-section along the downstream river network in the low discharge

The comparisons between the entry discharges and the modelled water surface elevation (WSE) at the first cross-section of each channel in the upstream river network model and the full network model are presented in Table 7.2-1. It can be seen that the modelled entry discharge and water surface elevation of the first cross-section of each channel in the two models were similar. The negative differences indicate the modelled value in the upstream river network models were lower than in the full network model. In fact, the maximum difference in the entry discharge was found in the first cross-section of Channel 2_4 (6.44 %) and the maximum difference in the model water surface elevation in the first cross-section of Channel 3 was 0.08 m. The modelled entry discharge of each channel according to the HEC-RAS model and the calculated entry discharge according to the cross-sectional area are presented in Table 7.2-2. Even though the estimated entry discharge at each channel was different from the modelled one, with the application of the *Flow Optimization* option, HEC-RAS could adjust the entry discharge at each channel to make the modelled water surface profiles acceptable (*i.e.* no hydraulic rise or drop at each bifurcation).

Table 7.2-1: Entry discharge and WSE at the 1st cross-section of each channel along the upstream channel network

	Entry discharge (m^3s^{-1})		Differences (m^3s^{-1})	Differences (%)
	Cross-sectional area approach	HEC-RAS result		
Channel6	2827.54	3847.98	1020.44	26.52%
Channel7	2318.62	2635.69	317.07	12.03%
Channel8	508.92	1212.29	703.37	58.02%
Channel9	1435.80	852.91	-582.89	-68.34%
Channel10	421.64	130.34	-291.30	**-223.49%**
Channel11	1896.98	2505.35	608.37	24.28%
Channel12	426.52	117.14	-309.38	**-264.11%**
Channel13	1470.46	2388.20	917.74	38.43%
Channel14	930.56	1342.63	412.07	30.69%
Channel15	2401.02	3730.83	1329.81	35.64%
Channel16	719.32	536.15	-183.17	-34.16%
Channel17	716.48	316.76	-399.72	**-126.19%**
Channel18	3120.34	4266.98	1146.64	26.87%
Channel19	3836.83	4583.74	746.91	16.29%
Channel20	4263.35	4700.88	437.53	9.31%

Table 7.2-2: Entry discharge of each channel along the downstream river network according to the HEC-RAS model and the assumption based on ratio of cross-sectional areas

	Cross-sectional area approach (m^3s^{-1})	HEC-RAS result (m^3s^{-1})	Difference (m^3s^{-1})
Channel 6	2827.54	3847.98	1020.44
Channel 7	2318.62	2635.69	317.07
Channel 8	508.92	1212.29	703.37
Channel 9	1435.80	852.91	-582.89
Channel 10	421.64	130.34	-291.30
Channel 11	1896.98	2505.35	608.37
Channel 12	426.52	117.14	-309.38
Channel 13	1470.46	2388.20	917.74
Channel 14	930.56	1342.63	412.07
Channel 15	2401.02	3730.83	1329.81
Channel 16	719.32	536.15	-183.17
Channel 17	2318.62	2635.69	317.07
Channel 18	3120.34	4266.98	1146.64
Channel 19	3836.83	4583.74	746.91
Channel 20	4263.35	4700.88	437.53

The modelled water surface profiles along the downstream river network are summarily presented in Figure 7.2-2, Figure 7.2-3 and Figure 7.2-4 for the water surface profile along Channel 6 –7 – 11 – 12 – 20, Channel 6 – 8 – 14 – 15 – 18 – 19 – 20 and Channel 9 – 17 – 19 – 20, respectively. The modelled water surface elevation (WSE) at the upstream boundary (Channoy) was 84.13 m, about 0.04 m above the recorded stage. The downstream boundary at the end of Channel 3 according to the full river network model met the modelled stage at 81.93 m in the upstream river network model. In addition, the modelled stage at the end of Channel 5 was 81.49 m; higher than that in the upstream river network model by 0.03 m. Details of the modelled stages at each cross-section are presented in *Appendix 3*.

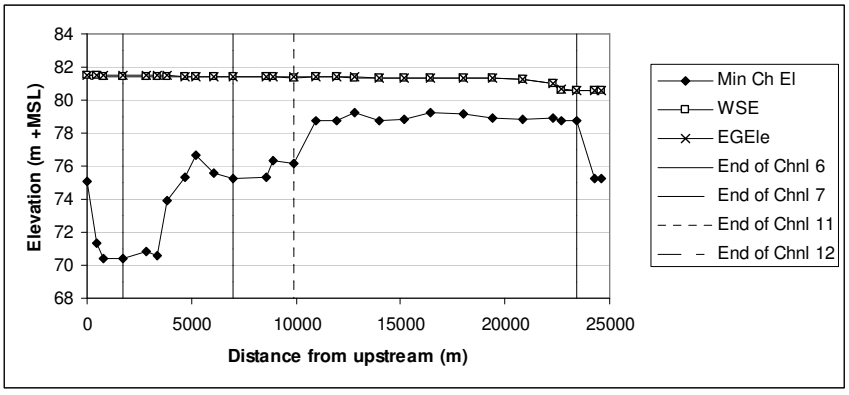

Figure 7.2-2: Water surface profile along Channel 6 – 7 – 11 – 12 and 20 in the low discharge

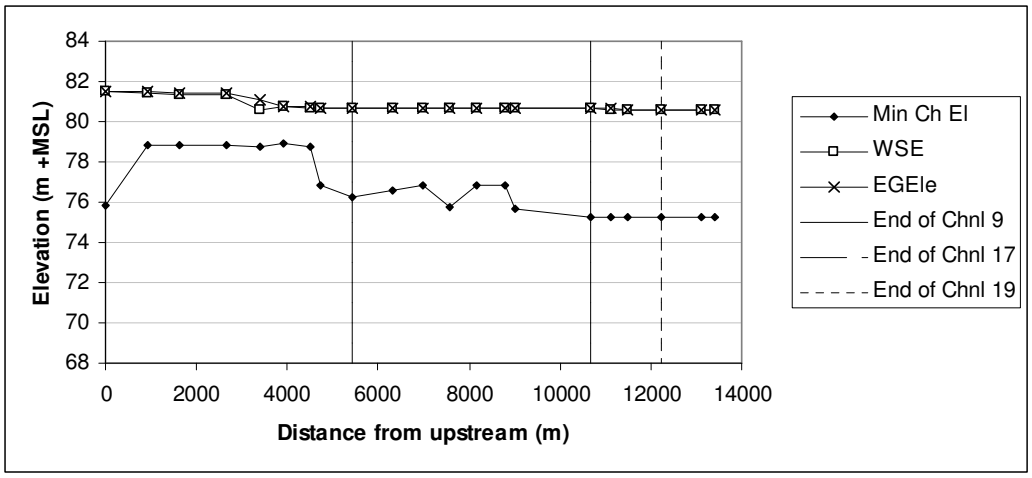

Figure 7.2-3: Water surface profile along Channel 9 – 17 – 19 and 20 in the low discharge

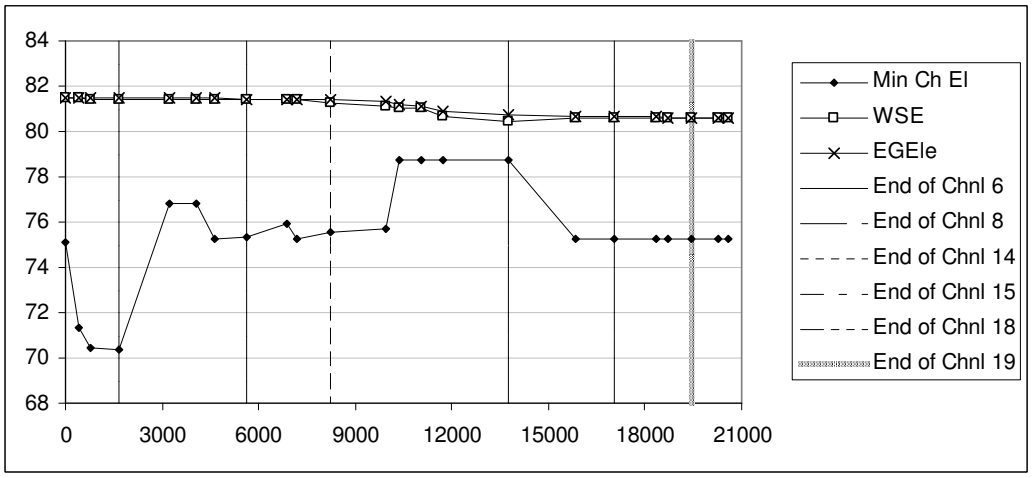

Figure 7.2-4: Water surface profile along Channel 6 – 8 – 14 – 15 – 18 – 19 and 20 in the low discharge

Table 7.2-3 presents the differences in the modelled water surface elevations (WSE) (i) at each bifurcation between the first two cross-sections of the two downstream channels and the last cross-section of the upstream channel; and, (ii) at each confluence between the last cross-section of the two upstream channels and the first cross-section of the downstream channel. By looking at the absolute value of the modelled stages at the cross-sections around the junction, there was a large gap between the upstream and downstream channel. For example, the maximum drop at bifurcation 1 was 0.19 m. However, by taking into account the distance between the last cross-section of the upstream channel and the first cross-sections of the downstream channel, the calculated maximum water surface slope was 2.0×10^{-4} mm^{-1}, which met the requirement that the water surface slope must be smaller than 1.0×10^{-3} mm^{-1}. In addition, even though the stage of the downstream channel was higher

than the stage of the upstream channel (*i.e.* Bifurcation 4, 5, 6 and 8 and Confluence 11 and 13), differences of the energy gradelines were always positive leading to the fact that the result was acceptable.

Table 7.2-3: Differences in modelled WSE at each junction and the WS slope between the surrounding cross-sections in the low discharge

	Channel	WSE (m +MSL)	Difference (m)	Length (m)	Slope (mm^{-1})
Bifurcation					
1	**Channel 1**	**83.95**			
	Channel 2	83.78	0.17	910	0.0002
	Channel 4	83.76	0.19	1300	0.0001
2	**Channel 2**	**83.30**			
	Channel 3	83.30	0.00	495	0.0000
	Channel 2_4	83.21	0.09	880	0.0001
4	**Channel 5**	**81.49**			
	Channel 9	81.50	-0.01	440	0.0000
	Channel 6	81.47	0.02	660	0.0000
5	**Channel 6**	**81.43**			
	Channel 8	81.44	-0.01	650	0.0000
	Channel 7	81.44	-0.01	650	0.0000
6	**Channel 7**	**81.41**			
	Channel 10	81.43	-0.02	800	0.0000
	Channel 11	81.41	0.00	870	0.0000
8	**Channel 11**	**81.30**			
	Channel 13	81.32	-0.02	610	0.0000
	Channel 12	81.39	-0.09	850	-0.0001
10	**Channel 9**	**80.66**			
	Channel 17	80.64	0.02	440	0.0000
	Channel 16	80.65	0.01	600	0.0000
Confluence					
3	Channel 2_4	82.34	0.04	850	0.0000
	Channel 4	82.35	0.05	450	0.0001
	Channel 5	**82.30**			
7	Channel 8	81.41	0.01	780	0.0000
	Channel 10	81.43	0.03	710	0.0000
	Channel 14	**81.40**			
9	Channel 14	81.29	0.21	1050	0.0002
	Channel 13	81.27	0.19	1030	0.0002
	Channel 15	**81.08**			
11	Channel 16	80.62	0.02	1900	0.0000
	Channel 15	80.48	-0.12	1900	-0.0001
	Channel 18	**80.60**			
12	Channel 17	80.64	0.07	810	0.0001
	Channel 18	80.58	0.01	820	0.0000
	Channel 19	**80.57**			
13	Channel 19	80.58	-0.01	580	0.0000
	Channel 12	80.59	0.00	700	0.0000
	Channel 20	**80.59**			

Figure 7.2-5 and Figure 7.2-6 present the comparison between the modelled top-widths and the top-widths extracted from the SPOT image along the upstream river network while Figure 7.2-7 and Figure 7.2-8 present the comparison between the modelled top-widths and those extracted from the SPOT image along the downstream river network. The positive differences in Figure 7.2-6 and Figure 7.2-8 indicate that the top-widths extracted from SPOT were generally larger than those extracted from

the HEC-RAS model. It can be seen that the linear regression calculated in both upstream and downstream river network was acceptable with R^2 of 0.95 and 0.85, respectively. Similar to what was found in Chapter 6, the main differences along the upstream river network appeared along Channel 2_4. Along the downstream river network, the significant differences appeared along the narrow channels (*e.g.* Channel 8 and Channel 14) while along the wide channels (*e.g.* Channel 15, Channel 18, Channel 19 and Channel 20), the absolute maximum difference was less than 20%.

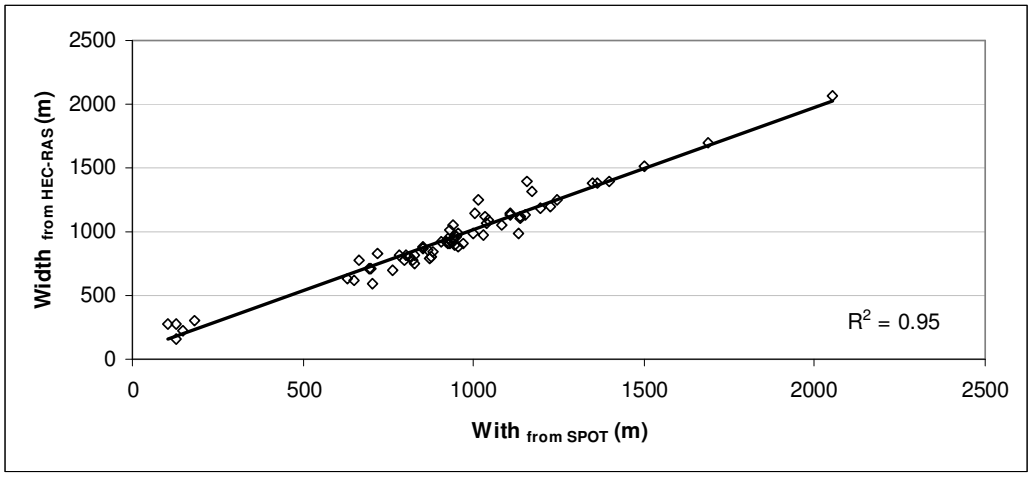

Figure 7.2-5: Linear comparison between the modelled top-width and that extracted from SPOT along the upstream river network in the low discharge

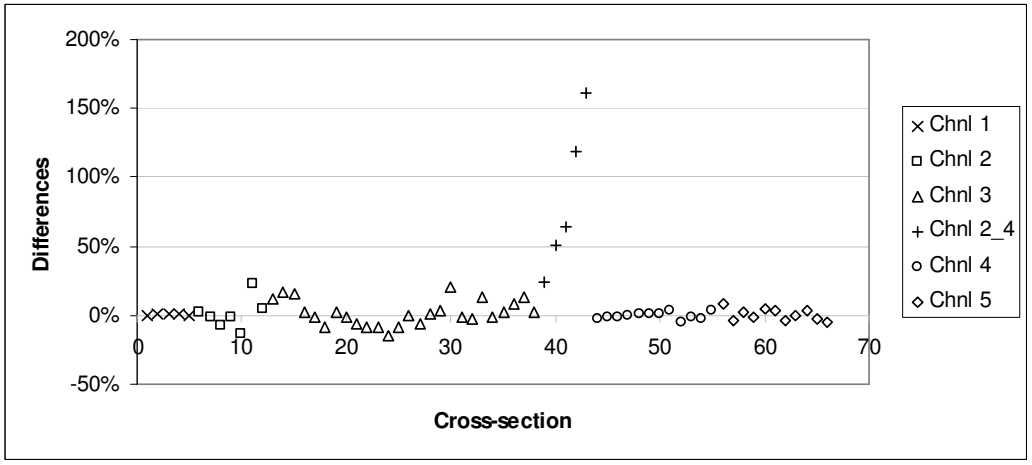

Figure 7.2-6: Differences in percentage between the modelled top-width and that extracted from SPOT along the upstream river network in the low discharge

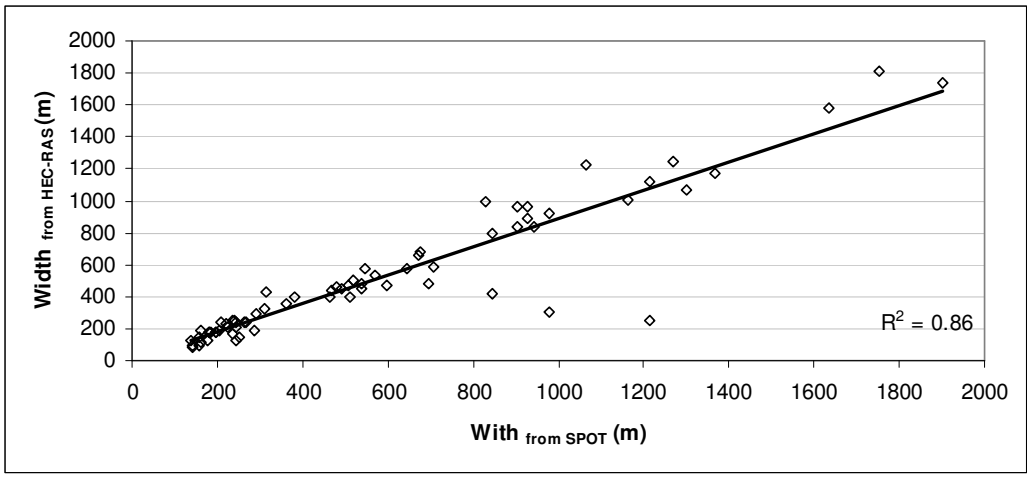

Figure 7.2-7: Linear comparison between the modelled top-width and that extracted from SPOT along the downstream river network in the low discharge

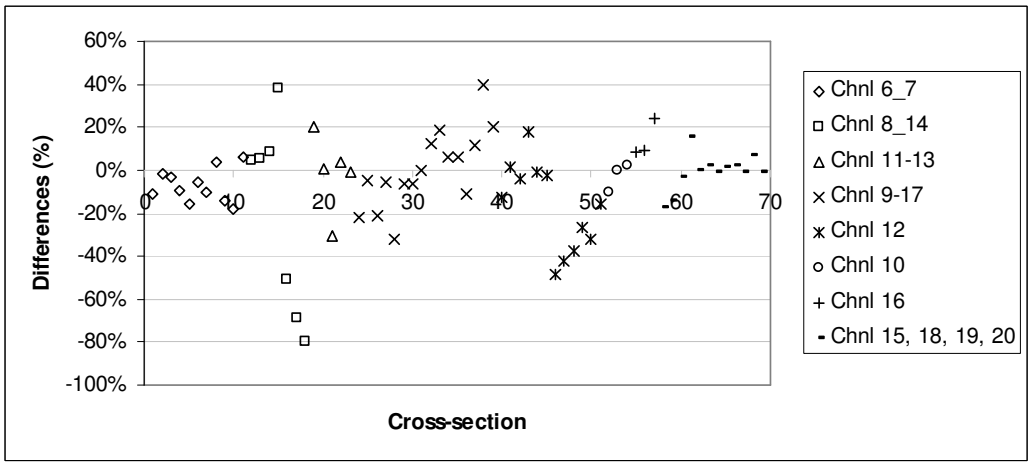

Figure 7.2-8: Differences in percentage between the modelled top-width and that extracted from SPOT along the downstream river network in the low discharge

Figure 7.2-9 presents the relationship between the modelled Froude number and the in-channel velocity along the downstream river network in the low discharge. Except cross-section 9.05 with the Froude number of 0.923 and cross-section 15.01 with the Froude number of 0.628, the calculated Froude number along the downstream river network was mainly less than 0.6.

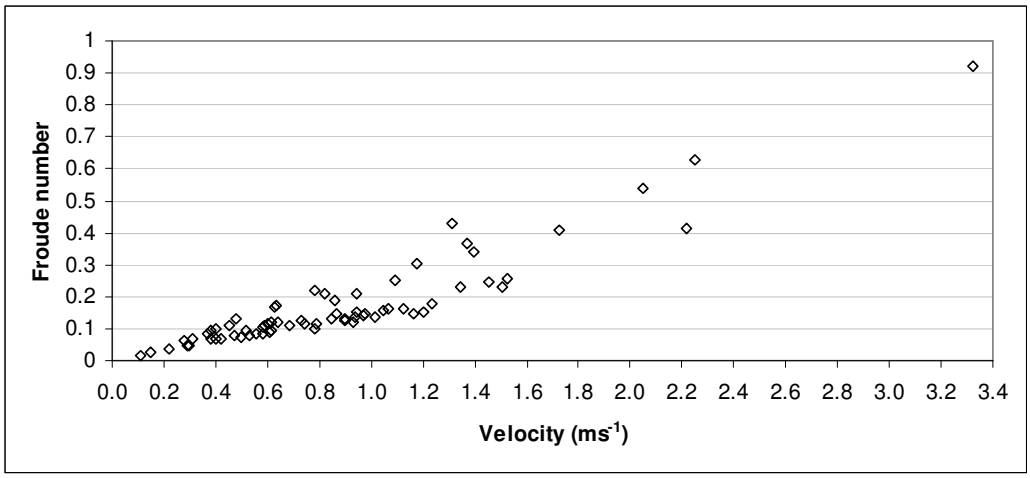

Figure 7.2-9: Froude number *vs.* mean in-channel velocity along the downstream river network in the low discharge

Figure 7.2-10 presents the water-way along the full river network in the case of the low entry discharge (6,450 m^3s^{-1}). Because the modelled entry discharge was much smaller than the bankfull discharge, the modelled water-way was well located in-channel along the river network.

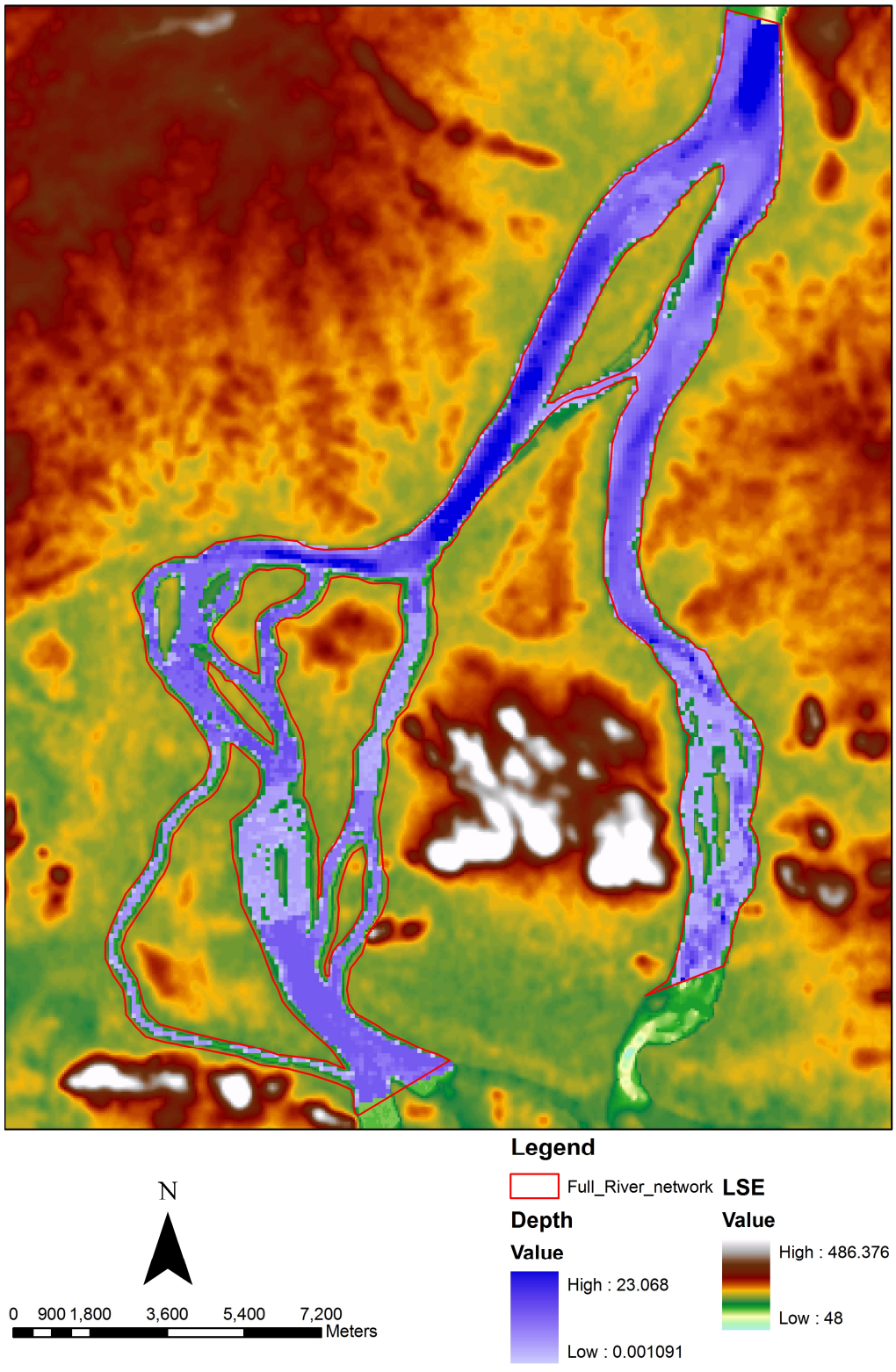

Figure 7.2-10: Modelled water-way along the full river network according to the low flow discharge (6,450 m^3s^{-1})

7.3 Hydraulic modelling in accordance to the historical average flood discharge (26,300 m^3s^{-1})

The Manning's *n* coefficient at each cross-section calculated according to the average flood discharge (26,300 m^3s^{-1}) along the downstream river network is presented in Figure 7.3-1. The calculated Manning's *n* ranged within 0.009 and 0.045 from which the minimum value was constrained to make an acceptable Manning's *n* set while the maximum value was as calculated according to the procedure presented in Chapter 4, section 4.5. Apart from the in-channel hydraulic roughness, the hydraulic roughness of the floodplain (Chapter 6) was also considered in the case of the average flood discharge. The analyses were done to examine the impact of the riparian hydraulic roughness on the stage at each cross-section leading to the (possible) changes of spatial flooding pattern.

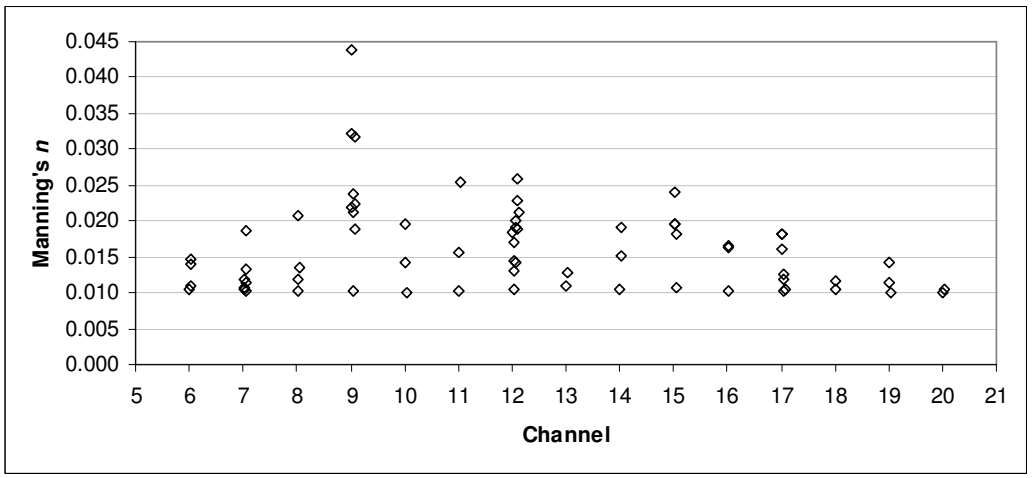

Figure 7.3-1: Manning's *n* coefficient at each cross-section along the downstream river network in the average flood discharge

7.3.1 Current land cover pattern

The comparisons between the entry discharge and the modelled water surface elevation (WSE) at the first cross-section of the channels of the upstream river network model and the full river network model are presented in Table 7.3-1. In the average flood discharge analysis, the differences in the entry discharges in each channel and the modelled stages between the upstream and full river network models were smaller than those in the low discharge analysis. The maximum difference in the discharge was -2.07 % (Channel 2_4) and in the modelled stage was -0.03 m (Channel 3).

Table 7.3-1: Entry discharge and WSE at the 1st cross-section of each channel along the upstream river network

	Discharge (m^3s^{-1})			WSE (m +MSL)		
	Upstream network	**Whole network**	**Difference (%)**	**Upstream network**	**Whole network**	**Difference (m)**
Channel 1	26294.09	26294.00	0.00	88.56	88.58	-0.02
Channel 2	13435.55	13392.88	0.32	88.20	88.22	-0.02
Channel 3	11279.93	11192.20	0.78	87.52	87.55	-0.03
Channel 2_4	2126.92	2170.99	-2.07	87.42	87.43	-0.01
Channel 4	12845.00	12900.80	-0.43	88.19	88.21	-0.02
Channel 5	15005.02	15101.90	-0.65	87.15	87.15	0.00

Table 7.3-2 presents the entry discharge at each channel along the full river network and a comparison between the entry discharges based on the ratio of cross-sectional areas and the entry discharge calculated according to HEC-RAS. In addition, the modelled water surface profiles along Channel 6 – 7 – 11 – 12 and 20, Channel 6 – 8 – 14 – 15 -18 – 19 and 20 and Channel 9 – 17 – 19 and 20 are presented in Figure 7.3-2, Figure 7.3-3 and Figure 7.3-4, respectively. The modelled stage at Channoy (upstream boundary condition) was 88.58 m +MSL; 0.05 m higher than the recorded stage. The downstream boundary condition at Hatxaykhoun was met (85.53 m +MSL) and at the end of Channel 20 was 85.95 m +MSL. In addition, the modelled WSE at the end of Channel 5 was 86.42 m +MSL, about 0.03 m lower than the modelled stage in the upstream river network model. Details of modelled stage at each cross-section are presented in *Appendix 3*.

Table 7.3-2: Entry discharge of each channel along the downstream river network according to the HEC-RAS model and the assumption based on ratio of cross-sectional areas

	Cross-sectional area assumption (m^3s^{-1})	HEC-RAS result (m^3s^{-1})	Difference (m^3s^{-1})
Channel6	9179.69	11466.72	2287.03
Channel7	5711.29	7747.76	2036.47
Channel8	3468.40	3718.96	250.56
Channel9	4648.52	3635.33	-1013.19
Channel10	833.09	590.52	-242.57
Channel11	4878.20	7157.24	2279.04
Channel12	1304.73	978.79	-325.94
Channel13	3573.47	6178.24	2604.77
Channel14	4301.49	4309.46	7.97
Channel15	7874.96	10487.72	2612.76
Channel16	2752.09	2021.95	-730.14
Channel17	5711.29	7747.76	2036.47
Channel18	10627.05	12509.79	1882.74
Channel19	12523.48	14123.02	1599.54
Channel20	13828.21	15101.94	1273.73

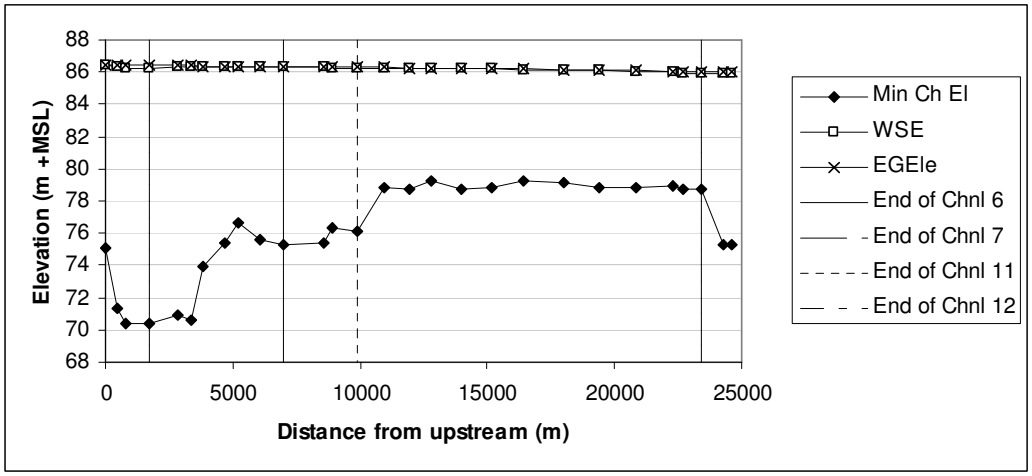

Figure 7.3-2: Water surface profile along Channel 6 – 7 – 11 – 12 and 20 in the average flood discharge

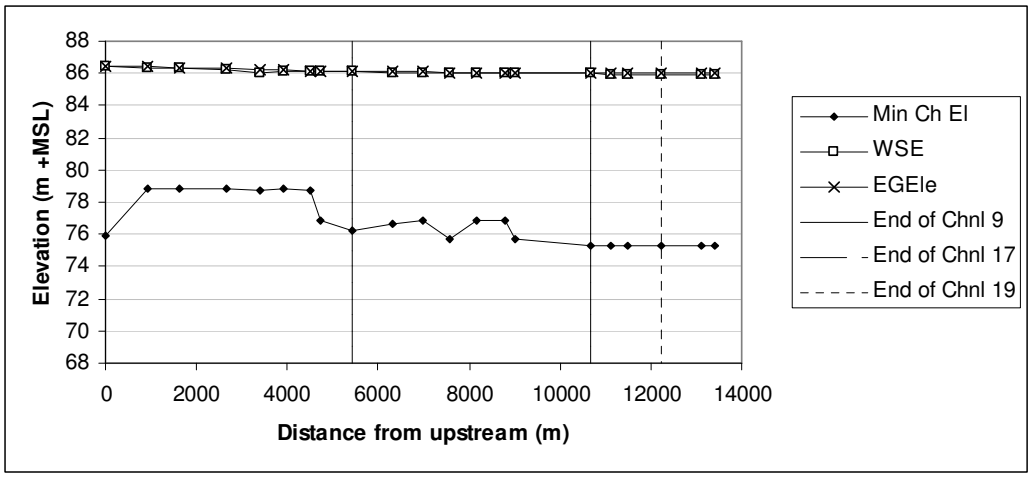

Figure 7.3-3: Water surface profile along Channel 9 – 17 – 19 and 20 in the average flood discharge

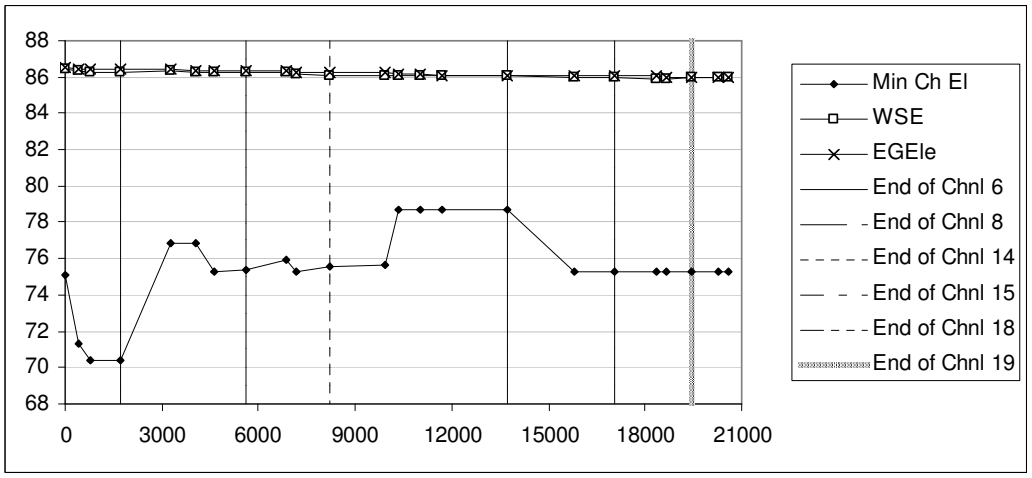

Figure 7.3-4: Water surface profile along Channel 6 – 8 – 14 – 15 -18 – 19 and 20 in the average flood discharge

Table 7.3-3 details the modelled water surface elevations (WSE) surrounding a junction of the full river network. In general, the maximum water surface slope at each junction was 2.0×10^{-4} mm^{-1}, which satisfies the assumption that the river network was gradually varied flow.

Table 7.3-3: Differences in modelled WSE at each junction and the WS slope between the surrounding cross-sections in the average flood discharge

	Channel	WSE (m +MSL)	Difference (m)	Length (m)	Slope (mm^{-1})
Bifurcation					
1	**Channel 1**	**88.32**			
	Channel 2	88.22	0.10	910	0.0001
	Channel 4	88.21	0.11	1300	0.0001
2	**Channel 2**	**87.58**			
	Channel 3	87.55	0.03	495	0.0001
	Channel 2_4	87.43	0.15	880	0.0002
4	**Channel 5**	**86.42**			
	Channel 9	86.44	-0.02	440	0.0000
	Channel 6	86.39	0.03	660	0.0000
5	**Channel 6**	**86.24**			
	Channel 8	86.33	-0.09	650	-0.0001
	Channel 7	86.29	-0.05	650	-0.0001
6	**Channel 7**	**86.30**			
	Channel 10	86.32	-0.02	800	0.0000
	Channel 11	86.30	0.00	870	0.0000
8	**Channel 11**	**86.19**			
	Channel 13	86.17	0.02	610	0.0000
	Channel 12	86.27	-0.08	850	-0.0001
10	**Channel 9**	**86.08**			
	Channel 17	86.04	0.04	440	0.0001
	Channel 16	86.05	0.03	600	0.0001
Confluence					
3	Channel 2_4	87.33	0.18	850	0.0002
	Channel 4	87.23	0.08	450	0.0002
	Channel 5	**87.15**			
7	Channel 8	86.29	0.04	780	0.0001
	Channel 10	86.32	0.07	710	0.0001
	Channel 14	**86.25**			
9	Channel 14	86.11	0.09	1050	0.0001
	Channel 13	86.12	0.10	1030	0.0001
	Channel 15	**86.02**			
11	Channel 16	86.00	0.04	1900	0.0000
	Channel 15	86.02	0.06	1900	0.0000
	Channel 18	**85.96**			
12	Channel 17	86.03	0.13	810	0.0002
	Channel 18	85.94	0.04	820	0.0000
	Channel 19	**85.90**			
13	Channel 19	85.93	-0.02	580	0.0000
	Channel 12	85.95	0.00	700	0.0000
	Channel 20	**85.95**			

Figure 7.3-5 presents the relationship between the modelled Froude number (most of the calculated Froude numbers were less than 0.3) and the in-channel velocity along the downstream river network in the average flood discharge. Figure 7.3-6 presents the flooding pattern over the full river network according to the average flood

discharge (26,300 m^3s^{-1}). Even though the average flood discharge was applied, the model flooding area along the floodplain was small (about 8.41 km^2).

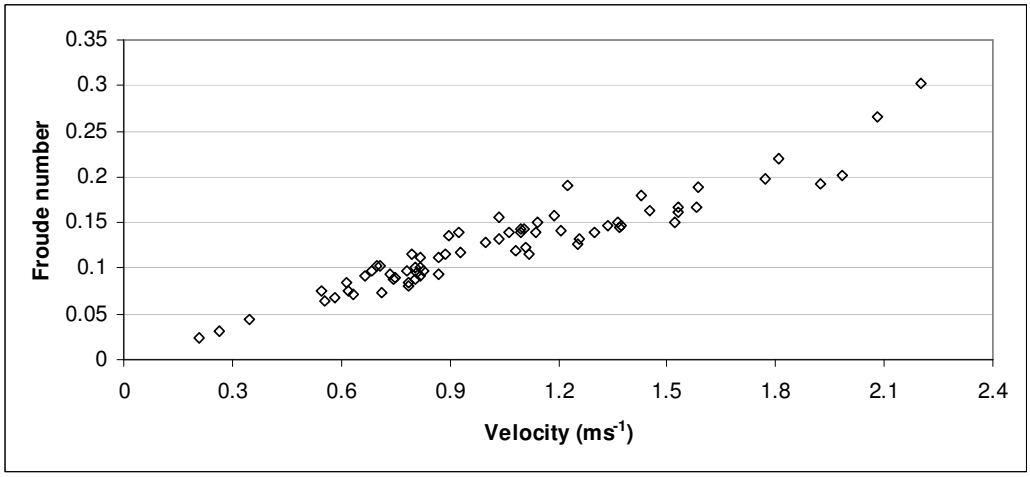

Figure 7.3-5: Froude number *vs.* mean in-channel velocity along the downstream river network in the average flood discharge

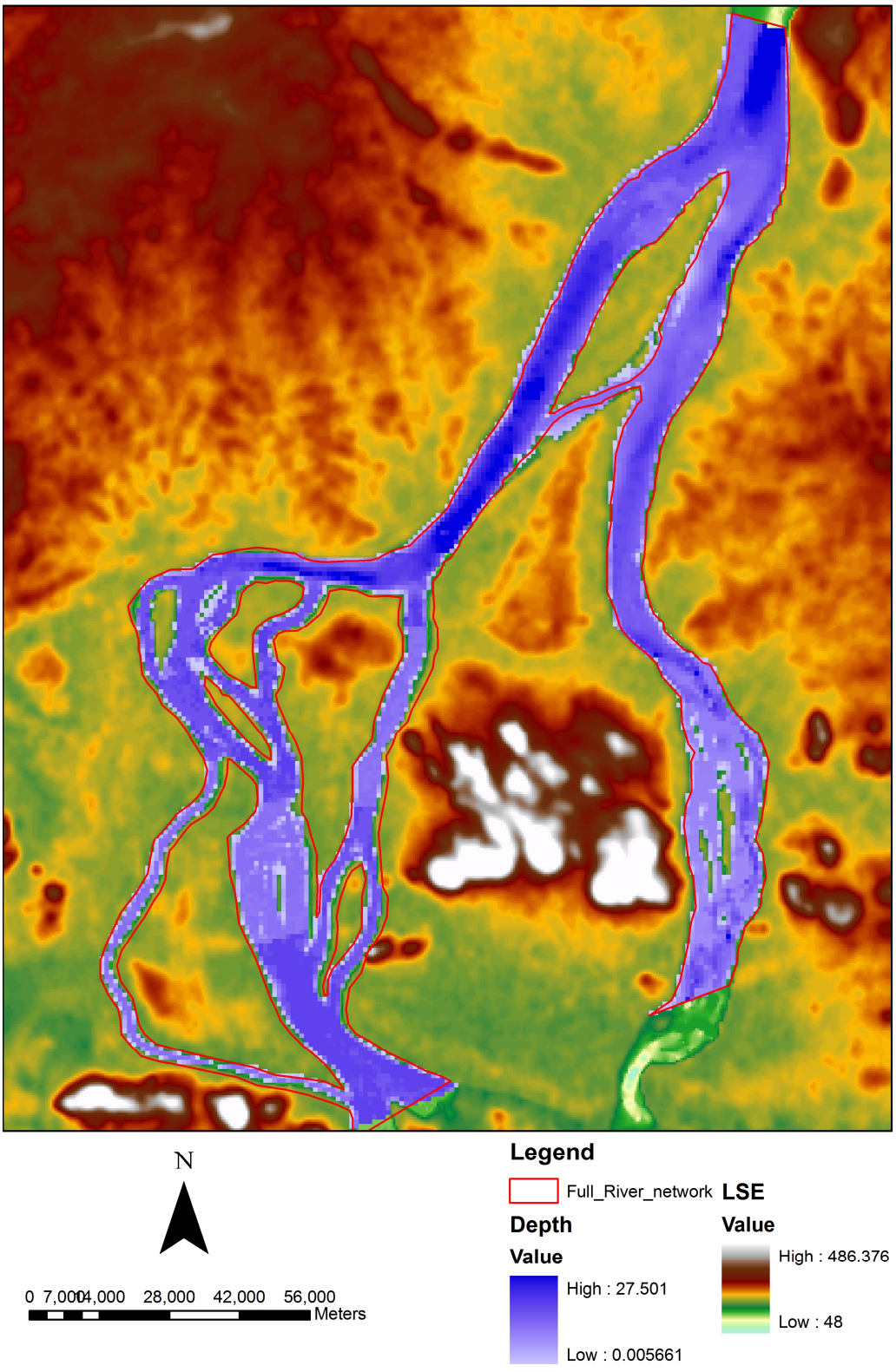

Figure 7.3-6: Modelled flooding pattern along the full river network according to the average flood discharge (26,300 m^3s^{-1})

7.3.2 Hypothetical scenarios of land cover pattern

Figure 7.3-7 and Figure 7.3-8 present the differences in the modelled water surface elevations (WSE) and the mean in-channel velocity at each cross-section along the full river network, respectively. In fact, the modelled stages along the full river network in all scenarios of the land cover pattern were approximately similar. Similarly, the differences in the mean in-channel velocity in all scenarios were very small; in fact, the modelled mean in-channel velocity between the past and current land cover pattern was similar while the modelled mean in-channel velocity in the future land cover pattern locally decreased with a maximum difference of about 0.013 ms^{-1} at cross-channel 2_4.

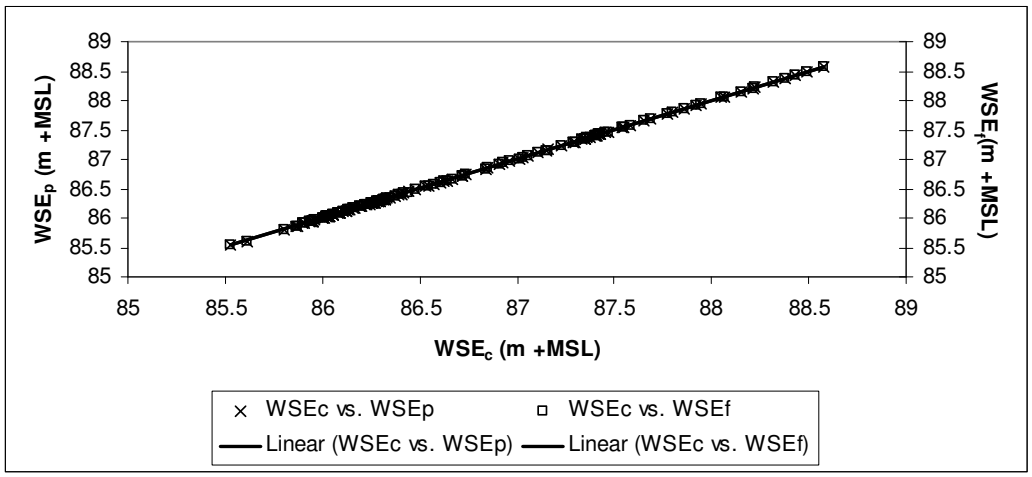

Figure 7.3-7: Modelled WSE at each cross-section according to the land cover change in the average flood discharge; $WSE_{c, p, f}$ – Water surface elevation for the current, past and future land cover pattern, respectively

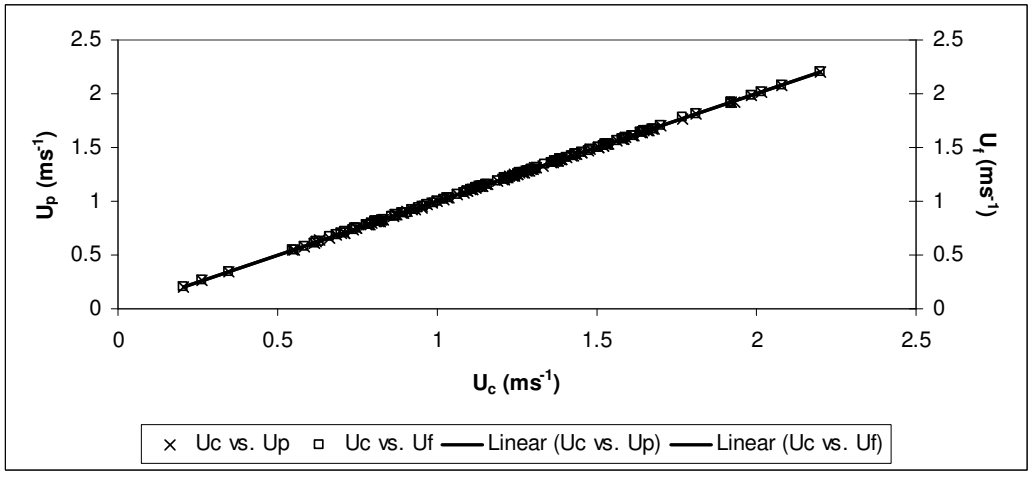

Figure 7.3-8: Modelled mean in-channel velocity at each cross-section according to the land cover change in the average flood discharge; $U_{c, p, f}$ – Average in-channel velocity for the current, past and future land cover pattern, respectively

Figure 7.3-9 and Figure 7.3-10 illustrate the differences in the mean riparian velocity based on a comparison between the current and past land cover pattern and current and future land cover pattern, respectively. With the reduction of the hydraulic roughness (Manning's *n*) from the past to current and future land cover patterns, the mean riparian velocity increased significantly. In fact, the average increase of the left and right riparian velocity between the past and current land cover patterns were 0.01 ms^{-1} and 0.02 ms^{-1}, respectively while the average decrease of the left and right riparian velocity between the current and future land cover patterns were 0.04 ms^{-1} and 0.05 ms^{-1}, respectively.

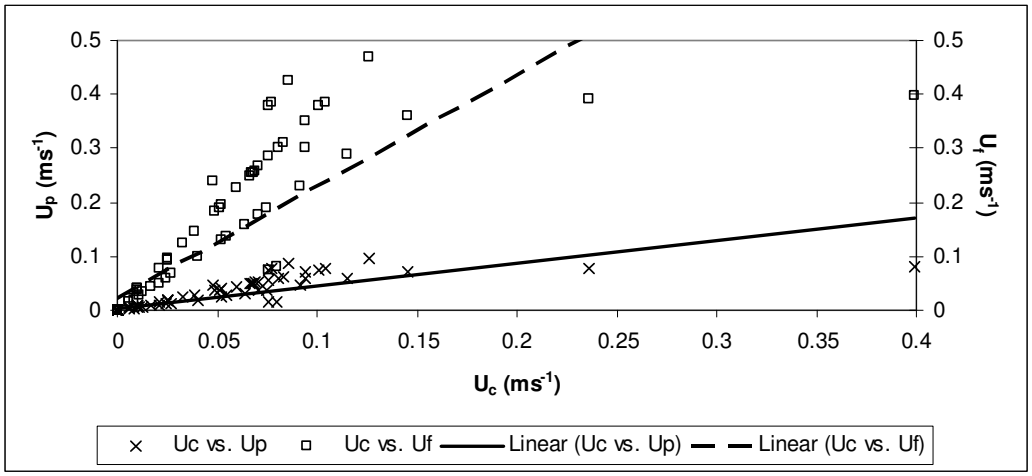

Figure 7.3-9: Modelled mean velocity in the floodplain along the left banks in the average flood discharge; $U_{c,\,p,\,f}$ – Average in-channel velocity for the current, past and future land cover pattern, respectively

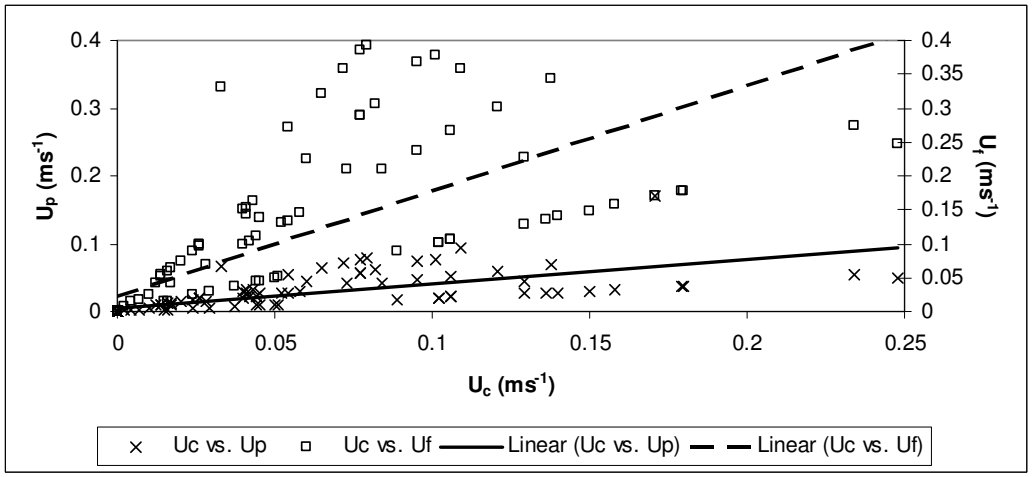

Figure 7.3-10: Modelled mean velocity in the floodplain along the right banks in the average flood discharge; $U_{c,\,p,\,f}$ – Average in-channel velocity for the current, past and future land cover pattern, respectively

7.4 Hydraulic modelling in accordance to the historical high flood discharge (45,149 m^3s^{-1})

As in Chapter 6, it is assumed that the in-channel hydraulic roughness (Manning's *n*) at each cross-section along the full river network in the high flood discharge was similar to that in the average flood discharge (Figure 7.3-1). The splitting discharge was calculated according to the entry high flood discharge and the changes of cross-sectional area.

7.4.1 Current land cover pattern

The entry discharge and the water surface elevation (WSE) at the first cross-section of each channel along the upstream river network are presented in Table 7.4-1. The maximum absolute differences between the (modelled) entry discharge and stages were 2.09 % and 0.04 m, respectively.

Table 7.4-1: Entry discharge and WSE at the 1st cross-section of each channel along the upstream river network

	Discharge (m^3s^{-1})			WSE (m +MSL)		
	Upstream network	**Whole network**	**Difference (%)**	**Upstream network**	**Whole network**	**Difference (m)**
Channel 1	45099.42	45098.25	0.00	91.21	91.23	-0.02
Channel 2	23446.75	23481.08	-0.15	90.69	90.72	-0.03
Channel 3	18911.87	18847.27	0.34	89.79	89.83	-0.04
Channel 2_4	4200.48	4288.40	-2.09	89.57	89.60	-0.03
Channel 4	21561.95	21590.24	-0.13	90.67	90.70	-0.03
Channel 5	26016.20	26182.12	-0.64	89.20	89.22	-0.02

Table 7.4-2 presents the entry discharge of each channel along the downstream river network. The modelled water surface profiles along Channel 6 – 7 – 11 – 12 and 20, Channel 6 – 8 – 14 – 15 -18 – 19 and 20 and Channel 9 – 17 – 19 and 20 are presented in Figure 7.4-1, Figure 7.4-2 and Figure 7.4-3. Details of stage at each cross-section are presented in *Appendix 3*.

Table 7.4-2: Entry discharge of each channel along the downstream river network according to the HEC-RAS model and the assumption of the ratio of cross-sectional areas

	Cross-sectional area (m^3s^{-1})	HEC-RAS result (m^3s^{-1})	Difference (m^3s^{-1})
Channel6	10606.70	19651.05	9044.35
Channel7	8638.88	13183.40	4544.52
Channel8	1967.82	6467.97	4500.15
Channel9	13132.08	6558.25	-6573.83
Channel10	905.18	923.17	17.99
Channel11	7733.70	12260.22	4526.52
Channel12	652.33	1868.94	1216.61
Channel13	7081.37	10388.84	3307.47
Channel14	2873.00	7390.31	4517.31
Channel15	9954.37	17780.10	7825.73
Channel16	6346.27	3615.07	-2731.20
Channel17	8638.88	13183.40	4544.52
Channel18	16300.64	21397.55	5096.91
Channel19	23086.44	24337.98	1251.54
Channel20	23738.78	26208.55	2469.77

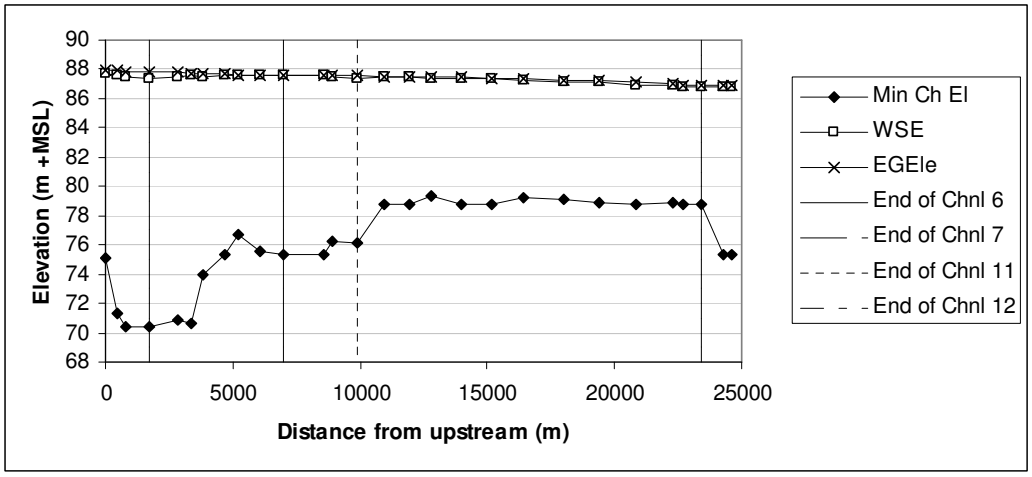

Figure 7.4-1: Water surface profile along Channel 6 – 7 – 11 – 12 and 20 in the high flood discharge

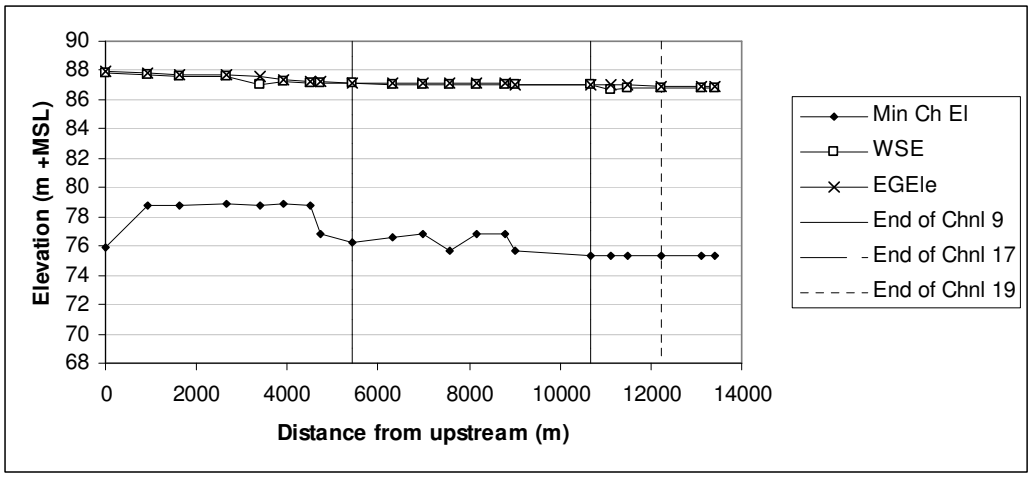

Figure 7.4-2: Water surface profile along Channel 9 – 17 – 19 and 20 in the high flood discharge

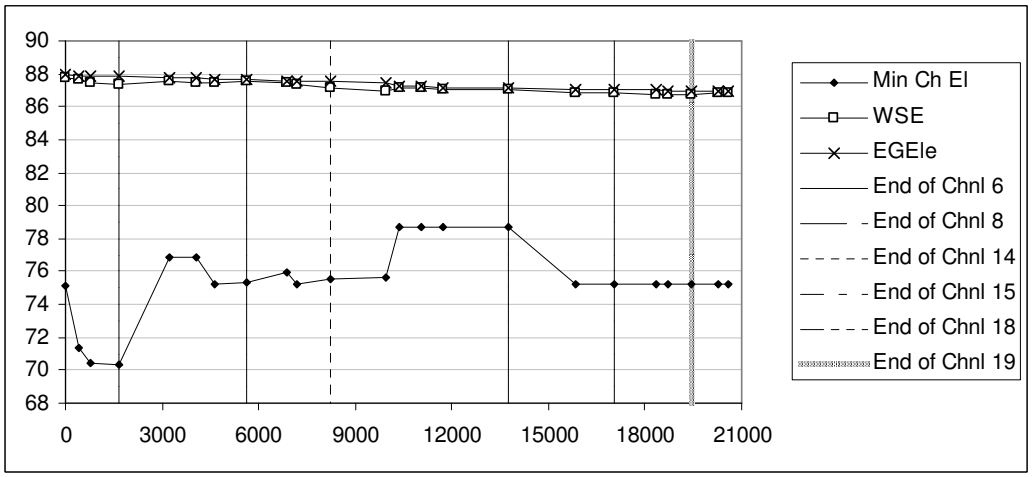

Figure 7.4-3: Water surface profile along Channel 6 – 8 – 14 – 15 -18 – 19 and 20 in the high flood discharge

Table 7.4-3 presents differences in the modelled water surface elevation (WSE) surrounding a junction. In general, the absolute maximum slope was 3.0×10^{-4} mm^{-1} which satisfied the assumption of the gradually varied flow applied to model the WS profiles along the full river network.

Table 7.4-3: Differences in modelled WSE at each junction and the WS slope between the surrounding cross-sections in the high flood discharge

	Channel	WSE (m +MSL)	Difference (m)	Length (m)	Slope (mm^{-1})
Bifurcation					
1	**Channel 1**	**90.84**			
	Channel 2	90.72	0.12	910	0.0001
	Channel 4	90.70	0.14	1300	0.0001
2	**Channel 2**	**89.85**			
	Channel 3	89.83	0.02	495	0.0000
	Channel 2_4	89.60	0.25	880	0.0003
4	**Channel 5**	**87.78**			
	Channel 9	87.86	-0.08	440	-0.0002
	Channel 6	87.74	0.04	660	0.0001
5	**Channel 6**	**87.38**			
	Channel 8	87.60	-0.22	650	-0.0003
	Channel 7	87.50	-0.12	650	-0.0002
6	**Channel 7**	**87.55**			
	Channel 10	87.60	-0.05	800	-0.0001
	Channel 11	87.55	0.00	870	0.0000
8	**Channel 11**	**87.34**			
	Channel 13	87.27	0.07	610	0.0001
	Channel 12	87.47	-0.13	850	-0.0002
10	**Channel 9**	**87.12**			
	Channel 17	87.05	0.07	440	0.0002
	Channel 16	87.07	0.05	600	0.0001
Confluence					
3	Channel 2_4	89.51	0.29	850	0.0003
	Channel 4	89.36	0.14	450	0.0003
	Channel 5	**89.22**			
7	Channel 8	87.52	0.08	780	0.0001
	Channel 10	87.60	0.16	710	0.0002
	Channel 14	**87.44**			
9	Channel 14	87.14	0.19	1050	0.0002
	Channel 13	87.15	0.20	1030	0.0002
	Channel 15	**86.95**			
11	Channel 16	86.94	0.08	1900	0.0000
	Channel 15	87.00	0.14	1900	0.0001
	Channel 18	**86.86**			
12	Channel 17	87.02	0.33	810	0.0004
	Channel 18	86.81	0.12	820	0.0001
	Channel 19	**86.69**			
13	Channel 19	86.78	-0.05	580	-0.0001
	Channel 12	86.83	0.00	700	0.0000
	Channel 20	**86.83**			

Figure 7.4-4 presents the relationship between the modelled Froude number (with the maximum value of about 0.438) and the in-channel velocity along the downstream river network in the high flood discharge. The modelled flooding pattern according to the high flood discharge along the full river network is presented in Figure 7.4-5 and the flooding area along the floodplain was 10.98 km^2.

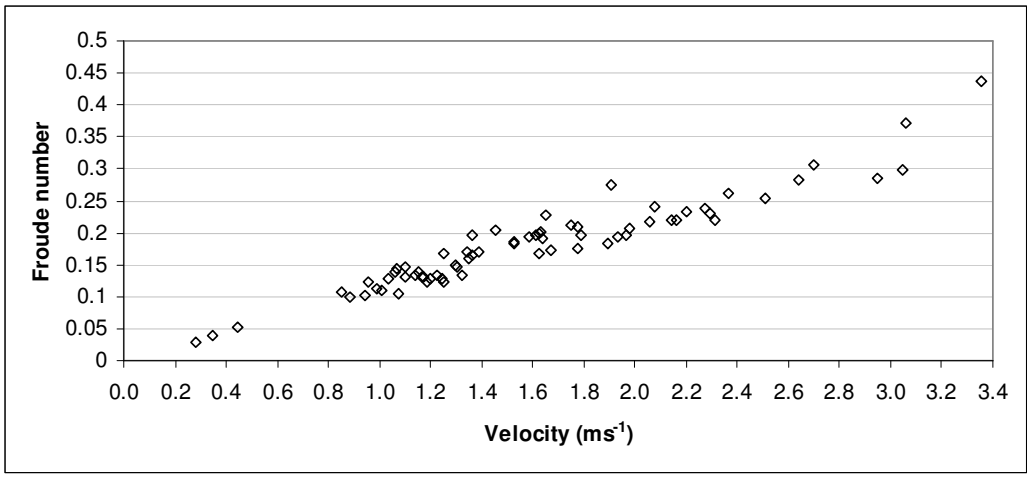

Figure 7.4-4: Froude number *vs.* mean in-channel velocity along the downstream river network in the high flood discharge

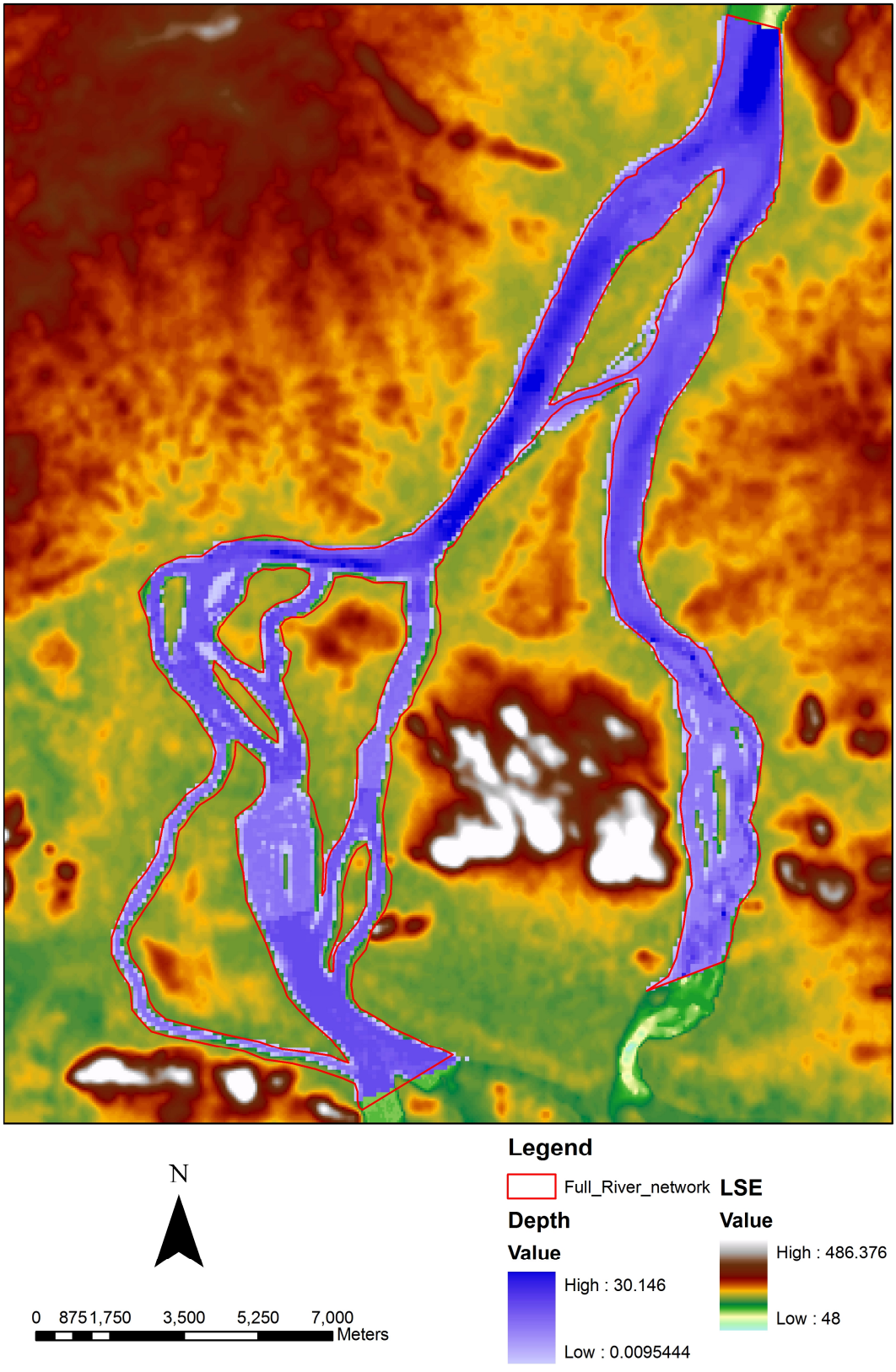

Figure 7.4-5: Modelled flooding pattern along the full river network according to the high flood discharge (45,149 m^3s^{-1})

7.4.2 Hypothetical scenarios of land cover pattern

Figure 7.4-6 and Figure 7.4-7 present the differences in the modelled water surface elevation (WSE) and the mean in-channel velocity at each cross-section along the full river network. Similar to the average flood discharge scenario, the modelled stage along the full river network was similar in all scenarios of the land cover pattern. Even though the differences between the mean in-channel velocity modelled according to different land cover patterns could be seen in Figure 7.4-7, they were in fact local changes (appeared along the Channel 2_4 - a *relatively small* cross-channel along the upstream network) and did not lead to significant differences in the mean values.

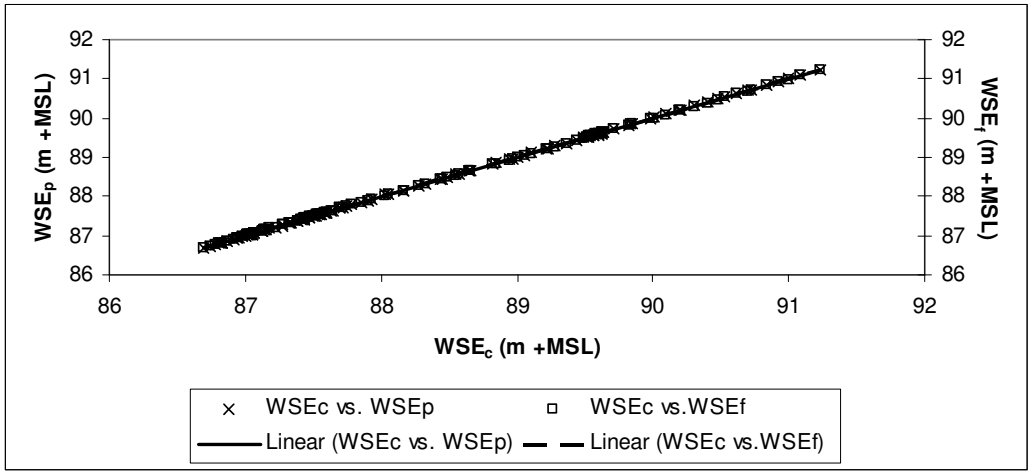

Figure 7.4-6: Modelled WSE at each cross-section according to the land cover change in the average flood discharge; $WSE_{c, p, f}$ – Water surface elevation for the current, past and future land cover pattern, respectively

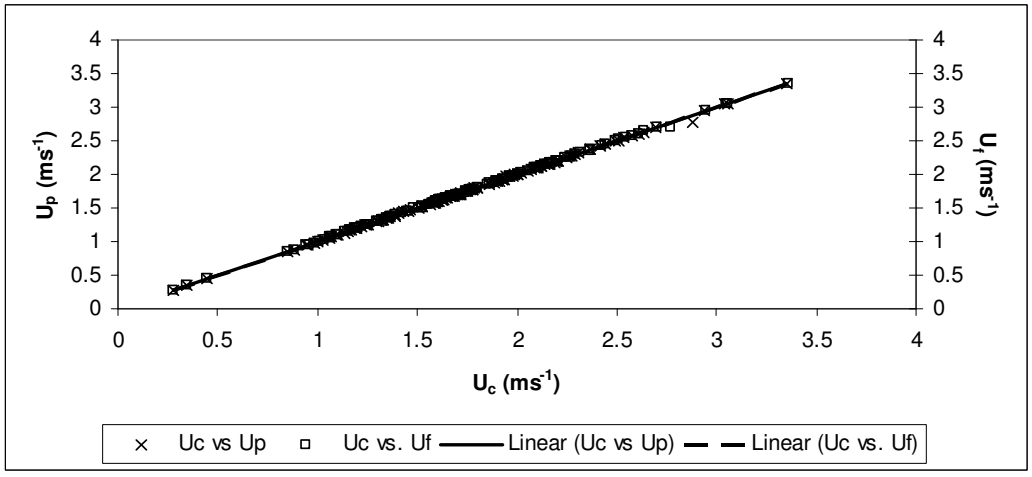

Figure 7.4-7: Modelled mean in-channel velocity at each cross-section according to the land cover change in the average flood discharge; $U_{c, p, f}$ – Average in-channel velocity for the current, past and future land cover pattern, respectively

Figure 7.4-8 and Figure 7.4-9 illustrate the differences in the mean riparian velocity based on a comparison between the current and past land cover pattern and current and future land cover pattern, respectively. Similar to what was found in the average flood discharge analysis, with the reduction of the hydraulic roughness (Manning's *n*) from the past to current and future land cover patterns, the mean riparian velocity increased significantly. In fact, the average increase of the left and right riparian velocity between the past and current land cover patterns were 0.03 ms^{-1} and 0.08 ms^{-1}, respectively while the average decrease of the left and right riparian velocity between the current and future land cover patterns were 0.10 ms^{-1} and 0.12 ms^{-1}, respectively.

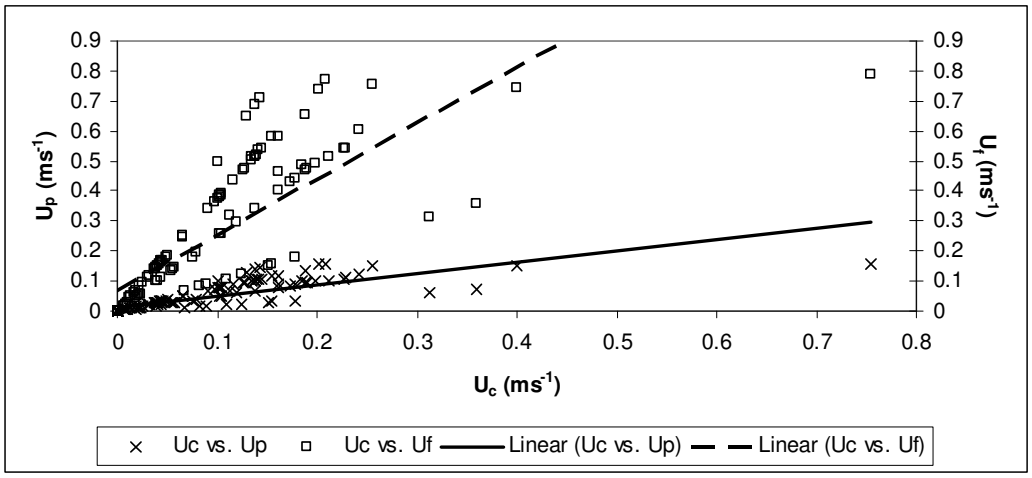

Figure 7.4-8: Modelled mean velocity in the floodplain along the left banks in the average flood discharge; $U_{c,\,p,\,f}$ – Average in-channel velocity for the current, past and future land cover pattern, respectively

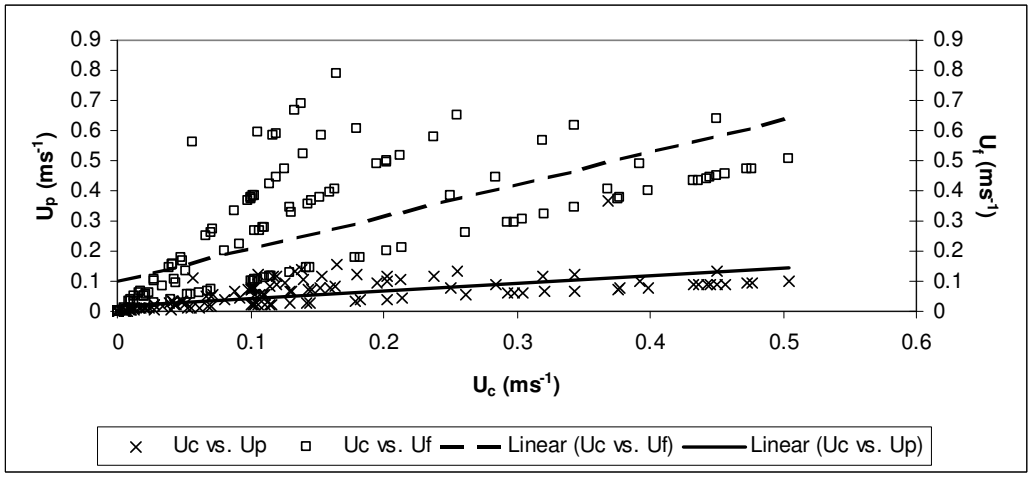

Figure 7.4-9: Modelled mean velocity in the floodplain along the right banks in the average flood discharge; $U_{c,\,p,\,f}$ – Average in-channel velocity for the current, past and future land cover pattern, respectively

7.5 Discussion

In general, in accordance with the high flood discharge (45,149 m^3s^{-1}) along the full river network, the large islands along Channel 2 and 3 and the downstream river network were still partly dry while most 'smaller' islands in the downstream river network were inundated. Even though the ratio of cross-sectional areas did not correctly reflect the entry discharge into each channel (Table 7.2-2, Table 7.3-2 and Table 7.4-2), the applied ratio together with the *Flow Optimization* option in HEC-RAS still could be applied in the case of lack of input data (in terms of entry discharge for each individual channel) to model the complex river network (Table 7.2-3, Table 7.3-3 and Table 7.4-3).

For acute angles at the bifurcations (Bi_5, Bi_8 and Bi_9; Chapter 3, Figure 3.3-10) along the downstream river network, the ratio of the splitting discharge needed to be adjusted iteratively by routing less discharge along the acute downstream channel. Even though the splitting discharge at each bifurcation might not reflect the actual splitting discharge in reality (due to the relation between the splitting discharge ratio and the combination of acute angle and cross-sectional area), together with the assigned Manning's *n* coefficient along the downstream network approximately within the predefined range of the Manning's *n* coefficients along the upstream network, the model can be used to simulate the water-way or flooding patterns along the complex river network in the case of the lack of input data (measured bathymetry and downstream boundary conditions). In fact, the modelled stages along the upstream river network for the full network models met those of the upstream river network models.

According to the literature, the findings from Carling and Grodek (1994) with the Manning's *n* coefficient of about 0.025 was the lowest for the bedrock-confined river (Chapter 2, section 2.1.2). However, for the downstream river network in this study, the minimum calculated Manning's *n* coefficient was constrained larger than 0.007; in fact, with the higher minimum value selected, the full river network could not be modelled accurately (*i.e.* either the modelled water surface profiles did not meet the recorded data at the upstream boundary condition or the modelled junctions did not reach the optimum solution (to eliminate the rise or drop of the water surface at each bifurcation) according to the *Flow Optimization* option in HEC-RAS). In addition, even though the top-width of the channels appeared on the developed DEM to be

quite accurate compared to that extracted from the SPOT image, the cross-sectional areas extracted from the pseudo-bathymetry are likely to be different from the natural non-surveyed cross-sectional areas. In fact, the downstream river network is anabranching while the upstream section is a network of meandering channels; therefore, the developed pseudo-bathymetry for the downstream network based on the relation between the SPOT reflectance and channel depth along the upstream network seemed to be deeper than the actual bathymetry. The differences between the calculated Manning's *n* coefficient along the downstream compared to the upstream river network indicate that the cross-sectional areas extracted from pseudo-bathymetry still need further adjustment (based on improved approaches and more intensive fieldtrip) for a better model. In fact, Figure 5.1-5 and 5.1-6 in Chapter 5 showed that the channel bed elevation along measured bathymetry of the upstream river network was lower than that along the pseudo-bathymetry of the downstream river network. Such the inaccurate interpolated pseudo-bathymetry lead to inappropriate assigned Manning's *n* coefficient. However, using an acceptable range of the Manning's *n* values (ranging from 0.007 to 0.9), the pseudo-bathymetry could be used to model the flows in the river network.

The distribution and mean value of the calculated Manning's *n* coefficients along the upstream and downstream river network in the case of the low discharge are presented in Figure 7.5-1and Figure 7.5-2, respectively. Figure 7.5-3 and Figure 7.5-4 present the distribution and mean value of the calculated Manning's *n* coefficient along the upstream and downstream river network in the case of the flood discharge, accordingly. For both low and flood discharge, the calculated Manning's *n* coefficients along the downstream multi-channel network were lower than those along the upstream river network. In the low discharge simulation, the mean Manning's *n* value was 0.055 in the upstream river network while it was 0.012 in the downstream river network. Similarly, the mean Manning's *n* value in the flooding simulations was 0.036 and 0.016 in the upstream and downstream river network, respectively. However, the mean value of the Manning's *n* coefficients along the downstream river network in the two levels of the entry discharge were still in the well-known range and due to the objective of this study which is to model the flooding extent along the river network, the modelled result was acceptable.

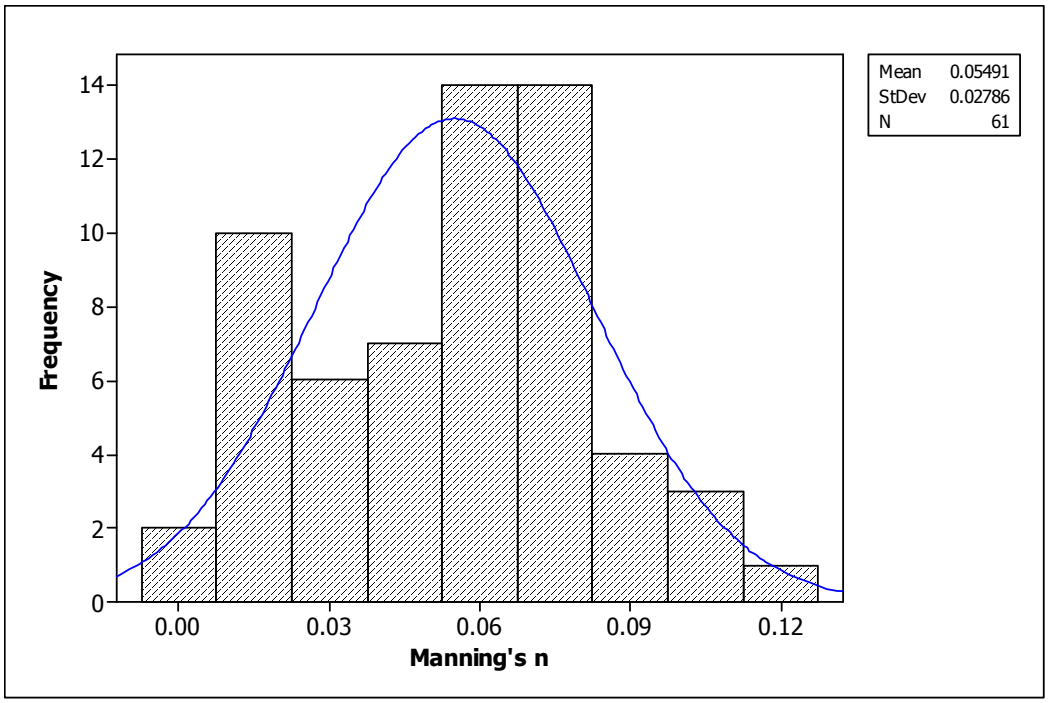

Figure 7.5-1: Distribution of the calculated Manning's *n* coefficient along the upstream river network in the low discharge according to the measured bathymetry

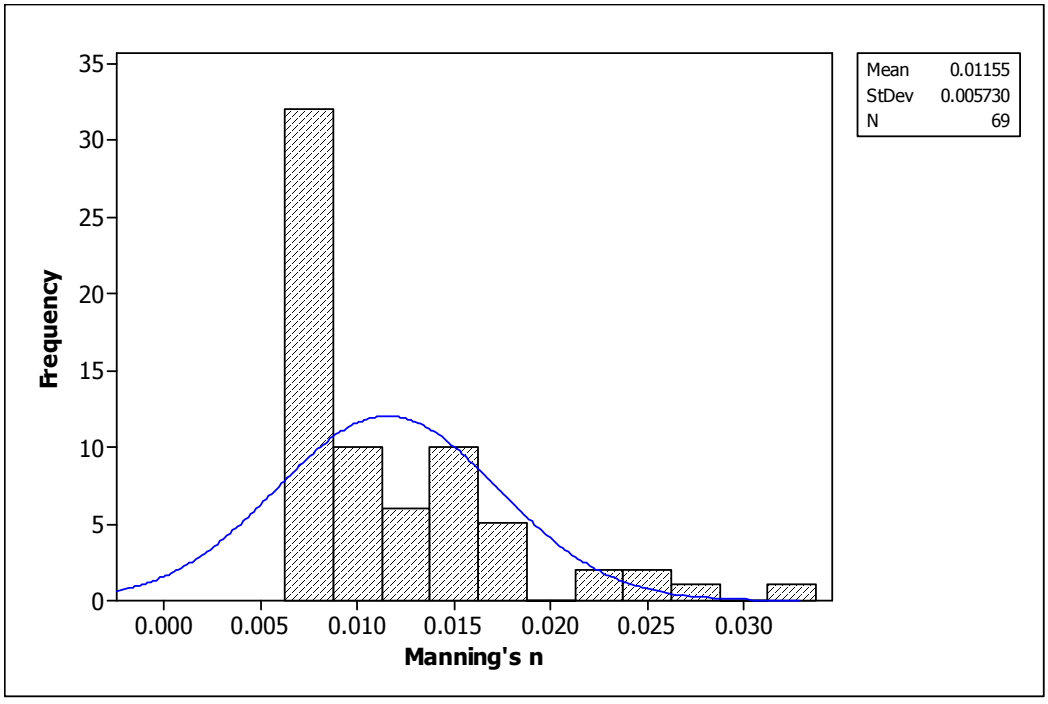

Figure 7.5-2: Distribution of the calculated Manning's *n* coefficient along the downstream river network in the low discharge according to the pseudo-bathymetry

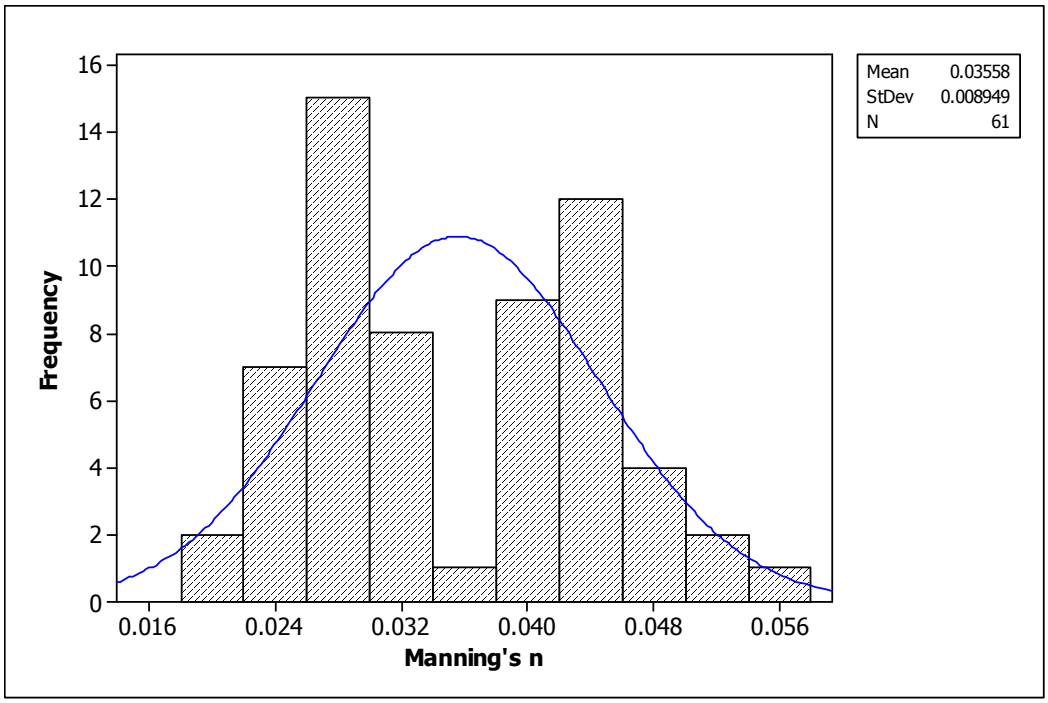

Figure 7.5-3: Distribution of the calculated Manning's *n* coefficient along the upstream river network in the flood discharge according to the measured bathymetry bathymetry

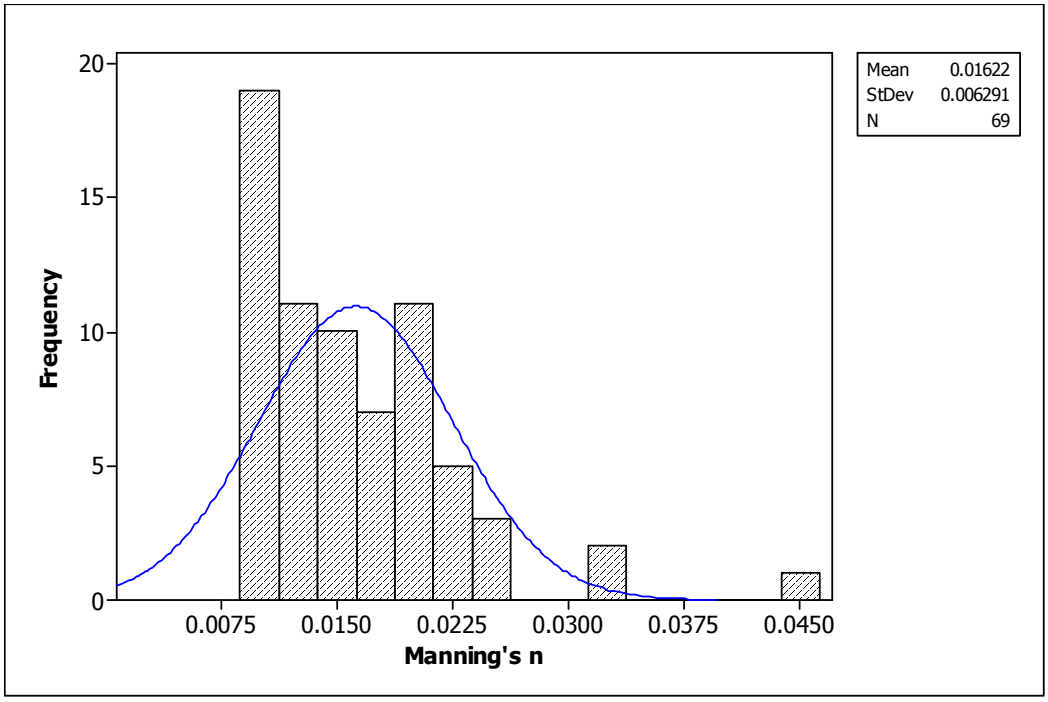

Figure 7.5-4: Distribution of the calculated Manning's *n* coefficient along the downstream river network in the flood discharge according to the pseudo bathymetry

In the low discharge model, due to a large range of the local water surface slope along Channel 2 and Channel 3, the calculated Manning's *n* coefficients were fluctuated greatly; the mean value along such channels was 0.045 with the standard deviation of 0.032. However, in the flooding model, the local water surface slope along Channel 2

and Channel 3 was more stable and therefore the calculated Manning's *n* coefficients along these channels were decreased with the mean value of 0.028 and the smaller standard deviation of 0.003. Such changes of water surface slope with the entry discharge were reported by Friedkin (1945) and Leopold and Wolman (1957). In addition, along Channel 4 and Channel 5, the calculated Manning's *n* coefficients were higher but more stable than those along Channel 2 and Channel 3. In fact, the Manning's *n* coefficients along Channel 4 and Channel 5 in low discharge and average flood discharge were 0.066 ± 0.016 and 0.045 ± 0.004, respectively. The bimodal distribution of the calculated hydraulic roughness coefficient in the flood discharge was caused by the separation of the hydraulic roughness along Channel 2 and 3 and Channel 4 and 5 with mean value of 0.028 and 0.045, respectively. In addition, along the downstream river network, even though the calculated hydraulic roughness was low (in comparison to those along the upstream network), due to the impact of the bedrock-constraint nature, the calculated hydraulic roughness coefficient increases with discharge.

The calculated Manning's *n* coefficients along the downstream river network in both the low discharge and average flood discharges are presented in Figure 7.5-5. Even though the set of Manning's *n* values calculated for the low and flood discharges along the downstream river network approximated the calculated range for the upstream river network, it can also be seen that the Manning's *n* set along the downstream network in the flood discharge scenario was much lower than that in the low discharge scenario. In fact, because the pseudo-bathymetry was developed for this section of the river network, the hydraulic nature at each cross-section along the network cannot be examined in any detail. Rather, the acceptability of the model is justified with the wetted-section data only. In addition, even though Patro *et al.* (2009) used SRTM data to estimate the bathymetry of a large river during low discharge when the channel bed was mainly exposed, the bathymetry they used was also simplified within the wetted-section. With the application of a 1D hydraulic model, Patro *et al.* (2009) found that the results obtained met the measured data. In fact, it helps to confirm that with the application of the energy approach of a 1D hydraulic model, the bathymetry of a river network can be simplified. In that case and the hydraulic roughness needs to be adjusted, to account for the over-simplified bathymetry, to make the modelled results meet the recorded data. Nevertheless, the

roughness is still required to be within a predefined range, otherwise the modelling exercise would be deemed a failure.

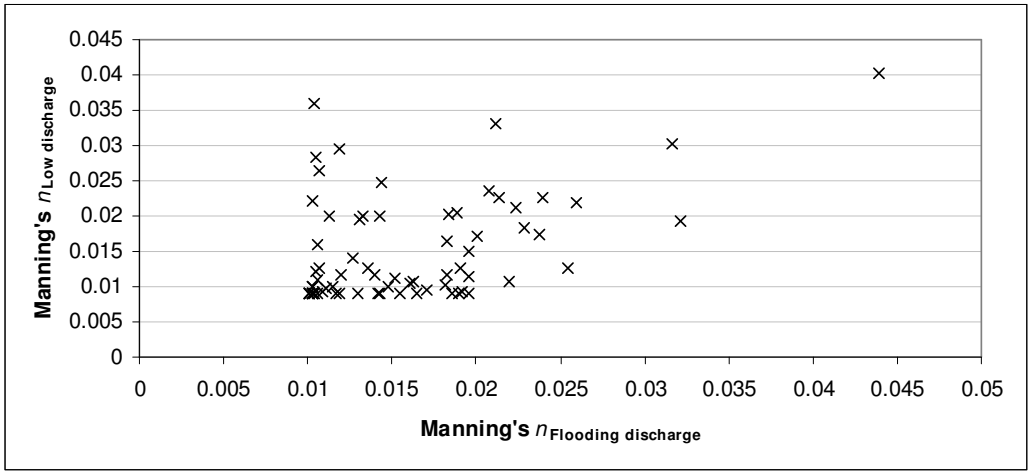

Figure 7.5-5: The calculated Manning's *n* at each cross-section along the downstream river network in the low (6,450 m^3s^{-1}) and flooding entry discharge (26,300 m^3s^{-1})

In a large river network, the assigned Manning's *n* coefficient of different land cover types along the floodplain did not have a strong impact on the modelled stage due to a large proportion of discharge routed along the channels but not the floodplain. The findings in this chapter agree with what was found in Chapter 6 and Latrubesse (2008). The *normal depth* conditions applied in this chapter present the largest flood along the downstream river network. If the *normal depth* condition increased, the flooding pattern along the downstream river network decreased. Therefore, without the known downstream end condition, the maximum flooding can be calculated only.

The *normal depth* applied as the downstream boundary condition of the downstream river network was increasing from 2.3 x 10^{-6} mm^{-1} to 3.8 x 10^{-6} mm^{-1} and 7.5 x 10^{-6} mm^{-1} corresponding to the low discharge, average and high flood discharge, respectively. The findings in the downstream river network agree with what was found in the upstream river network (the higher the entry discharge, the higher the water surface slope). In addition, according to Knighton (1998), alluvial anabranching rivers usually have lower water surface slopes than meandering rivers. The steepening water surface slopes were found along the upstream river network (meandering channels) compared to the more gentle water surface slopes along the downstream river network (anabranching network) in all three scenarios of the entry discharges.

The obtained results from the full network models confirm that in the case of the lack of the measured bathymetry, the energy approach in a 1D hydraulic model still can be

used to estimate the hydraulic parameters of the complex river network. The calculated Froude number in relation to the hydraulic depth and the mean in-channel velocity in all three discharges (low discharge, average and high flood discharge) are presented in Figure 7.5-6. The Froude number was spread over a wide range of values in the low discharge scenario (from 0.02 to 0.92) while such the number ranged from 0.02 to 0.30 and from 0.03 to 0.44 in the average and high flood discharge scenarios, respectively. Comparing to the modelled Froude number along the upstream network (Chapter 6), the Froude number calculated in the low discharge along the downstream network was significantly different while it is not that significantly different in the flood discharge scenarios (Table 7.5-1). The greatly fluctuated Froude number was caused by the greatly fluctuated modelled mean velocity while the modelled hydraulic depth was not significantly different along the downstream river network. However, according to Ashmore (1985), the Froude number along an anabranching network was from 0.41 to 1.08 which was higher than that calculated in the downstream anabranching network. The possible reason might be the pseudo-bathymetry which was interpolated based on the measured bathymetry of the upstream network was deeper than the actual bathymetry of the anabranching downstream network. The high modelled velocity was caused by the low Manning's *n* at the cross-section; for example, the Manning's *n* at cross-section 9.05 was assigned to 0.0081 leading to the high mean in-channel velocity (3.32 ms^{-1}) and therefore resulting in the high calculated Froude number (0.923). The Froude number decreased from the low discharge to the average flood discharge due to the increase of channel depth while the velocity did not significantly increase. However, the Froude number increased from the average to high flood discharge due to the significant increase of the mean in-channel velocity. The findings lead to the fact that the geometry and/or the boundary conditions (assigned Manning's *n* coefficient) of the hydraulic model were arguable, especially in the case of the low discharge where the water surface slope in each channel was considered to be greatly different compared to the neighbours. However, the approach is valuable in terms of identifying which channels need to be measured in detail, especially in the case of a multi-channel network located in a remote area. Even though the local Froude number was quite high at certain cross-sections (Figure 7.5-6), especially at the low discharge simulation, the maximum value was still lower than 1 and the majority of the calculated Froude numbers were

less than 0.4 therefore the subcritical model was still suitable to model the river network.

Table 7.5-1: Calculated Froude number along the upstream and downstream river network in different scenarios of the upstream discharge

		Low discharge	Average flood discharge	High flood discharge
Upstream network	Min	0.05	0.02	0.03
	Max	0.33	0.29	0.31
Downstream network	Min	0.02	0.02	0.03
	Max	0.92	0.30	0.44

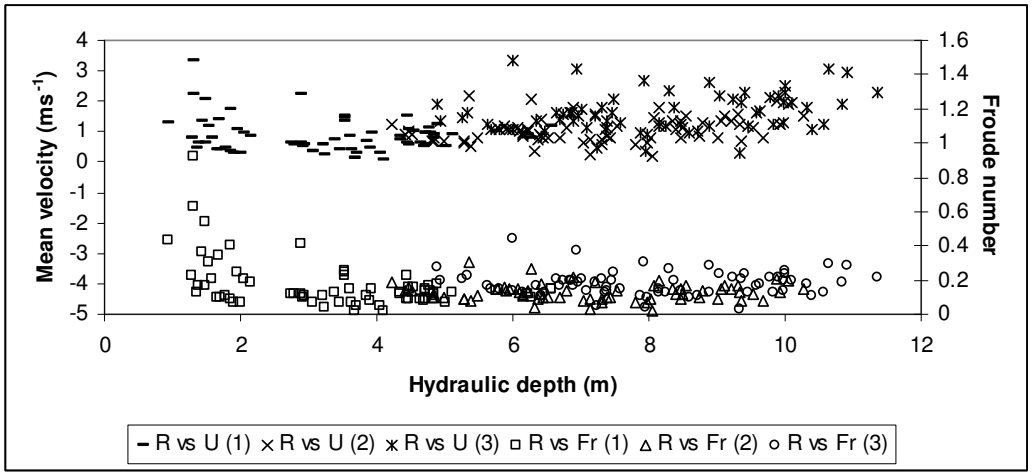

Figure 7.5-6: Hydraulic depth, mean in-channel velocity *vs.* Froude number in the low discharge, average and high flood discharge along the downstream river network; Notes: 1 – Low discharge; 2 – Average mean flood discharge; 3 – High flood discharge

Broadhurst and Heritage (1998) introduced the 'multiple stage' model for the bedrock-influenced river system in South Africa in which at a certain discharge, the modelled stage at a certain cross-section cutting through different channels were different. This feature was found in the downstream river network of the study area. Figure 7.5-7 illustrates the cross-sections laterally across the downstream river network and Figure 7.5-8 presents the modelled stages across the cross-sections in the low discharge, average and high flood discharge. It can be seen that the larger lateral distance between the channels, the higher the difference between the modelled water surface elevation. For example, at all three applied discharges, the modelled water surface elevation at 1_b and 1_c was similar but greatly different from the modelled water surface elevation at 1_a. Similarly, the modelled water surface elevation at 2_e was significantly different from the rest across the cross-section. However, there was no evidence to confirm that the differences between the cross-sections were higher in the low discharge compared with the high discharges.

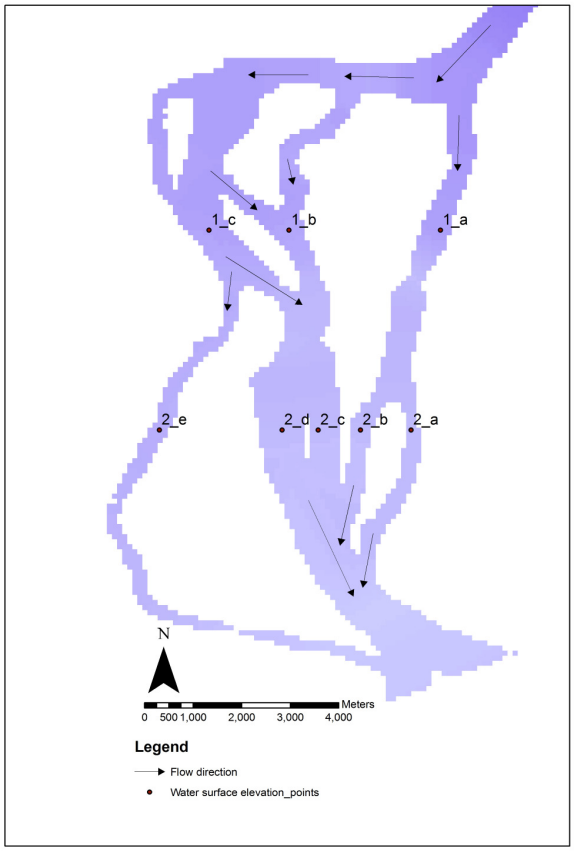

Figure 7.5-7: Cross-sections across the downstream river network

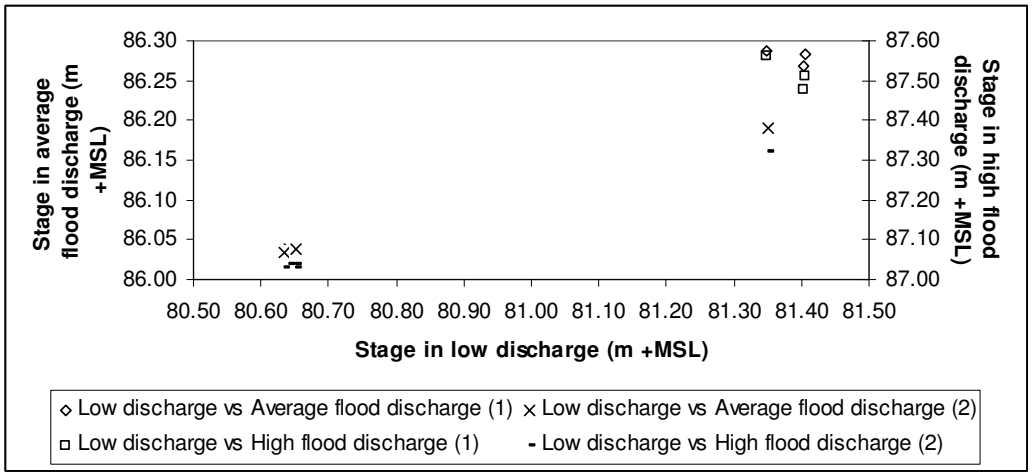

Figure 7.5-8: Water surface elevation at each channel across the cross-sections; Notes: 1 - Cross-section 1 and 2 – Cross-section 2 in Figure 7.5-7

Chapter 8: General discussion

Introduction

The first section of this discussion summarises the current issues faced in the Siphandone wetlands in terms of the physical setting. Even though a comparison between different segments of the Mekong River was not defined as a specific goal of the study, differences between the in-channel hydraulic parameters at Pakse and Channoy are clarified to provide greater understanding of how the Mekong River behaves hydraulically in different segments. Then, detailed explanations of how each defined goal of the study has been considered to be fulfilled are presented. Finally, suggestions on future work in order to get a better understanding of the hydraulic nature of a bedrock-confined river network are given.

In general, the 1D hydraulic models were successfully developed (for both the upstream and full river network) to estimate the hydraulic nature (*i.e.* water surface profiles, mean velocity and Froude (*Fr*) number) along a large and sediment-laden bedrock-confined river network with multiple outlet sections. The novelty of the study is that the hydraulic models were built even with limited input data based on: (i) the measured bathymetry (along the upstream river network) and pseudo-bathymetry (along the downstream river network); (ii) the assumed division of discharge at each junction (based on the ratio of the first cross-sectional area of the downstream channels); (iii) the calculated Manning's *n* coefficient at each cross-section; and, (iv) the *Flow Optimization* function in HEC-RAS. The sediment entrainment conditions within the entry channel of the river network could be estimated as a pointer to future study of sediment transport along the Siphandone wetlands via the outcomes of the hydraulic models. The weaknesses of the study will also be discussed in the last section.

8.1 Changes in the physical setting of the Siphandone wetlands

A range of issues in terms of physical setting are currently faced in the Siphandone wetlands, including: global climate change, local land cover change and planned dam construction for hydroelectric power. Such issues are projected to affect strongly the hydraulic nature of the river network and are receiving considerable attention from different international organizations like the MRC, WWF and the International Rivers

Organization. This study mainly focused on the hydraulic aspects of the Siphandone river network. In fact, the scientific challenge was to understand the nature of low and high flows in such a complex river network and to compare and contrast this behaviour with that of single-thread bedrock channels and alluvial anabranching networks (reviewed from the literature). This study will benchmark the current hydraulic nature within the Siphandone wetlands before any significant physical changes happen due to the alteration of the global environmental context and local anthropogenic impacts. To address the scientific hypotheses, the objective of the study was subdivided into different specific goals and each of the goals is discussed in different sections in this chapter.

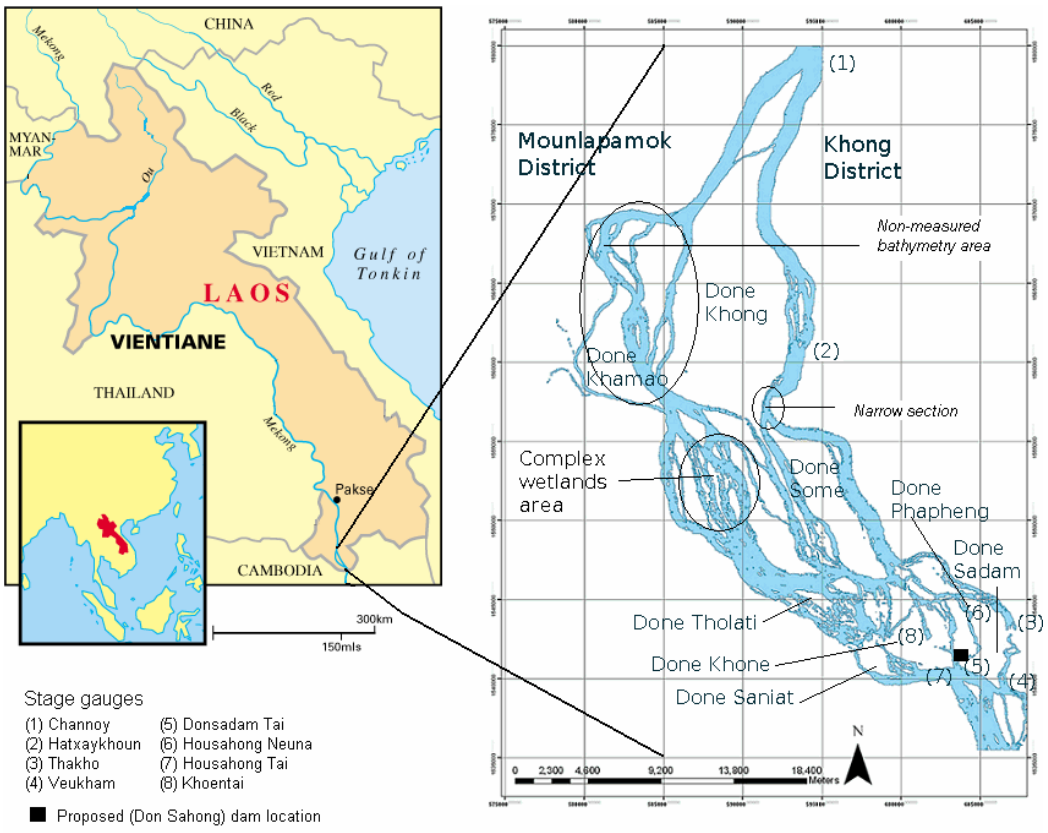

Figure 8.1-1: The Pakse gauging station and the Siphandone wetlands

8.2 Hydraulic nature at Pakse and Channoy

The reaches of the Mekong River at Pakse and Channoy (Figure 8.1-1) are bedrock-confined. While Pakse is located within a lengthy single channel section, Channoy is the entry section of a large and complex anabranching network; such differences lead

to significant variations in the hydraulic nature at the cross-sections of the two locations.

Although along the two segments (from Pakse to Channoy and from Channoy to Hatxaykhoun), the water surface slopes increase with discharge, the relationship between the water surface slope and discharge is different in the two segments; the water surface slopes in the segment from Pakse to Channoy ($S = 1x10^{-5}Q^{0.156}$, R^2 = 0.87) increased more slowly than that in the segment from Channoy to Hatxaykhoun ($S = 2x10^{-5}Q^{0.203}$, R^2 = 0.77). Such trends in water surface slope are unusual; with increasing discharge, water surface slope usually decreases (Friedkin, 1945; Yatsu, 1955; Depetris and Gaiero, 1998; Wohl, 2007); but similar results have been found for bedrock-confined rivers in field-based studies (Heritage *et al.*, 2004; Richardson and Carling, 2006). The trend in water surface slope as a function of discharge between Channoy and Hatxaykhoun could be explained by the morphological controls along the river network. The river network in Siphandone is subcritical ($Fr < 1$; Chapter 6 and Chapter 7). Therefore with a rise of the channel bed such as the rise at the end of Channel 3, the local water surface elevation decreases (Figure 8.2-1). In addition, due to the impact of such a rise in the channel bed, the water surface elevation upstream of the rise increases faster than that over the rise itself; therefore, with an increase in discharge, the water surface slope increases. This effect might be exacerbated if the bed rise is located also at a narrowing river section.

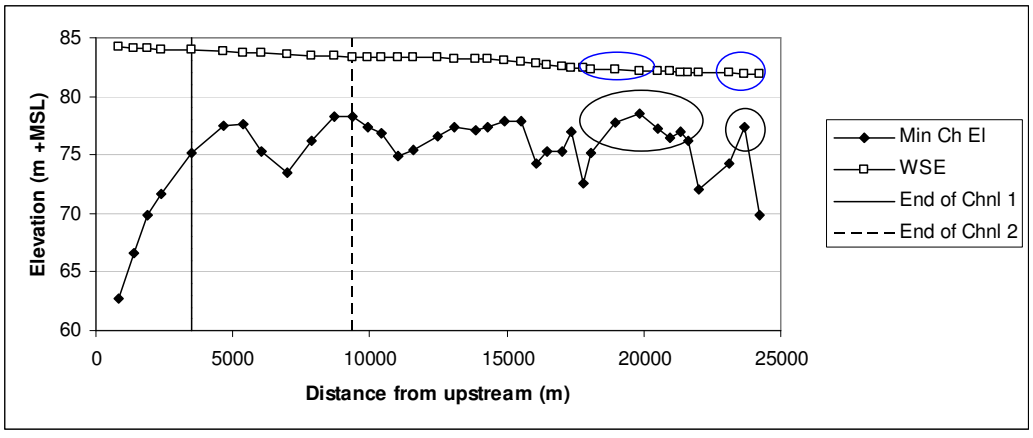

Figure 8.2-1: Water surface elevation and the channel bed elevation along Channel 1, 2 and 3; black circles – the rise of the channel bed and blue circles – the drop of water surface elevation

A classification of natural rivers proposed by Rosgen (1994) was well-referred to classify different natural rivers (Savery *et al,*, 2001; Juracek and Fitzpatrick, 2003;

Roper *et al.*, 2008). According to the Rosgen's classification (1994), the Mekong segment at Pakse could be considered as 'C' stream type, which is characterised by low gradient (water surface slope smaller than 0.02 mm^{-1}), meandering (sinuosity larger than 1.4), the width and depth ratio (of about 161) larger than 12, point bar and riffle/pool. However, Rosgen (1994) did not include bedrock-confined channels in his classification, class 'C' strictly applied only to alluvial channels. At Channoy, even though it is at the entry section of the anabranching channel network, the river meets the criteria of class 'DA' which is characterised by stable channel banks and low water surface slope. However, the width to depth (*w/d*) ratio of the Channoy section is greater than 40, which does not satisfy the criteria of Rosgen (1994) for class 'DA' channels. In fact, the *w/d* ratio in alluvial and bedrock-confined anabranching networks ranges from 20 to 122 (Makaske, 2001; Latrubesse, 2008; Nanson and Knighton, 1996). However, none of these studies measured the *w/d* ratio of the Mekong, and according to the cross-section extracted from the DEM at Channoy (Figure 3.3-6), the *w/d* ratio in Channoy was about 107 at the bankfull discharge. The value is within the published range of the *w/d* ratios for anabranching networks.

Figure 8.2-2 and Figure 8.2-3 present the relationship between the hydraulic radius, cross-sectional area, general water surface slope (from Pakse to Channoy and from Channoy to Hatxaykhoun) and entry discharge at Pakse and Channoy. At similar entry discharge, the smaller Manning's *n* coefficient at Pakse compared with Channoy might be caused by the combination of the two parameters: (i) the smaller cross-sectional areas at Pakse than that at Channoy; and, (ii) the smaller water surface slope from Pakse to Channoy than that from Channoy to Hatxaykhoun. In addition, the hydraulic radius at Channoy is higher than that at Pakse for an identical discharge. While the hydraulic radius at Channoy increases monotonically with increasing discharge, the hydraulic radius at Pakse increases with discharge up to a discharge of about 30,000 m^3s^{-1}, and then decreases with further increases in discharge. This is due to the rapid increase in cross-sectional width compared to the increase in cross-sectional area during the overbank flow (Figure 8.2-3). Moreover, the cross-sections at Pakse and Channoy are located in sand-bedded and rock-bedded segments, accordingly; therefore, the Manning's *n* coefficient at Channoy is higher than that at Pakse.

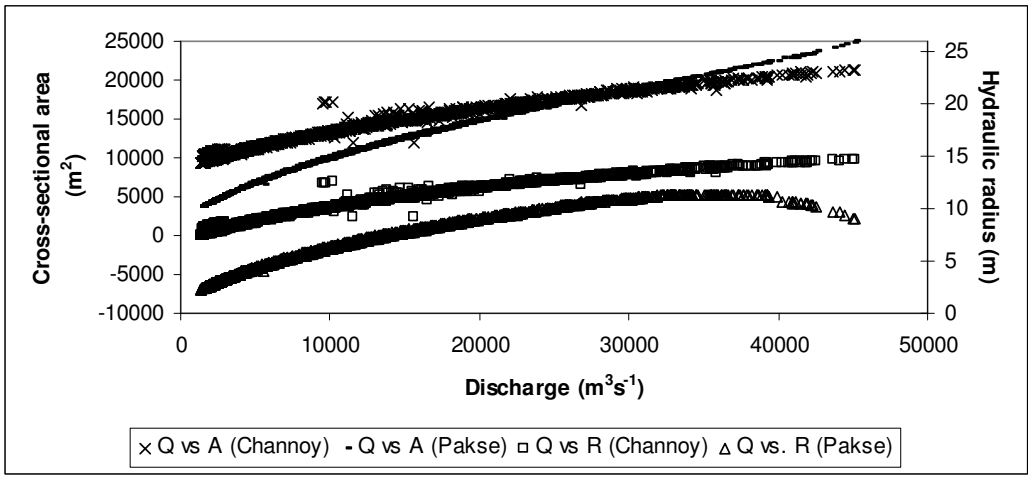

Figure 8.2-2: Cross-sectional area, hydraulic radius *vs.* discharge at Pakse and Channoy

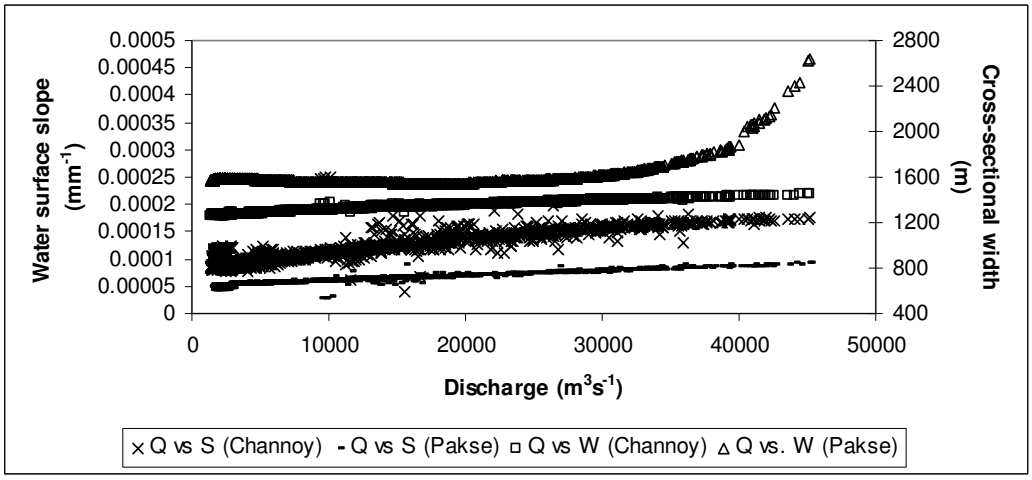

Figure 8.2-3: Water surface slope (from Pakse to Channoy and from Channoy to Hatxaykhoun), top-width *vs.* discharge at Pakse and Channoy

The mean velocity at Channoy ($U = 6.0x10^{-4}Q^{0.78}$) increases more rapidly than that at Pakse ($U = 1.5x10^{-2}Q^{0.46}$), which might reflect the drop in the Manning's *n* coefficient with discharge at Channoy. The trends of the Manning's *n* coefficients at Pakse and Channoy calculated for entry discharges from 1,300 m^3s^{-1} to 45,100 m^3s^{-1} are presented in Figure 8.2-4. Even though the Manning's *n* coefficient at Pakse was lower than that at Channoy at all entry discharges, the ranges of the Manning's *n* coefficient (from 0.018 to 0.033 and from 0.022 to 0.293 at the Pakse and Channoy cross-section, respectively) are within the published range of the Manning's *n* coefficient for bedrock-confined rivers (Carling and Grodek, 1994; Kidson *et al.*, 2006; Heritage *et al.*, 2004; Wohl and Wilcox, 2005; Carrivick *et al.*, 2004; Carrivick, 2009) and reflect the fact that both cross-sections are located in the bedrock section of

the Mekong River. In fact, the Pakse section is mainly sand bedded within a bedrock section while the Channoy section is mainly bedrock with little filling of sand. According to the literature, the hydraulic roughness (Manning's *n*) coefficients for bedrock-confined channels vary from a minimum value of 0.025 (Carling and Grodek, 1994) to a maximum value of 0.9 in the case of 'the major obstacle' in channels (Carrivick, 2009).

The range of the calculated Manning's *n* coefficient (from 0.022 to 0.29) at Channoy is similar to the range of the Manning's *n* values in previously reported bedrock-confined channels. In addition, the Manning's *n* coefficient decreased with discharge, which is normal behaviour. However, the range of Manning's *n* coefficient from 0.018 to 0.033 at the full range of entry discharge at Pakse was lower than the published range where the minimum value was much smaller than that documented by Carling and Grodek (1994); however, the mean calculated Manning's *n* coefficient was 0.027 with a standard deviation of about 0.0015 (Figure 8.2-4) and, therefore, it could be confirmed that the cross-section at Pakse is a bedrock-confined section with alluvial fill. The trend of the Manning's *n* coefficient at Pakse is more complex than that at Channoy because it is located in a strong bedrock-constrained segment, with the channel width relatively stable over a large range of discharge. In fact, the Manning's *n* coefficient at Pakse decreased (from 0.029 to 0.026) when discharge increased to 14,000 m^3s^{-1}; after this discharge the Manning's *n* coefficient slightly increased (from 0.026 to 0.027) when discharge reached about 35,000 m^3s^{-1}. Beyond this discharge, the Manning's *n* coefficient decreased to 0.02 as a minimum. Because the cross-sectional area at Pakse has a constant top-width for a large range of discharges (from 1,300 m^3s^{-1} up to more than 30,000 m^3s^{-1}) leading to a constant value of the ratio of Q/RU over a large range of discharge, the calculated Manning's *n* coefficient at Pakse was also relatively constant. In both the Pakse and Channoy cross-sections, the greatest contribution to flow resistance is not skin friction but form roughness which changes as river stage varies. The calculated Manning's *n* coefficient decreases with increasing discharge at Pakse and Channoy because velocity increases rapidly with increasing stage while cross-sectional area and hydraulic radius increase more slowly.

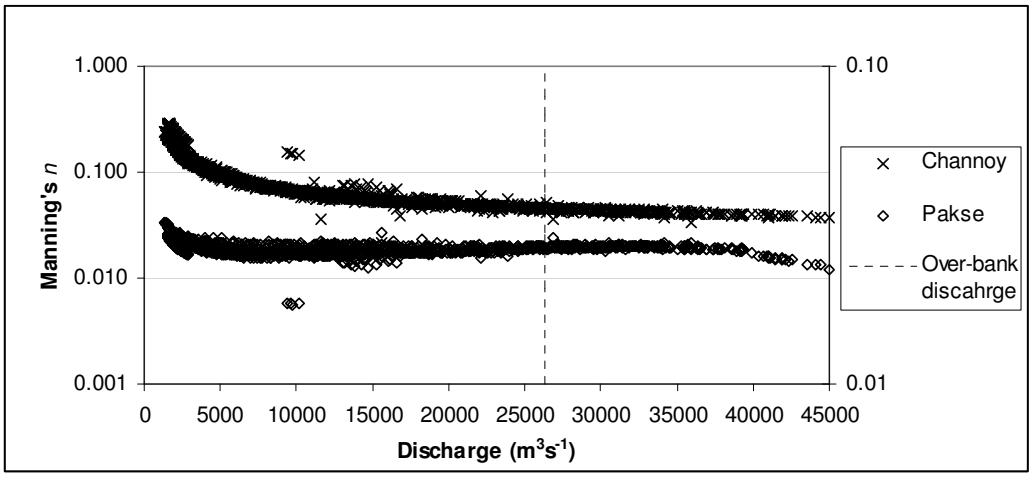

Figure 8.2-4: Calculated Manning's *n* at Pakse and Channoy

The at-a-station hydraulic geometry analysis at Pakse and other single meandering channels were analyzed and are presented within Figure 8.2-5. The R^2 values of relationships between the range of discharge (from the low flow to the overbank discharges) *versus* top-width, hydraulic radius and mean velocity were 0.91, 0.95 and 0.97, respectively at Pakse. The Mekong segment at Pakse, which is characterized by a meandering pattern, has values of *b*, *f* and *m* equal to - 0.0074, 0.41 and 0.58, respectively. With a wide cross-section (approximately 1,700 m) and relatively small hydraulic radius (approximately 11 m), the *w/d* ratio at Pakse is high. According to different research, the exponent values are positive (*e.g.* Leopold and Maddock, 1953; Parker, 1979; Whipple, 2004). However, the exponent values might be negative as well. According to Huang and Nanson (1997) and Knighton and Nanson (2002), along an alluvial anabranching network in Australia, the *f* and *m* exponent were negative. In fact, the width of the cross-section at Pakse is quite stable (Figure 3.2-2) when the water surface elevation rises from about 88 m +MSL to 95 m +MSL, due to the bedrock-confined section. At Pakse, the channel section is relatively wide and therefore, the increase of discharge might cause little impact on the increase of depth. The *f* value (0.41) at Pakse was quite similar with what was found by Gupta *et al.* (1999) (0.46) and within the published range of values (from 0.20 to 0.63 (Deodhar and Kale, 1999); and, from 0.28 to 0.41 (Turowski, 2008)). In addition, the *m* exponent at Pakse (0.38), within the published range of values from 0.08 to 0.58 (Deogkar and Kale, 1999), shows the fact that the increase of discharge has a strong impact on the increase of mean velocity. The summation of the exponents (*b*, *f* and *m*) at Pakse was 0.98, which is not significantly different from the predefined value of 1.

A comparison between the at-a-station hydraulic geometry between the alluvial and bedrock-confined meandering channels is also presented in Figure 8.2-5. In fact, the maximum value of the *b* and *f* exponents of the bedrock-confined river was higher than those of the alluvial channel. In addition, the *b* and *f* exponents of the bedrock-confined river had a wider range compared to those of the alluvial river. This could be explained by the fact that within the alluvial river, the river's geometry could be adjusted easily. Therefore, the *b* and *f* exponents of the different rivers were within a small range. In contrast, along the bedrock-constrained river, the river's geometry could not be freely adjusted; therefore, the *b* and *f* exponents of each individual river were defined and driven by the geological controls.

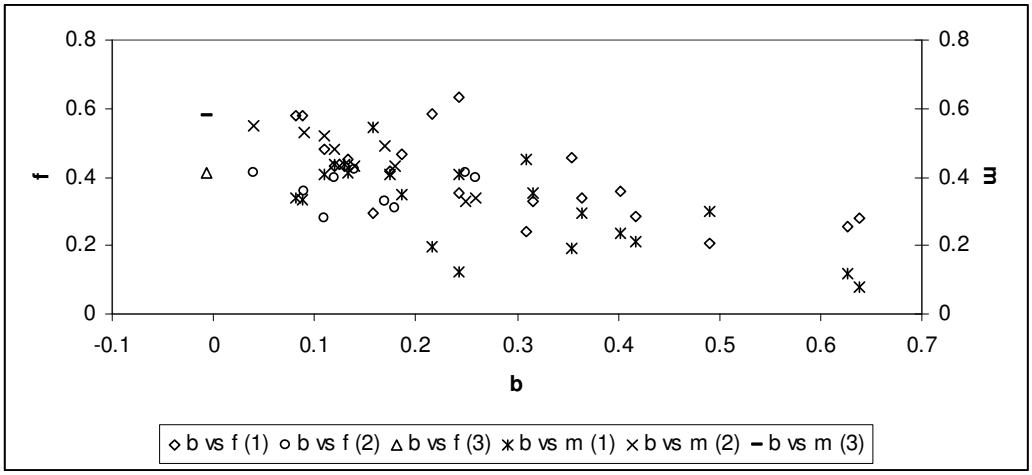

Figure 8.2-5: At-a-station hydraulic geometry at different bedrock-confined meandering channel (1) (*after* Deodhar and Kale, 1999), alluvial meandering channel, (2) (*after* Dingman, 2007) and at the Pakse cross-section (3)

Similarly, the at-a-station hydraulic geometry analysis at Channoy and other anabranching networks were analyzed and presented in Figure 8.2-6. The R^2 values of relationships between the range of discharges (from the low flow to the overbank discharge) *versus* top-width, hydraulic radius and mean velocity were 0.93, 0.97 and 0.99, respectively at Channoy. Even though the Channoy section is not within the anabranching network of the Mekong, it was shown above that the hydraulic characteristics were useful to help constrain and describe other sections within the network. Even though the exponent values of *b*, *f* and *m* at Channoy (0.06, 0.19 and 0.78, respectively) were within the range of values of other anabranching river networks (Latrubesse, 2008), the differences between the exponent values at Channoy and others anabranching network could be explained by the local controls such as

channel cross-sectional shape and the hydraulic roughness in relation to the stage (Wolh, 2007). At Channoy, the mean in-channel velocity is the variable most affected by changes in discharge. In addition, the *f* coefficient is much larger than the *b* coefficient, which means that with the increase of discharge, the hydraulic radius increases much faster than the width. In fact, the cross-section has quite steep banks (Figure 3.3-2, Figure 3.3-6 and Figure 3.3-7).

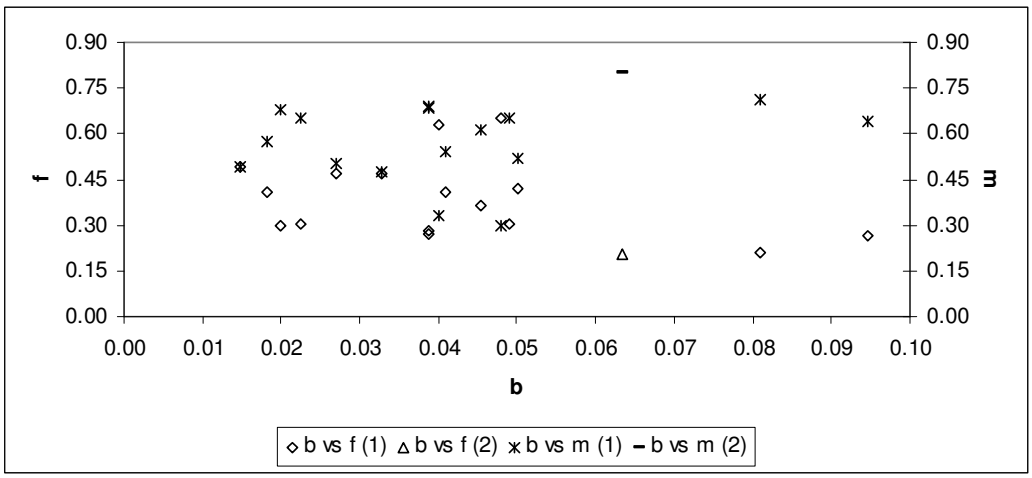

Figure 8.2-6: At-a-station hydraulic geometry at different alluvial anabranching networks (1) (*after* Latrubesse, 2008) and at Channoy (2)

Whereas, for both Pakse and Channoy, the values of the exponents *f* and *m* are significantly different to zero at the 0.1% level using an *F*-test (Davis, 1986), the values of the exponent *b* for both Pakse and Channoy also for the 0.1% level are not significantly different to zero. In fact, using the regression methods in Minitab, Excel and Matlab, the sign of the power-law exponent for Pakse could be either positive or negative but with values typically between – 0.00074 and + 0.04. In the case of Pakse, the gauge section (Figure 3.2-2) is of near rectangular form for a wide range of median discharges such that the wetted width is practically constant. In the case of Channoy although the section is less regular (Figure 3.3-6) it also has a near-rectangular form for a range of median discharges such that the exponent is small (although always positive) and not significantly different to zero.

8.3 The in-channel hydraulic nature and riparian hydraulic roughness at each cross-section along the river network

In a bedrock-confined anabranching network, the use of hydraulic roughness (Manning's *n*) coefficients obtained from tabulated data in texts and guidelines is

incorrect and, therefore, leads to poor estimation of the modelled hydraulic characteristics along a river network (Heritage *et al.*, 2004). With the application of a single Manning's *n* value for the whole river reach, the modelled wetted-section locally under or over estimates the measured stage (Schumann *et al.*, 2007). In addition, the Manning's *n* at one cross-section throughout one channel could be significantly different from that of the neighbour due to relatively extreme variations in the channel geometry (Kale *et al.*, 1996; Wohl, 1999), such as narrow and broad sections and bedrock rapids as well as variation in spill resistance due to structural control. Therefore, the assumption of a single Manning's *n* coefficient or a 'smooth' variation in the Manning's *n* values along the channel (as is commonly applied when modelling alluvial rivers; *e.g.* Huang and Lee, 2009) in a bedrock confined river network is not realistic. In fact, this was reflected by the findings of this study; the calculated Manning's *n* coefficient at a given cross-section could be significantly different from that of the neighbours (Chapter 6, section 6.2.3 and section 6.2.4) and the modelled geometrical aspects along the upstream river network was highly complex (Chapter 6, section 6.7). In addition, the assumption that the hydraulic roughness along the river network was stable over a full range of flood discharge was valid (Chapter 6, section 6.7). Moreover, the hydraulic roughness along the floodplain of a large river network has no significant impact on the modelled water surface elevation because most of the discharge going through a cross-section was routed in the main channel rather than the floodplain in the flood discharge scenarios. However, in this study, the hydraulic roughness of the riparian zone had a strong impact on the mean riparian velocity, which might lead to modification of the geomorphology of the floodplain as well as minor influences on the in-channel velocity.

8.3.1 In-channel hydraulic nature

In alluvial river networks, there are 'smooth' transitions in channel geometry including bifurcations and confluences (Schumm, 1971) and, therefore, the splitting discharge ratio at bifurcations is often quite symmetric and remains stable over a range of discharges (Frings and Kleinhans, 2008). However, this was not the case in the bedrock-confined network modelled in this study; in fact, according to the acute angle (Kale *et al.*, 1996; Tooth and Nanson, 1999, 2000; Whipple *et al.*, 2000), the splitting discharge ratio at a bifurcation in the low discharge scenario was highly

asymmetric. With an increase of discharge, the ratio of discharge tends to be symmetric at all bifurcations in the river network.

Although it is assumed that the ratio of the splitting discharge at a bifurcation was equal to the ratio of first cross-sectional areas of the channels downstream of the bifurcation in each channel, the splitting discharge so obtained is just the initial condition to calculate the hydraulic roughness (Manning's *n*) coefficient at each cross-section and to initiate the HEC-RAS model. The splitting discharge was subsequently adjusted automatically in HEC-RAS to minimize any drop or rise of the modelled water surface profile at each bifurcation. The differences between the initial discharge based on the above assumption, and the discharge adjusted in HEC-RAS are presented in Chapter 6, section 6.7 for the upstream river network and in Chapter 7, section 7.2, 7.3 and 7.4 for the downstream river network for the low discharge, average and high flood discharge, respectively. These differences were highest in the low discharge model while in the flood discharge models, the differences were significantly decreased. Furthermore, in the low discharge model the bifurcating angle has a stronger impact on splitting the entry discharge than in the flood discharge.

According to the approach applied in this study to calculate the Manning's *n* coefficient at each cross-section along the river network (Chapter 4, section 4.5), the water surface slope along channels need to be predefined. Therefore, the calculated Manning's *n* coefficient could be 'biased' due to the pre-defined water surface slope. However, the trend of the Manning's *n* coefficient along the upstream river network was found in the Optimization Algorithm (OpA) as well (Chapter 8, section 8.5). The higher calculated Manning's *n* along Channel 4 and Channel 5 might reflect the existence of the bedrock outcrops.

Among other hydraulic parameters, the water surface slope is not appropriate to classify the channel patterns of mega river networks (Latrubesse, 2008). In fact, there is a wide range of water surface slopes in different alluvial anabranching networks; the water surface slope is less than 5.0×10^{-3} mm^{-1} (Knighton, 1998) or ranges from 9.5×10^{-5} mm^{-1} to 2.5×10^{-2} mm^{-1} for the Australian anabranching network described by Nanson and Knighton (1996) and from 2.0×10^{-5} mm^{-1} to 3.9×10^{-3} mm^{-1} for several abranching networks located in different climatic settings described by Makeske (2001); from 1.4×10^{-2} mm^{-1} to 2.0×10^{-4} mm^{-1} for the mixed bedrock-alluvial anabranching rivers (Tooth and McCathy, 2004) and from 1.6×10^{-5} mm^{-1} to

1.5 x 10^{-4} mm^{-1} for large abranching networks (Latrubesse, 2008). These values contrast with the general higher values (from 4.0 x 10^{-1} mm^{-1} to 2.0 x 10^{-3} mm^{-1}) obtained in modelling a glacial outburst flood through a bedrock-confined anabranching network (Carrivick, 2009). In general, the water surface slope along the upstream river network was quite low, which is within the described range of Knighton (1998) for alluvial anabranching networks and Latrubesse (2008) for large river networks at the global scale. In addition, due to the impact of the bedrock-constraint leading to differences in the cross-sectional areas between the neighboured cross-sections, the local water surface slopes at different segments along a channel were significantly different from others, especially during the low discharge. The findings were supported by Tooth and McCarthy (2004).

8.3.2 Floodplain hydraulic roughness

Even though the floodplain hydraulic roughness generally is considered to be one of the key elements of hydrodynamic modelling during a period of overbank discharge (Fathi-Maghadam and Kouwen, 1997; Huthoff *et al.*, 2006; Thomas and Nisbet, 2007; Straatsma and Baptist, 2008; Yagci and Kabdasli, 2008), in the application of the steady 1D hydraulic model for the large river network modelled in this study, the floodplain hydraulic roughness coefficient does not have any significant influence on the modelled water surface elevation, but the mean riparian velocity is affected. In fact, in this study, most of the entry discharge was routed along the main channel which is similar to what was found by Latrubesse (2008) – the small inundated area along the anabranching river network and the low mean velocity on the floodplain compared with the mean in-channel velocity; the discharge entering the floodplain area was insignificant compared to the total discharge entering an individual cross-section. Such results confirm that the application of HEC-RAS for the study river network is acceptable due to the main assumption of the HEC-RAS model (*i.e.* horizontal exchange between channels and floodplains are insignificant (Brunner, 2006)). In fact, the discharge entering the left and right riparian zone had maximum values of 1.74 % and 5.85 % of the total discharge at a cross-section (Chapter 6, section 6.5.1 and section 6.5.2). In addition, the calculated water surface elevation at each cross-section did not change significantly under different scenarios of land cover pattern along the floodplain in the study area (for example, Chapter 7, section 7.32

and section 7.4.2), despite different hydraulic roughness values of the different land cover types.

In this study, the mean in-channel velocity was much greater than the mean riparian velocity, which does not agree with the results found by Wyzga (1999). Wyzga (1999) measured the mean in-channel and riparian velocity in a small channel (maximum channel width about 70 m) with a wide floodplain (in comparison to the channel width) during the flooding period for three cross-sections. Wyzga (1999) found that at the highest discharge, maximum ratios between the floodplain and in-channel velocity at the three cross-sections were about 22.3 %, 64.6 % and 52.3 %. Even though the mean riparian velocity measured by Wyzga (1999) was much higher than those in the Siphandone wetlands, the differences between the planimetric wetted-area in the floodplain compared to that in the main channel might be a reasonable explanation; in fact, the proportion of planimetric wetted-area in the floodplain compared to that of the in-channel in the study area was much smaller than that of the river described by Wyzga (1999).

Knight and Brown (2001) conducted a flume study on the influence of the floodplain hydraulic roughness on the mean floodplain and in-channel velocity. They confirmed that with a rough floodplain, the mean in-channel velocity was from 0.40 ms^{-1} to 0.78 ms^{-1} while the mean riparian velocity was from 0.25 ms^{-1} to 0.48 ms^{-1}. However, in a 'smooth' floodplain, the differences between the two mean velocities were not significantly different and the majority of the measured velocities both of the in-channel and floodplain ranged from 0.60 ms^{-1} to 0.80 ms^{-1}. The latter situation was not found in the present study because in the Knight and Brown study, the floodplain was relatively wide (approximately 1.5 times wider than the channel cross-section) in comparison to that of this study. However, the river network in this study has narrow riparian zone and a large proportion of the entry discharge was routed along the channel but not the riparian zone.

Knighton and Nanson (2002) presented in-channel and floodplain velocities of four locations along an alluvial anabranching network in Australia. They found that the mean velocity of a cross-section increases with discharge; the mean overbank velocity ranged from 0.02 ms^{-1} to 0.55 ms^{-1} while the mean in-channel velocity ranged from 0.51 ms^{-1} to 1.37 ms^{-1}. Along the Siphandone river network, the highest riparian velocity corresponding to the average and high flood discharge was 0.12 ms^{-1} and 0.3

ms^{-1}, respectively. In fact, the findings in this study agree with what was found by Knighton and Nanson (2002).

In conclusion, the assigned hydraulic roughness coefficient of the floodplain in this study is not a driving factor to estimate the flooding pattern along the river network in the flooding scenarios. However, if the geomorphological changes of the riparian zone were the objective of a study, a 2D or 3D hydraulic model needs to be developed and the hydraulic roughness value along the riparian zone should be strongly calibrated in order to deal with the complex hydraulic nature in the riparian zone, particularly the area of interaction between the main channel and floodplain (Knight and Shiono, 1996). In fact, a suggestion is to measure the flow velocity on the riparian zone during a flood event in order to be able to accurately calibrate the hydraulic roughness of the riparian zone for a better understanding of the hydraulic roughness caused by land cover and other geomorphological features (*e.g.* natural obstacles, irregularity of the land surface) in the floodplain area.

8.4 The application of a steady 1D hydraulic model for a large bedrock-confined river network with limited input data

The findings from this study show that, with limited input data (measured bathymetry, boundary conditions), the energy approach of a steady 1D hydraulic model could be used to understand the mean hydraulic nature at each cross-section along the river network and, therefore, the flooding pattern could also be modelled. There were different ways to overcome the problem of lack of input data. In this study, a pseudo-bathymetry was developed for the downstream river network by interpolating a SPOT image. Together with the assumption of the splitting discharge at each bifurcation according to the first cross-sectional area of the first cross-section of the downstream channels, the application of the *Flow Optimization* function in HEC-RAS was applied to model the river network with acceptable results (no rise and/or drop of the modelled water surface profile at each bifurcation and the modelled stages met the recorded ones). The water surface slope along the channels without any gauged data was interpolated according to the top-width extracted from a SPOT image and from the available DEM. However, with the lack of the input data (*i.e.* the rating curve at each cross-section of each individual channel within the river network), the unsteady 1D hydraulic model could not be applied for the river network.

Apart from the lack of the boundary condition for the hydraulic modelling, another limitation of the study is that the available DEM was not validated in the field. The errors in the planform of the river network might lead to too high or too low calculated Manning's *n* coefficient at each cross-section along the river network. It is suggested to validate the DEM before applying it for the HEC-RAS models. In addition, in contrast to alluvial rivers which are free to adjust their dimension, shape, pattern and gradient in response to hydraulic change (Schumm, 1971), the bedrock-confined river networks have less freedom to adjust their geomorphological features and therefore, abrupt changes in the channel planform (Kale *et al.*, 1996; Wohl, 1999) and acute angles at the bifurcations occur (Tooth and Nanson, 1999, 2000; Whipple *et al.*, 2000). These features could be found along the downstream river network in Siphandone and were a great challenge in modelling the network. However, with the assumption of the ratio of splitting discharge at each bifurcation together with the application of the *Flow Optimization* in HEC-RAS, the modelling results of the river network were acceptable (there was no rise and/or drop of water surface profile at each bifurcation and the upstream and downstream boundary conditions were met) in the case of the limited input data. Further improvement of this study might be made by doing a field-survey to validate the splitting discharge at each bifurcation.

In this study, only the energy approach was applied in the hydraulic model but not the momentum approach. In fact, in the momentum approach, the split of discharge at each bifurcation was based on the angles between the upstream channel and the downstream channels, and the cross-sectional areas of the first downstream cross-sections. The former could be measured according to the planform of the river network; however, the latter could be estimated only in the downstream river network where the pseudo-bathymetry was applied. In addition, the momentum calculation is mainly utilized in situations where the water surface profile is varied rapidly (Bruner, 2006) (*i.e.* significantly non-uniform; including hydraulic jumps or drops with sudden significant changes in the hydraulic radius of the flow). Such an approach requires a well-defined bathymetry because it considers the depth from the water surface to the centroid of each cross-section which could not be well reflected in the pseudo-bathymetry. In fact, when the momentum approach was applied, there were significant drops and rises at each junction along the river network which could not be validated from the real nature of the flows.

In addition, in order to reject the application of the energy approach, the modelled water surface must pass through the critical depth (Bruner, 2006); however, this feature was not found in the results of the modelled upstream and full river network and therefore the application of the energy approach was validated. Furthermore, because the flow in the Siphandone river network is subcritical ($Fr << 1$) (Chapter 6, section 6.4.1, 6.6.1. and 6.6.2 and Chapter 7, section 7.1, 7.2 and 7.3), for the range of flows modelled, the energy approach could be applied due to the insignificant influence of the junction flow angles.

8.4.1 Lack of sufficient bathymetry along the river network and calibrating data for the hydraulic model

Significant issues addressed within this study are the lack of the measured bathymetry of the downstream river network and calibrating data. The available Hydrographic Atlas, with little information on the land surface elevations, mainly contains the elevations of the areas nearby the channel-banks and the bathymetry of the upstream river network; therefore, such data alone could not be used to generate the geometry of a cross-section including the channel and floodplains in the HEC-RAS model. The SRTM was used to develop the geometry of the floodplain instead. However, the SRTM contains local error of ±10 m in the elevation of the land surface (Patro *et al.*, 2009), which might lead to error in the modelled flooding extent. Even though the modelled WSE was validated according to the recorded stage at the stage gauges at Channoy and Hatxaykhoun, there was no available information for validating the spatial extent of the flood and interviews with local people proved inconclusive. In fact, only the SPOT image taken during the low discharge was available to calibrate and validate the hydraulic model but there was none during the flooding period; if in time there is any other available data which could be used to confirm the modelled flooding results, the model could be validated more thoroughly.

To overcome the problem of lack of bathymetry in the downstream river network, the pseudo-bathymetry was created. The pseudo-bathymetry was developed based on the reflectance from the SPOT image and consideration of the geomorphological features described in Brambati and Carulli (2001). Even though the developed pseudo-bathymetry did not reflect the actual channel bed elevation, the differences between the cross-sectional areas extracted from the measured and pseudo-bathymetry along the upstream river network were not of such significance (Chapter 6, section 6.8).

This result is largely because, in a 1D hydraulic model with the energy approach application, the cross-sectional area is more important than the cross-sectional shape. In addition, the ranges of the Manning's *n* along the downstream river in all levels of modelled discharge were within the range of those derived in the upstream river network. In fact, one of the main aims of this study was not to understand in detail the differences of the hydraulic nature at each cross-section along the downstream river network but rather to understand the mean hydraulic parameters at each cross-section and define the wetted-width of channels at different discharges. The model of the upstream river network achieved this rigorously whilst the pseudo-bathymetry allowed the downstream river network to be assessed more generally and, thus, met the objective of the study.

For the upstream river network, to model Channel 4 and 5 with the lack of the downstream boundary conditions, for the low discharge simulation, the water surface elevation at the end of Channel 5 was estimated based on the wetted-width extracted from the SPOT image and the available DEM for the cross-sectional shape extraction. For the flooding scenario, the assumption of similar water surface slope over the whole river network in the flooding simulation was given. The full river network was calibrated according to: (i) the modelled WSE and the entry discharge into each channel within the upstream river network; and, (ii) the wetted-width at each cross-section along the full river network in the case of the low discharge model.

Even though it was not possible to validate the land cover maps created from the SPOT images taken in 2003 and 2005 by field work, the set of a simplified land cover map created by the MRC in 2003 (Chapter 4, section 4.2.1) and a standard approach applied to interpolate the land cover maps in ENVI, the new maps interpolated from the SPOT images were considered to be acceptable (Chapter 6, section 6.1.1). In addition, because a large proportion of the entry discharge at a cross-section was routed mainly in the channel, the hydraulic roughness (mainly controlled by the land cover type) along the floodplain areas did not have a strong impact on the hydraulic modelling results (Chapter 8, section 8.3.2).

8.4.2 Splitting discharge at each bifurcation

The ratio of the splitting discharge was calculated based on the ratio of the cross-sectional areas of the first cross-section of each downstream channel. Even though the

applied ratio of splitting discharge was useful to set an initial condition for modelling the river network without any measured data on the entry discharge at each downstream channel, the splitting discharge based on the ratio of the cross-sectional area might not be thoroughly correct. Makaske *et al.* (2009) observed that the ratio of splitting discharge at a bifurcation (along the alluvial anabranching network in Canada) was not equal to that of the cross-sectional area. They found that, at the bankfull discharge along the upper Columbia River, at a bifurcation within the river network, the ratio of cross-sectional area between the side and main channel was 0.065 while the ratio of splitting discharge between the side and main channel was 0.012. However, in the case of lack of input data, the ratio of splitting discharge at each bifurcation according to the ratio of the cross-sectional area was useful and in fact it is just an initial condition before the *Flow Optimization* option in HEC-RAS was applied. The *Flow Optimization* option in HEC-RAS calculates the water surface profile along the river network according to the initial assigned discharge at each channel and then adjusts the initial condition of the splitting discharge at each bifurcation to eliminate any rise and/or drop of the water surface at each junction. In addition, based on the modelled hydraulic nature, the discharge entering each individual channel was confirmed to be acceptable via the modelled hydraulic parameters along the river network.

The ratio of the top-width of the first cross-sections after a bifurcation was applied to identify the ratio of the splitting discharge. However, the application of such a ratio to set the initial condition of the entry discharges within the HEC-RAS model was not perfect (*i.e.* there were a rise and/or drop at some bifurcations along the river network). The modelling problem might be caused by the bedrock-constrained nature of the river network; in fact, with the bedrock-constraints, the width of channels could not be freely adjusted during the intermediate discharges but the adjustment occurs mainly in the depth (Knighton, 1998; Hartshorn *et al.*, 2002).

8.4.3 The water surface slope along the river network

The assumption of water surface slope along Channel 4 and Channel 5 similar to that along Channel 2 and Channel 3 in the flood discharge scenario requires further examination and validation. In fact, based on the pre-calculated Manning's *n* (by using the Winxspro program) along Channel 4 and 5, the calculated water surface slopes (in HEC-RAS) in both low and high discharge were quite similar. Due to the

assumption of similar water surface slope along the river network in the flooding scenario, there is no clue to reject the result of the models. Apart from the validated findings along the upstream river network model (by comparing the wetted-section at each cross-section modelled by HEC-RAS and extracted from the SPOT image in the low discharge scenario and referring to the recorded stages at Channoy and Hatxaykhoun), the full network model was also validated according to the wetted-width at each cross-section and the WSE along the upstream river network created in both models (upstream and full river network models) similarly was found.

8.4.4 Particular issues related to the application of 1D hydraulic modelling for a bedrock-confined river network

The 1D hydraulic model has a long tradition of application, especially to understand the hydraulic nature of a large river (Pappenberger, 2005; Shahrokhnia and Javan, 2005, 2007; Mosquera-Machado and Ahmad, 2007; Remo and Pinter, 2007; Roberts *et al.*, 2007; Thompson *et al.*, 2007; Patro *et al.*, 2009). However, to understand the hydraulics of a river network with more than one outlet section is still a great challenge, especially in the case of lack of boundary conditions and geometry of the river network. In addition, due to the impact of bedrock-control, the nature of the bedrock-confined river network is more complex (*e.g.* the fluctuation of the hydraulic roughness coefficient from one cross-section to the neighbours and acute angle between the upstream and downstream channels at each junction) and, therefore, is a great challenge to be modelled.

The energy approach of the steady 1D hydraulic model is suitable to study the general hydraulic nature of a large river network with a lack of input data like the in-channel geometry Together with the assumption that the ratio of the splitting discharge at each bifurcation is equal to the ratio of the first cross-sectional areas of the downstream channels, the model is able to deal with the lack of the entry discharge into each individual channel of the river network. Even though there are deep pools in the downstream river network, such pools are local and therefore would not have significant impacts on the modelled water surface profiles. The applied 1D hydraulic model did not deal with the unsteady flow of a flood wave (as has been considered for a bedrock-confined channel by Carrivick, 2006); however, it would be possible to develop an unsteady 1D hydraulic model if the entry discharge of each individual

channel of the river network could be assumed and validated over the full range of the annual hydrograph. In fact, the study provided a brief description of the splitting discharge at three entry discharges, which could be further developed for the whole range of the annual hydrograph if there are enough data for calibrating and validating the hydraulic models. In addition, to consider the local variation in the hydraulic conditions would require additional field data primarily for validation.

One of the well-known limitations of 1D hydraulic models is that such models could not be used to model the detailed hydraulics of complex river systems such as anabranching rivers (Merwade *et al.*, 2008), due to its numerical-computation simplicity. This study based on the steady 1D hydraulic model has in fact helped to identify the general hydraulic nature along a complex river network at a certain level of the entry discharges and is a strong base for a more comprehensive hydraulic model (*e.g.* unsteady 1D hydraulic model) to provide greater understanding of the river network.

8.5 Other possibilities to model a complex bedrock-confined river network

The results of the flooding patterns modelled according to the HEC-RAS models and the tilted-DEM agree with each other quite well; even with the high flood discharge, the modelled overland flooding extents from the two types of modelling were not large. It confirms that the tilted-DEM approach is useful in terms of determining the likely extent of the flooded area along a river network where preliminary data on the flooding extent are not available.

Hydraulic roughness is one of the main sources of error in hydraulic calculations (Lopez *et al.*, 1998). To adjust the roughness coefficient is normally time-consuming according to the experience of the modeller (Visser *et al.*, 2001). Even though Ramesh *et al.* (2000) used the 1D shallow water flow equations and the OpA to estimate the hydraulic roughness of a network with a confluence, they modelled a channel network with only one exit channel. In addition, the hydraulic roughness achieved from their OpA is a single value for each channel. In general, the model developed by Ramesh *et al.* (2000) worked well for a uniform channel bed (simple flume experiment) but is not suitable in the case of a bedrock-confined river network with a high variation of the cross-sectional area at each cross-section along a channel. In this study, an OpA was developed in Microsoft Excel and was used separately from

the HEC-RAS model. The *Solver* function in Microsoft Excel was applied and the objective function was to minimize the summation of differences in the simulated top-width at each cross-section achieved in the HEC-RAS model and that extracted from SPOT image. The changing parameter of the OpA was the Manning's *n* coefficient at each cross-section. The application of the OpA showed that the calculated Manning's *n* coefficient at each cross-section along channel 4 and 5 was generally higher than that in Channel 2 and 3. However, the OpA model was sensitive according to the water surface slope which was calculated separately in HEC-RAS. In fact, the OpA used the water surface slope results in the HEC-RAS model and after each run of the OpA, the Manning's *n* coefficient at each cross-section was changed and resulted in changes to the water surface slope in the HEC-RAS model. Thus the OpA developed within this present study was no better than using the optimization routine within HEC-RAS with the combination of the geometry analysis at each cross-section and was abandoned. However, with more recorded stages at different cross-section along the river network and the wetted-section extracted from the SPOT image, the OpA could be improved and applied for later research.

8.6 The implication of channel regulation and climate change on geomorphological processes

This study specifically set out to take a cautious approach and apply only a steady 1D hydraulic model to a complex river system. The philosophy has been that the greater understanding of the system obtained with the HEC-RAS model could then inform an improved field sampling regime to develop better models related to specific environmental issues usually applied at more local levels. These latter models would thus be 'embedded' within the larger picture delineated by the 1D model. The issue of sediment transport within the Mekong is a crucial issue with respect to ecological integrity, channel stability and indeed for the future function of the Mekong Delta in the light of the plans to build cascades of dams not only on the tributaries but also along the main stem. Fu *et al.* (2008) studied the impact of dams on the sediment loads along the UMB and they found that the dams have trapped a large amount of sediment from upstream and caused different impacts on the downstream channels (decrease sediment transport at different scales in different locations). Even though the dams have not changed the regime of monthly mean discharge, the seasonal water

storage changes the original hydraulic conditions of the river leading to changes in sediment transport dynamics (Fu *et al.*, 2008).

There are currently no detailed studies of the Mekong sediment transport regime. An intriguing issue is that much of the bed material throughout the system is fine sand and silt, coarse sand and gravel being in short supply. This fine material is readily entrained into suspension by the annual hydrograph. However, there is no information on the sediment size as well as sediment load in the Siphandone wetlands; although it has been estimated that around 160 million tonnes of suspended sediment pass the Pakse gauge each year (Walling, 2005, 2008). The fate of this sediment within the complex Siphandone river network is unknown; however, a similar load has been estimated at Stung Treng (Harden and Sundbord, 1992) immediately to the south of Siphandone, indicating a constant flux through the study area. An intriguing question is why some of the minor channels have not become filled with alluvium. Consequently, as an indicator of a future research direction, the initial motion criteria (Shields parameter *versus* particle Reynolds number) briefly has been considered to get some general ideas of the potential conditions related to the sustained sediment flux through Siphandone. Because there was no available information on the sediment size at the Channoy section, the sediment size and hydraulic data at Pakse were used instead. Due to the lack of the hydrograph in the downstream channels along the river network, conditions within the modelled reach were considered for Channoy alone.

Figure 8.6-1 and Figure 8.6-2 present the calculated Shields parameter *versus* the particle Reynolds number in Pakse and Channoy, respectively. The figures were plotted with different values of the sediment size from 7.50×10^{-5} to 4.75×10^{-3} m measured at Pakse (Unpublished data of Yamanashi University). It could be seen that the range of calculated Shields parameters at Pakse was significantly lower than that at Channoy. For the sediment size of 4.75×10^{-3} m, the sediment could be transported as bedload only by discharges in excess of about 5,600 m^3s^{-1} at Pakse (about more than 52 % of the flow duration curve; Chapter 3) while at Channoy all the sediment was transported at all level of the recorded discharge. In addition, at Pakse, the sediment finer than 4.25×10^{-4} m would be suspended by the discharge greater than 3,800 m^3s^{-1} (about more than 62 % of the flow duration curve; Chapter 3). At Channoy, at all discharges, sediment finer than 4.25×10^{-4} m was suspended while sediment larger than 4.25×10^{-4} m could be transported as bedload. Thus, sediment

transport should be more prevalent at Channoy than Pakse and there is a greater propensity for suspension transport at Channoy. By applying an identical sediment size range to calculate the Shields parameter and the Particle Reynolds number at Pakse and Channoy for different upstream discharges, it could be concluded that one of the major factors contributing to the lower sufficient ability for sediment transport at Pakse is the water surface slope. The mean water surface slope along each channel in Siphandone and at Pakse against the entry discharge of each channel is presented in Figure 8.6-3; it could be seen that the upstream network where the channels could be classified as meandering had higher water surface slope than that from Pakse to Channoy for all levels of discharge. However, along the downstream river network where the anabranching pattern could be found, the water surface slope at each channel was smaller than that in the upstream river network and that from Pakse to Channoy. The findings agree with Knighton (1998) who concludes that the water surface slope along the anabranching network is lower than that along the meandering channel. According to Jansen and Nanson (2004), the anabranching network exhibits large sediment transporting capacity per unit available stream power, which could explain why the channels within the downstream river network are still active.

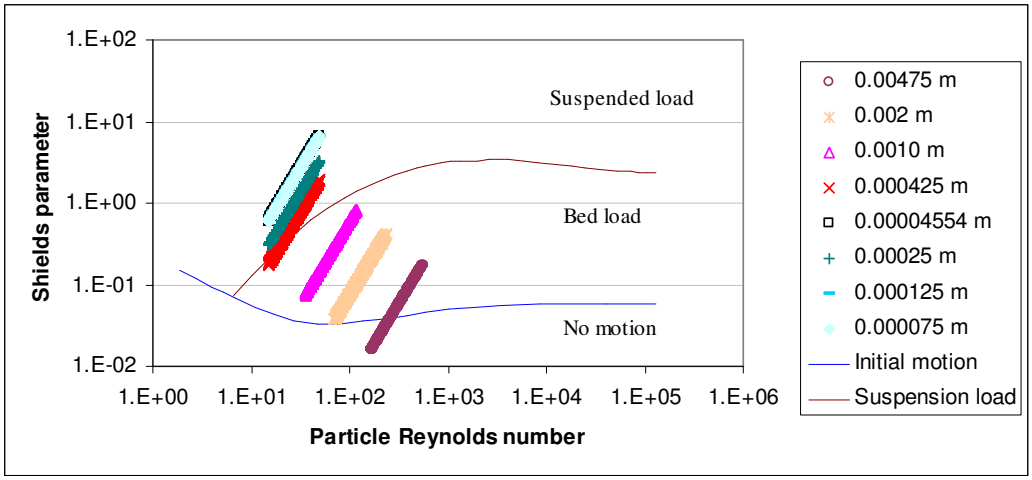

Figure 8.6-1: Shields diagram at Pakse

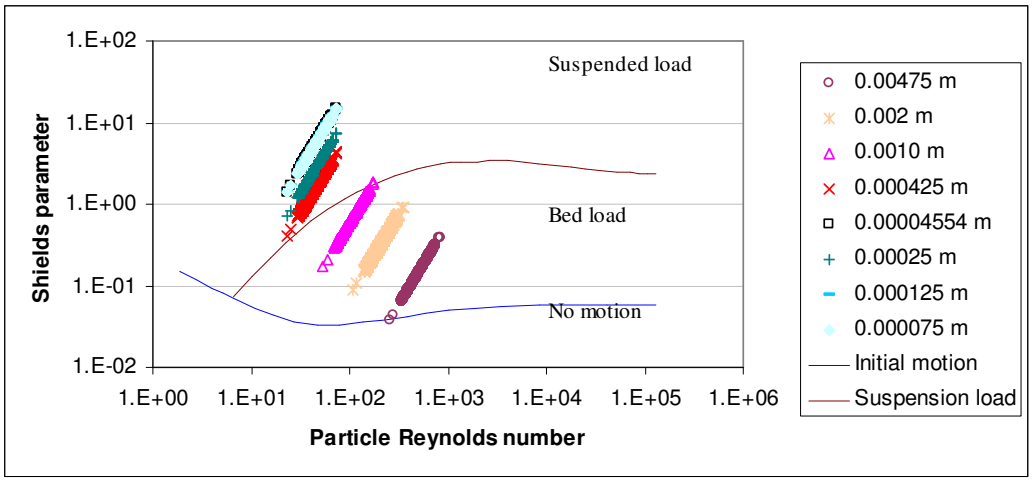

Figure 8.6-2: Shields diagram at Channoy

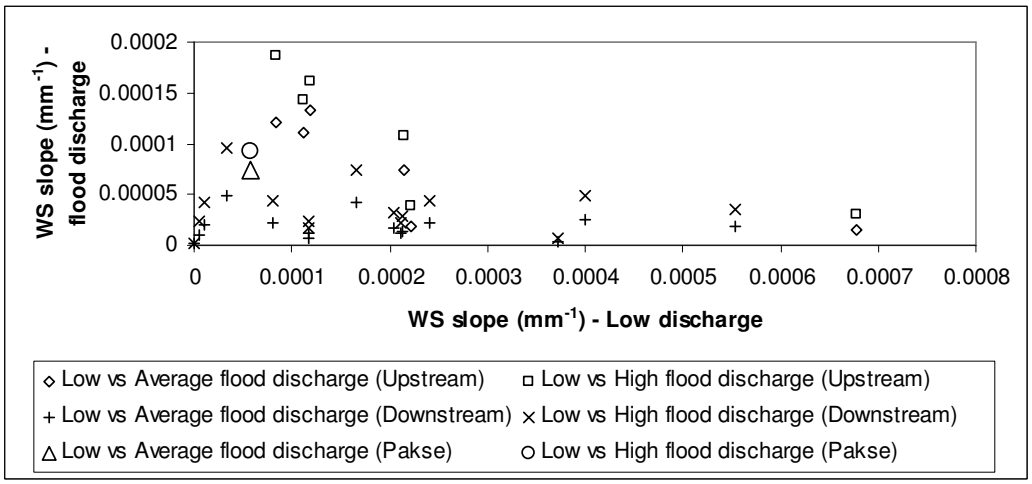

Figure 8.6-3: Water surface slope from Pakse to Channoy and along the Siphandone river network; Notes: WS – Water surface.

In addition, climate change is going to change the hydrological features of the watershed along the Mekong River leading to changes of discharge entering the Mekong from different tributaries. By the change of discharge at each segment, the hydraulic nature of the channels would be changed which requires further study on the impact of climate change on the geomorphological nature of the Siphandone wetlands. In fact, the recent meeting organized by the WWF (September, 2009) focused on the impact of climate change on the livelihood of the local people with great attention to the changes of hydraulic characteristics, including sediment load, of the river network.

The International Rivers Organization is currently focusing on the sediment load in the river network in the Siphandone wetlands and actually want to develop a

benchmark on the current conditions of the hydraulic nature and sediment load and to provide a brief scientific report on the future changes in hydraulic nature and sediment load if several dams within the area are built. In fact, the Don Sahong dam located in the south of the Siphandone wetland is proposed to be built and it is projected to cause great disturbance for the local and regional environment in terms of hydraulic nature, sediment transport, and other severe ecological and socio-economical impacts.

8.7 Suggesting future work

The main aims of the study were to (i) estimate the wetted-section along the river network based on the recorded discharges at the Pakse gauging station and the recorded stages at Channoy and Hatxaykhoun stage gauges; and, (ii) model the hydraulic parameters along the complex bedrock-confined river network within the Siphandone wetlands. Therefore, the steady flow analysis in the HEC-RAS model was used but not the unsteady flow analysis. However, to better understand the impact of flow regulation and climate change on the study area, it is important to develop the unsteady flow hydraulic model based on what was examined in this study (*i.e.* the splitting discharge at each bifurcation, the boundary conditions, pseudo-bathymetry). In fact, due to climate change, the annual hydrograph might be strongly affected and changed.

The interpolated pseudo-bathymetry could be applied in a 1D hydraulic model with the application of the energy approach. However, it is necessary to have a further study on the interpolation of the pseudo-bathymetry based on the SPOT images and data for calibrating and validating the approach is essentially required. With a better pseudo-bathymetry, the detailed hydraulic nature of the river network could be studied.

Due to lack of sediment data in the study area, the sediment transport model in HEC-RAS was not considered. Even if the sediment data collected in Pakse could be used to model the sediment transport in Siphandone, detailed rating curves at each individual channel within the river network are not available and, therefore, the sediment transport could not be modelled (for each individual channel). However, a sediment transport simulation would provide greater understanding of the river network; for example: (i) Why the river remains multi-channel rather than blocking minor channels with sediment and increasing the transport efficiency of the main

channels? (ii) What is happening if the river network change is driven by climate change?

For greater understanding on the changing of the annual hydrograph of the river network over time, it is important to investigate the hydrological nature of the watershed. In fact, an integrated hydrological and hydraulic study is suggested to increase understanding of the complex natural system and projecting the future changes in the global climate change context. Even though a sensitivity analysis was partly done in this study (changes of the modelled water surface profiles according to different sets of the Manning's *n* coefficient along the river network; Chapter 6, section 6.3.2), the sensitivity of the hydraulic model based on different boundary conditions needs to be more thoroughly examined. In addition, to increase understanding of the hydraulic model results, further analysis on uncertainty of the models need to be investigated.

One of the findings of the study was that the riparian hydraulic roughness did not have significant impact on the spatial flooding extent; however, the changes of the land cover leading to changes of the hydraulic roughness along the floodplain might have a strong impact on the period of the flood (Anderson *et al.*, 2006) due to the changes of the mean velocity in the floodplain (Chapter 6, section 6.6). To increase understanding of the influence of the hydraulic roughness in the floodplain on the timing and magnitude of the flood, an unsteady 1D flow analysis is suggested; however, the great challenge for building such an unsteady 1D flow model is that the rating curve at each single channel within the network must be available or should be able to be calculated. In addition, a 2D hydraulic model is suggested for the measured bathymetry channels of the Siphandone river network in order to make a comprehensive sediment transport model for detailed understanding of the sediment transport pattern in a complex river network in the context of the increasing impacts due to global climate change and anthropogenic activities.

Even though the classification of an anabranching network proposed by Nanson and Knighton (1996) has been applied to classify different categories of the anabranching network, such a classification has been applied only to alluvial networks. In fact, Tooth and McCarthy (2004) did research on understanding the geomorphological nature of a mixed bedrock-alluvial network but did not put the river network into any category suggested by Nanson and Knighton (1996); therefore, it is necessary to

conduct a more detailed study on the geomorphological, hydraulics and sediment transport along the bedrock-confined river network to suggest a suitable category other than the Nanson and Knighton (1996) classification.

Daconti (2001) concluded that there was significant bank erosion along the Siphandone wetlands; however, the channel planform in a single-thread bedrock-confined channel is stable (Richardson and Carling, 2005) and the planform of anabranching alluvial networks is quite stable as well (Schumm, 1985, Wang *et al.*, 2005). In addition, from the fieldtrip observation in the Siphandone wetlands, there was rare bank protection in the study area and little evidence of significant bankline recession. According to Meshkova (2009, *per. com.*), there is no significant bank erosion along the Mekong between Stung Treng and Kratie where a similar bedrock-confined anabranching network is found. In fact, there should be another study to investigate the geomorphological changes with specific focus on the bank erosion issue in the Siphandone wetlands.

In this study, considerable effort was given to exploring and applying a reduced complexity (raster-based) model (CAESAR – Cellular Automaton Evolutionary Slope And River) to route discharge along the river network. The idea was that such a model might be applied well in a situation with limited input data and where the main objective would be to determine the water levels and hence the flooding extents. However, the obtained results of the approaches have not been reported herein due to the lack of robust results.

Even though the CAESAR model is based on simple rules to route discharge downstream and it could not accurately simulate any hydraulic parameters within a channel network, it is expected that it would be able to simulate the wetted-section along a river network with limited input data, especially in the case of the application of the pseudo-bathymetry and no entry discharge data for most of the channels within the network. However, in the Siphandone river network, even when the Manning's n along the river network was calibrated according to the calculated Manning's n at Pakse, the wetted-section was not well simulated (*i.e.* the water surface profile significantly rose and dropped without any clear link with the geomorphological features of the channel bed or river planform). Due to the asymmetry of bifurcations especially in terms of the bifurcation angles, discharge from the upstream channel was routed mainly along the smaller angle channel downstream. In fact, CAESAR could

not correctly model the water surface elevation. However, the edited version of the CAESAR model with specific focus on adjusting the algorithm to route discharge along each downstream channel after a bifurcation might be useful to route discharge a long a large river network with input data-constrained.

Chapter 9: Conclusions

The project was developed to investigate the bulk hydraulic flow structure of a bedrock-constrained anabranching river network with more than one outlet section within the Mekong River in the Siphandone Wetlands, Laos. The main challenge of the study was to model the hydraulic variables along the complex river network within acceptable tolerances in a situation where the available data for calibrating and validating the outputs are limited. In fact, the wetted-section and flood patterns were modelled with specific attention to calibrating individual value of the in-channel hydraulic roughness at each cross-section for specific entry-section discharges. The hydraulic roughness value of each land cover pattern of the floodplain was considered and the modelled results showed that the hydraulic roughness values of the land cover pattern did not have any significant impact on the modelled stage due to a large proportion of discharge in each cross-section being routed through the channels with minimal inundation of the riparian zone during the selected overbank floods.

The study river network is a bedrock-constrained channel with an alluvial overprint. Such mixed bedrock and alluvial channels lead to the hydraulic characteristics spatially varying along the river network, with especially significant differences in the modelled hydraulic characteristics between the upstream and downstream river network. Even though there is a lack of information on the measured hydraulic parameters along the river network for validating the hydraulic models, the modelled parameters sit quite well within the range of the referenced data.

Even though the developed integrated DEM contains certain errors (estimated bathymetry along the cross-channel in the upstream network and the interpolated pseudo-bathymetry along the downstream network), the integrated DEM was a strong base to model the river network (especially in the case of lack of measured bathymetry) with acceptable errors of the modelled water surface elevations at the downstream and upstream boundary conditions and differences between the modelled wetted-section and that extracted from the SPOT image.

In fact, due to the use of the energy calculation in the 1D hydraulic model, the cross-sectional shape was less important than the cross-sectional area. In addition, despite the lack of downstream boundary conditions of one of the outlet sections, it was still possible to develop the hydraulic model and the results were acceptable when

comparing the results obtained from the better parameterised upstream river network model and the full river network model which was less well-constrained.

In the Siphandone wetlands, the significant land cover change in recent years (from 2001 and 2005) due to conversion of forest to scrub and rice paddy was identified. However, with the application of a 1D hydraulic model for a large river network where a large proportion of discharge was routed along the main channels in the flood period, the land cover change leading to the changes of the hydraulic roughness of the land surface did not have significant influence on the modelled water surface elevation. However, the changes of the land cover altered the flow velocity along the riparian area, which may cause significant changes of the geomorphological features of the floodplain area. The influence of land cover change on the flow pattern in the riparian area requires a comprehensive study to understand the nature of the overland flow and its impacts not only on the geomorphological features of the floodplain but also on the cropping calendar (caused by the flood duration) and therefore the livelihood of the local people.

The hydraulic roughness at each cross-section was calculated individually. In the bedrock-confined channel, the hydraulic roughness in one cross-section can be significantly different from the neighbours (caused by the abrupt changes of channel geometry, the local water surface slope and the presence or absence of an alluvial fill within the bedrock channel), especially in the case of the low discharge simulation; therefore, the assumption that along an alluvial channel, the same hydraulic roughness can be assigned through the model is not applicable to mixed alluvial-bedrock systems.

In order to apply a 1D hydraulic model for a river network, an initial set of entry discharge values at each individual channel within the river network needs to be identified. The results of the study confirmed that the ratio of cross-sectional areas is a rational basis for splitting discharge at a bifurcation. Even though the ratio of the splitting discharge is not perfect, with the application of the *Flow Optimization* in HEC-RAS, the splitting discharge ratio can be adjusted and identified. In addition, whereas in alluvial systems bifurcation geometry might adjust through time, within the bedrock-confined river network, for a given discharge, there was high inequality in terms of the splitting discharge at each bifurcation, especially in the case of the low

discharge. However, when discharge increased, the splitting discharge ratios tended to be more equal than in the low discharge scenario.

In conclusion, this study provides a benchmark describing the current bulk hydraulic properties of the river network. The results of the study are meaningful when global climate change and strong anthropogenic impacts are progressively occurring and projected to alter the hydraulic properties and sediment load of the river network. In addition, the study provides a strong base for a more comprehensive hydraulic model (*e.g.* unsteady 1D hydraulic model or 2D/3D hydraulic model given sufficient data are available) in order to better understand how the river network behaves temporally and spatially.

REFERENCES

1. Abbado, D., Slingerland, R., & Smith, N. D. 2005. Origin of anastomosis in the upper Columbia River, British Columbia, Canada. In M. D. Blum & S. B. Marriot & S. M. Leclair (Eds.), Fluvial Sedimentology VII, Special Publication of the International Association of Sedimentologists Vol. 35: 3-15. Oxford, UK: Blackwell.
2. Abernethy, B. & Rutherfurd, I. D. 2000. The effect of riparian tree roots on the mass-stability of riverbanks. Earth Surface Processes and Landforms, 25(9): 921-937.
3. Ackerman, C. T. 2005. HEC-GeoRAS: An extension for support of HEC-RAS using ArcGIS: U.S. Army Corps of Engineers - Hydrologic Engineering Center, HEC.
4. Alho, P., Roberts, M. J., & Käyhkö, J. 2007. Estimating the inundation area of a massive, jökulhlaup from northwest Vatnajökull, Iceland Natural Hazards, 41(1): 21-42.
5. Altobelli, A. & Daconto, G. 2001. Study of land cover in Siphandone wetlands through remote sensing and development of a wetland GIS. In G. Daconto (Ed.), Siphandone Wetlands.
6. Anderson, D. M., Overpeck J.T., Gupta A.K. 2002. Increase in the Asian southeast monsoon during the past four centuries. Science, 291(5581): 596 - 599.
7. Anderson, B. G., Rutherfurd, I. D., & Western, A. W. 2006. An analysis of the influence of riparian vegetation on the propagation of flood waves. Environmental Modelling & Software, 21(9): 1290-1296.
8. Arcement, G. J. & Schneider, V. R. 1989. Guide for Selecting Manning's Roughness Coefficients for Natural Channels and Flood Plains.
9. Aronica, G., Hankin, B., & Beven, K. 1998. Uncertainty and equifinality in calibrating distributed roughness coefficients in a flood propagation model with limited data. Advances in Water Resources, 22(4): 349-365.
10. Arora, V. K. & Boer, G. J. 2001. Effects of simulated climate change on the hydrology of major river basins. J. Geophys. Res., 106(D4): 3335–3348.
11. Ashley, G. M., Renwick, W. H., & Haag, G. H. 1988. Channel form and processes in bedrock and alluvial reaches of the Raritan River, New Jersey. Geology, 16(5): 436-439.
12. Ashmore, P. 1985. Process and Form in Gravel Braided Streams: Lab- oratory Modelling and Field Observations University of Alberta, Edmonton.
13. Baird, I. G. 1999. Fishes and Forests: Fish foods and the Importance of Seasonally Flooded Riverine Habitats for Mekong River Fish, Environmental Protection and Community Development in Siphandone Wetland Project, CESVI Cooperation and Development, Pakse, Lao PDR.

14. Baird, I. G. 2000. Aquatic Biodiversity in the Siphandone Wetlands, Environmental Protection and Community Development in Siphandone Wetland Project, CESVI Cooperation and Development, Pakse, Lao PDR.

15. Baird, I. G. 2009. The Don Sahong dam: potential impact on regional fish migrations, livelihoods and human health: University of Victoria.

16. Baker, V. R. & Kale, V. S. 1998. The role of extreme floods in shaping bedrock channels. In K. Tinkler & E. Wohl (Eds.), Rivers Over Rock: Fluvial Processes in Bedrock Channels: 153 – 165. Washington, DC: American Geophysical Union.

17. Barnes, H. H. 1967. Roughness characteristics of natural channels. United States Geological Survey Water Supply Paper, 1849.

18. Bates, P. D. & De Roo, A. P. J. 2000. A simple raster-based model for flood inundation simulation. Journal of Hydrology, 236(1-2): 54-77.

19. Bates, P. D., Dawson, R. J., Hall, J. W., Horritt, M. S., Nicholls, R. J., Wicks, J., & Hassan, M. A. A. M. 2005. Simplified two-dimensional numerical modelling of coastal flooding and example applications. Coastal Engineering, 52(9): 793-810.

20. Bates, P. D., Wilson, M. D., Horritt, M. S., Mason, D. C., Holden, N., & Currie, A. 2006. Reach scale floodplain inundation dynamics observed using airborne synthetic aperture radar imagery: Data analysis and modelling. Journal of Hydrology Measurement and Parameterization of Rainfall Microstructure, 328(1-2): 306-318.

21. Benito, G., Díez-Herrero, A., & Villalta, M. F. d. 2003. Magnitude and Frequency of Flooding in the Tagus Basin (Central Spain) over the Last Millennium. Climatic Change, 58(1): 171-192.

22. Best, J. L. & Rhoads, B. L. 2008. Sediment Transport, Bed Morphology and the Sedimentology of River Channel Confluences. In A. G. R. B. L. R. Stephen P. Rice (Ed.), River Confluences, Tributaries and the Fluvial Network: 45-72.

23. Bhaskaran, B. & Mitchell, J. F. B. 1998. Simulated changes in Southeast Asian monsoon precipitation resulting from anthropogenic emissions. International Journal of Climatology, 18(13): 1455-1462.

24. Biron, P. M. & Lane, S. N. 2008. Modelling hydraulics and sediment transport at river confluences. In S. P. Rice & A. G. Roy & B. L. Rhoads (Eds.), River confluences, tributaries and the fluvial network. West Sussex, England: John Wiley & Sons, Ltd.

25. Boruah, S., Gilvear, D., Hunter, P., & Sharma, N. 2008. Quantifying channel planform and physical habitat dynamics on a large braided river using satellite data - the Brahmaputra, India. River Research and Applications, 24(5): 650-660.

26. Bradbrook, K. F., Biron, P. M., Lane, S. N., Richards, K. S., & A. G. Roy. 1998. Investigation of controls on secondary circulation in a simple confluence geometry using a three-dimensional numerical model. Hydrological Processes, 12(8): 1371-1396.

27. Brambati, A. & Carulli, G. B. 2001. Geology, geomorphology and hydrogeology. In G. Daconto (Ed.), Siphandone Wetlands: Environmental Protection and Community Development in Siphandone Wetlands Project.

28. Bridge, J. 2003. Rivers and Floodplains - Forms, Processes and Sedimentary Record Oxford, UK Blackwell Science Ltd.

29. Brierley, G. J. & Fryirs, K. A. 2005. Geomorphology and river management: Blackwell Publising.

30. Broadhurst, L. J. & Heritage, G. L. 1998. Modelling stage-discharge relationships in anastomosed bedrock-influenced sections of the Sabie River system. Earth Surface Processes and Landforms, 23(5): 455-465.

31. Brown, A. G., Gregory, K. J., & Milton, E. J. 1987. The use of Landsat multispectral scanner data for the analysis and management of flooding on the river Severn, England. Environmental Management, 11(5): 695-701.

32. Brunner, G. W. 2002. HEC-RAS, River analysis system Hydraulic reference manual: U.S. Army Corps of Engineers - Hydrologic Engineering Center, HEC.

33. Brunner, G. W. 2006. HEC-RAS, River analysis system: U.S. Army Corps of Engineers - Hydrologic Engineering Center, HEC.

34. Cameron, D. 2007. Flow, frequency, and uncertainty estimation for an extreme historical flood event in the Highlands of Scotland, UK. Hydrological Processes, 21(11): 1460-1470.

35. Campbell, B. J. 1996. Introduction to remote sensing. New York: The Guilford Press.

36. Cao, Z. & Carling, P. A. 2002. Mathematical modelling of alluvial rivers: reality and myth. Part I: General review. Water and Maritime Engineering , ICE, 154(3): 207- 219.

37. Cao, Z. & Carling, P. A. 2002. Mathematical modelling of alluvial rivers: reality and myth. Part II: special issues. Water and Maritime Engineering , ICE, 154(4): 297- 307.

38. Carling, P. A. 1991. An appraisal of the velocity-reversal hypothesis for stable pool-riffle sequences in the river severn, England. Earth Surface Processes and Landforms, 16(1): 19-31.

39. Carling, P. A. & Grodek, T. 1994. Indirect estimation of ungauged peak discharges in a bedrock channel with reference to design discharge selection. Hydrological Processes, 8(6): 497-511.

40. Carling, P. A. & Wood, N. 1994. Simulation of flow over pool-riffle topography: A consideration of the velocity reversal hypothesis. Earth Surface Processes and Landforms, 19(4): 319-332.

41. Carling, P. 2006. The hydrology and geomorphology of bedrock rivers. Geomorphology, 82(1-2): 1-3.

42. Carling, P. A., Herget, J., Lanz, J. K., Richardson, K., & Pacifici, A. 2009. Channel-scale erosional bedforms in bedrock and in loose granular material:

character, processes and implications. In D. M. Burr & P. A. Carling & V. R. B. Baker (Eds.), Megaflooding on Earth and Mars: Cambridge University Press.

43. Carrivick, J. L., Russell, A. J., Tweed, F. S., & Twigg, D. 2004. Palaeohydrology and sedimentary impacts of jökulhlaups from Kverkfjöll, Iceland. Sedimentary Geology, 172(1-2): 19-40.

44. Carrivick, J. L. 2006. Application of 2D hydrodynamic modelling to high-magnitude outburst floods: An example from Kverkfjöll, Iceland. Journal of Hydrology, 321(1-4): 187-199.

45. Carrivick, J. L. 2009. Jokulhlaups from Kverkfjoll volcano, Iceland: modelling transient hydraulic phenomena. In D. M. Burr & P. A. Carling & V. R. Baker (Eds.), Megaflooding on earth and mars: Cambridge.

46. Casas, A., G. Benito, V.R. Thorndycraft, M. Rico,. 2006. The topographic data source of digital terrain models as a key element in the accuracy of hydraulic flood modelling. Earth Surface Processes and Landforms, 31(4): 444-456.

47. Chanson, H. 1999. The Hydraulics of Open Channel Flow: John Wiley & Sons Inc.

48. Chinvanno, S. Information for sustainable development in light of Climage Change in Mekong River Basin.

49. Chow, V. T. 1959. Open Channel Hydraulics: McGraw-Hill Book Company, Inc.

50. Chow, V. T., D.R. Maidment, L.W. Mays. 1988. Applied Hydrology: McGraw-Hill Book Company, Inc.

51. Chung, C.-J. & Fabbri, A. G. 2008. Predicting landslides for risk analysis -- Spatial models tested by a cross-validation technique. Geomorphology, 94(3-4): 438-452.

52. Conlan, I. A., Rutherfurd, I. D., Finlayson, B. L., & Western, A. W. 2008. Sediment transport through a forced pool on the Mekong River: sand dunes superimposed on a larger sediment wave? , Marine and River Dune Dynamics. Leeds, United Kingdom.

53. Costelloe, J. F., Grayson, R. B., & McMahon, T. A. 2006. Modelling streamflow in a large anastomosing river of the arid zone, Diamantina River, Australia. Journal of Hydrology, 323(1-4): 138-153.

54. Coulthard, T. J., M. J. Kirkby, M. G. Macklin. 1999. Modelling the impacts of Holocene environmental change in an upland river catchment, using a cellular automaton approach. In A. G. Brown, T. A. Quine (Ed.), Fluvial processes and environmental change: Jonh Wiley & Sons.

55. Coulthard, T. J., M. G. Macklin,. 2001. How sensitive are river systems to climate and land-use changes? A model-based evaluation. Journal of Quaternary Science, 16(4): 347-351.

56. Coulthard, T. J., M. G. Macklin, M. J. Kirkby,. 2002. A cellular model of Holocene upland river basin and alluvial fan evolution. Earth Surface Processes and Landforms, 27(3): 269-288.

57. Coulthard, T. J., J. Lewin, M.G. Macklin. 2005. Modelling differential catchment response to environmental change. Geomorphology, 69(1-4): 222-241.

58. Coulthard, T. J., M. J. Van De Wiel,. 2006. A cellular model of river meandering. Earth Surface Processes and Landforms, 31(1): 123-132.

59. Coulthard, T. J., D.N. Hicks, M.J. van de Wiel. 2007. Cellular modelling of river catchments and reaches: advantages, limitations and prospects. Geomorphology, In Press, Accepted manuscript.

60. Cowan, W. L. 1956. Estimating hydraulic roughness coefficients. Agricultural Engineering 7(7): 473- 475.

61. Daconto, G. (Ed.). 2001. Siphandone Wetlands: Environmental Protection and Community Development in Siphandone Wetlands Project.

62. Darby, S. E., van de Wiel M.J. 2003. Models in Fluvial Geomorphology. In G. M. Kondolf, H. Piégay (Ed.), Tools in Fluvial Geomorphology: 539-576.

63. Davis, W. M. 1899. The geographical cycle. Geography Journal 14: 481-504.

64. Davis, J. C. 1986. Statistics and Data Analysis in Geology (2nd ed.). New York: John Wiley & Sons.

65. Deng, Z., Ji, M., & Zhang, Z. 2008. Mapping bathymetry from multi-source remote sensing images: A case study in the Beilun estuary, Guangxi, China. Paper presented at the The International Archives of the Photogrammetry, Remote Sensing and Spatial Information Sciences. , Beijing, China.

66. Dennis, I. A., Mark G. Macklin, Tom J. Coulthard, Paul A. Brewer,. 2003. The impact of the October-November 2000 floods on contaminant metal dispersal in the River Swale catchment, North Yorkshire, UK. Hydrological Processes, 17(8): 1641-1657.

67. Deodhar, L. A. & Kale, V. S. 1999. Downstream adjustments in allochthonous rivers: Western Deccan Trap upland region, India. In A. J. Miller & A. Gupta (Eds.), Varieties of Fluvial Form. Chichester Wiley.

68. Depetris, P. J. & Gaiero, D. M. 1998. Water-surface slope, total suspended sediment and particulate organic carbon variability in the Paraná River during extreme flooding. Naturwissenschaften, 85(1): 26-28.

69. Dingman, S. L. 2007. Analytical derivation of at-a-station hydraulic-geometry relations. Journal of Hydrology, 334(1-2): 17-27.

70. Downs, P. W. & Thorne, C. R. 2000. Rehabilitation of a lowland river: Reconciling flood defence with habitat diversity and geomorphological sustainability. Journal of Environmental Management, 58(4): 249-268.

71. Ehernfeld, S. & Littauer, S. B. 1964. Introduction to statistical method: McGraw-Hill Book Company.

72. ENVI. 2008. User's Guide - The enviroment for visualizing images, 4.5 ed.: Research Systems, Inc.

73. Fathi-Maghadam, M. & Kouwen, N. 1997. Nonrigid, Nonsubmerged, Vegetative Roughness on Floodplains. Journal of Hydraulic Engineering, 123(1): 51-57.

74. Ferguson, R. I., Parsons, D. R., Lane, S. N., & Hardy, R. J. 2003. Flow in meander bends with recirculation at the inner bank. Water Resour. Res., 39.

75. Fleming, M. C. & Nellis., J. G. 2000. Principles of applied statistics : an integrated approach using MINITAB and Excel London: Thomson.

76. Formann, E., Habersack, H. M., & Schober, S. 2007. Morphodynamic river processes and techniques for assessment of channel evolution in Alpine gravel bed rivers. Geomorphology, 90(3-4): 340-355.

77. Fotherby, L. M. 2009. Valley confinement as a factor of braided river pattern for the Platte River. Geomorphology, 103(4): 562-576.

78. French, R. H. 1985. Open-Channel Hydraulics: McGraw-Hill Book Company.

79. Friedkin, J. F. 1945. A laboratory study of the meanderings of alluvial rivers. Mississippi: U.S waterways experiment station.

80. Frings, R. M. & Kleinhans, M. G. 2008. Complex variations in sediment transport at three large river bifurcations during discharge waves in the river Rhine. Sedimentology, 55(5): 1145-1171.

81. Fu, K. D., He, D. M., & Lu, X. X. 2008. Sedimentation in the Manwan reservoir in the Upper Mekong and its downstream impacts. Quaternary International, 186(1): 91-99.

82. Fuller, I. C., Large, A. R. G., & Milan, D. J. 2003. Quantifying channel development and sediment transfer following chute cutoff in a wandering gravel-bed river. Geomorphology, 54(3-4): 307-323.

83. Gao, J. 2009. Bathymetric mapping by means of remote sensing: methods, accuracy and limitations. Progress in Physical Geography, 33(1): 103-116.

84. García Díaz, R. 2005. Analysis of Manning coefficient for small-depth flows on vegetated beds. Hydrological Processes, 19(16): 3221-3233.

85. Gates, T. K. & Ahmed, S. I. 1995. Sensitivity of predicted irrigation-delivery performance to hydraulic and hydrologic uncertainty. Agricultural Water Management, 27(3-4): 267-282.

86. Gilbert, G. K. 1877. Geology of the Henry Mountains, U.S. Geographical and Geological Survey of the Rocky Mountain region: 160. Washington, D.C., U.S. : Government Printing Office.

87. Gradzinski, R., Baryla, J., Doktor, M., Gmur, D., Gradzinski, M., Kedzior, A., Paszkowski, M., Soja, R., Zielinski, T., & Zurek, S. 2003. Vegetation-controlled modern anastomosing system of the upper Narew River (NE Poland) and its sediments. Sedimentary Geology, 157(3-4): 253-276.

88. Green, J. C. 2005. Modelling flow resistance in vegetated streams: review and development of new theory. Hydrological Processes, 19(6): 1245-1259.

89. Gupta, A., Kale, V. K., & Rajanguru, S. N. 1999. The Narmada River, India, Through Space and Time. In A. J. Miller & A. Gupta (Eds.), Varieties of fluvial form: John Wiley & Sons.

90. Gupta, A., Hock, L., Xiaojing, H., & Ping, C. 2002. Evaluation of part of the Mekong River using satellite imagery. Geomorphology, 44(3-4): 221-239.

91. Gupta, A. K., D. M. Anderson, J.T. Overpeck. 2003. Abrupt changes in the Asian southwest monsoon during the Holocene and their links to the North Atlantic Ocean. 421(6921n): 354-357.

92. Gupta, A., S.C. Liew. 2007. The Mekong from satellite imagery: A quick look at a large river. Geomorphology Monsoon Rivers of Asia, 85(3-4): 259-274.

93. Harden, P. O. & Sundborg, A. 1992. The Lower Mekong Basin Suspended Sediment Transport and Sedimentation Problems: 71. Uppsala, Sweden Computer Processing and Editorial Work: AB Hydroconsult.

94. Hartshorn, K., Hovius, N., Dade, W. B., & Slingerland, R. L. 2002. Climate-Driven Bedrock Incision in an Active Mountain Belt. Science, 297(5589): 2036-2038.

95. Harvey, D. 1969. Explanation in Geography. London: Edward Arnold.

96. Harwood, K. & Brown, A. G. 1993. Fluvial processes in a forested anastomosing river: Flood partitioning and changing flow patterns. Earth Surface Processes and Landforms, 18(8): 741-748.

97. HEC-RAS. 2006. HEC-RAS: River Analysis System - Release notes: U.S. Army Corps of Engineers - Hydrologic Engineering Center, HEC.

98. Heer, A. F. M. D. & Mosselman, E. 2004. Flow structure and bedload distribution at alluvial diversions, Proceedings Riverflow 2004. Naples.

99. Heinimann, A. 2006. Pattern of land cover change in the Lower Mekong Basin. The relevance of mesoscale approaches. University of Bern, Bern, Switzerland.

100. Heritage, G. L., B. P. Moon, L. J. Broadhurst, C. S. James,. 2004. The frictional resistance characteristics of a bedrock-influenced river channel. Earth Surface Processes and Landforms, 29(5): 611-627.

101. Hessel, R., Jetten, V., & Guanghui, Z. 2003. Estimating Manning's n for steep slopes. CATENA, 54(1-2): 77-91.

102. Hicks, D. M. & Mason, P. J. 1991. Roughness characteristics of New Zealand rivers. Paper presented at the New Zealand Water Resources Survey, DSIR Marine and Freshwater, Wellington.

103. Hook, J., N. Susan, J. Robyn. 2003. Social Atlas of the Lower Mekong Basin. Phnom Penh: Mekong River Comission, Campodia.

104. Horritt, M. S. & Bates, P. D. 2002. Evaluation of 1D and 2D numerical models for predicting river flood inundation. Journal of Hydrology, 268(1-4): 87-99.

105. Horritt, M. S. 2006. A methodology for the validation of uncertain flood inundation models. Journal of Hydrology, 326(1-4): 153-165.

106. Howard, A. D. 1980. Thresholds in river regimes. In D. R. Coates & J. D. Vitek (Eds.), Thresholds in Geomorphology. Boston: Allen and Unwin.

107. Howard, A. D. 1994. A detachment limited model of drainage basin evolution. Water Resources Research, 30(7): 2251-2260.

108. Howard, A. D., Dietrich, W. E., & Seidl, M. A. 1994. Modeling fluvial erosion on regional to continental scales. J. Geophys. Res., 99(B7): 13971-13986.

109. Huang, H. Q. & Nanson, G. C. 1997. Vegetation and channel variation; a case study of four small streams in southeastern Australia. Geomorphology, 18(3-4): 237-249.

110. Huang, H. Q. & Nanson, G. C. 2007. Why some alluvial rivers develop an anabranching pattern. Washington, DC, ETATS-UNIS: American Geophysical Union.

111. Huang, J.-K. & Lee, K. T. 2009. Influences of spatially heterogeneous roughness on flow hydrographs. Advances in Water Resources, 32(11): 1580-1587.

112. Huthoff, F., Augustijn, D. C. M., & Hulscher, S. J. M. H. 2007. Analytical solution of the depth-averaged flow velocity in case of submerged rigid cylindrical vegetation. Water Resour. Res., 43(6): W06413.

113. Islam, T. G. M., Kabir, M. R., & Nishat, A. 2006. Nodal point relation for the distribution of sediments at channel bifurcation. Reston, VA, ETATS-UNIS: American Society of Civil Engineers.

114. Jacobs, J. W. 1996. Adjusting to climate change in the Lower Mekong. Global Environmental Change, 6(1): 7-22.

115. Jagers, H. R. A. 2003. Modelling planform changes of braided rivers. Unpublished PhD thesis, University of Twente, the Netherlands.

116. Jain, V. & Sinha, R. 2004. Fluvial dynamics of an anabranching river system in Himalayan foreland basin, Baghmati river, north Bihar plains, India. Geomorphology, 60(1-2): 147-170.

117. Jamieson, S. S. R., Sinclair, H. D., Kirstein, L. A., & Purves, R. S. 2004. Tectonic forcing of longitudinal valleys in the Himalaya: morphological analysis of the Ladakh Batholith, North India. Geomorphology, 58(1-4): 49-65.

118. Jansen, J. D. & Nanson, G. C. 2004. Anabranching and maximum flow efficiency in Magela Creek, northern Australia. Water Resour. Res., 40(4): W04503.

119. Jarrett, R. D. 1984. Hydraulics of high gradient streams. ASCE J. Hydraul. Eng., 110.

120. Judd, D. A., I.D. Rutherfurd, J.W. Tilleard, R.J. Keller. 2007. A case study of the processes displacing flow from the anabranching Ovens River, Victoria, Australia. Earth Surface Processes and Landforms, 9999(9999): n/a.

121. Juracek, K. E. & Fitzpatrick, F. A. 2003. Limitations and implicationgs of stream classification. Journal of the American Water Resources Association, 39(3): 659-670.

122. Kale, V. S., Baker, V. R., & Mishra, S. 1996. Multi-channel patterns of bedrock rivers: An example from the central Narmada basin, India. CATENA, 26(1-2): 85-98.

123. Kale, V. S. 2005. The sinuous bedrock channel of the Tapi River, Central India: Its form and processes. Geomorphology, 70(3-4): 296-310.

124. Kasper, K. E., C.I. Thornton, S.R. Abt, M.D. Robeson, C.C. Watson. 2005. Accuracy of HEC-RAS to calculate flow depths and total energy loss with and without bendway weirs in a meander bend: Colorado State University.

125. Kasper, K. E., Thornton, C. I., Abt, S. R., Robeson, M. D., & Watson, C. C. 2005. Accuracy of HEC-RAS to calculate flow depths and total energy loss with and without bendway weirs in a meander bend. Albuquerque, New Mexico: U.S. Department of the Interior.

126. Katiyar, S. K. & K.K.Rampal. 1991. Bathymetric mapping over coastal Andhra Pradesh using landsat Mss data. Journal of the Indian Society of Remote Sensing, 19(3).

127. Kellerhals, R., Bray, D. I., & Church, M. 1976. Classification and Analysis of River Processes. Journal of the Hydraulics Division, 102(7): 813 - 829

128. Khanna, M. & Malano, H. M. 2006. Modelling of basin irrigation systems: A review. Agricultural Water Management, 83(1-2): 87-99.

129. Kidson, R., K. Richards, P. Carling,. 2003. Manning's n Expert Panel experiment: an invitation. Hydrological Processes, 17(7): 1469.

130. Kidson, R. L., K. S. Richards, P. A. Carling,. 2006. Hydraulic model calibration for extreme floods in bedrock-confined channels: case study from northern Thailand. Hydrological Processes, 20(2): 329-344.

131. Kiem, S. A., Hapuarachchige P. H., Kuniyosi T. 2004. Impacts of climate change variability on streamflow in the Mekong River: an interest challenge for hydrological modelling. Paper presented at the Proc. 7th International River Symposium, 31 August - 3 Sept. 2004, Brisbane, Australia.

132. Kinghton, D. 1998. Fluvial forms and processes - a new perspective: Hodder Arnold, a member of the HodderHeadline Group.

133. Kite, G. 2000. Developing a hydrological model for the Mekong Basin. Impacts of basin development on fi sheries productivity. Working Paper 2. Colombo, Sri Lanka: International Water Management Institute.

134. Kleinen, T. & Petschel-Held, G. 2007. Integrated assessment of changes in flooding probabilities due to climate change. Climatic Change, 81(3): 283-312.

135. Kleinhans, M. G., Jagers, H. R. A., Mosselman, E., & Sloff, C. J. 2008. Bifurcation dynamics and avulsion duration in meandering rivers by one-dimensional and three-dimensional models. Water Resour. Res., 44.

136. Knebl, M. R., Yang, Z.-L., Hutchison, K., & Maidment, D. R. 2005. Regional scale flood modeling using NEXRAD rainfall, GIS, and HEC-HMS/RAS: a case study for the San Antonio River Basin Summer 2002 storm event. Journal of Environmental Management Sustainable planning in a semi-arid fast growing region, 75(4): 325-336.

137. Knight, D. W. & Shiono, K. 1996. River channel and floodplain hydraulics. In M. G. Anderson & D. E. Walling & P. D. Bates (Eds.), Floodplain processes: John Wiley & Sons Ltd.

138. Knighton, A. D. 1998. Fluvial forms and processes. A new perspective. London: Arnold.

139. Knighton, D. W. & Brown, F. A. 2001. Resistance studies of overbank flowin rivers with sediment using the flood channel facility. Journal of Hydraulic Research, 39(3).

140. Knighton, A. D. & Nanson, G. C. 2002. Inbank and overbank velocity conditions in an arid zone anastomosing river. Hydrological Processes, 16(9): 1771-1791.

141. Kolding, J. 2002. The use of hydro-acoustic surveys for the monitoring of fish abundance in the deep pools and Fish Conservation Zones in the Mekong River, Siphandone area, Champassak Province, Lao PDR. Vientiane: Mekong River Commission, Laos.

142. Kondolf, G. M., H. Piegay. 2003. Tools in Fluvial Geomorphology. The Atrium, Southern Gate, Chichester, West Sussex, England: John Wiley and Sons Ltd.

143. Kummu, M., J. Koponen, J. Sarkkula. 2005. Assessing impacts of the Mekong development in the Tole Sap Lake. Paper presented at the Role of Water Sciences in Transboundary River Basin Management, Thailand.

144. Kummu, M., O. Varis. 2007. Sediment-related impacts due to upstream reservoir trapping, the Lower Mekong River. Geomorphology Monsoon Rivers of Asia, 85(3-4): 275-293.

145. Kummu, M., Lu, X. X., Rasphone, A., Sarkkula, J., & Koponen, J. 2008. Riverbank changes along the Mekong River: Remote sensing detection in the Vientiane-Nong Khai area. Quaternary International, 186(1): 100-112.

146. Kundzewicz, Z. W., Nohara, D., Tong, J., Oki, T., Buda, S., & Takeuchi, K. 2009. Discharge of large Asian rivers - Observations and projections. Quaternary International, 208(1-2): 4-10.

147. Lane, E. W. 1957. A study of the shape of channels formed by natural streams flowing in erodible material, Missouri River Division Sediment Series, Vol. 9. Omaha, NE: U.S. Army Corps of Engineers.

148. Lane, S. N. 1998. Hydraulic modelling in hydrology and geomorphology: a review of high resolution approaches. Hydrological Processes, 12(8): 1131-1150.

149. Lane, S. N. 2005. Roughness - time for a re-evaluation? Earth Surface Processes and Landforms, 30(2): 251-253.

150. Lane, S. N. 2006. Numerical Modelling in Physical Geography: Understanding, Explanation and Prediction. In G. V. Nicholas Clifford (Ed.), Key Methods in Geography: SAGE Publications Ltd.

151. Lane, S. N., Parsons, D. R., Best, J. L., Orfeo, O., Kostaschuk, R. A., & Hardy, R. J. 2008. Causes of rapid mixing at a junction of two large rivers: RÃ-o ParanÃ¡ and RÃ-o Paraguay, Argentina. J. Geophys. Res., 113.

152. Latrubesse, E. M. 2008. Patterns of anabranching channels: The ultimate end-member adjustment of mega rivers. Geomorphology, 101(1-2): 130-145.

153. Laushey, L. M. 1989. A dimensionless Manning-type equation. In B. C. Yen (Ed.), nternational Conference on Channel Flow and Catchment Runoff: Centennial of Manning's Formula and Kuichling's Rational Formula. Charlottesville: American Society of Civil Engineers.

154. LeFavour, G. & Alsdorf, D. 2005. Water slope and discharge in the Amazon River estimated using the shuttle radar topography mission digital elevation model. Geophys. Res. Lett., 32.

155. Lejot, J., Delacourt, C., Piégay, H., Fournier, T., Trémélo, M.-L., & Allemand, P. 2007. Very high spatial resolution imagery for channel bathymetry and topography from an unmanned mapping controlled platform. Earth Surface Processes and Landforms, 32(11): 1705-1725.

156. Leopold, L. B. & Maddock, T. 1953. The hydraulic geometry of stream channels and some physiographic implications. U.S. Geological Survey Professional Paper: 1–57.

157. Leopold, L. B. & Wolman, M. G. 1957. River channel patterns: braided, meandering and straight. Paper presented at the U.S. Geol. Surv. Prof. Pap.

158. Leopold, L. B., M.G. Wolman, J.P. Miller. 1964. Fluvial processes in geomorphology: Dover Publications, Inc., New York.

159. Li, Z. & Zhang, J. 2001. Calculation of Field Manning's Roughness Coefficient. Agricultural Water Management, 49(2): 153-161.López, F. & García, M. 1998. Open-Channel Flow through Simulated Vegetation: Suspended Sediment Transport Modeling. Water Resour. Res., 34(9): 2341-2352.

160. Lu, X. X. & Siew, R. Y. 2006. Water discharge and sediment flux changes over the past decades in the Lower Mekong River: possible impacts of the Chinese dams. Hydrol. Earth Syst. Sci., 10(2): 181-195.

161. Lu, X. & Jiang, T. 2009. Larger Asian rivers: Climate change, river flow and sediment flux. Quaternary International, 208(1-2): 1-3.

162. MacAlister, C. & Mahaxay, M. 2009. Mapping wetlands in the Lower Mekong Basin for wetland resource and conservation management using Landsat ETM images and field survey data. Journal of Environmental Management, 90(7): 2130-2137.

163. Makaske, B. 2001. Anastomosing rivers: a review of their classification, origin and sedimentary products. Earth-Science Reviews, 53(3-4): 149-196.

164. Makaske, B., Smith, D. G., Berendsen, H. J. A., de Boer, A. G., van Nielen-Kiezebrink, M. F., & Locking, T. 2009. Hydraulic and sedimentary processes causing anastomosing morphology of the upper Columbia River, British Columbia, Canada. Geomorphology, 111(3-4): 194-205.

165. Mandlburger, G., Hauer, C., Hofle, B., Habersack, H., & Pfeifer, N. 2009. Optimisation of LiDAR derived terrain models for river flow modelling. Hydrol. Earth Syst. Sci., 13(8): 1453 - 1466.

166. Manusthiparom, C., C. Apirumanekul, M. Mahaxay. 2005. Flood forcasting and river monitoring system in the Mekong River Basin, The second Southeast Asia Water Forum. Bali, Indonesia.

167. Mariza, C. C., Jeffrery E. Richey, Gopi Goteti, Dennis P. Lettenmaier, Christoph Feldkotter, Anond Snidvong. 2007. Landscape structure and use, climate, and water movement in the Mekong River Basin.

168. Marsik, M. & Waylen, P. 2006. An application of the distributed hydrologic model CASC2D to a tropical montane watershed. Journal of Hydrology, 330(3-4): 481-495.

169. Mason, D. C., Cobby, D. M., Horritt, M. S., & Bates, P. D. 2003. Floodplain friction parameterization in two-dimensional river flood models using vegetation heights derived from airborne scanning laser altimetry. Hydrological Processes, 17(9): 1711-1732.

170. Maxwell, J. F. 2001. Vegetation in the Siphandone wetlands. In G. Daconto (Ed.), Siphandone Wetlands.

171. Melching, C. 1992. An improved first order reliability approach for assessing uncertainties in hydrologic modeling. Journal of Hydrology, 132: 157-177.

172. Melsheimer, C. & Liew, S. C. 2001. Extracting bathymetry from multi-temporal SPOT images. Paper presented at the Proceedings of the 22nd Asian Conference on Remote Sensing, 5-9 November 2001, Singapore.

173. Merwade, V., Cook, A., & Coonrod, J. 2008. GIS techniques for creating river terrain models for hydrodynamic modeling and flood inundation mapping. Environmental Modelling & Software, 23(10-11): 1300-1311.

174. Métivier & Gaudemer. 1999. Stability of output fluxes of large rivers in South and East Asia during the last 2 million years: implications on floodplain processes. Basin Research, 11(4): 293-303.

175. Métivier, F., Gaudemer, Y., Tapponnier, P., & Klein, M. 1999. Mass accumulation rates in Asia during the Cenozoic. Geophysical Journal International, 137(2): 280-318.

176. Millar, R. G. 2000. Influence of Bank Vegetation on Alluvial Channel Patterns. Water Resour. Res., 36(4): 1109-1118.

177. Mishra, S. K., Vijay P.S. 2003. Role of dimensionless numbers in wave analysis. Hydrological Processes, 17(3): 651-669.

178. Montanari, M., Hostache, R., Matgen, P., Schumann, G., Pfister, L., & Hoffmann, L. 2009. Calibration and sequential updating of a coupled hydrologic-hydraulic model using remote sensing-derived water stages. Hydrol. Earth Syst. Sci., 13(3): 367-380.

179. Montgomery, D. R., Abbe, T. B., Buffington, J. M., Peterson, N. P., Schmidt, K. M., & Stock, J. D. 1996. Distribution of bedrock and alluvial channels in forested mountain drainage basins. Nature, 381(6583): 587-589.

180. Morisawa, M. 1968. Streams - their dynamic and morphology: McGraw-Hill Book Company.

181. Morisawa, M. 1985. Rivers - form and process. In K. M. Clayton (Ed.), Geomorphology texts: Longman Group Limited.

182. Mosquera-Machado, S. & Ahmad, S. 2007. Flood hazard assessment of Atrato River in Colombia. Water Resources Management, 21(3): 591-609.

183. MRC. 2006. Annual flood report 2005. Vientiane: Mekong River Commission, Laos.

184. Nanson, G. C., A.D. Knighton. 1996. Anabraching rivers: their causes, character and classification. Earth Surface Processes and Landforms, 21(3): 217-239.

185. Nanson, G. C. & Huang, H. Q. 1999. Anabranching rivers: divided efficiency leading to fluvial diversity. In A. J. Miller & A. Gupta (Eds.), Varieties of Fluvial Form: 477–494. Chichester: Wiley.

186. Nanson, G. C. & Huang, H. Q. 2008. Least action principle, equilibrium states, iterative adjustment and the stability of alluvial channels. Earth Surface Processes and Landforms, 33(6): 923-942.

187. Nelson, J. M., J.P. Bennett, S.M. Wiele. 2003. Flow and Sediment-Transport Modeling. In G. M. Kondolf, H. Piégay (Ed.), Tools in Fluvial Geomorphology: 539-576.

188. Niekerk, A. W. v., Heritage, G. L., Broadhurst, L. W., & Moon, B. P. 1999. Bedrock anastomosing channel systems: morphology and dynamics of the Sabie River, Mpumulanga Province, South Africa. In A. J. Miller & A. Gupta (Eds.), Varieties of Fluvial Form: 33 - 51. Chichester: Wiley.

189. Nijssen, B., O'Donnell, G. M., Hamlet, A. F., & Lettenmaier, D. P. 2001. Hydrologic Sensitivity of Global Rivers to Climate Change. Climatic Change, 50(1): 143-175.

190. Oreskes, N., Shrader-Frechetted, K., & Belitz, K. 1994. Verification, validation, and confirmation of numerical models in the earth science. Science, 263: 6.

191. Pantulu, V. R. 1986. The Mekong river system. In B. R. Davies & K. F. Walker (Eds.), The Ecology of Rivers. Dordrecht: Dr. W. Junk Publishers.

192. Pappenberger, F., Beven, K., Horritt, M., & Blazkova, S. 2005. Uncertainty in the calibration of effective roughness parameters in HEC-RAS using inundation and downstream level observations. Journal of Hydrology, 302(1-4): 46-69.

193. Parker, G. 1979. Hydraulic Geometry of active gravel rivers. Journal of the Hydraulics Division, 105(9): 1185-1201

194. Parsons, D. R., Best, J. L., Orfeo, O., Hardy, R. J., Kostaschuk, R., & Lane, S. N. 2005. Morphology and flow fields of three-dimensional dunes, Rio Paraná, Argentina: Results from simultaneous multibeam echo sounding and acoustic Doppler current profiling. J. Geophys. Res., 110(F4): F04S03.

195. Parsons, D. R., Best, J. L., Lane, S. N., Thomas, R. E., Keevil, G., & Hardy, R. J. 2007. Flow structures and controls at river bifurcations: a laboratory flume experiment. Paper presented at the AGU Fall Meeting, San Francisco.

196. Patro, S., Chatterjee, C., Singh, R., & Raghuwanshi, N. S. 2009. Hydrodynamic modelling of a large flood-prone river system in India with limited data. Hydrological Processes, 23(19): 2774-2791.

197. Penny, D. 2006. The Holocene history and development of the Tonle Sap, Cambodia. Quaternary Science Reviews, 25(3-4): 310-322.

198. Phovisay, A. 2003. Monitoring of Fish Trade Study of the Siphandone Fishery, Champassak Province, 2003, Living Aquatic Resources Research Center, National Agriculture and Forestry Research Institute Ministry of Agriculture and Forestry, Vientiane, Lao PDR. Vientiane: The Data and Information Unit Living Aquatic Resources Research Center.

199. Pilgrim, D. H. 1976. Travel times and nonlinearity of flood runoff from tracer measurements on a small watershed. Water Resour. Res. , 123: 487 - 496.

200. Polcyn, F. C. & D.R., L. 1979. Landsat bathymetric mapping by multispectal prossing. Paper presented at the Proceedings of thirdteenth international symposium on remote sensing of environment.

201. Ramesh, R., Datta, B., Bhallamudi, S. M., & Narayana, A. 2000. Optimal Estimation of Roughness in Open-Channel Flows. Journal of Hydraulic Engineering, 126(4): 299-303.

202. Rathburn, S. & Wohl, E. 2003. Predicting fine sediment dynamics along a pool-riffle mountain channel. Geomorphology, 55(1-4): 111-124.

203. Remo, J. W. F. & Pinter, N. 2007. Retro-modeling the Middle Mississippi River. Journal of Hydrology, 337(3-4): 421-435.

204. Richard, H. F. P. 1967. Fluid dynamics. Columbus, Ohio: Charles E. Merrill Books, Inc.

205. Richards, K. 1982. Rivers - form and process in alluvial channels: Methuen & Co. Ltd.

206. Richardson, W. R. & Thorne, C. R. 2001. Multiple thread flow and channel bifurcation in a braided river: Brahmaputra-Jamuna River, Bangladesh. Geomorphology, 38(3-4): 185-196.

207. Richardson, K. & Carling, P. A. 2005. A typology of sculpted forms in open bedrock channels. Paper presented at the Special Paper-Geological Society of America.

208. Richardson, K. & Carling, P. A. 2006. The hydraulics of a straight bedrock channel: Insights from solute dispersion studies. Geomorphology, 82(1-2): 98-125.

209. Roberts, R. G. 1991. Sediment budgets and Quaternary history of the Magela Creek catchment, tropical Northern Australia. Wollongong, Australia.

210. Roberts, S. J., Gottgens, J. F., Spongberg, A. L., Evans, J. E., & Levine, N. S. 2007. Assessing Potential Removal of Low-Head Dams in Urban Settings: An Example from the Ottawa River, NW Ohio. Environmental Management, 39(1): 113-124.

211. Roper, B. B., Buffington, J. M., Archer, E., Moyer, C., & Ward, M. 2008. The Role of Observer Variation in Determining Rosgen Stream Types in Northeastern Oregon Mountain Streams¹. JAWRA Journal of the American Water Resources Association, 44(2): 417-427.

212. Rosgen, D. L. 1994. A classification of natural rivers. CATENA, 22(3): 169-199.

213. Rykiel, E. J. 1996. Testing ecological models: the meaning of validation. Ecological Modelling, 90(3): 229-244.

214. Sargent, R. G. 2005. Verification and validation of simulation models, Proceedings of the 37th conference on Winter simulation. Orlando, Florida: Winter Simulation Conference.

215. Savery, T. S., Belt, G. H., & Higgins, D. A. 2001. Evaluation of the Rosgen stream classification system in Chequamegon-Nicolet national forest, Wisconsin. Journal of the American Water Resources Association, 37(3): 641-654.

216. Schaller, M., Hovius, N., Willett, S. D., Ivy-Ochs, S., Synal, H.-A., & Chen, M.-C. 2005. Fluvial bedrock incision in the active mountain belt of Taiwan from in situ-produced cosmogenic nuclides. Earth Surface Processes and Landforms, 30(8): 955-971.

217. Schumann, G., Hostache, R., Puech, C., Hoffmann, L., Matgen, P., Pappenberger, F., & Pfister, L. 2007. High-resolution 3-D flood information from radar imagery for flood hazard management. Geoscience and Remote Sensing, IEEE Transactions on, 45(6): 1715-1725.

218. Schumm, S. A. 1971. Fluvial morphology: the historical perspective. In H. W. Shen (Ed.), Fluvial geomorphology in river mechanics. Fort Collins, Colorado: Water resources publication.

219. Schumm, S. A. 1985. Patterns of alluvial rivers. Annu. Rev. Earth Planet. Sci.(13): 5 - 27.

220. Shahrokhnia, M. A. & Javan, M. 2005. Performance assessment of Doroodzan irrigation network by steady state hydraulic modeling. Irrigation and Drainage Systems, 19(2): 189-206.

221. Shahrokhnia, M. A. & Javan, M. 2007. Influence of roughness changes on offtaking discharge in irrigation canals. Water Resources Management, 21(3): 635-647.

222. Sibson, R. 1981. A Brief Description of Natural Neighbor Interpolation. New York: John Wiley & Sons.

223. Sibson, R. 1981. A brief description of natural neighbor interpolationts. In V. Barnett (Ed.), nterpreting Multivariate Data. Chichester: John Wiley.

224. Smith, D. G. & Smith, N. D. 1980. Sedimentation in anastomosed river systems; examples from alluvial valleys near Banff, Alberta. JOURNAL OF SEDIMENTARY RESEARCH, 50(1): 157-164.

225. Smith, D. G. 1986. Anastomosing river deposits, sedimentation rates and basin subsidence, Magdalena River, northwestern Colombia, South America. Sedimentary Geology, 46(3-4): 177-196.

226. Smith, N. D., McCarthy, T. S., Ellery, W. N., Merry, C. L., & Rüther, H. 1997. Avulsion and anastomosis in the panhandle region of the Okavango Fan, Botswana. Geomorphology, 20(1-2): 49-65.

227. Snidvongs, A. 2006. Vulnerability to climate change related water resesource changes and extreme hydrological events in Southeast Asis. Washington DC, USA: The International START Secretariat.

228. Stark, C. P. 2006. A self-regulating model of bedrock river channel geometry. Geophys. Res. Lett., 33(4): L04402.

229. START. 2006. Final technical report: Assessment of Impact and Adaptation to Climate Change in Multiple Sectors and Multiple Regions (AIACC): Regional Study AS07 – Southeast Asia Regional Vulnerability to Changing Water Resources and Extreme Hydrological due to Climate Change (2003-2006).

230. Straatsma, M. W. & Baptist, M. J. 2008. Floodplain roughness parameterization using airborne laser scanning and spectral remote sensing. Remote Sensing of Environment, 112(3): 1062-1080.

231. Ta, T. K. O., Nguyen, V. L., Tateishi, M., Kobayashi, I., Tanabe, S., & Saito, Y. 2002. Holocene delta evolution and sediment discharge of the Mekong River, southern Vietnam. Quaternary Science Reviews, 21(16-17): 1807-1819.

232. Tabacchi, E., Lambs, L., Guilloy, H., Planty-Tabacchi, A.-M., Muller, E., & Décamps, H. 2000. Impacts of riparian vegetation on hydrological processes. Hydrological Processes, 14(16-17): 2959-2976.

233. Tabata, K. K. & Hickin, E. J. 2003. Interchannel hydraulic geometry and hydraulic efficiency of the anastomosing Columbia River, southeastern British Columbia, Canada. Earth Surface Processes and Landforms, 28(8): 837-852.

234. Takagi, T., Oguchi, T., Matsumoto, J., Grossman, M. J., Sarker, M. H., & Matin, M. A. 2007. Channel braiding and stability of the Brahmaputra River, Bangladesh, since 1967: GIS and remote sensing analyses. Geomorphology, 85(3-4): 294-305.

235. Takeuchi, K. 2004. A role of distributed hydrological models in the Mekong River Basin management. Paper presented at the Advances in Integrated Mekong River Management, Lao PDR.

236. Takeuchi, K. 2004. Preface. Paper presented at the Advances in Integrated Mekong River Management, Lao PDR.

237. Tayefi, V., S. N. Lane, R. J. Hardy, D. Yu,. 2007. A comparison of one- and two-dimensional approaches to modelling flood inundation over complex upland floodplains. Hydrological Processes, 9999(9999): n/a.

238. Thomas, H. & Nisbet, T. R. 2007. An assessment of the impact of floodplain woodland on flood flows. Hertford, ROYAUME-UNI: LeadMedia.

239. Thompson, C., Rhodes, E., & Croke, J. 2007. The storage of bed material in mountain stream channels as assessed using Optically Stimulated Luminescence dating. Geomorphology Mountain Rivers II: Channel Processes - Mountain Rivers II, 83(3-4): 307-321.

240. Tilman, E., L. Saravuth, V. Sisomvang, J. Tospornsampan, T. H. Ngan, C. Krittasudthacheewa, C. Apirumanekul. 2006. MRC Annual flood report 2005: Mekong River Commission.

241. Tinkler, K. & Wohl, E. 1998. A primer on bedrock channels. In K. Tinkler & E. Wohl (Eds.), Rivers Over Rock: Fluvial Processes in Bedrock Channels, Vol. 107: 1 - 18. Washington, D. C.: Geophys. Monogr. Ser.

242. Tooth, S. & Nanson, G. C. 1999. Anabranching rivers on the Northern Plains of arid central Australia. Geomorphology, 29(3-4): 211-233.

243. Tooth, S. & Nanson, G. C. 2000. The role of vegetation in the formation of anabranching channels in an ephemeral river, Northern plains, arid central Australia. Hydrological Processes, 14(16-17): 3099-3117.

244. Tooth, S. & McCarthy, T. S. 2004. Controls on the transition from meandering to straight channels in the wetlands of the Okavango Delta, Botswana. Earth Surface Processes and Landforms, 29(13): 1627-1649.

245. Topa, P. & Paszkowski, M. 2002. Anastomosing Transportation Networks, Parallel Processing and Applied Mathematics : 4th International Conference, PPAM 2001 Na: czÃ³w, Poland, September 9-12, 2001. Revised Paper: 904.

246. Totz, C. 2003. Floodplain mapping using HEC-RAS: Waterburry Com. - Haestad Press.

247. Tripathi, N. K. & Rao, A. M. 2002. Bathymetric mapping in Kakinada Bay, India, using IRS-1D LISS-III data. International Journal of Remote Sensing, 23(6): 1013 - 1025.

248. Tucker, G. E., R.L. Singerland. 1994. Erosional dynamics, flexural isostasy, and long-lived escarpments: A numerical modelling study. Journal of Geophysical Research, 99: 12229-12243.

249. Turowski, J. M., Hovius, N., Wilson, A., & Horng, M.-J. 2008. Hydraulic geometry, river sediment and the definition of bedrock channels. Geomorphology, 99(1-4): 26-38.

250. van den Berg, J. H. 1995. Prediction of alluvial channel pattern of perennial rivers. Geomorphology, 12(4): 259-279.

251. van Gelder, P. 2000. Statistical methods for the risk-based design of civil structures. Delft University of Technology.

252. van Zalinge, N., P. Degen , C. Pongsri, S. Nuov, J.G. Jensen, V.H. Nguyen, X. Choulamany. 2004. The Mekong River System. Paper presented at the The Second International Symposium on the Management of Large Rivers for Fisheries, Phnom Penh, Kingdom of Cambodia.

253. Varis, O., M. Keskinen. 2003. Socio-economic analysis of the Tonle Sap Region, Cambodia: Building links and capacity for targeted poverty alleviation. Water Resources Management, 19(2): 295-310.

254. Varis, O., M. Keskinen. 2006. Policy analysis for the Tonle Sap Lake, Cambodia: A Bayesian network model approach. Water Resources Management, 22(3): 417-431.

255. Verhaar, P. M., Biron, P. M., Ferguson, R. I., & Hoey, T. B. 2008. A modified morphodynamic model for investigating the response of rivers to short-term climate change. Geomorphology, 101(4): 674-682.

256. Vidal, J.-P., Moisan, S., Faure, J.-B., & Dartus, D. 2007. River model calibration, from guidelines to operational support tools. Environmental Modelling & Software, 22(11): 1628-1640.

257. Visser, M., Duits, M., & Lee, W. v. d. 2001. An automatic calibration method for hydraulic models: HKV LIJN IN WATER, P.O. Box 2120, 8203 AC Lelystad.

258. Wallerstein, N. P. & Thorne, C. R. 2004. Influence of large woody debris on morphological evolution of incised, sand-bed channels. Geomorphology, 57(1-2): 53-73.

259. Walling, D. E. 2005. Tracing suspended sediment sources in catchments and river systems. Science of The Total Environment, 344(1-3): 159-184.

260. Walling, D. E. 2008. The changing sediment load of the Mekong River. Ambio, 37(3).

261. Wang, S., Chen, Z., & Smith, D. G. 2005. Anastomosing river system along the subsiding middle Yangtze River basin, southern China. CATENA, 60(2): 147-163.

262. Wang, J. J. & Lu, X. X. 2008. Influence of the changing environment on sediment loads of the Lower Mekong River. Paper presented at the Sediment dynamics in changing environments, Christchurch, NewZealand.

263. Wassmann, R., Hien, N. X., Hoanh, C. T., & Tuong, T. P. 2004. Sea Level Rise Affecting the Vietnamese Mekong Delta: Water Elevation in the Flood Season and Implications for Rice Production. Climatic Change, 66(1): 89-107.

264. Watson, D. F. 1988. Natural neighbor sorting on the n-dimensional sphere. Pattern Recognition 21(1): 63 - 67.

265. Watson, D. 1992. Contouring: A Guide to the Analysis and Display of Spatial Data. London: Pergamon Press.

266. Wende, R. & Nanson, G. C. 1998. Anabranching rivers: ridge-form alluvial channels in tropical northern Australia. Geomorphology, 22(3-4): 205-224.

267. Werner, B. T. 1995. Eolian dunes: Computer simulations and attractor interpretation. Geology, 23(12): 1107 - 1110.

268. Wheater, H. S. 2002. Progress in and prospects for fluvial flood modelling. Philosophical Transactions of the Royal Society A: Mathematical, Physical and Engineering Sciences, 360(1796): 1409-1431.

269. Whipple, K. X. & Tucker, G. E. 1999. Dynamics of the stream-power river incision model: Implications for height limits of mountain ranges, landscape response timescales, and research needs. J. Geophys. Res., 104(B8): 17661-17674.

270. Whipple, K. X., Snyder, N. P., & Dollenmayer, K. 2000. Rates and processes of bedrock incision by the Upper Ukak River since the 1912 Novarupta ash flow in the Valley of Ten Thousand Smokes, Alaska. Geology, 28(9): 835-838.

271. Whipple, K. X. 2004. Bedrock rivers and the geomorphology of the active orogens. Annual Review of Earth and Planetary Sciences, 32(1): 151-185.

272. Wilcock, P. R. & Crowe, J. C. 2003. Surface-based Transport Model for Mixed-Size Sediment. Journal of Hydraulic Engineering, 129(2): 120-128.

273. Wilson, C. A. M. E. & Horritt, M. S. 2002. Measuring the flow resistance of submerged grass. Hydrological Processes, 16(13): 2589-2598.

274. Wilson, M. D. & Atkinson, P. M. 2007. The use of remotely sensed land cover to derive floodplain friction coefficients for flood inundation modelling. Hydrological Processes, 21(26): 3576-3586.

275. Wobus, C. W., Tucker, G. E., & Anderson, R. S. 2006. Self-formed bedrock channels. Geophys. Res. Lett., 33(18): L18408.

276. Wohl, E. E. 1999. Incised bedrock channels. In S. E. Darby & A. Simon (Eds.), Incised river channels: processes, forms, engineering and management: John Wiley and Sons.

277. Wohl, E. E. & Wilcox, A. 2005. Channel geometry of mountain streams in New Zealand. Journal of Hydrology, 300(1-4): 252-266.

278. Wohl, E. 2007. Channel-Unit Hydraulics on a Pool-Riffle Channel. Physical Geography, 28(3): 233-248.

279. Wyzga, B. 1999. Estimating mean flow velocity in channel and floodplain areas and its use for explaining the pattern of overbank deposition and floodplain retention. Geomorphology, 28(3-4): 281-297.

280. Yagci, O. & Kabdasli, M. S. 2008. The impact of single natural vegetation elements on flow characteristics. Hydrological Processes, 22(21): 4310-4321.

281. Yamashita, A. 2003. Outline of the Mekong River - From Tibetan Moutains to the Mekong Delta, Vol. 2007.

282. Yatsu, E. 1955. On the long profile of the graded river. Transaction, American Geophysical Union, 36(4).

283. Yu, D. & Lane, S. N. 2006. Urban fluvial flood modelling using a two-dimensional diffusion-wave treatment, part 2: development of a sub-grid-scale treatment. Hydrological Processes, 20(7): 1567-1583.

284. Zalinge, N., Deap, L., Ngor, P., Sarkkula, J., & Koponen, J. 2003. Mekong flood levels and Tonle Sap fish catches. Paper presented at the Second International Symposium on the Management of Large Rivers for Fisheries, Phnom Penh.

285. Zavadil, E., Stewardson, M., Ladson, A., & Rutherfurd, I. 2007. Which confluences should we use to differentiate stream segments for management? A geomorphic assessment. Paper presented at the Proceedings of the 5th Australian Stream Management Conference. Australian rivers: making a difference, Charles Sturt University, Thurgoona, New South Wales.

Appendices

Appendix 1: Open Letter on the Don Sahong Dam, Proposed for the Mainstream Mekong River, Southern Laos

August 26, 2009

To Whom it May Concern:

We, the undersigned scientists, fisheries specialists, nutritionists and development workers, are writing to offer our support to the Lao people, and to express our concern about plans to construct the Don Sahong Dam across the Hou Sahong channel in the Khone Falls area of Khong District, Champasak Province, southern Laos. We believe the project will have grave consequences for regional fisheries and the food security and livelihood of millions of people in the Mekong River Basin.

According to an independent scientific paper recently released[1], the Don Sahong project would block migrations of many important fish species that move up and down the Mekong River past the Khone Falls at various times of the year. Through fieldwork and a review of the available scientific literature, the paper reveals that many fish species migrate very long distances through the Hou Sahong Channel to upstream areas, where they form an important part of the diet of local people. The paper concludes that through blocking the migration of these fish, there is a "high risk that the dam could cause serious impacts to fisheries both far upstream and downstream from the Khone Falls, in Laos, Cambodia, Thailand and Viet Nam, thus jeopardising the livelihoods of large numbers of people".

According to the paper, the mitigation measures proposed in the project's draft environmental impact assessment are unlikely to be effective. There is no known fish pass that could cope with the unique biological requirements of all the fish species that migrate past the Khone Falls each year. The proposal to widen the Hou Sadam is also likely to be ineffective because it would require major engineering works that would be extremely costly.

The paper concludes that fisheries losses in the region, and especially in Laos and Cambodia, could negatively impact the nutritional status of hundreds of thousands or even millions of people dependent on these fisheries, thus affecting the health of a

large number of people. Figures indicate that in Stung Treng Province of Cambodia, almost 45% of children under five years old are underweight. As Cambodians depend on fisheries for the majority of their protein needs, losing a large quantity of wild-caught fish due to the Don Sahong Dam would further exacerbate the situation.

In Laos, recent research by the World Food Programme (WFP) has found that Laos' rural population is experiencing serious nutritional problems, with 50% of all children being chronically malnourished. The Lao people are particularly lacking in meat, fish and edible oils, the exact food types that are threatened by the dam. If the dam causes even a 10% reduction in fisheries in central and southern Laos, the areas expected to be most seriously impacted by the Don Sahong Dam, this could have a serious impact on the nutritional status of people already living at the margins of food security.

For these reasons, we are concerned that the Don Sahong Dam would cause more problems than it would bring benefits to the Lao people, or other peoples in the region. If the dam goes forward, the corresponding drop in nutritional status for Lao and Cambodian citizens could result in setbacks in government and international donor efforts to alleviate poverty and meet various health-related United Nations Millennium Development goals. It could also negatively affect the nutritional status of people in Thailand and Viet Nam. This is a risk that we simply do not believe is worth taking.

We are respectively writing this letter with the hope that the information being provided here will be useful to decision-makers when considering the development of the Don Sahong Dam. We believe that it would be beneficial for everyone to prioritize alternative options for meeting Laos' development needs, options that would protect natural resources while supporting people's food security and decreasing poverty.

Sincerely,

Dr. Ian G. Baird, Affiliate, POLIS Project on Ecological Governance, University of Victoria, Canada

Keith Barney, PhD Candidate, Geography Department, York University, Canada

Andrew Bartlett, Chief Technical Adviser, Laos Extension for Agriculture Project NAFES/Helvetas, Vientiane, Laos

Dr. Isabel Beasley, Wildlife Biologist, Department of Primary Industries and Water, Hobart, Australia

David J.H. Blake, Postgraduate Researcher, School of International Development, University of East Anglia, United Kingdom

Grazia Borrini-Feyerabend, President, Paul K. Feyerabend Foundation, Co coordinator ICCA Consortium

Dr. Simon Bush, Environmental Policy Group. Wageningen University, The Netherlands

Dr Andrew Cock, Postdoctoral Research Fellow, Centre of Southeast Asian Studies, Monash Asia Institute, Monash University, Australia

Dr Jonathan Cornford, Director, Manna Gum, Australia

Peter Cunningham, Fisheries Biologist, Wester Ross Fisheries Trust, Scotland

Dr. Justin McDaniel, Associate Professor, University of Pennsylvania, USA

Pete Davidson, Program Manager, Bird Studies Canada

Dr. Anthony Davis, Associate Vice-President (Research), Mount Saint Vincent University, Nova Scotia, Canada

Dr. Phillip Dearden, Professor and Chair, Department of Geography, University of Victoria, Canada

Michael B. Dwyer, Doctoral candidate, Energy & Resources Group, University of California, Berkeley, USA

Dr. Christian Erni, IWGIA, Denmark

Dr. Tom Evans, Deputy Director, Wildlife Conservation Society (WCS) Cambodia Program, Cambodia

Dr. Jefferson Fox, Senior Fellow, East-West Center, Honolulu, Hawaii, USA

Dr. Charles R. Goldman, Professor, Department of Environmental Science and Policy University of California, Davis, USA

Dr. Carl Grundy-Warr, Senior Lecturer, Geography Department, National University of Singapore

Dr. Philip Hirsch, Professor of Human Geography and Director, Australian Mekong Resource Centre, School of Geosciences, University of Sydney, Australia

Dr. Zeb Hogan, Fisheries biologist, University of Nevada, USA

Dr. Glen Hvenegaard, Professor of Geography and Environmental Studies, University of Alberta, Canada

Ronald W. Jones, Technical Advisor, FACT, Cambodia

Dr. Hjorleifur Jonsson, Associate Professor of Anthropology, SHESC, Arizona State University, Tempe, USA

Vanessa Lamb, PhD Student, York University, Canada

Dr. Guy R. Lanza, Professor of Microbiology and Director, Environmental Science Program, University of Massachusetts, USA

Dr. Pinkaew Laungaramsri, Faculty of Social Sciences, Chiang Mai University, Thailand

Dr. Leedom Lefferts, Professor of Anthropology Emeritus, Drew University, New Jersey, USA and Research Associate, Department of Anthropology, Smithsonian Institution, Washington, DC, USA

Mak Sithirith, PhD Candidate, Department of Geography, National University of Singapore

Dr. Kanokwan Manorom, Director of Mekong Sub-region Social Research Center, Faculty of Liberal Arts, Ubon Ratchathani University, Thailand

Dr. Michael M'Gonigle, Professor, Faculty of Law, University of Victoria, Canada

Dr. Thomas Murphy, Adjunct professor, Buffalo State, State University of New York, USA

Peng Bun, NGOR, Fisheries researcher, IFReDI/Fisheries Administration, Phnom Penh, Cambodia

Dr. Alan Potkin, Ecologist, Team Leader, Digital Conservation Facility Laos, c/o Center for Southeast Asian Studies, Northern Illinois University, USA

Michael Køie Poulsen, Biologist, M.Sc., Nordic Agency for Ecology and Environment, Denmark

Dr. Boike Rehbein, Director, Global Studies Programme, University of Freiburg, Germany

Dr. Kenneth Ruddle, Director, International Resources Management Institute, Hong Kong

Dr. Guido Sprenger, Junior Professor, Institute of Ethnology, University of Münster, Germany

Dr. Simon Springer, Assistant Professor, Geography Department, National University of Singapore

Pam Stacey, Biologist, Sessional Instructor, University of Alberta, Canada

Dr. David B Thomson, Consultant to World Bank, ADB, FAO, UNDP, EU, former Assistant Professor, University of Rhode Island, USA, presently Scotland

Dr. Peter Ward, Adjunct Professor of Civil Engineering, University of British Columbia, Canada

Kevin Woods, PhD Program, University of California, Berkeley, USA

Reference:

[1] Baird, Ian G. 2009. The Don Sahong Dam: Potential Impacts on Regional Fish Migrations, Livelihoods and Human Health, Victoria, B.C., Canada. Downloadable at: http://polisproject.org/PDFs/Baird%202009_Don%20Sahong.pdf

Appendix 2: Discriminant analysis results

Analysis 1:

Left Channel; Section 1

- **Discriminant Analysis: Re_class versus Elevation**

```
Linear Method for Response: Re_class

Predictors: Elevation

Group         1         2
Count       479       660

Summary of classification

                 True Group
Put into Group       1      2
1                  342    324
2                  137    336
Total N            479    660
N correct          342    336
Proportion       0.714  0.509

N = 1139           N Correct = 678           Proportion Correct = 0.595
```

- **Descriptive Statistics: Elevation**

```
Variable  Re_class    N  N*    Mean  SE Mean  StDev  Minimum      Q1  Median
Ele       1          479   0  79.315   0.0686  1.501   71.620  78.440  79.440
          2          660   0  78.513   0.0707  1.817   62.640  77.440  78.440

Variable  Re_class      Q3  Maximum
Ele       1          80.440   80.540
          2          79.440   80.440
```

Left Channel; Section 2

- **Discriminant Analysis: Re_class versus Elevation**

```
Linear Method for Response: Re_class

Predictors: Elevation

Group         1         2
Count       456       808

Summary of classification

                 True Group
Put into Group       1      2
1                  296    400
2                  160    408
Total N            456    808
N correct          296    408
Proportion       0.649  0.505

N = 1264           N Correct = 704           Proportion Correct = 0.557
```

- **Descriptive Statistics: Elevation**

```
Variable  Re_class    N  N*    Mean  SE Mean  StDev  Minimum      Q1  Median
Ele       1          456   0  78.360   0.0685  1.463   74.330  77.340  78.350
          2          808   0  77.725   0.0424  1.204   74.580  77.350  77.860
```

```
Variable  Re_class      Q3  Maximum
Ele       1         79.380   80.370
          2         78.350   80.960
```

Left Channel; Section 3

- **Discriminant Analysis: Re_class versus Elevation**

```
Linear Method for Response: Re_class

Predictors: Elevation

Group         1         2
Count      2485      1108

Summary of classification

                 True Group
Put into Group       1      2
1                 1629    521
2                  856    587
Total N           2485   1108
N correct         1629    587
Proportion       0.656  0.530

N = 3593           N Correct = 2216           Proportion Correct = 0.617
```

- **Descriptive Statistics: Elevation**

```
Variable  Re_class     N  N*    Mean  SE Mean  StDev  Minimum      Q1
Median
Ele       1         2485   0  79.119   0.0372  1.856   53.060  78.260
80.270
          2         1108   0  78.271   0.0710  2.365   57.860  77.250
78.280

Variable  Re_class      Q3  Maximum
Ele       1         80.290   81.020
          2         80.270   80.320
```

Right Channel; Section 1

- **Discriminant Analysis: Re_class versus Elevation**

```
Linear Method for Response: Re_class

Predictors: Elevation

Group         1         2
Count       662       833

Summary of classification

                 True Group
Put into Group       1      2
1                  520    398
2                  142    435
Total N            662    833
N correct          520    435
Proportion       0.785  0.522

N = 1495           N Correct = 955           Proportion Correct = 0.639
```

- **Descriptive Statistics: Elevation**

```
Variable  Re_class    N  N*    Mean  SE Mean  StDev  Minimum      Q1  Median
```

Ele	1	662	0	78.763	0.0665	1.711	69.100	78.430	78.450
	2	833	0	77.407	0.0845	2.439	67.880	75.400	77.430

Variable	Re_class	Q3	Maximum
Ele	1	80.430	80.450
	2	79.400	80.450

Right Channel; Section 2

- **Discriminant Analysis: Re_class versus Class**

Linear Method for Response: Re_class

Predictors: Class

Group	1	2
Count	348	837

Summary of classification

	True Group	
Put into Group	1	2
1	348	0
2	0	837
Total N	348	837
N correct	348	837
Proportion	1.000	1.000

N = 1185 N Correct = 1185 Proportion Correct = 1.000

- **Descriptive Statistics: Elevation**

Variable	Re_class	N	N*	Mean	SE Mean	StDev	Minimum	Q1	Median
Ele	1	348	0	76.201	0.0926	1.727	66.560	75.360	75.360
	2	837	0	74.690	0.111	3.208	67.060	70.380	75.360

Variable	Re_class	Q3	Maximum
Ele	1	77.360	80.380
	2	77.360	80.380

Analysis 2:

Left Channel; Section 1

- **Discriminant Analysis: Re_class versus Elevation**

```
Linear Method for Response: Re_class

Predictors: Elevation

Group         1         2
Count       546       834

Summary of classification

                 True Group
Put into Group       1      2
1                  346    344
2                  200    490
Total N            546    834
N correct          346    490
Proportion       0.634  0.588

N = 1380           N Correct = 836           Proportion Correct = 0.606
```

- **Descriptive Statistics: Elevation**

```
Variable  Re_class    N  N*    Mean  SE Mean  StDev  Minimum      Q1  Median
Ele       1         546   0  79.072   0.0676  1.580   71.620  78.390  79.420
          2         834   0  78.351   0.0597  1.726   62.640  77.390  78.420

Variable  Re_class      Q3  Maximum
Ele       1         80.420   80.440
          2         79.420   80.540
```

Left Channel; Section 2

- **Discriminant Analysis: Re_class versus Elevation**

```
Linear Method for Response: Re_class

Predictors: Elevation

Group         1         2
Count       651       230

Summary of classification

                 True Group
Put into Group       1      2
1                  411     92
2                  240    138
Total N            651    230
N correct          411    138
Proportion       0.631  0.600

N = 881            N Correct = 549           Proportion Correct = 0.623
```

- **Descriptive Statistics: Elevation**

```
Variable  Re_class    N  N*    Mean  SE Mean  StDev  Minimum      Q1  Median
Ele       1         651   0  78.136   0.0432  1.103   75.030  77.350  78.340
          2         230   0  77.338   0.0872  1.322   74.330  76.070  77.370

Variable  Re_class      Q3  Maximum
Ele       1         78.370   80.370
          2         78.350   80.960
```

Left Channel; Section 3

- **Discriminant Analysis: Re_class versus Elevation**

```
Linear Method for Response: Re_class

Predictors: Elevation

Group         1         2
Count      2621      1138


Summary of classification
                 True Group
Put into Group       1      2
1                 1692    544
2                  929    594
Total N           2621   1138
N correct         1692    594
Proportion       0.646  0.522

N = 3759           N Correct = 2286           Proportion Correct = 0.608
```

- **Descriptive Statistics: Elevation**

```
Variable  Re_class     N  N*    Mean  SE Mean  StDev  Minimum      Q1
Median
Ele       1         2621   0  79.090   0.0364  1.864   53.060  78.260
80.270
          2         1138   0  78.298   0.0698  2.355   57.860  77.250
78.280

Variable  Re_class      Q3  Maximum
Ele       1         80.290   81.020
          2         80.270   80.320
```

Right Channel; Section 1

- **Discriminant Analysis: Re_class versus Elevation**

```
Linear Method for Response: Re_class

Predictors: Elevation

Group         1         2
Count       538      2068

Summary of classification

                 True Group
Put into Group       1      2
1                  374    706
2                  164   1362
Total N            538   2068
N correct          374   1362
Proportion       0.695  0.659

N = 2606           N Correct = 1736           Proportion Correct = 0.666
```

- **Descriptive Statistics: Elevation**

```
Variable  Re_class     N  N*    Mean  SE Mean  StDev  Minimum      Q1
Median
Ele       1          538   0  79.431   0.0426  0.989   75.400  78.430
79.450
          2         2068   0  78.721   0.0278  1.266   69.100  78.430
78.450
```

```
Variable  Re_class      Q3  Maximum
Ele       1         80.430   80.450
          2         79.450   80.450
```

Right Channel; Section 2

- **Discriminant Analysis: Re_class versus Elevation**

```
Linear Method for Response: Re_class

Predictors: Elevation

Group         1         2
Count       454       546

Summary of classification
                  True Group
Put into Group      1      2
1                 241    208
2                 213    338
Total N           454    546
N correct         241    338
Proportion      0.531  0.619

N = 1000           N Correct = 579           Proportion Correct = 0.579
```

- **Descriptive Statistics: Elevation**

```
Variable  Re_class    N  N*    Mean  SE Mean  StDev  Minimum      Q1  Median
Ele       1         454   0  76.827   0.0974  2.074   70.380  75.400  76.990
          2         546   0  75.282    0.116  2.708   67.880  74.880  75.400
Variable  Re_class      Q3  Maximum
Ele       1         79.380   80.400
          2         77.400   80.400
```

Right Channel; Section 3

- **Discriminant Analysis: Re_class versus Elevation**

```
Linear Method for Response: Re_class

Predictors: Elevation

Group         1         2
Count       397       332


Summary of classification

                  True Group
Put into Group      1      2
1                 356    173
2                  41    159
Total N           397    332
N correct         356    159
Proportion      0.897  0.479

N = 729           N Correct = 515           Proportion Correct = 0.706
```

- **Descriptive Statistics: Elevation**

```
Variable  Re_class    N  N*    Mean  SE Mean  StDev  Minimum      Q1  Median
Ele       1         397   0  76.256    0.116  2.309   70.060  75.360  75.360
          2         332   0  73.438    0.153  2.796   68.560  70.360  75.360
```

Variable	Re_class	Q3	Maximum
Ele	1	77.360	80.380
	2	75.380	80.360

Appendix 3: Hydraulic nature at each cross-section along the full river network

- ***Low discharge (6,450 m^3s^{-1}) scenario***

Reach	River Station	Q Channel	W.S. Elev	E.G. Slope	Vel Chnl	Flow Area Ch	Top W Act Chan	Mann Wtd Chnl	Froude # Chl	Hydr Depth C	Vel Left	Vel Right
		(m^3/s)	(m)	(m/m)	(m/s)	(m^2)	(m)			(m)	(m/s)	(m/s)
Channel1	1.05	6450	84.14	8.69E-05	0.543	11876.78	1246.28	0.0769	0.056	9.53	0	0
Channel1	1.04	6450	84.08	7.67E-05	0.51	12651	1376.45	0.0753	0.054	9.19	0	0
Channel1	1.03	6450	84.03	8.53E-05	0.515	12522.17	1511.37	0.0734	0.057	8.29	0	0
Channel1	1.02	6450	83.99	8.54E-05	0.502	12858.77	1699.16	0.071	0.058	7.57	0	0
Channel1	1.01	6450	83.95	8.72E-05	0.515	12513.33	2059.57	0.0603	0.067	6.08	0	0
Channel2	2.07	2224.12	83.78	2.76E-05	0.394	5649.95	1381.7	0.034123	0.062	4.09	0	0
Channel2	2.06	2224.12	83.71	0.000146	0.491	4530.66	1130.95	0.0621	0.078	4.01	0	0
Channel2	2.05	2224.12	83.59	0.000174	0.595	3739.23	880.29	0.0582	0.092	4.25	0	0
Channel2	2.04	2224.12	83.5	0.000129	0.488	4557.2	918.44	0.0677	0.07	4.96	0	0
Channel2	2.03	2224.12	83.32	0.00028	0.527	4220.76	983.33	0.0838	0.081	4.29	0	0
Channel2	2.02	2224.12	83.31	3.95E-06	0.501	4439.41	1246.03	0.00925	0.085	3.56	0	0
Channel2	2.01	2224.12	83.3	2.13E-05	0.515	4315.81	1097.72	0.0223	0.083	3.93	0	0
Channel3	3.26	1749.12	83.3	2.58E-06	0.39	4488.2	1057.53	0.0108	0.06	4.24	0	0
Channel3	3.25	1749.12	83.3	1.12E-05	0.527	3316.22	776.44	0.0167	0.081	4.27	0	0
Channel3	3.24	1749.12	83.29	1.27E-05	0.406	4312.71	832.01	0.0263	0.057	5.18	0	0
Channel3	3.23	1749.12	83.28	4.3E-05	0.375	4665.6	941.42	0.05083	0.054	4.96	0	0
Channel3	3.22	1749.12	83.25	7.77E-05	0.392	4466.41	987.07	0.061572	0.059	4.52	0	0
Channel3	3.21	1749.12	83.12	0.000314	0.49	3572.23	754.86	0.102041	0.072	4.73	0	0
Channel3	3.2	1749.12	83.07	3.87E-05	0.443	3952.46	819.28	0.0401	0.064	4.82	0	0
Channel3	3.19	1749.12	83.03	0.000089	0.464	3767.01	801.33	0.057	0.068	4.7	0	0
Channel3	3.18	1749.12	82.96	0.000233	0.529	3307.06	771.47	0.0761	0.082	4.29	0	0
Channel3	3.17	1749.12	82.81	0.00025	0.564	3099.84	800.37	0.0691	0.092	3.87	0	0
Channel3	3.16	1749.12	82.67	0.000242	0.474	3689.35	696.06	0.0997	0.066	5.3	0	0
Channel3	3.15	1749.12	82.51	0.000324	0.579	3021.29	596.97	0.0916	0.082	5.06	0	0
Channel3	3.14	1749.12	82.35	0.000563	0.52	3365.4	793.86	0.119499	0.081	4.24	0	0

Channel3	3.13	1749.12	82.26	6.84E-05	0.643	2719.82	919.69	0.0265	0.119	2.96	0	0
Channel3	3.12	1749.12	82.23	0.000197	0.512	3418.13	909.8	0.0662	0.084	3.76	0	0
Channel3	3.11	1749.12	82.12	0.000261	0.544	3213.74	916.59	0.0713	0.093	3.51	0	0
Channel3	3.1	1749.12	82.08	4.37E-05	0.769	2274.17	1070.02	0.0142	0.168	2.13	0	0
Channel3	3.09	1749.12	82.06	9.91E-06	0.759	2303	1397.96	0.00596	0.189	1.65	0	0
Channel3	3.08	1749.12	82.04	6.73E-05	0.785	2226.99	1181.42	0.017	0.183	1.89	0	0
Channel3	3.07	1749.12	82.01	5.89E-05	0.566	3092.56	1109.32	0.0303	0.108	2.79	0	0
Channel3	3.06	1749.12	81.97	1.91E-05	0.87	2011.43	1141.36	0.00787	0.209	1.76	0	0
Channel3	3.05	1749.12	81.94	6.85E-05	1.089	1606.16	859.83	0.0121	0.254	1.87	0	0
Channel3	3.04	1749.12	81.94	4.24E-05	0.716	2444.41	968.86	0.0185	0.144	2.52	0	0
Channel3	3.03	1749.12	81.93	2.54E-05	0.716	2441.44	1112.56	0.0128	0.154	2.19	0	0
Channel3	3.02	1749.12	81.93	4.15E-06	0.573	3054.02	1320.15	0.00622	0.12	2.31	0	0
Channel3	3.01	1749.12	81.93	3.04E-05	0.388	4503.34	1138.55	0.0355	0.062	3.96	0	0
Channel16	16.03	536.15	80.65	3.42E-06	0.583	920.02	286.58	0.0069	0.104	3.21	0	0
Channel16	16.02	536.15	80.64	6.59E-06	0.641	836.97	290.88	0.0081	0.121	2.88	0	0
Channel16	16.01	536.15	80.62	8.05E-06	0.864	620.21	172.01	0.0077	0.145	3.61	0	0
Channel12	12.12	117.14	81.39	3.59E-05	0.367	319.31	173.54	0.0245	0.086	1.84	0	0
Channel12	12.11	117.14	81.39	8.48E-06	0.275	426.12	225.15	0.0162	0.064	1.89	0	0
Channel12	12.1	117.14	81.37	1.93E-05	0.403	290.41	175.68	0.0152	0.1	1.65	0	0
Channel12	12.09	117.14	81.36	7.08E-06	0.308	380.03	189.94	0.0137	0.07	2	0	0
Channel12	12.08	117.14	81.35	1.18E-05	0.384	304.92	178.36	0.0128	0.094	1.71	0	0
Channel12	12.07	117.14	81.33	1.34E-05	0.479	244.7	179.34	0.0094	0.131	1.36	0	0
Channel12	12.06	117.14	81.31	1.03E-05	0.63	185.86	126.15	0.0066	0.166	1.47	0	0
Channel12	12.05	117.14	81.3	4.72E-06	0.454	258.14	145.78	0.007	0.109	1.77	0	0
Channel12	12.04	117.14	81.26	0.000262	0.824	142.1	89.34	0.0267	0.209	1.59	0	0
Channel12	12.03	117.14	80.99	0.000149	0.785	149.31	116.69	0.0183	0.221	1.28	0	0
Channel12	12.02	117.14	80.59	0.000382	1.31	89.4	94.19	0.0144	0.429	0.95	0	0
Channel12	12.01	117.14	80.59	5.82E-05	0.632	185.39	133.67	0.015	0.171	1.39	0	0
Channel10	10.03	130.34	81.43	4.5E-07	0.218	598.39	184.76	0.0067	0.039	3.24	0	0
Channel10	10.02	130.34	81.43	1.8E-07	0.147	886.32	241.12	0.0068	0.024	3.68	0	0
Channel10	10.01	130.34	81.43	1.3E-07	0.107	1223.4	298.13	0.0085	0.017	4.1	0	0
Channel2_4	24.05	475	83.21	0.000868	1.393	341.06	160.07	0.035	0.305	2.13	0	0

Channel2_4	24.04	475	83.08	0.000376	0.95	500.19	222.64	0.035	0.202	2.25	0	0
Channel2_4	24.03	475	82.95	0.00023	0.732	649.23	296.2	0.035	0.158	2.19	0	0
Channel2_4	24.02	475	82.68	0.000738	1.067	444.97	275.77	0.035	0.268	1.61	0	0
Channel2_4	24.01	475	82.34	0.001173	1.231	385.87	273.36	0.035	0.331	1.41	0	0
Channel8	8.04	1212.29	81.44	1.36E-05	0.945	1283.25	326.83	0.0097	0.152	3.93	0	0
Channel8	8.03	1212.29	81.38	1.6E-05	1.344	901.97	254.9	0.0069	0.228	3.54	0	0
Channel8	8.02	1212.29	81.39	1.15E-05	1.044	1160.79	255.47	0.0089	0.156	4.54	0	0
Channel8	8.01	1212.29	81.41	1.56E-05	0.607	1998.74	431.36	0.0181	0.09	4.63	0	0
Channel14	14.03	1342.63	81.4	3.61E-06	0.743	1806.69	416.35	0.0068	0.114	4.34	0	0
Channel14	14.02	1342.63	81.38	6.7E-06	0.901	1490.09	308.4	0.0082	0.131	4.83	0	0
Channel14	14.01	1342.63	81.29	1.89E-05	1.527	879.32	248.92	0.0066	0.259	3.53	0	0
Channel9	9.09	852.91	81.5	2.15E-05	0.469	1820.18	467.6	0.0245	0.076	3.89	0	0
Channel9	9.08	852.91	81.43	7.96E-05	0.862	988.88	457.05	0.0173	0.187	2.16	0	0
Channel9	9.07	852.91	81.37	2.62E-05	1.091	781.49	402.21	0.0073	0.25	1.94	0	0
Channel9	9.06	852.91	81.34	0.000114	0.942	905.32	442.35	0.0183	0.21	2.05	0	0
Channel9	9.05	852.91	80.56	0.0005	3.32	256.91	194.69	0.0081	0.923	1.32	0	0
Channel9	9.04	852.91	80.71	0.000157	1.178	724.28	473.8	0.0141	0.304	1.53	0	0
Channel9	9.03	852.91	80.63	8.9E-05	1.368	623.44	432.53	0.0088	0.364	1.44	0	0
Channel9	9.02	852.91	80.66	2E-05	0.588	1449.54	492.21	0.0156	0.109	2.94	0	0
Channel9	9.01	852.91	80.66	3.23E-05	0.399	2137.66	617.3	0.0326	0.068	3.46	0	0
Channel17	17.07	316.76	80.64	1.36E-05	0.599	528.85	189.09	0.0122	0.114	2.8	0	0
Channel17	17.06	316.76	80.64	4.73E-06	0.616	514.21	187.87	0.0069	0.119	2.74	0	0
Channel17	17.05	316.76	80.64	3.65E-06	0.42	754.34	208.65	0.0107	0.07	3.62	0	0
Channel17	17.04	316.76	80.63	3.24E-05	0.516	613.82	210.13	0.0225	0.096	2.92	0	0
Channel17	17.03	316.76	80.64	2.11E-06	0.379	835.82	272.05	0.0081	0.069	3.07	0	0
Channel17	17.02	316.76	80.64	2.38E-06	0.295	1073.18	289.36	0.0125	0.049	3.71	0	0
Channel17	17.01	316.76	80.64	8.2E-07	0.294	1078.05	267.12	0.0078	0.047	4.04	0	0
Channel4	4.12	4225.88	83.76	0.000315	0.769	5494.59	1059	0.0691	0.108	5.19	0	0
Channel4	4.11	4225.88	83.63	0.000242	0.779	5422.72	1117.3	0.0572	0.113	4.85	0	0
Channel4	4.1	4225.88	83.44	0.000476	0.907	4657.06	1201.83	0.0593	0.147	3.87	0	0
Channel4	4.09	4225.88	83.13	0.000213	0.741	5700.36	1389.44	0.0505	0.117	4.1	0	0
Channel4	4.08	4225.88	82.98	0.000109	0.75	5634.84	1125.07	0.0407	0.107	5.01	0	0

Channel4	4.07	4225.88	82.86	0.000127	0.647	6527.05	966.85	0.0621	0.08	6.75	0	0
Channel4	4.06	4225.88	82.75	0.00015	0.66	6401.98	948.07	0.0663	0.081	6.75	0	0
Channel4	4.05	4225.88	82.69	9.5E-05	0.683	6188.58	984.91	0.0486	0.087	6.28	0	0
Channel4	4.04	4225.88	82.63	0.00037	0.711	5943.06	890.79	0.0959	0.088	6.67	0	0
Channel4	4.03	4225.88	82.51	0.000233	0.758	5573.02	914.26	0.0672	0.098	6.1	0	0
Channel4	4.02	4225.88	82.4	0.00025	0.708	5964.87	903.11	0.0786	0.088	6.6	0	0
Channel4	4.01	4225.88	82.35	8.83E-05	0.6	7042.39	883.02	0.062478	0.068	7.98	0	0
Channel5	5.11	4700.88	82.3	7.36E-05	0.77	6104.89	1012.27	0.0369	0.1	6.03	0	0
Channel5	5.1	4700.88	82.26	0.000303	0.853	5507.84	847.99	0.071	0.107	6.5	0	0
Channel5	5.09	4700.88	82.18	0.00014	0.734	6405.38	874.55	0.0607	0.087	7.32	0	0
Channel5	5.08	4700.88	82.11	0.000223	0.734	6402.44	817.67	0.0802	0.084	7.83	0	0
Channel5	5.07	4700.88	82.04	0.000114	0.786	5978.44	817.97	0.0511	0.093	7.31	0	0
Channel5	5.06	4700.88	81.98	0.00012	0.845	5564.06	711.62	0.0511	0.096	7.82	0	0
Channel5	5.05	4700.88	81.91	0.000308	0.801	5868.24	623.28	0.0975	0.083	9.42	0	0
Channel5	5.04	4700.88	81.82	0.000195	0.777	6053.69	630.85	0.081	0.08	9.6	0	0
Channel5	5.03	4700.88	81.75	0.000134	0.767	6131.87	716.38	0.0632	0.084	8.56	0	0
Channel5	5.02	4700.88	81.66	0.000267	0.852	5519.05	778.39	0.0708	0.102	7.09	0	0
Channel5	5.01	4700.88	81.49	0.000477	0.812	5788.98	979.28	0.0879	0.107	5.91	0	0
Channel6	6.04	3847.98	81.47	4.9E-06	0.898	4282.75	839.75	0.0073	0.127	5.1	0	0
Channel6	6.03	3847.98	81.46	5.6E-06	0.932	4130.4	662.65	0.0086	0.119	6.23	0	0
Channel6	6.02	3847.98	81.43	5.85E-06	1.162	3310.97	503.14	0.0073	0.145	6.58	0	0
Channel6	6.01	3847.98	81.43	5.32E-06	1.205	3192.67	486.77	0.0067	0.15	6.56	0	0
Channel7	7.07	2635.69	81.44	2.59E-05	1.013	2600.71	452.12	0.0161	0.135	5.75	0	0
Channel7	7.06	2635.69	81.44	1.14E-05	0.785	3359.56	535.19	0.0146	0.1	6.28	0	0
Channel7	7.05	2635.69	81.42	2.5E-05	0.968	2723.32	578.66	0.0145	0.142	4.71	0	0
Channel7	7.04	2635.69	81.44	1.84E-06	0.579	4551.01	963.38	0.0066	0.085	4.72	0	0
Channel7	7.03	2635.69	81.42	3.69E-05	0.682	3862.11	1001.07	0.0219	0.111	3.86	0	0
Channel7	7.02	2635.69	81.41	1.54E-05	0.732	3601.98	1065.79	0.012685	0.127	3.38	0	0
Channel7	7.01	2635.69	81.41	2.46E-06	0.617	4271.01	961.39	0.0069	0.093	4.44	0	0
Channel11	11.03	2505.35	81.41	2.7E-06	0.5	5006.17	999.57	0.0096	0.071	5.01	0	0
Channel11	11.02	2505.35	81.38	4.7E-06	0.849	2950.82	678	0.0068	0.13	4.35	0	0
Channel11	11.01	2505.35	81.3	1.82E-05	1.456	1720.67	485.73	0.0068	0.247	3.54	0	0

Channel13	13.02	2388.2	81.32	8.55E-06	1.236	1932.59	396.31	0.0068	0.179	4.88	0	0
Channel13	13.01	2388.2	81.27	1.52E-05	1.504	1588.39	358.03	0.007	0.228	4.44	0	0
Channel15	15.05	3730.83	81.08	0.000121	2.214	1685.37	583.1	0.0101	0.416	2.89	0	0
Channel15	15.04	3730.83	81.07	0.000115	1.728	2158.49	1175.95	0.0093	0.407	1.84	0	0
Channel15	15.03	3730.83	81.03	0.000309	1.394	2675.92	1583.32	0.0179	0.342	1.69	0	0
Channel15	15.02	3730.83	80.68	0.000344	2.049	1820.76	1226.33	0.0118	0.537	1.48	0	0
Channel15	15.01	3730.83	80.48	0.000178	2.25	1658.21	1267.43	0.0071	0.628	1.31	0	0
Channel18	18.02	4266.98	80.6	5.52E-06	0.94	4539.98	948.27	0.0071	0.137	4.79	0	0
Channel18	18.01	4266.98	80.58	1.42E-05	1.064	4009.83	898.01	0.0096	0.161	4.47	0	0
Channel19	19.03	4583.74	80.57	7.94E-06	1.123	4081.66	857.35	0.0071	0.164	4.76	0	0
Channel19	19.02	4583.74	80.57	7.58E-06	0.978	4684.57	995.63	0.0079	0.144	4.71	0	0
Channel19	19.01	4583.74	80.58	1.9E-05	0.788	5820.09	1204.56	0.0158	0.114	4.83	0	0
Channel20	20.02	4700.88	80.59	2.78E-06	0.532	8844.42	1881.76	0.0088	0.078	4.7	0	0
Channel20	20.01	4700.88	80.59	2.2E-06	0.559	8404.6	1884.39	0.0072	0.085	4.46	0	0

- ***Historical average flooding discharge (26,300 m^3s^{-1}) scenario***

Reach	River Station	Q Channel	W.S. Elev	E.G. Slope	Vel Chnl	Flow Area Ch	Top W Act Chan	Mann Wtd Chnl	Froude # Chl	Hydr Depth C	Vel Left	Vel Right
		(m^3/s)	(m)	(m/m)	(m/s)	(m^2)	(m)			(m)	(m/s)	(m/s)
Channel1	1.05	26294	88.58	0.000117	1.506	17461.06	1263.66	0.0412	0.129	13.82	0	0.065
Channel1	1.04	26289.6	88.49	0.000119	1.388	18945.32	1432.46	0.0439	0.122	13.23	0.077	0.077
Channel1	1.03	26293.37	88.43	0.00012	1.356	19384.83	1568.62	0.04318	0.123	12.36	0.076	0.072
Channel1	1.02	26293.26	88.38	0.000122	1.282	20509.38	1760.01	0.0442	0.12	11.65	0.086	0.054
Channel1	1.01	26294.66	88.32	0.000123	1.212	21692.84	2114.19	0.0432	0.121	10.26	0.048	0.121
Channel2	2.07	13392.88	88.22	0.000109	1.12	11962.33	1433.16	0.0383	0.124	8.35	0.081	0.077
Channel2	2.06	13392.85	88.05	0.000114	1.387	9654.69	1203.07	0.0308	0.156	8.03	0.094	0.129
Channel2	2.05	13397.87	87.92	0.000122	1.658	8078.89	1089.58	0.0253	0.194	7.41	0.071	0
Channel2	2.04	13394.1	87.86	0.000108	1.531	8749.24	975.41	0.0293	0.163	8.97	0.068	0.106
Channel2	2.03	13380.13	87.77	0.000103	1.475	9069.24	1130.99	0.0276	0.166	8.02	0.115	0.138
Channel2	2.02	13395.66	87.69	0.000108	1.282	10451.69	1418.12	0.0307	0.151	7.37	0	0.077
Channel2	2.01	13393.5	87.58	0.00011	1.43	9366.8	1212.01	0.0286	0.164	7.73	0.075	0.109
Channel3	3.26	11192.2	87.55	9.56E-05	1.218	9186.8	1132.35	0.0324	0.137	8.11	0.094	0.171
Channel3	3.25	11197.63	87.42	0.0001	1.664	6730.65	867.03	0.0236	0.191	7.76	0	0.041
Channel3	3.24	11193.39	87.4	9.67E-05	1.389	8061.32	952.24	0.0294	0.152	8.47	0.092	0.179
Channel3	3.23	11194.86	87.35	9.54E-05	1.294	8651.6	995.45	0.0319	0.14	8.69	0.069	0.073
Channel3	3.22	11193.37	87.3	9.38E-05	1.289	8685.26	1061.68	0.0305	0.144	8.18	0.083	0.06
Channel3	3.21	11197.67	87.16	9.52E-05	1.644	6811.34	836.7	0.024	0.184	8.14	0	0.04
Channel3	3.2	11197.73	87.11	0.000095	1.503	7452.09	901.66	0.0265	0.167	8.26	0	0.041
Channel3	3.19	11197.94	87.03	9.88E-05	1.562	7166.85	897.41	0.0254	0.176	7.99	0	0
Channel3	3.18	11197.71	86.96	9.6E-05	1.7	6586.91	858.74	0.0224	0.196	7.67	0	0.052
Channel3	3.17	11197.72	86.91	9.05E-05	1.679	6670.44	928.2	0.0211	0.2	7.19	0	0.045
Channel3	3.16	11197.94	86.85	0.000123	1.644	6813.04	798.55	0.0282	0.18	8.53	0	0
Channel3	3.15	11197.94	86.72	0.000127	1.923	5822.76	724.77	0.0235	0.217	8.03	0	0
Channel3	3.14	11197.86	86.72	0.000125	1.59	7044.8	887.5	0.027971	0.18	7.94	0	0.044
Channel3	3.13	11197.94	86.64	0.000124	1.61	6954.55	1011.66	0.025	0.196	6.87	0	0

Channel3	3.12	11197.85	86.62	0.000128	1.437	7794.67	1088	0.0292	0.171	7.16	0.039	0
Channel3	3.11	11197.56	86.57	0.00011	1.385	8083.47	1254.27	0.028	0.174	6.44	0.013	0.102
Channel3	3.1	11197.93	86.53	0.000169	1.403	7983.02	1417.52	0.0293	0.189	5.63	0.025	0
Channel3	3.09	11197.16	86.41	0.000146	1.267	8839.39	1609.2	0.029808	0.173	5.49	0	0.15
Channel3	3.08	11197.94	86.25	0.000169	1.377	8133.69	1583.56	0.029136	0.194	5.14	0	0
Channel3	3.07	11197.79	86.14	0.000159	1.309	8551.46	1432.08	0.033015	0.171	5.97	0.052	0
Channel3	3.06	11197.91	86.05	0.000184	1.453	7705.71	1534.48	0.027918	0.207	5.02	0.033	0
Channel3	3.05	11197.94	85.87	0.00022	2.014	5559.45	1143.36	0.021727	0.292	4.86	0	0
Channel3	3.04	11197.92	85.86	0.000187	1.615	6935.45	1298.95	0.027036	0.223	5.34	0	0.026
Channel3	3.03	11197.94	85.8	0.00018	1.524	7347.44	1411.41	0.027464	0.213	5.21	0	0
Channel3	3.02	11197.53	85.61	0.000195	1.38	8112.02	1415.25	0.0324	0.184	5.73	0.025	0.14
Channel3	3.01	11197.94	85.53	0.000136	1.273	8798.14	1242.7	0.0338	0.153	7.08	0	0
Channel16	16.03	2021.95	86.05	1.07E-05	0.744	2717.78	372.34	0.0165	0.088	7.3	0	0.037
Channel16	16.02	2021.26	86.05	1.07E-05	0.748	2702.59	379.26	0.0162	0.089	7.13	0.021	0.05
Channel16	16.01	2022.07	86	1.07E-05	1.136	1779.28	261.66	0.0103	0.139	6.8	0	0
Channel12	12.12	978.79	86.27	2.16E-05	0.664	1473.68	279.16	0.0212	0.092	5.28	0.025	0.016
Channel12	12.11	979	86.27	2.14E-05	0.547	1790.14	332.85	0.0259	0.075	5.38	0	0
Channel12	12.1	979	86.23	2.16E-05	0.699	1400.45	291.42	0.0189	0.102	4.81	0	0
Channel12	12.09	979	86.22	2.14E-05	0.615	1592.59	301.5	0.0228	0.085	5.28	0	0
Channel12	12.08	979	86.19	2.2E-05	0.683	1434.01	287.72	0.02	0.098	4.98	0	0
Channel12	12.07	979	86.16	2.21E-05	0.709	1381.75	284.81	0.019	0.103	4.85	0	0.016
Channel12	12.06	979	86.12	2.23E-05	0.895	1093.4	246.97	0.0142	0.136	4.43	0	0
Channel12	12.05	979	86.09	2.26E-05	0.797	1227.75	253.99	0.017	0.116	4.83	0.006	0
Channel12	12.04	979	86.01	2.39E-05	1.224	800.04	189.68	0.0104	0.19	4.22	0	0
Channel12	12.03	978.84	86	2.38E-05	0.923	1060.05	235.24	0.0144	0.139	4.51	0.027	0
Channel12	12.02	978.27	85.95	2.5E-05	1.034	946.17	211.66	0.0131	0.156	4.47	0.076	0.017
Channel12	12.01	977.75	85.95	2.36E-05	0.819	1193.73	218.12	0.0184	0.112	5.47	0.08	0.04
Channel10	10.03	590.52	86.32	1.05E-06	0.346	1708.85	269.87	0.0101	0.044	6.33	0	0
Channel10	10.02	590.52	86.32	1.03E-06	0.262	2249.86	315.53	0.0143	0.031	7.13	0	0
Channel10	10.01	590.45	86.32	1.03E-06	0.207	2847.48	353.41	0.0196	0.023	8.06	0.008	0.004
Channel2_4	24.05	2170.99	87.43	0.000165	1.919	1131.38	193.16	0.0217	0.253	5.86	0.126	0.234
Channel2_4	24.04	2194.49	87.45	0.000161	1.305	1681.19	290.5	0.0313	0.173	5.79	0.052	0.101

Channel2_4	24.03	2200.27	87.43	7.49E-05	0.987	2229.96	392.5	0.0279	0.132	5.68	0.051	0
Channel2_4	24.02	2176.57	87.38	0.000158	0.943	2307.52	425.24	0.0411	0.129	5.43	0.399	0.082
Channel2_4	24.01	2191.51	87.33	0.000156	0.827	2650.9	507.16	0.0455	0.115	5.23	0.104	0.079
Channel8	8.04	3718.96	86.33	1.84E-05	1.208	3079.84	409.59	0.0136	0.141	7.52	0	0
Channel8	8.03	3718.88	86.25	1.88E-05	1.585	2346.33	325.08	0.0102	0.188	7.22	0	0.017
Channel8	8.02	3718.92	86.25	1.85E-05	1.452	2561.21	316.89	0.0119	0.163	8.08	0	0.014
Channel8	8.01	3716.5	86.29	1.8E-05	0.868	4280.38	489.15	0.0207	0.094	8.75	0.021	0.106
Channel14	14.03	4309.46	86.25	2.51E-05	1.082	3981.78	474.17	0.0191	0.119	8.4	0.01	0.014
Channel14	14.02	4309.37	86.2	2.55E-05	1.363	3161.23	378.96	0.0152	0.151	8.34	0	0.02
Channel14	14.01	4308.32	86.11	2.71E-05	1.81	2379.81	345.42	0.0104	0.22	6.89	0.04	0.042
Channel9	9.09	3635.33	86.44	4.54E-05	0.81	4486.91	604.76	0.0316	0.095	7.42	0	0
Channel9	9.08	3635.33	86.37	4.7E-05	1.035	3511.41	564.04	0.0224	0.132	6.23	0	0
Channel9	9.07	3635.33	86.31	4.83E-05	1.189	3058.4	521.11	0.019	0.157	5.87	0	0.024
Channel9	9.06	3635.33	86.28	4.78E-05	1.096	3316.8	534.11	0.0213	0.14	6.21	0	0
Channel9	9.05	3635.33	86.03	5.49E-05	2.2	1652.56	308.2	0.0103	0.303	5.36	0	0
Channel9	9.04	3635.33	86.13	5.04E-05	1	3633.85	594.85	0.0237	0.129	6.11	0	0
Channel9	9.03	3635.33	86.09	5.15E-05	1.064	3417.03	579.98	0.022	0.14	5.89	0	0
Channel9	9.02	3635.33	86.08	4.97E-05	0.829	4387.13	594.53	0.0322	0.097	7.38	0	0
Channel9	9.01	3635.33	86.08	4.86E-05	0.633	5742.94	720.13	0.0439	0.072	7.97	0	0
Channel17	17.07	1613.27	86.04	7.47E-06	0.871	1851.22	301.34	0.0105	0.112	6.14	0	0
Channel17	17.06	1613.27	86.04	7.49E-06	0.89	1813.08	294.8	0.0103	0.115	6.15	0	0
Channel17	17.05	1613.27	86.04	7.44E-06	0.736	2190.77	343.82	0.0127	0.093	6.37	0	0
Channel17	17.04	1613.26	86.03	7.56E-06	0.818	1972.28	294.86	0.0119	0.101	6.69	0	0.015
Channel17	17.03	1612.85	86.03	7.41E-06	0.62	2603.01	370.29	0.0161	0.075	7.03	0	0.044
Channel17	17.02	1613.27	86.03	7.24E-06	0.553	2919.1	399.74	0.0183	0.065	7.3	0	0
Channel17	17.01	1612.85	86.03	7.23E-06	0.583	2764.87	354.42	0.0181	0.067	7.8	0	0.045
Channel4	4.12	12900.8	88.21	0.000143	1.235	10448.2	1153.54	0.042	0.131	9.06	0.055	0.054
Channel4	4.11	12895.14	88.15	0.000135	1.21	10654.06	1170.4	0.0418	0.128	9.1	0.145	0
Channel4	4.1	12892.28	88.07	0.000133	1.242	10376.23	1257.27	0.0379	0.138	8.25	0	0.248
Channel4	4.09	12899.35	87.95	0.000135	1.019	12653.41	1472.08	0.0478	0.111	8.6	0.068	0.084
Channel4	4.08	12898.44	87.8	0.000135	1.141	11306.43	1203.16	0.0453	0.119	9.4	0.066	0.095
Channel4	4.07	12898.76	87.65	0.00014	1.133	11388.55	1042.1	0.0515	0.109	10.93	0.076	0.158

Channel4	4.06	12899.07	87.54	0.00014	1.151	11209.36	1042.46	0.0501	0.112	10.75	0.064	0.18
Channel4	4.05	12900.45	87.47	0.000143	1.159	11132.39	1067.63	0.0492	0.115	10.43	0.071	0.129
Channel4	4.04	12900.56	87.41	0.000147	1.227	10514.08	1009.27	0.0471	0.121	10.42	0	0.136
Channel4	4.03	12901.03	87.35	0.000148	1.243	10379.27	1086.53	0.0441	0.128	9.55	0.025	0.002
Channel4	4.02	12901.02	87.29	0.000146	1.208	10683.72	1021.18	0.0478	0.119	10.46	0.01	0.024
Channel4	4.01	12900.97	87.23	0.000145	1.113	11593.98	978.36	0.0562	0.103	11.85	0	0.089
Channel5	5.11	15101.9	87.15	0.000159	1.25	12077.92	1424.91	0.0419	0.137	8.48	0	0.106
Channel5	5.1	15102.03	87.06	0.000156	1.521	9930.39	986.3	0.0383	0.153	10.07	0	0.026
Channel5	5.09	15102.05	87.01	0.000185	1.372	11010.38	1128.51	0.0452	0.14	9.76	0	0
Channel5	5.08	15102.05	86.93	0.000166	1.42	10633.18	953.25	0.0452	0.136	11.15	0	0
Channel5	5.07	15101.89	86.84	0.000157	1.479	10213.73	933.31	0.0418	0.143	10.94	0.049	0
Channel5	5.06	15101.88	86.74	0.000163	1.649	9158.59	791.5	0.0396	0.155	11.57	0	0.058
Channel5	5.05	15101.95	86.67	0.00016	1.674	9022.4	699.95	0.0415	0.149	12.89	0	0.102
Channel5	5.04	15102.05	86.61	0.000159	1.636	9229.54	693.89	0.0432	0.143	13.3	0	0
Channel5	5.03	15102.05	86.55	0.000169	1.539	9813.93	820.04	0.0441	0.142	11.97	0	0
Channel5	5.02	15102.05	86.48	0.000162	1.581	9550.64	891.9	0.0391	0.154	10.71	0	0.012
Channel5	5.01	15102.04	86.42	0.000164	1.384	10913.92	1096.56	0.0428	0.14	9.95	0	0.028
Channel6	6.04	11466.72	86.39	2.01E-05	1.301	8814.78	1001.45	0.0147	0.14	8.8	0	0
Channel6	6.03	11466.72	86.35	2.03E-05	1.52	7542.19	734.37	0.014	0.151	10.27	0	0
Channel6	6.02	11466.72	86.26	2.07E-05	1.922	5967.42	593.76	0.011	0.193	10.05	0	0
Channel6	6.01	11466.72	86.24	2.1E-05	1.986	5773.31	584.74	0.0106	0.202	9.87	0	0
Channel7	7.07	7747.76	86.29	1.31E-05	1.53	5063.33	556.21	0.0103	0.162	9.1	0	0
Channel7	7.06	7747.76	86.31	1.31E-05	1.254	6176.53	621.95	0.0133	0.127	9.93	0	0
Channel7	7.05	7747.76	86.29	1.32E-05	1.335	5803.47	684.29	0.0113	0.146	8.48	0	0
Channel7	7.04	7747.76	86.32	1.3E-05	0.805	9618.62	1133.87	0.0186	0.088	8.48	0	0
Channel7	7.03	7747.76	86.32	5.19E-06	0.805	9625.16	1476.17	0.010432	0.101	6.52	0	0
Channel7	7.02	7747.76	86.31	1.92E-05	0.78	9939.23	1543.49	0.01995	0.098	6.44	0	0
Channel7	7.01	7747.76	86.3	5.65E-06	0.818	9473.9	1179.57	0.0118	0.092	8.03	0	0
Channel11	11.03	7157.24	86.3	1.67E-05	0.71	10079.77	1078.01	0.0255	0.074	9.35	0	0
Channel11	11.02	7157.24	86.25	1.71E-05	1.11	6445.29	758.16	0.0155	0.122	8.5	0	0.007
Channel11	11.01	7157.04	86.19	1.79E-05	1.429	5008.47	780.97	0.0102	0.18	6.41	0	0.051
Channel13	13.02	6178.24	86.17	2.24E-05	1.529	4041.92	473.53	0.0129	0.167	8.54	0	0

Channel13	13.01	6178.24	86.12	2.28E-05	1.771	3487.93	427.26	0.0109	0.198	8.16	0	0
Channel15	15.05	10487.72	86.02	4.29E-05	2.08	5041.45	803.56	0.0107	0.265	6.27	0	0
Channel15	15.04	10487.72	86.09	4.2E-05	1.14	9196.92	1591.98	0.0183	0.151	5.78	0	0
Channel15	15.03	10487.71	86.09	4.15E-05	0.929	11289.46	1764.51	0.0239	0.117	6.4	0.01	0
Channel15	15.02	10487.72	86.05	4.15E-05	1.096	9570.88	1605.52	0.019502	0.143	5.96	0	0
Channel15	15.01	10487.72	86.02	4.22E-05	1.107	9470	1556.64	0.0196	0.143	6.08	0	0
Channel18	18.02	12509.79	85.96	1.11E-05	1.26	9931.57	1063.39	0.0117	0.132	9.34	0	0
Channel18	18.01	12509.79	85.94	1.1E-05	1.374	9106.57	1004.08	0.0105	0.146	9.07	0	0
Channel19	19.03	14123.02	85.9	1.31E-05	1.583	8922.75	957.96	0.0101	0.166	9.31	0.017	0
Channel19	19.02	14123.05	85.91	1.28E-05	1.368	10326.03	1120.11	0.0115	0.144	9.22	0	0
Channel19	19.01	14122.87	85.93	1.27E-05	1.121	12599.39	1320.16	0.0143	0.116	9.54	0.024	0
Channel20	20.02	15101.94	85.95	3.36E-06	0.785	19226.34	1986.83	0.0106	0.081	9.68	0.011	0.01
Channel20	20.01	15101.71	85.95	3.35E-06	0.787	19193.67	2127.87	0.0101	0.084	9.02	0.006	0.029

- ***Historical high flooding discharge (45,149 m^3s^{-1}) scenario***

Reach	River Station	Q Channel	W.S. Elev	E.G. Slope	Vel Chnl	Flow Area Ch	Top W Act Chan	Mann Wtd Chnl	Froude # Chl	Hydr Depth C	Vel Left	Vel Right
		(m^3/s)	(m)	(m/m)	(m/s)	(m^2)	(m)			(m)	(m/s)	(m/s)
Channel1	1.05	45098.25	91.23	0.000193	2.167	20808.41	1263.66	0.0412	0.17	16.47	0.138	0.138
Channel1	1.04	45079.75	91.09	0.000192	1.988	22670.28	1432.46	0.0439	0.16	15.83	0.143	0.165
Channel1	1.03	45108.42	91	0.000188	1.927	23412.51	1568.62	0.04318	0.159	14.93	0.13	0.133
Channel1	1.02	45101.24	90.92	0.000185	1.805	24986.02	1760.01	0.0442	0.153	14.2	0.138	0.117
Channel1	1.01	45067.68	90.84	0.000174	1.667	27031.32	2114.19	0.0432	0.149	12.79	0.1	0.344
Channel2	2.07	23481.08	90.72	0.00014	1.511	15539.66	1433.16	0.0383	0.146	10.84	0.145	0.18
Channel2	2.06	23458.51	90.48	0.000144	1.865	12578.96	1203.07	0.0308	0.184	10.46	0.154	0.392
Channel2	2.05	23499.65	90.3	0.000148	2.201	10674.78	1090.87	0.0253	0.225	9.79	0.134	0.344
Channel2	2.04	23485.64	90.21	0.000153	2.126	11044.44	975.41	0.0293	0.202	11.32	0.137	0.238
Channel2	2.03	23433.05	90.1	0.000135	2.002	11704.36	1130.99	0.0276	0.199	10.35	0.198	0.255
Channel2	2.02	23512	90.01	0.000134	1.709	13759.71	1428.05	0.0307	0.176	9.64	0.038	0.14
Channel2	2.01	23470.93	89.85	0.000142	1.936	12123.86	1212.01	0.0286	0.195	10	0.173	0.203
Channel3	3.26	18847.27	89.83	0.000119	1.601	11772.18	1132.35	0.0324	0.158	10.4	0.228	0.369
Channel3	3.25	18930.86	89.63	0.000126	2.185	8663.65	876.76	0.0236	0.222	9.88	0	0.101
Channel3	3.24	18868.84	89.62	0.000126	1.854	10177.09	952.24	0.0294	0.181	10.69	0.161	0.399
Channel3	3.23	18879.68	89.56	0.000128	1.74	10851.01	995.45	0.0319	0.168	10.9	0.127	0.284
Channel3	3.22	18892.5	89.49	0.000121	1.715	11015.36	1061.68	0.0305	0.17	10.38	0.126	0.202
Channel3	3.21	18932.39	89.28	0.000128	2.201	8603.52	852.47	0.024	0.221	10.09	0.018	0.098
Channel3	3.2	18920.55	89.23	0.000128	2.02	9365.82	908.08	0.0265	0.201	10.31	0.046	0.25
Channel3	3.19	18931.28	89.11	0.000133	2.09	9057.91	916.4	0.0254	0.212	9.88	0	0.262
Channel3	3.18	18930.8	89.01	0.000127	2.263	8365.07	878.3	0.0224	0.234	9.52	0	0.143
Channel3	3.17	18930.46	88.94	0.000114	2.204	8587.2	945.31	0.0211	0.233	9.08	0.044	0.129
Channel3	3.16	18937.27	88.85	0.00018	2.243	8444.58	823.88	0.0282	0.224	10.25	0.037	0.131
Channel3	3.15	18936.72	88.65	0.000182	2.611	7252.13	747.45	0.0235	0.268	9.7	0.048	0.107
Channel3	3.14	18932.01	88.66	0.000175	2.154	8787.99	903.75	0.027971	0.221	9.72	0.125	0.16
Channel3	3.13	18932.1	88.57	0.000157	2.123	8918.9	1023.55	0.025	0.23	8.71	0.03	0.293
Channel3	3.12	18921.37	88.55	0.000165	1.911	9902.34	1093.26	0.0292	0.203	9.06	0.103	0.305

Channel3	3.11	18907.13	88.49	0.000141	1.802	10493.72	1254.27	0.028177	0.199	8.37	0.119	0.376
Channel3	3.1	18935.65	88.45	0.000183	1.763	10743	1442.19	0.0293	0.206	7.45	0.097	0.214
Channel3	3.09	18911.13	88.33	0.000156	1.579	11979.31	1657.38	0.029845	0.187	7.23	0.104	0.377
Channel3	3.08	18938.47	88.16	0.000182	1.669	11350.46	1802.96	0.029468	0.212	6.3	0	0.182
Channel3	3.07	18936.4	88.03	0.000191	1.671	11331.2	1509.34	0.033092	0.195	7.51	0.116	0.028
Channel3	3.06	18936.47	87.93	0.000188	1.777	10658.06	1602.04	0.027977	0.22	6.65	0.101	0.142
Channel3	3.05	18934.73	87.7	0.000229	2.442	7752.38	1246.65	0.02185	0.313	6.22	0	0.298
Channel3	3.04	18935.93	87.7	0.000212	2.005	9445.91	1442.92	0.027127	0.25	6.55	0.056	0.102
Channel3	3.03	18937.35	87.64	0.000197	1.886	10042.47	1509.33	0.027617	0.233	6.65	0.113	0.07
Channel3	3.02	18913.33	87.42	0.000222	1.77	10683.41	1415.25	0.0324	0.206	7.55	0.102	0.433
Channel3	3.01	18939.32	87.32	0.000191	1.712	11064.69	1288.73	0.0338	0.186	8.59	0.022	0
Channel16	16.03	3615.07	87.07	2.23E-05	1.166	3099.79	375.98	0.0165	0.13	8.24	0.012	0.103
Channel16	16.02	3611.15	87.06	0.000022	1.17	3086.36	379.26	0.0162	0.131	8.14	0.04	0.116
Channel16	16.01	3617.5	86.94	2.38E-05	1.778	2034.27	278.41	0.0103	0.21	7.31	0	0
Channel12	12.12	1868.94	87.47	3.98E-05	1.033	1810.01	279.16	0.0212	0.129	6.48	0.05	0.041
Channel12	12.11	1870.25	87.47	4.07E-05	0.851	2198.03	341.58	0.0259	0.107	6.43	0	0.111
Channel12	12.1	1871	87.41	4.01E-05	1.065	1757.31	309.6	0.0189	0.143	5.68	0	0.034
Channel12	12.09	1871.25	87.39	4.25E-05	0.957	1955.93	318.49	0.0228	0.123	6.14	0	0.016
Channel12	12.08	1870.25	87.32	4.13E-05	1.059	1765.32	294.22	0.02	0.138	6	0.013	0.106
Channel12	12.07	1869.7	87.27	4.19E-05	1.098	1702.11	293.28	0.019	0.146	5.8	0	0.115
Channel12	12.06	1871.28	87.18	4.46E-05	1.364	1371.69	277.1	0.0142	0.196	4.95	0	0
Channel12	12.05	1871.03	87.12	4.52E-05	1.251	1495.36	265.18	0.017	0.168	5.64	0.032	0
Channel12	12.04	1870.95	86.94	4.73E-05	1.904	982.45	200.35	0.0104	0.275	4.9	0.089	0
Channel12	12.03	1869.15	86.92	4.84E-05	1.457	1282.52	244.32	0.0144	0.203	5.25	0.076	0
Channel12	12.02	1865.28	86.82	5.02E-05	1.65	1130.2	211.66	0.0131	0.228	5.34	0.154	0.052
Channel12	12.01	1863.08	86.83	5.23E-05	1.345	1385.04	218.12	0.0184	0.17	6.35	0.178	0.081
Channel10	10.03	923.17	87.6	1.46E-06	0.447	2065.41	285.2	0.0101	0.053	7.24	0.007	0.006
Channel10	10.02	923.19	87.6	1.55E-06	0.346	2665.37	334.73	0.0143	0.039	7.96	0	0
Channel10	10.01	922.46	87.6	1.53E-06	0.28	3299.22	353.41	0.0196	0.029	9.34	0.019	0.009
Channel2_4	24.05	4288.4	89.6	0.000225	2.769	1548.98	193.16	0.0217	0.312	8.02	0.202	0.45
Channel2_4	24.04	4556.22	89.64	0.000238	1.966	2317.47	290.5	0.0313	0.222	7.98	0.188	0.126
Channel2_4	24.03	4581.17	89.62	0.000109	1.48	3095.55	393.73	0.0279	0.168	7.86	0.161	0.072
Channel2_4	24.02	4451.3	89.56	0.000214	1.375	3236.68	425.24	0.0411	0.159	7.61	0.754	0.154

Channel2_4	24.01	4533.1	89.51	0.000209	1.208	3753.39	507.16	0.0455	0.142	7.4	0.256	0.12
Channel8	8.04	6467.97	87.6	3.5E-05	1.789	3615.26	431.95	0.0136	0.197	8.37	0	0
Channel8	8.03	6466.67	87.44	3.48E-05	2.366	2733.21	329.28	0.0102	0.262	8.3	0	0.049
Channel8	8.02	6467.19	87.43	3.66E-05	2.199	2940.7	325.59	0.0119	0.234	9.03	0	0.039
Channel8	8.01	6454.91	87.52	3.49E-05	1.322	4883.64	489.15	0.0207	0.134	9.98	0.057	0.203
Channel14	14.03	7390.31	87.44	4.75E-05	1.625	4546.57	474.17	0.0191	0.168	9.59	0.038	0.042
Channel14	14.02	7389.81	87.33	5.06E-05	2.056	3595.09	389.4	0.0152	0.216	9.23	0	0.048
Channel14	14.01	7383.82	87.14	5E-05	2.699	2735.85	345.42	0.0104	0.306	7.92	0.079	0.092
Channel9	9.09	6558.25	87.86	8.68E-05	1.223	5362.96	633.86	0.0316	0.134	8.46	0.041	0
Channel9	9.08	6558.31	87.72	8.42E-05	1.528	4292.21	595.1	0.0224	0.182	7.21	0	0
Channel9	9.07	6555.81	87.6	8.25E-05	1.752	3742.87	532.9	0.019	0.211	7.02	0.025	0.178
Channel9	9.06	6557.65	87.56	8.38E-05	1.64	3999.07	535.92	0.0213	0.192	7.46	0.044	0.042
Channel9	9.05	6558.31	86.98	0.00011	3.356	1954.47	326.52	0.0103	0.438	5.99	0	0
Channel9	9.04	6558.31	87.22	9.85E-05	1.526	4296.91	616.86	0.0237	0.185	6.97	0	0
Channel9	9.03	6557.48	87.15	9.86E-05	1.623	4039.71	591.83	0.022	0.198	6.83	0.007	0.145
Channel9	9.02	6558.3	87.12	0.000108	1.306	5020.77	615.28	0.0322	0.146	8.16	0.022	0
Channel9	9.01	6558.31	87.12	0.000109	1.007	6510.68	746.74	0.0439	0.109	8.72	0	0
Channel17	17.07	2940.75	87.05	1.56E-05	1.36	2162.08	313.74	0.0105	0.165	6.89	0	0.013
Channel17	17.06	2940.8	87.04	1.63E-05	1.388	2118.82	316.52	0.0103	0.171	6.69	0	0
Channel17	17.05	2940.46	87.05	1.59E-05	1.155	2546.84	359.6	0.0127	0.138	7.08	0	0.055
Channel17	17.04	2939.97	87.02	1.61E-05	1.297	2265.92	298.84	0.0119	0.15	7.58	0	0.071
Channel17	17.03	2937.01	87.03	1.62E-05	0.987	2976.87	378.03	0.0161	0.112	7.87	0	0.101
Channel17	17.02	2940.79	87.03	1.65E-05	0.884	3328.24	417.67	0.0183	0.1	7.97	0	0.012
Channel17	17.01	2937.28	87.02	1.65E-05	0.941	3120.52	362.93	0.0181	0.102	8.6	0	0.102
Channel4	4.12	21590.24	90.7	0.000178	1.621	13318.1	1153.54	0.042	0.152	11.55	0.178	0.163
Channel4	4.11	21574.31	90.62	0.00017	1.591	13557.67	1175.53	0.0418	0.15	11.53	0.242	0.103
Channel4	4.1	21508.01	90.53	0.000156	1.595	13482.22	1262.83	0.0379	0.156	10.68	0.066	0.473
Channel4	4.09	21581	90.4	0.000164	1.328	16252.27	1472.08	0.0478	0.128	11.04	0.161	0.212
Channel4	4.08	21555.52	90.19	0.000177	1.52	14185.48	1203.16	0.0453	0.141	11.79	0.14	0.319
Channel4	4.07	21557.2	89.98	0.000206	1.56	13815.95	1042.1	0.0515	0.137	13.26	0.188	0.477
Channel4	4.06	21548.3	89.82	0.000206	1.587	13582	1042.46	0.0501	0.14	13.03	0.19	0.505
Channel4	4.05	21571.77	89.71	0.000209	1.595	13526.69	1067.63	0.0492	0.143	12.67	0.227	0.443
Channel4	4.04	21577.37	89.62	0.000219	1.69	12764.44	1022.87	0.0471	0.153	12.48	0.044	0.456

Channel4	4.03	21599.3	89.53	0.000209	1.694	12753.45	1086.53	0.0441	0.158	11.74	0.185	0.103
Channel4	4.02	21604.57	89.44	0.000219	1.677	12882.83	1021.18	0.0478	0.151	12.62	0.105	0.114
Channel4	4.01	21585.81	89.36	0.000235	1.578	13677.22	981.23	0.0562	0.135	13.94	0.313	0.437
Channel5	5.11	26182.12	89.22	0.000231	1.739	15053.94	1434.82	0.0419	0.171	10.49	0.104	0.445
Channel5	5.1	26194.41	89.05	0.000258	2.201	11899.99	990.13	0.0383	0.203	12.02	0.36	0.119
Channel5	5.09	26206.61	88.97	0.000316	1.967	13325.87	1190.76	0.0452	0.188	11.19	0.066	0.146
Channel5	5.08	26168.29	88.82	0.0003	2.1	12459.78	970.63	0.0452	0.187	12.84	0.212	0.111
Channel5	5.07	26204.33	88.65	0.000288	2.199	11917.99	944.16	0.0418	0.198	12.62	0.138	0.11
Channel5	5.06	26200.97	88.44	0.000312	2.494	10506.44	793.56	0.0396	0.219	13.24	0.091	0.195
Channel5	5.05	26195.92	88.28	0.000329	2.579	10158.05	707.13	0.0415	0.217	14.37	0	0.45
Channel5	5.04	26206.94	88.16	0.000336	2.541	10315.14	701.02	0.0432	0.211	14.71	0.102	0.321
Channel5	5.03	26209.23	88.05	0.000353	2.37	11059.46	840.42	0.0441	0.209	13.16	0.039	0.067
Channel5	5.02	26207.47	87.9	0.000326	2.422	10820.81	899.83	0.0391	0.223	12.03	0.152	0.1
Channel5	5.01	26206.49	87.78	0.000325	2.111	12415.93	1106.3	0.0428	0.201	11.22	0	0.152
Channel6	6.04	19651.05	87.74	3.75E-05	1.93	10184.47	1021.69	0.0147	0.195	9.97	0	0.028
Channel6	6.03	19651.35	87.63	4.12E-05	2.313	8496.35	747.58	0.014	0.219	11.37	0	0.018
Channel6	6.02	19651.37	87.43	4.35E-05	2.946	6671.63	611.51	0.011	0.285	10.91	0	0.01
Channel6	6.01	19651.37	87.38	4.47E-05	3.046	6451.22	606.33	0.0106	0.298	10.64	0	0
Channel7	7.07	13183.4	87.5	2.59E-05	2.292	5751.54	574.83	0.0103	0.231	10.01	0.01	0.01
Channel7	7.06	13183.41	87.54	2.66E-05	1.894	6959.5	642.89	0.0133	0.184	10.83	0	0
Channel7	7.05	13183.41	87.51	2.54E-05	1.98	6657.65	710.18	0.0113	0.206	9.37	0	0
Channel7	7.04	13182.84	87.59	2.45E-05	1.189	11088.34	1173.42	0.0186	0.123	9.45	0.067	0
Channel7	7.03	13183.11	87.58	8.77E-06	1.137	11595.1	1572.07	0.010508	0.134	7.38	0	0.02
Channel7	7.02	13183.09	87.58	3.12E-05	1.101	11979.07	1629.21	0.019774	0.13	7.35	0	0.044
Channel7	7.01	13183.37	87.55	1.06E-05	1.2	10987.03	1234.62	0.011802	0.128	8.9	0	0.028
Channel11	11.03	12260.22	87.55	3.3E-05	1.072	11438.09	1099.68	0.0255	0.106	10.4	0	0
Channel11	11.02	12259.68	87.43	3.27E-05	1.669	7347.72	762.59	0.0155	0.172	9.64	0.016	0.043
Channel11	11.01	12256.57	87.34	3.07E-05	2.076	5903.23	787.79	0.0102	0.242	7.49	0	0.13
Channel13	13.02	10388.84	87.27	4.35E-05	2.273	4571.25	486.53	0.0129	0.237	9.4	0.008	0.062
Channel13	13.01	10388.94	87.15	4.51E-05	2.637	3940.15	443.27	0.0109	0.282	8.89	0	0
Channel15	15.05	17780.1	86.95	8.1E-05	3.059	5811.69	837.05	0.0107	0.371	6.94	0	0
Channel15	15.04	17779.93	87.14	7.13E-05	1.632	10895.03	1637.31	0.0183	0.202	6.65	0.082	0.022
Channel15	15.03	17779.6	87.14	7.27E-05	1.352	13148.56	1780.21	0.0239	0.159	7.39	0.042	0

Channel15	15.02	17780.07	87.05	7.24E-05	1.585	11219.41	1667.81	0.019511	0.195	6.73	0.022	0.007
Channel15	15.01	17779.79	87	7.5E-05	1.612	11028.36	1607.7	0.019605	0.196	6.86	0.109	0.053
Channel18	18.02	21397.55	86.86	2.42E-05	1.964	10892.82	1077.82	0.0117	0.197	10.11	0	0.02
Channel18	18.01	21397.61	86.81	2.42E-05	2.142	9987.95	1020.75	0.0105	0.219	9.78	0	0.005
Channel19	19.03	24337.98	86.69	2.99E-05	2.512	9689.72	968.32	0.0101	0.253	10.01	0.044	0
Channel19	19.02	24338.37	86.74	2.91E-05	2.162	11257.03	1137.54	0.0115	0.219	9.9	0	0.04
Channel19	19.01	24337.07	86.78	2.86E-05	1.773	13727.35	1330.58	0.0143	0.176	10.32	0.053	0
Channel20	20.02	26208.55	86.83	7.58E-06	1.249	20975.76	1986.83	0.0106	0.123	10.56	0.023	0.024
Channel20	20.01	26206.68	86.83	7.4E-06	1.244	21074.18	2146.24	0.010102	0.127	9.82	0.02	0.068